

WL-TR-96-3109

**INVESTIGATION OF PILOT INDUCED
OSCILLATION TENDENCY AND PREDICTION
CRITERIA DEVELOPMENT**



ALEXANDER V. EFREMOV, PhD., et al.

**MOSCOW AVIATION INSTITUTE
MOSCOW, RUSSIA**

VICTOR V. RODCHENKO, PhD., et al.

**CENTRAL AEROHYDRODYNAMIC INSTITUTE
ZHUKOVSKY, RUSSIA**

SERGEY BORIS, PhD., et al.

**GROMOV FLIGHT RESEARCH INSTITUTE
ZHUKOVSKY, RUSSIA**

MAY 1996

FINAL REPORT FOR PERIOD FEBRUARY 1994 - - MARCH 1995

19970314 056

APPROVED FOR PUBLIC RELEASE, DISTRIBUTION IS UNLIMITED

**FLIGHT DYNAMICS DIRECTORATE
WRIGHT LABORATORY
AIR FORCE MATERIEL COMMAND
WRIGHT-PATTERSON AFB OH 45433-7562**

DTIC QUALITY INSPECTED 1

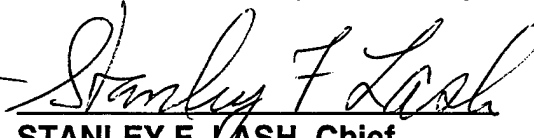
NOTICE

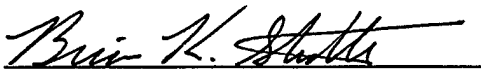
When Government drawings, specifications, or other data are used for any purpose other than in connection with a definitely Government-related procurement, the United States Government incurs no responsibility or any obligation whatsoever. The fact that the Government may have formulated, or in any way supplied the said drawings, specifications, or other data, is not to be regarded by implication, or otherwise as in any manner construed, as licensing the holder, or any other person or corporation; or as conveying any rights or permission to manufacture, use, or sell any patented invention that may in any way be related thereto.

This report is releasable to the National Technical Information Service (NTIS). At NTIS, it will be available to the general public, including foreign nations.

This technical report has been reviewed and is approved for publication.


DAVID B. LEGGETT
Flying Qualities Section


STANLEY F. LASH, Chief
Control Dynamics Branch


BRIAN K. STADLER
Simulation Programs Section


DON R. GUM, Chief
Control Integration & Assessment Branch


DAVID P. LEMASTER, Chief
Flight Control Division

If your address has changed, if you wish to be removed from our mailing list, or if the addressee is no longer employed by your organization, please notify WL/FIGD, Bldg 145, 2180 Eighth St, Ste 1, Wright Patterson AFB, OH 45433-7505, to help maintain a current mailing list.

Copies of this report should not be returned unless return is required by security considerations, contractual obligations, or notice on a specific document.

REPORT DOCUMENTATION PAGE			Form Approved OMB No. 0704-0188	
Public reporting burden for this collection of information is estimated to average 1 hour per response, including the time for reviewing instructions, searching existing data sources, gathering and maintaining the data needed, and completing and reviewing the collection of information. Send comments regarding this burden estimate or any other aspect of this collection of information, including suggestions for reducing this burden, to Washington Headquarters Services, Directorate for Information Operations and Reports, 1215 Jefferson Davis Highway, Suite 1204, Arlington, VA 22202-4302, and to the Office of Management and Budget, Paperwork Reduction Project (0704-0188), Washington, DC 20503.				
1. AGENCY USE ONLY (Leave blank)		2. REPORT DATE May 96		3. REPORT TYPE AND DATES COVERED Feb 1994 - Mar 95
4. TITLE AND SUBTITLE Investigation of Pilot Induced Oscillation and Tendency and Prediction Criteria Development			5. FUNDING NUMBERS PE: 62201F	
6. AUTHOR(S) Alexander V. Efremov, et al. Victor V. Rodchenko, et al. Sergey Boris, et al.				
7. PERFORMING ORGANIZATION NAME(S) AND ADDRESS(ES) Moscow Aviation Institute Gromov Flight Research Institute Moscow, Russia Zhukovsky, Russia Central Aerohydrodynamic Institute Zhukovsky, Russia			8. PERFORMING ORGANIZATION REPORT NUMBER SPC-94 4028 SPC-94 4027 SPC-94 4029	
9. SPONSORING/MONITORING AGENCY NAME(S) AND ADDRESS(ES) Flight Dynamics Directorate Wright Laboratory Air Force Materiel Command Wright-Patterson AFB OH 45433-7562 POC: Brian K. Stadler, WL/FIGD, (937) 255-6526			10. SPONSORING/MONITORING AGENCY REPORT NUMBER WL-TR-96-3109	
11. SUPPLEMENTARY NOTES				
12a. DISTRIBUTION / AVAILABILITY STATEMENT Approved for public release; distribution unlimited.			12b. DISTRIBUTION CODE	
13. ABSTRACT (Maximum 200 words) This report documents the results of work of three Russian institutions directed towards the development of criteria for analysis and prediction of pilot-induced oscillation (PIO) tendencies. The first section of the report covers work done at the Moscow Aviation Institute to determine some of the basic influences of PIO and develop new criteria or modify existing criteria for the prediction of PIO tendencies. The second section describes work done at the Central Aerohydrodynamic Institute to investigate PIO tendencies utilizing a ground-based simulator to evaluate the effects of feel system dynamics and control sensitivities on PIO tendencies. The third section describes work done at the Gromov Flight Research Institute on the use of TU-154 in-flight simulator to evaluate and validate various criteria for the prediction of PIO tendencies in flight for Class III aircraft.				
14. SUBJECT TERMS Flight Control, Flying Qualities, Pilot-Induced Oscillation, Flight Simulation, Feel System Dynamics			15. NUMBER OF PAGES 293	
			16. PRICE CODE	
17. SECURITY CLASSIFICATION OF REPORT UNCLASS	18. SECURITY CLASSIFICATION OF THIS PAGE UNCLASS	19. SECURITY CLASSIFICATION OF ABSTRACT UNCLASS	20. LIMITATION OF ABSTRACT SAR	

TABLE OF CONTENTS

<u>SECTION</u>	<u>PAGE</u>
1 ANALYSIS OF REASONS FOR PILOT INDUCED OSCILLATION TENDENCY AND DEVELOPMENT OF CRITERIA FOR ITS PREDICTION	1
Alexander V. Efremov, PhD., et al. Moscow Aviation Institute Moscow, Russia	
2 INVESTIGATION OF FEEL SYSTEM AND CONTROL SENSITIVITY CHARACTERISTICS INFLUENCING PIO OF UNMANEUVERABLE AIRCRAFT	139
Victor V. Rodchenko, PhD., et al. Central Aerohydrodynamic Institute Zhukovsky, Russia	
3 IN-FLIGHT SIMULATION OF LARGE AIRCRAFT PILOT INDUCED OSCILLATION TENDENCY AND ITS CRITERIA DEVELOPMENT	219
Sergey Boris, PhD., et al. Gromov Flight Research Institute Zhukovsky, Russia	

FOREWORD

This report documents the results of three efforts sponsored by Wright Laboratory through the European Office of Aerospace Research and Development (EOARD) with three Russian research institutes: the Moscow Aviation Institute (MAI), the Central Aerohydrodynamics Institute (TsAGI), and the Gromov Flight Research Institute (GFRI). The overall objective of these three efforts was the development and assessment of criteria for the analysis and prediction of pilot-induced oscillation (PIO) tendencies. The three efforts are documented in the three sections of this report.

The first section, by MAI, focuses on pilot modeling. The primary tasks of this effort were to: 1) determine some of the basic influences on PIO tendency, 2) develop common methodology, algorithms, and software for use in different stages of the study (simulation on a workstation, a ground-based simulator, and in-flight simulator), 3) conduct experiments with different aircraft dynamics to determine the pilot and pilot-vehicle system frequency response characteristics, and 4) develop new criteria or modify existing criteria for the prediction of PIO tendencies.

The second section, by TsAGI, focuses on ground-based simulation. The primary objectives of this effort were: 1) development of methods to investigate PIO tendencies on a ground-based simulator, 2) evaluation of the effects of feel system dynamics and control sensitivity on PIO tendencies, and 3) evaluation of the effects of limb-manipulator dynamics characteristics coupled with elastic structural modes on PIO tendencies.

The third section, by GFRI, focuses on in-flight simulation. The primary purpose of this effort was to evaluate and validate various criteria for the prediction of PIO tendencies in flight for Class III aircraft (large aircraft with low maneuverability). Four criteria were selected for evaluation: 1) Smith-Geddes, 2) Gibson, 3) Bandwidth, and 4) a "pilot-in-the-loop" technique developed by R. A. Hess and R. M. Kalteis.

The three efforts documented in this report represent a comprehensive treatment of the PIO problem, offering new perspectives by the three Russian institutes and authors.

SECTION 1

ANALYSIS OF REASONS FOR PILOT INDUCED OSCILLATION TENDENCY AND DEVELOPMENT OF CRITERIA FOR ITS PREDICTION

**Alexander V. Efremov, PhD
Alexander V. Ogloblin, PhD
Alexander V. Koshelenko
Vladimir A. Naumov**

**MOSCOW AVIATION INSTITUTE
PILOT-VEHICLE LABORATORY**

MOSCOW, RUSSIA

CONTENTS

	Page
LIST OF FIGURES.....	4
LIST OF SYMBOLS	8
PREFACE.....	11
INTRODUCTION	12
1.0 THE VARIABLES DEFINING THE PILOT-VEHICLE SYSTEM	
CHARACTERISTICS	15
1.1 THE TASK VARIABLES	15
1.1.1 The Controlled Element Dynamics	15
1.1.2 Manipulators	25
1.1.3 Display	25
1.1.4 Input Signal $i(t)$ or $d(t)$	29
1.2 THE PILOT'S VARIABLES	29
2.0 ANALYSIS OF THE REASONS FOR PIO TENDENCY IN	
MODERN AIRCRAFT	31
2.1 THE INFLUENCE OF SOME DYNAMICS PECULIARITIES IN ATTITUDE	
LONGITUDINAL MOTION OF SUPERAUGMENTED VEHICLES	33
2.2 THE INFLUENCE OF DIFFERENT TASK VARIABLES	41
2.3 THE INFLUENCE OF PILOT'S VARIABLES (π, σ).....	61
3.0 DEVELOPMENT OF CRITERIA FOR HANDLING QUALITIES RESULTING	
FROM EXPERIMENTAL RESEARCH ON PILOT-VEHICLE SYSTEM	
CHARACTERISTICS	69
3.1 THE TASK OF EXPERIMENTAL RESEARCH	69
3.2 ANALYSIS OF RESULTS	71
4.0 THE DEVELOPMENT OF CRITERIA FOR PREDICTION OF PIO	
TENDENCY	85
4.1 THE PREDICTION OF PIO TENDENCY AND REQUIREMENTS FOR	
HANDLING QUALITIES BASED ON THE STRUCTURAL APPROACH	86
4.2 APPLICATION OF THE OPTIMAL PILOT BEHAVIOR MODEL FOR	
PREDICTION OF PIO TENDENCY	92
4.2.1 The Structure of OCM and Description of its Computer Implementation	92
4.2.2 OCM Application to PIO Tendency Investigation	99
GENERAL CONCLUSIONS AND RECOMMENDATIONS	118
A General Conclusions	118
B Recommendations	120

REFERENCES	121
APPENDIX A Method for Experimental Measurement of Pilot-Vehicle System	
Characteristics	123
A.1 The Unified Fourier Coefficient Method	123
A.2 The Input Signal Development	125
APPENDIX B Standard Dynamics in Precise Tracking Tasks	130
APPENDIX C The Workstation for Manual Control Task Research	135

LIST OF FIGURES

	Page
Figure 1.1 PIOR Scale	16
Figure 1.2 Pilot-Vehicle System	17
Figure 1.3 Examples of Controlled Element Dynamics for Different Tasks	18
Figure 1.4 The Influence of Limitation on Velocity of Surface Deflection	21
Figure 1.5 The Influence of FCS Nonlinear Filter on Control Element Dynamics	22
Figure 1.6 The Influence of Manipulator Dynamics	26
Figure 1.7 Types of Display and Ways of Preservation of Information	28
Figure 2.1 MAI's Facilities Used for Experiments: The Workstation and Moving-Base Simulator	34
Figure 2.2 The Comparison of Experimental Results	35
Figure 2.3 The Comparison of Experimental Results	37
Figure 2.4 The Connection of Amplitude Margin and Resonance Peak	39
Figure 2.5 The Realization of LAHOS's Configuration on In-Flight Simulator Tu-154	39
Figure 2.6 The Comparison of Experimental Results	40
Figure 2.7 Correlated and Uncorrelated with Input Parts of Power Spectral Density Error	42
Figure 2.8 The Influence of FCS Nonlinear Filter on Closed-Loop System Characteristics	42
Figure 2.9 The Comparison of Experimental Results	44
Figure 2.10 The Comparison of Experimental Results	45
Figure 2.11 The Dual-Loop Pilot-Vehicle System (Parallel Scheme)	47
Figure 2.12 Ranges of Stability	49
Figure 2.13 The Comparison of Results Received by Different Criteria	50

Figure 2.14a The Comparison of Experimental Results	51
Figure 2.14b The Comparison of Experimental Results	52
Figure 2.15 The Block-Scheme of Experiment	54
Figure 2.16a The Comparison of Experimental Results	56
Figure 2.16b The Comparison of Experimental Results	57
Figure 2.17 The Comparison of Experimental Results	58
Figure 2.18 The Comparison of Experimental Results	60
Figure 2.19 The Comparison of Experimental Results	62
Figure 2.20 The Comparison of Experimental Results	63
Figure 2.21 The Comparison of Experimental Results	64
Figure 2.22 The Comparison of Experimental Results	67
Figure 2.23 The Comparison of Experimental Results	68
Figure 3.1 The Approximation of LAHOS Input Signal	70
Figure 3.2 The Pilot Frequency Response Characteristics for the Optimal Control Dynamics .	73
Figure 3.3 The Pilot Phase Compensation and Workload Parameters for 2D and 2G Configurations	75
Figure 3.4 The Levels of Handling Qualities	76
Figure 3.5 The Correlation of Closed-Loop Parameters with Developed Criteria	79
Figure 3.6 The Correlation of Closed-Loop Parameters with PR (for the Case When Pilot Phase Compensation is Defined on $\omega=\omega_{BW}$)	80
Figure 3.7 The Correlation Between PIOR and PR	82
Figure 3.8 The Correlation between PIOR and PR (from [5])	83
Figure 3.9 The Criteria for PIO Tendency	84
Figure 4.1 The Modeling of Effect of Permissible Interval d by the Threshold $a=d$	93

Figure 4.2 The Modeling of Effect of Permissible Interval d by the Residual Remnant	94
Figure 4.3 The Human Optimal Control Model	98
Figure 4.4 Comparison of Mathematical Modeling and Experimental Results. Pilot Frequency Response Corresponding to the Optimal Control Dynamics	101
Figure 4.5 Comparison of Mathematical Modeling and Experimental Results (Conf. 1B)	103
Figure 4.6 Comparison of Mathematical Modeling and Experimental Results (Conf. 1D)	104
Figure 4.7 Comparison of Mathematical Modeling and Experimental Results (Conf. 1E)	105
Figure 4.8 Comparison of Mathematical Modeling and Experimental Results (Conf. 1F)	106
Figure 4.9 Comparison of Mathematical Modeling and Experimental Results (Conf. 1G)	107
Figure 4.10 Comparison of Mathematical Modeling and Experimental Results (Conf. 6C) ...	108
Figure 4.11 Comparison of Mathematical Modeling and Experimental Results (Conf. LAHOS 1.4)	109
Figure 4.12 Results of Optimal Control Analysis	110
Figure 4.13 Comparison of Mathematical Modeling and Experimental Results (Conf. 2C) ...	111
Figure 4.14 Comparison of Mathematical Modeling and Experimental Results (Conf. 2G) ...	112
Figure 4.15 Comparison of Mathematical Modeling and Experimental Results (Conf. 1E, $d=0$ sm)	114
Figure 4.16 Comparison of Mathematical Modeling and Experimental Results (Conf. 1E, $d=0.85$ sm)	115
Figure 4.17 Comparison of Mathematical Modeling and Experimental Results (Conf. 1E, $d=2$ sm)	116
Figure A.1 The Distribution of Power Function	127
Figure A.2 The Input Signal.....	129
Figure B.1 The Optimal Aircraft Dynamics	131
Figure B.2 The Frequency Response of Optimal Aircraft Dynamics	134

Figure C.1 The Graphical Presentation of Results	137
--	-----

LIST OF SYMBOLS

A_k	- Amplitude of One of Sinusoids
\hat{a}_k and \hat{b}_k	- Measured Fourier Coefficients
c	- Control Action Signal
d	- Disturbance Input Signal
"d", $\pm d$	- Permissible Interval of Error
e	- Error Signal
f, f_i	- Fraction of Attention Coefficient
H_{cg}	- Altitude in the Center of Gravity
H_p	- Altitude in the Place of Pilot Location
I	- Command Input Signal
$I_{ii}(\omega)$	- Input Signal Distribution of Power Function
$j\omega$	- Fourier Operator
K_c	- Controlled Element Gain Coefficient
K_D	- Display Gain Coefficient
K_p	- Pilot Gain Coefficient
m	- Order of Input Spectral Density Model
	$S_{ii}(\omega) = \frac{K_i^2}{(\omega_i^2 + \omega^2)^2}$
M_q	- Pitching Acceleration Due to Pitch Rate, $q = \dot{\theta}$
M_W	- Pitching Acceleration Due to Velocity Along Z Axis, w
$M_{\dot{w}}$	- Pitching Acceleration Due to Linear Acceleration Along Z Axis, \dot{w}
M_α	- $U_0 M_W$
$M_{\dot{\alpha}}$	- $U_0 M_{\dot{w}}$
M_{δ_e}	- Pitching Acceleration Due to Elevator Deflection δ_e
$N(\bullet)$	- Describing Function Gain of Threshold in Perception of (\bullet) Signal
n_z	- Normal Acceleration
P	- Procedure Variables
q	- Pitch Rate;
r, R	- Resonance Peak
S	- Laplace Operator
$S_{ii}(\omega)$	- Input Signal Spectral Density
$S_{e_i e_i}$	- Spectral Density of Error Signal Correlated with Input
$S_{e_n e_n}$	- Spectral Density of Error Signal Correlated with Remnant

$S_{n_e n_e}(\omega)$	- Remnant Spectral Density
$S_{n_{eo}}$	- Residual Remnant
T_L	- Pilot Lead Time
T_N	- Neuromuscular Time Constant
u	- Vector of Control Action Signals
$W_C(j\omega)$	- Controlled Element Dynamics
$W_{CL}(j\omega)$	- Close-Loop System Frequency Response Characteristic
W_D	- Display Transfer Function
$W_{OL}(j\omega)$	- Open-Loop System Frequency Response Characteristic
$W_P(j\omega)$	- Pilot Describing Function (Control Response)
W_P^{vest}	- Pilot Describing Function Defining his Reaction to Motion Cues
W_P^{vis}	- Pilot Describing Function Defined his Reaction to Visual Cues
x	- Aircraft Phase Coordinate Defined the Piloting Task or Vector of Aircraft Phase Coordinates
Z_W	- Acceleration Along Z Axis Due to Velocity Along Z Axis, w
Z_α	- $U_O Z_{\dot{w}}$
Z_{δ_e}	- Acceleration Along Z Axis Due to Elevator Deflection δ_e
α	- Angle of Attack
ΔL	- Amplitude Margin
$\Delta\phi$	- Phase Margin
$\Delta\phi_P$	- Pilot Phase Compensation
δ_e^x	- Deflection of Elevator
δ_{\max}	- Limitation on Surface Deflection
δ_{\max}^x	- Limitation on Velocity of Surface Deflection
ε	- Angle of Sight Control
θ	- Pitch Angle;
θ_C	- Commanded Pitch Angle
θ_e	- Pitch Angle Tracking Error ($\theta_e = \theta_C - \theta$)
λ	- Pole of Unstable First-Order Plant ($W = \frac{\lambda}{s - \lambda}$)
ξ_{SP}	- Short Period Damping Ratio
$\rho_{O(\bullet)}$	- Noise Ratio of (\bullet) Signal
σ	- Pilot-Centered Variables

$\sigma(\bullet)$	- Mean Square of Signal (\bullet)
τ	- Time Delay of Element $e^{-s\tau}$
Φ	- Physiological Characteristics
φ_P^{opt}	- Pilot Phase Frequency Response for the Optimal Dynamics
φ	- Psychophysiological Characteristics
ω_{BW}	- Bandwidth Frequency
ω_c	- Crossover Frequency
ω_i	- Characterized Frequency of Input Spectral Density Model

$$S_{ii}(\omega) = \frac{K_i^2}{(\omega_i^2 + \omega^2)^2}$$

ω_k	- Frequency of One of Sinusoids
ω_{SP}	- Short Period Frequency
$\omega _{\varphi=-180^\circ}$	- Frequency when Open-Loop Phase is Equal 180°
\in	- Environmental Variables

Abbreviations

DLC	- Direct Lift Control
FCS	- Flight Control System
ICR	- Instantaneous Center of Rotation
HDD	- Head Down Display
HUD	- Head Up Display
PIO	- Pilot Induced Oscillation
OCM	- Optimal Control Model

PREFACE

The research reported here was accomplished for the United States Air Force by Pilot-Vehicle Laboratory of the Moscow Aviation Institute under contract SPC-94-4028. The program was sponsored by the Wright Laboratory and the European Office of Aerospace Research and Development.

The Contractor's principal investigator was:
Prof. Alexander V. Efremov

The Contractor's senior research scientist was:
Dr. Alexander V. Ogloblin

The Contractor's research scientist was:
Alexander V. Koshelenko

The postgraduate student:
Vladimir A. Naumov

The research was performed during the period from February 1994 through March 1995.

INTRODUCTION

The basis for the aviation development is the aspiration of increase of its efficiency and safety of flight. Improved are flight performance, extended flight envelope, mastered new flight regimes, and tasks (low-altitude and high angle-of-attack flight and others). However all of these factors lead to the increase of pilot workload which can reduce the accuracy and safety of flight. The solution of these problems can be achieved by creating of special methods to decrease pilot workload and to exclude or minimize the conditions required to use the maximum human potentialities. The more perspective way here is the creation of superaugmented control systems, integrated displays, and new types of manipulators. The level of modern control system potentialities allows us to solve the problem of optimal control performance synthesized for each piloting task. It is obvious that these problems cannot be solved without deep study of pilot behavior characteristics, his potentialities, and regularities. All that is necessary is to search for the best ways to eliminate the side effects accompanied by superaugmented aircraft and aircraft with nontraditional aerodynamic configurations. All these effects appear when a pilot closes the loop. The study of pilot behavior in closed-loop systems has a history. The considerable input in its development was made by American scientists. They discovered the adaptation of pilot behavior to task variables (controlled element dynamics and input power spectral density characteristics); worked out the methods for measurement of pilot control behavior characteristics, offered the pilot control models, determined the influence of motion cues on some pilot-vehicle system performance, defined the standard controlled element dynamics ($W_C = \frac{k}{s}$) widely used for handling qualities and control system design. These and other results were summarized in [1, 14]. Some new results in the study of pilot-vehicle system performances were also received in Russia. In particular, these results were worked out in Pilot-Vehicle Laboratory of the Moscow Aviation Institute (PVL MAI): the methods, algorithms and software of the unified Fourier coefficients method, and the estimation of its accuracy. Extended was the knowledge of pilot adaptation in the low frequency range, the method of synthesis of the optimal controlled element dynamics in each piloting task, the structural approach to pilot behavior modeling, and "Paper Pilot" techniques.

All of these results are summarized in [1]. The results of pilot behavior regularities were widely used for the following applied manual control tasks:

- requirements for aircraft handling qualities;
- flight control system design;
- development of piloting technique; and
- simulator design.

The analysis of dynamics peculiarities arising in a pilot-vehicle closed-loop system is a task, investigated from the pilot-vehicle system analysis point of view. One of such peculiarities is so-called "Pilot Induced Oscillations" - the phenomenon which can lead to accidents in some cases. This phenomena appeared at different stages of aviation history since the first flight of the Wright Brothers. The augmentation of aircraft and the extension of its flight envelope provoked additional PIO tendencies. There was some research dedicated to the investigation of these peculiarities. Some of the research [2, 3] was dedicated to influence of the effects of elevator

control system dynamics and well-known handling qualities parameters ($F^n, \xi_{SP}, \omega_{SP}$) on the PIO tendency. The creation of highly augmented aircraft, whose dynamics are essentially different from a second order system, required additional investigations for understanding new peculiarities. In this connection it is necessary to mention that the research [4, 5, 6] showed that the existence of additional filters, typical for superaugmented aircraft control systems, leads to the considerable increase in PIO tendency. The understanding that the peculiarities in aircraft control appear in closed-loop systems and the second-order dynamics cannot be used for development of criteria, leads to the necessity of developing generalized criteria for handling qualities. From the majority of approaches developed, two of the more interesting and widely used are discussed below. The first is the equivalent system approach, where the high order system (HOS) dynamics of modern aircraft is approximated with a low order system (LOS). The requirements for parameters of LOS are defined by the current requirements. The second approach uses a model of pilot describing function and attempts to apply the system approach to the problem, by confederating the characteristics of closed-loop system and pilot rating. Both approaches allowed us to move forward in the definition of requirements for handling qualities for the highly augmented aircraft. These approaches have one common considerable shortcoming which leads to the difference in recommendations and results of experimental investigations on the ground and in-flight simulators. That is, inaccuracy in description of the aircraft dynamics in the first approach and in the pilot mathematical model used in the second approach. Such inaccuracy is one of the basic in difference between predicted and experimental pilot ratings. In the second approach it is necessary to notice the Neal and Smith research [4]. The influence of flight control system augmentation here was evaluated with the help of pilot ratings (PR) and associated commentaries. The direct measurements of pilot-vehicle frequency response characteristics in this work did not allow to get the reliable correlation between PR and parameters of frequency response characteristics. The last are standardized according to Neal-Smith criteria. The procedure for calculation of pilot and pilot-vehicle system frequency response characteristics developed in this criteria gives the parameters not corresponding to experimental PR. The modified procedure for calculation of the parameters was offered in [15]. It was based on pilot optimal control model (OCM). It allows us to make more precise use of pilot-vehicle system parameters and to avoid the fixation of bandwidth frequency. However, it was not carried out in this experimental research work, which didn't allow us to check the offered recommendations. Neal-Smith criteria and its modification don't take into account characteristics other than controlled element dynamics, of pilot-vehicle systems. This limitation decreases its reliability for prediction of handling qualities. But, this criteria catches the tendency of the closed-loop system to oscillate and therefore can be used as the basis for prediction of this phenomenon. It is necessary to carry out wide ranging research to develop such criteria as the following:

- determination of the basic reasons for PIO tendency;
- development of the common methodology, algorithms, and software for the possibility of realizing different stages of experimental research (preliminary the simulations used the workstation, ground-based, and in-flight simulators);
- fulfillment of wide experimental research of the different aircraft dynamic configurations to define the pilot and pilot-vehicle system frequency response characteristics;
- modification of Neal-Smith criteria or development of new criteria.

The goal of the current research was to investigate and solve these problems. The analysis and prediction of PIO are considered here from the common basis of analysis and synthesis of pilot-vehicle systems and the systems approach to analysis of PIO tendency. The first chapter defines the main variables influencing pilot-vehicle system characteristics. The second chapter considers the influence of different tasks and pilot's variables on PIO tendency. The conditions are defined for the experiments recommended for further investigations at TsAGI and LII. The third chapter details the experimental investigation of pilot-vehicle closed-loop system characteristics and pilot ratings for all Neal-Smith and the majority of LAHOS configurations. The experiments were carried out basically on the PVL MAI workstation for the manual control task and the moving-based simulator. As a result of this research we developed the requirements for closed-loop and pilot workload parameters. The fourth chapter is dedicated to the development of calculation procedures used in the development of criteria for prediction of requirements for handling qualities and PIO tendency. Two approaches were considered for the calculation: one is based on a structural approach and the second on the use of modern control theory for the description of pilot behavior. Good correlation of results between experimental research and mathematical modeling was demonstrated. The appendixes presents information about the method of identification of pilot and pilot-vehicle system characteristics, the equipment used for research, and the optimal aircraft dynamics used in development of criteria.

1.0 THE VARIABLES DEFINING THE PILOT-VEHICLE SYSTEM CHARACTERISTICS

The analysis of the known PIO facts and their pilot's commentaries leads to the appearance of the specialized scale for evaluation of PIO tendency (fig. 1.1). The numerical values of this scale PIOR define the level of this tendency which is described in the left part of the scale. The attentive reading of it shows that the scale can be divided in two parts which defines two levels of PIO tendency.

The first part (PIOR 1 to 4) defines a level of PIO tendency taking place in a stable pilot-vehicle closed-loop system. The maximum rating of this level PIOR = 4 corresponds to the case where the oscillations arising in the loop can be removed or decreased by the decrease of pilot gain only. In particular, it can be achieved by decreasing the requirement for accuracy of task fulfillment. The latter will be shown in chapter 2.

The second part of the scale (PIOR 5 to 6) includes the cases of the unstable oscillations arising when a pilot just attempts to close the loop.

Thus the PIO tendency takes place in the closed-loop system and its analysis has to be done by means of the system analysis. Such analysis takes into account that the pilot-vehicle system characteristics defining its peculiarities depend on a wide range of the variables, which has to be adequate to the investigated piloting task (or mission). All the variables can be divided on two groups: the task variables and variables connected with the pilot (pilot's variables). All of them influence control, physiological (ϕ), and psycophysiological (Ψ) pilot characteristics (fig. 1.2). Further investigation considered only two of them: control response (pilot describing function $W_P(j\omega)$ and remnant spectral density $S_{n_e n_e}$), and psycophysiological (pilot rating, PR) characteristics. The change of pilot control characteristics leads to the change of pilot-vehicle system parameters and as a consequence to the change of PR.

1.1 THE TASK VARIABLES

There are the following task variables (fig. 1.2): a controlled element, including the flight control system (FCS), the interfaces (display and manipulator), and input signals (command input signal $i(t)$ and/or disturbance $d(t)$). All or part of them are different for each investigated mission (piloting task).

1.1.1 The Controlled Element Dynamics

It is characterized by the mathematical model of transformation of a control action $c(t)$ into aircraft phase coordinate $x(t)$ defining the piloting task. In general, case $x(t)$ and $c(t)$ are the vectors. In the majority of cases of tracking tasks, controlled element dynamics can be considered as a linear element. For this reason, it can be represented by the linear differential equations with constant coefficients or transfer functions (W_C). In table 1.1 (see fig. 1.3), a number of transfer

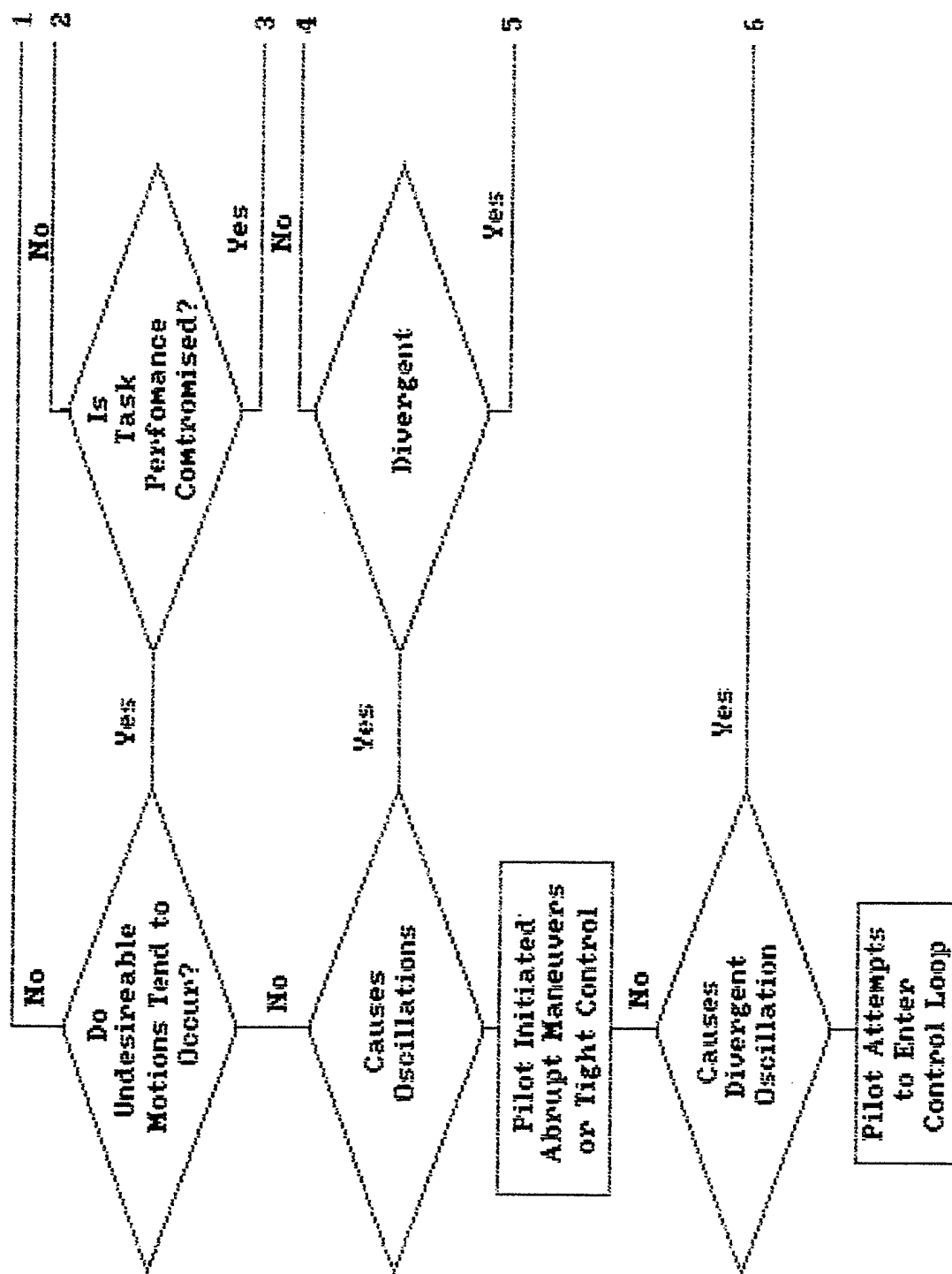


Fig. 1.1.1. PIOR scale

PILOT-VEHICLE SYSTEM

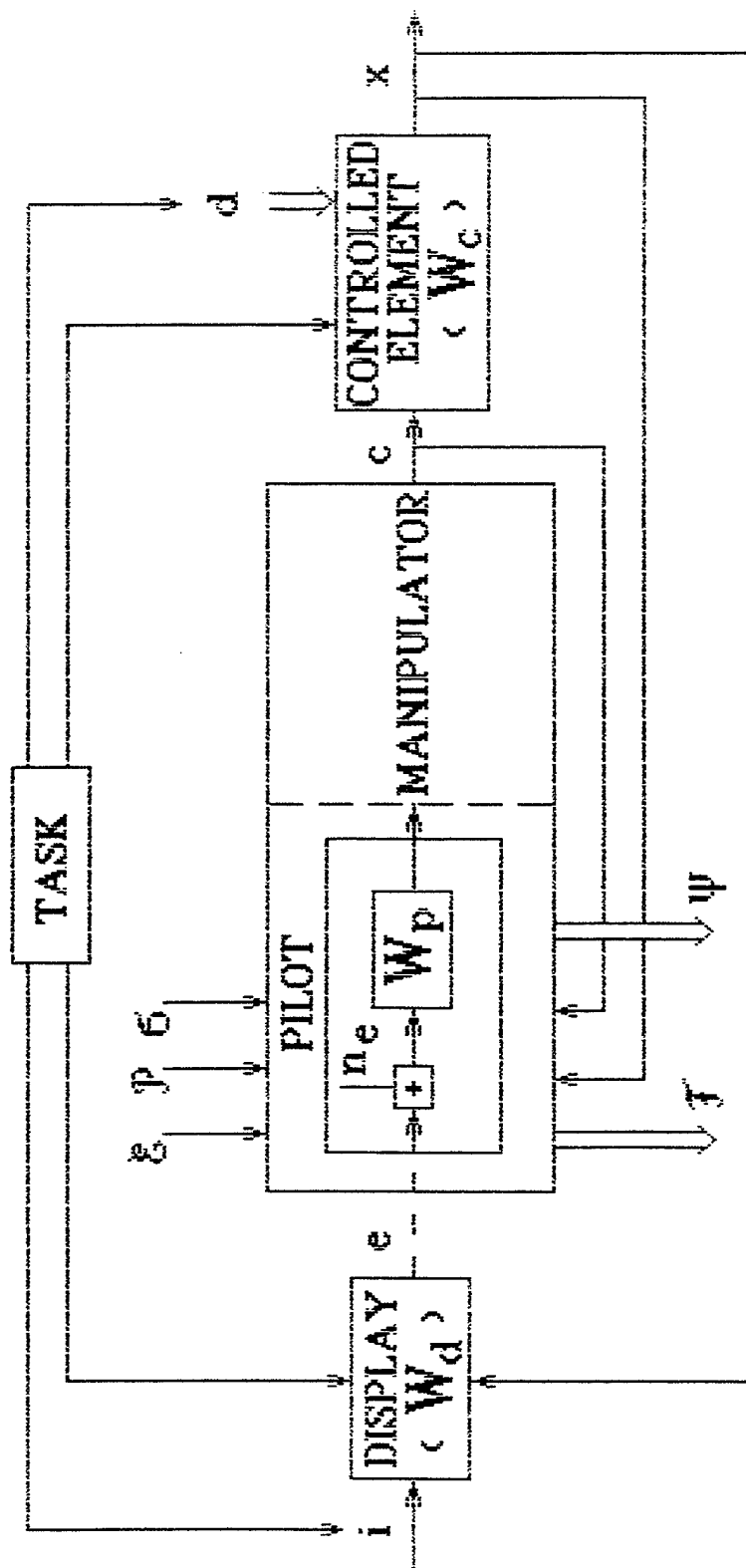


Fig. 1.2. Pilot-vehicle system

CONTROLLED ELEMENT DYNAMICS (W_c)

(low level of augmentation)

N	Output	W_c	Manual control task
1	θ pitch angle	$\frac{K_c(s - Z_w) e^{-\tau s}}{s(s^2 + 2 \xi_{sp} \omega_{sp} s + \omega_{sp}^2)}$	stabilization and control angular motion (conventional configuration)
2	ϵ_z angle of sight	$\frac{K_c(s^2 - Z_w s - Z_w \frac{V}{L})}{s^2(s^2 + 2 \xi_{sp} \omega_{sp} s + \omega_{sp}^2)}$	taking aim ($\epsilon_z = \vartheta + \arcsin \frac{H}{L}$)
3	ΔH altitude	$\frac{K_c n_\alpha g}{s^2(s^2 + 2 \xi_{sp} \omega_{sp} s + \omega_{sp}^2)}$	formation flight, flare
4	γ bank angle	$\frac{K_c}{s(s - L_p)}$	stabilization and control of angular motion
5	ΔZ lateral coordinate	$\frac{K}{s^3(s - L_p)}$	path control in landing
6	X logitudi- nal coordinate	$\frac{K}{s^2(s + a)}$ $\frac{K_c}{s(s^3 + a_1 s^2 + a_2 s + a_3)}$	hovering with thrust control hovering with pitch angle control

Fig. 1.3. Examples of controlled element dynamics for different tasks

functions $W_C(s)$ are shown for different piloting tasks for the low level of aircraft augmentation. For these tasks, the controlled element dynamics differs significantly. This peculiarity defines the different requirements of the character of pilot's actions.

In practical engineering tasks, it is sometimes necessary to use more complex mathematical models taking into account the nonlinear effects, discrete dynamics of some FCS filters, and other complex effects. In these cases, it is convenient to use the concept of describing function $W_C(j\omega)$. For nonlinear systems it depends on the signal $c(t)$ and in some cases nonlinear effects of controlled element dynamics can be considerable. It takes place when the limits on surface deflection and its velocity are reached. In that case, the describing function can differ significantly from the type corresponding to the linear type. Because of the dependence of $c(t)$ from many factors (for example from the input signal or the piloting manner), the variability of such describing function $W_C(c(t), j\omega)$ from experiment to experiment can be high. It has to be taken into account in analysis of results and in a process of preparation of experiments on ground- and in-flight simulators.

Analysis of Some Peculiarities in Dynamics of Highly Augmented Aircraft and Nontraditional Aerodynamics Configurations.

Only some peculiarities in longitudinal motion are discussed.

a) The Peculiarities in Dynamics of Highly Augmented Aircraft.

1. The High Frequency Delay

The high frequency delay is the typical characteristic for the highly augmented aircraft. It is connected with the existence of the different filters in FCS, computers for their realization, and some other reasons. It leads to the difference in the highly augmented aircraft dynamics from the airframe dynamics. This peculiarity can be described approximately by the time delay element $e^{-\tau s}$. In this case, the dynamics of modern aircraft in the pitch control task can be represented by the following:

$$W_C \frac{K_C(S+a)e^{-\tau_c s}}{S(S^2 + 2\xi_{SP}\omega_{SP}S + \omega_{SP}^2)}$$

Here the parameter "a" is not defined by the aerodynamic derivative (Z^α) for some FCS (it takes place in the Space Shuttle aerospace vehicle). The value of τ can be considerable for some aircraft. For example, it is equal 0.152 sec for the Space Shuttle [7] and 0.26 sec for Russian "Buran."

2. Significant Influence of Nonlinearities on Aircraft Dynamics.

Only three nonlinearities are considered:

- the limitation on velocity of surface deflection $\dot{\delta}_{\max}$;
 - the limitation on the surface deflection δ_{\max} ;
- nonlinear filters in FCS.

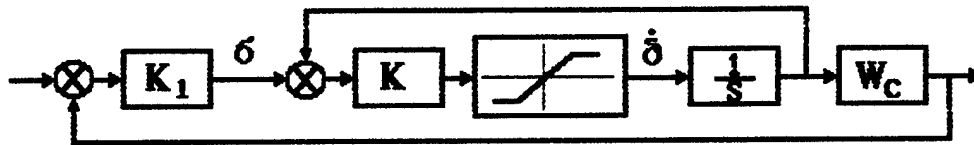
Two first cases of limitation take place for aircraft with a low level of augmentation. They begin to show themselves when δ or $\dot{\delta}$ reach maximum values. However, the small feedback coefficients and the limitation on feedback signals practically do not allow development of unstable processes for these aircraft. The describing function for such controlled elements demonstrates some changes only in a case of very tight limitation. The limitation on the elevator velocity leads to an increase of equivalent time constant of first order dynamics approximated by the actuator dynamics. The variability of the describing function evaluated in several experiments is insignificant which allows us to approximate the nonlinear model of actuator by its equivalent

$$W_a = \frac{1}{T_a j\omega + 1}.$$

The peculiarity of highly augmented aircraft is the existence of high values of feedback coefficients which change its dynamics considerably. In such conditions the use of an actuator with a small value of $\dot{\delta}_{\max}$ or its decrease because of the accidents can lead (if there is not installed special filters) to the development of instability in FCS. The effect of nonlinearity is evident in this case. The measurement of the describing function $W_C(j\omega)$ in the process of the investigation of pilot-aircraft closed-loop system with periodic appearance of such processes demonstrates its high variability from experiment to experiment. The average value of W_C shows the decrease of control element dynamics damping and a dramatic change of its phase (fig. 1.4). The significant difference in aircraft dynamics and the system "airframe + highly augmented FCS dynamics" can lead to the sharp change in dynamics when the deflection of the surfaces reaches the maximum value (δ_{\max}). In particular, the stable control element can become unstable in this case. The dynamics can change considerably when a direct lift control surface used for decoupling attitude and flight path motion reaches the maximum level. Nonlinear coefficients [8] and filters [9] are used in the practice of modern FCS design. The nonlinear filters (fig. 1.5) installed on the "Buran" aerospace vehicle FCS are used to avoid the instability which can arise from the limitation on $\dot{\delta}$. This nonlinear filter has a limiter with regulated values from the feedback signals. In the case of an increase in normal acceleration n_z or pitch rate q , these values decrease, which leads to a decrease of the signal sent to the actuator. Analysis shows that in this case it is possible to avoid instability in FCS, but it leads to the appearance of other sources of nonlinearity. The transfer from considerable to small deflection of the stick causes an increase of gain frequency response characteristics $|W_C(j\omega)|$ in the crossover frequency range and to some change of the phase (see fig. 1.5).

3. Discrepancy Between the Attitude and Path Motion Transfer Function Parameters

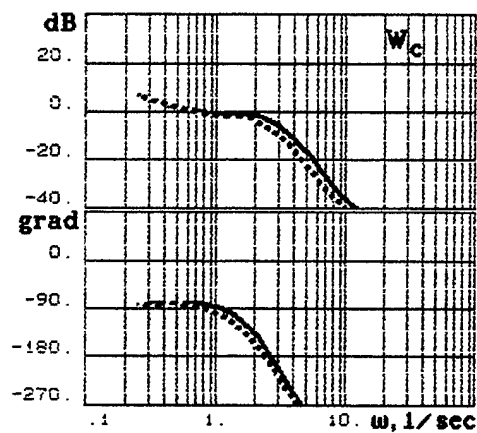
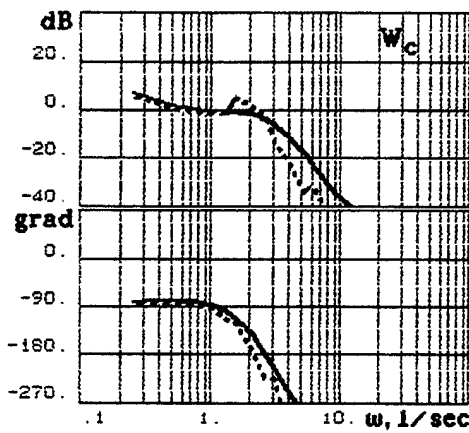
The limitation on surface deflection velocity $\dot{\delta}_{\max}$



Highly augmented
aircraft
 $\delta = \delta_1$

$$\delta_1 \gg \delta_2$$

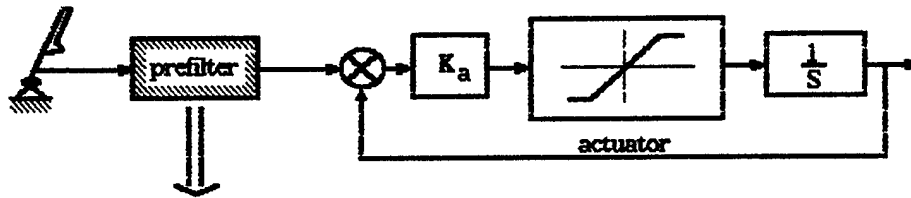
Low augmented
aircraft
 $\delta = \delta_2$



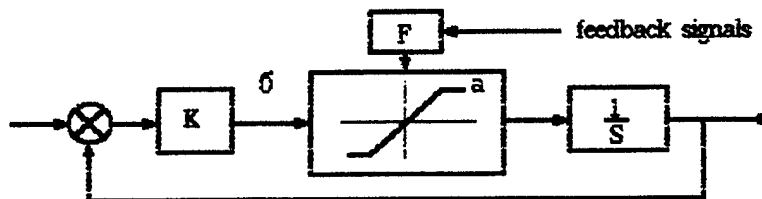
— $\dot{\delta}_{\max} = 126 \text{ deg/sec}$
 - - - $\dot{\delta}_{\max} = 15 \text{ deg/sec}$

Fig. 1.4. The influence of limitation on velocity of surface deflection

The significant influence of nonlinearity on a dynamic response



Buran's basic prefilter



$$W = \frac{1}{T j\omega + 1}, \quad T = \frac{1}{K \operatorname{erf}\left(\frac{a}{\sqrt{2} \sigma}\right)}$$

$$\sigma_1 > \sigma_2$$

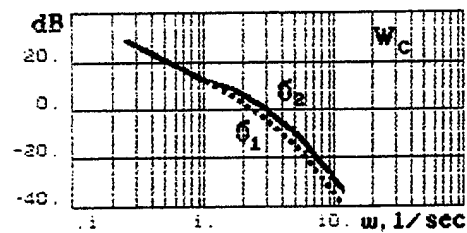


Fig. 1.5. The influence of FCS nonlinear filter on control element dynamics

The aim to get the desirable pitch dynamics for highly augmented aircraft can lead to the case where the zeros of transfer function W_{C_2} don't equal the poles of transfer function for coupled path and angular motions (W_{C_1}). Such a case occurs for the Space Shuttle vehicle [7]. Here the zero of W_{C_2} is defined by the parameter of FCS filter, $a = 1/T_q$. For this vehicle, it is equal to 1.5 rad/sec which doesn't correspond to the lift derivative $-Z_W = 0.7$ rad/sec. This derivative is the zero in W_{C_2} for the conventional configuration. For that reason the transfer function $\frac{H(S)}{X(S)}$ has the slope $20 \lg \frac{d(|H/x|)}{d \lg \omega} \cong -60$ dB/dec in the frequency range (0.7÷1.5 rad/sec). It is a well-known fact that it is impossible to control such a plant.

b) The Dynamic Peculiarities of Nontraditional Aerodynamic Configuration.

Discussed below are two nontraditional aerodynamic configurations.

1. Potentiality of Configuration with Direct Lift Control (DLC) for Considerable Change Of Aircraft Dynamics and Creation of the New Motion Modes

Table 1.2 shows some examples of transfer functions supplied in the new motion modes for aircraft with DLC [17].

All of these transfer functions are correct until the deflection of the direct lift control surface reaches the maximum value. The potentiality of using new motion modes leads to the necessity of revising the handling qualities standards because the current standards are based on the dynamics of conventional aircraft configurations having traditional coupling between attitude and flight path motions.

Table 1.2

N	Motion Mode	$W_C(S)$
1	θ =Variable α =Constant	$\frac{\theta(S)}{C(S)} = \frac{K_C M_\delta}{S(S - M_q)}$
2	α =Variable θ =Constant	$\frac{H(S)}{C(S)} = \frac{K_C n_{\delta_{DLC}}}{S(S + Z_\alpha)}$
3	$n_Z = 0$; $\gamma = 0$ θ =Variable	$\frac{\vartheta(S)}{X(S)} = \frac{K_C M_\delta}{S^2 - M_q S - M_\alpha}$

2. The Specific Coupling Between the Attitude and Flight Path Motion for Some Aerodynamic Configurations.

In the flare, it is supposed that a pilot closes two loops. In the outer one, he tries to control altitude at his location (H_p) and in the inner - pitch angle (θ). It is a known fact [12] that the complexity of control in dual-loop systems depends on the transfer function coupling between the outer and inner coordinates, $H_p(s)$ and $\theta(s)$ in our case. The increased phase delay in the frequency response characteristic ($H_p(j\omega)/\theta(j\omega)$) requires the pilot gain to increase in the inner loop which necessitates more complex adaptation in the outer loop to achieve good accuracy.

Because of the coupling between $H_p(s)$ and $\theta(s)$, the transfer function $H_p(s)/\theta(s)$ can be defined by the division of $H_p(s)/\delta(s)$ and $\theta(s)/\delta(s)$. These transfer functions have to take into account the elevator lift coefficient Z_δ . It can be considerable for the aircraft with an elevator or for a "flying wing" configurations.

Because of the change of the altitude at the pilot location

$$H_p = H_{cg} + l \cdot \theta,$$

where $H_{cg}(s) = \frac{V}{S} (\theta(s) - \alpha(s))$ - altitude in the center of gravity (c.g.),

l - the distance between the pilot and c.g., and taking into account the well-known transfer functions for $\alpha(s)/\delta(s)$ and $\theta(s)/\delta(s)$, it is possible to get the following equation for $H_p(s)/\theta(s)$:

$$\frac{H_p(s)}{\theta(s)} = \frac{[-Z_{\delta_e} + l(M_{\delta_e} + Z_{\delta_e} M_{W\delta})]s^2 + [Z_{\delta_e}(M_q + M_{\dot{\delta}}) + l(Z_W M_{\delta_e} - Z_{\delta_e} M_W)]s -}{[M_{\delta_e} + Z_{\delta_e} M_W]s^2 + (-Z_W M_{\delta_e} + Z_{\delta_e} M_W)s - (Z_\alpha M_{\delta_e} - Z_{\delta_e} M_\alpha)} \quad (1.1)$$

The numerator of this transfer function can be rewritten the following way:

$$K_1 (s^2 + 2\xi\omega_1 + \omega_1^2), \text{ where}$$

$$\omega_1^2 = \frac{-Z_\alpha M_{\delta_e} + Z_{\delta_e} M_\alpha}{-Z_{\delta_e} + l(M_{\delta_e} + Z_{\delta_e} M_{W\delta})}$$

The last can be simplified and

$$\omega_1^2 \cong \frac{-Z_\alpha}{\Delta l}, \quad (1.2)$$

here $\Delta l = 1 - \frac{Z_{\delta_e}}{M_{\delta_e}}$ - defines the distance between a pilot location and an instantaneous

center of rotation (ICR) (the positive value corresponds to the case when the ICR is behind the pilot).

For aircraft with an elevator or for a "flying wing" configurations, Δl is considerably less in comparison with conventional aerodynamic configurations. In some cases (aerospace vehicles like the Space Shuttle or Buran), Δl can be negative. For these cases the frequency response characteristic (1.1) has the additional phase delay in comparison with the case where $\Delta l > 0$.

1.1.2 Manipulators

The manipulator remained the most conservative element in aircraft for many years. Basically the wheel was used for the transport or civil airplanes and the control stick for the maneuverable aircraft. Only in recent times have the new types of manipulators begun to be used: the miniwheel (TU-204), and sidestick (F-16, A-300). As for the rudder control, rudder pedals are used for all airplanes. The characteristics of these manipulators (stiffness, damping, mass and etc.) used for different aircraft are considerably different.

Because of the system "hand + manipulator" works in tight interaction (fig. 1.6), the parameters of the manipulator also influence pilot characteristics. The difference between the parameters of manipulators in each channel has to be taken into account in the investigation of concrete piloting task. The specific peculiarity of the pilot and modern aircraft interaction is the complete loss of the "elevator sensation" because a pilot doesn't feel the force and moment of the control surfaces.

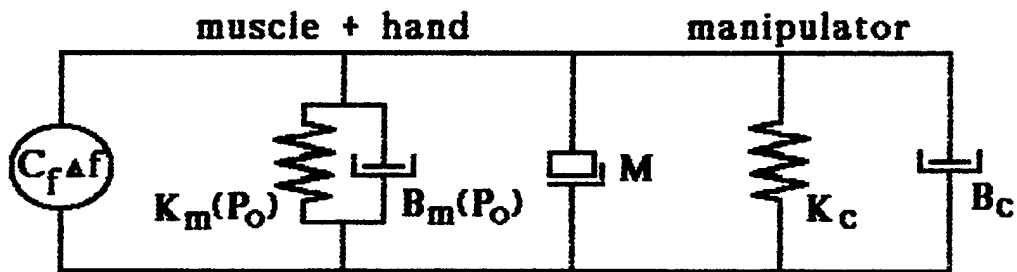
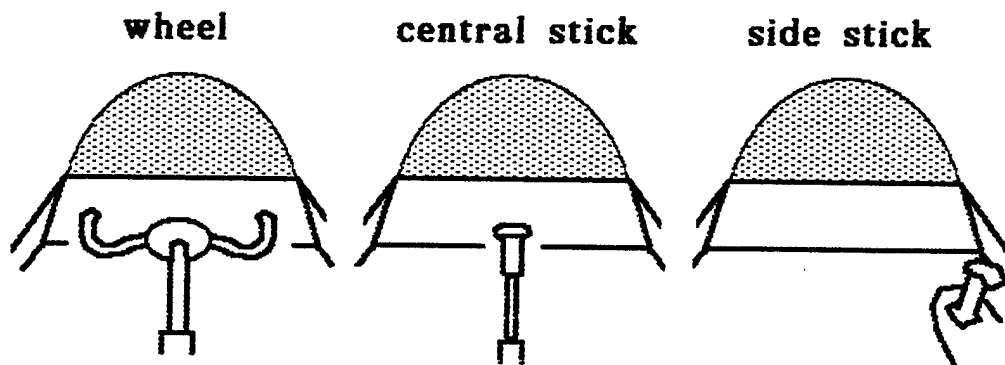
The usage of the small sidestick with low gradient dF/dx stimulates a pilot to actions which do not conform with flight control system potentialities. This circumstance requires the development of special means for regulation of forces. One of them is considered in [1].

1.1.3 Display

As a rule, a display is considered a special technical device. Basically the displays used are: Head Up and Head Down Displays (HUD and HDD), and instruments. Information can be transferred through the other sensory systems (for example tactical, auditory) as well.

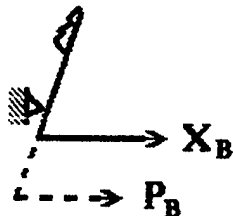
The simulator's moving base system can be considered as a display device having influence on the vestibular system and presenting information about the linear and angular accelerations to the pilot. The necessary outside visual information can be received through the windshield glass, by reference to marks on aircraft nose or windshield glass and the horizon information from objects (the ground, clouds, other aircraft, etc.). The chosen system of the reference points can be considered as a display for visual flight.

MANIPULATOR



$$\frac{C}{\Delta f} = \frac{C_f / M}{s^2 + \frac{B_m(P_O) + B_c}{M} s + \frac{K_m(P_O) + K_c}{M}}$$

manipulator
output



type of
manipulators

$F^X = 0$ - free moving

$F^X \rightarrow \infty$ - pressure

Fig. 1.6. The influence of manipulator dynamics

Depending on the composition of the command stimulus, all displays can be divided into three categories: compensatory, pursuit, and preview (fig. 1.7). The simplest mathematical model for the compensatory display is the gain coefficient $W_D = K_D$. As a rule for the HDD or instruments $K_D \ll 1$. As for the HUD or in the visual flight, the coefficient K_D has to correspond to the indication of angular position. When the distance between the pilot and windshield glass (L) is equal 53.7 cm, $K_D = 1$ and the perceived signal $\bar{e}(t)$ is equal to the error $e(t)$.

The flight director indicator is a rather complex instrument and its transfer function is also rather complex. The perceived signal \bar{e} calculated here is the weighted sum of coordinates

$$\bar{X}_K = X_K + X_K^T,$$

$$\bar{e} = \sum_{k=1}^n W_k X_k \text{ where}$$

X_K - aircraft output signal from elevator deflection and

X_K^T - the change of the aircraft phase coordinate from the turbulence velocity W_0 :

$X_K^T = W_{X_K}^T W_T$. Here $W_{X_K}^T$ is the transfer function corresponding to the airframe dynamics.

W_k - the display transfer functions. In the simplest case it is gain coefficients.

The display transfer function W_d can be combined with the controlled element dynamics $W_C * W_D$. It is necessary to notice that except for the change of controlled element dynamics, the director indicator leads to the change of equivalent input signal. In that case

$$i(t) = \sum_{k=1}^n W_k * X_k^T.$$

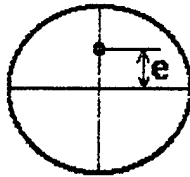
Table 1.3 shows some examples for W_X^T . As for the pursuit display, it depicts the input and/or output signal in addition to error signal. Except for the current value of input and error signals, the preview display gives a prediction about $i(t)$ over some interval τ_0 . The visual display is characterized with other variables. Each considered display corresponds to a specific type of pilot-vehicle system, reflecting the investigated task. For example, the first form of discussed displays corresponds to the compensatory system, and the second, to the pursuit system.

For the case where the computer is used for generation of displayed information, additional parameters are introduced. That is time discretization which can be characterized as a time delay (T_D). It appears to influence the pilot-vehicle system characteristics when $T_D > 0.1 \text{ sec}$. Except for time discretization, the display is characterized by the number of lines which can influence the system characteristics in the case of small scales or number of lines on the unit of screen.

DISPLAY

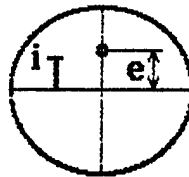
TYPES OF DISPLAY

Compensatory



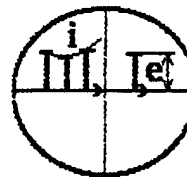
director
control

Pursuit



taking aim; flight
against a ground
(clouds)

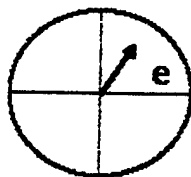
Preview



flight in canyon;
terrain following

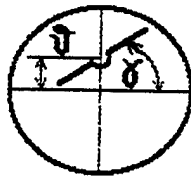
WAY OF REPRESENTATION OF INFORMATION

Vector



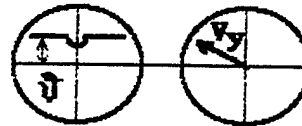
refueling

Coordinative



stabilization in
longitudinal and
lateral motion

Coordinative (with
separation of
stimulus)



landing (without
director indicator)

Fig. 1.7. Types of display and ways of presentation of information

There are other factor influencing the perceived information such as the way information is presented. The vector and two versions of a display for presenting information about two stimulus $e_1(t)$ and $e_2(t)$ are shown in fig. 1.7.

The single loop compensatory system is the simplest one. Here, a pilot perceives only one stimulus error signal $e(t)$. The case where he perceives the information about the other phase coordinates coupled with the output signal corresponds to the multiloop system. It takes place in the altitude control task, when a pilot reacts to the pitch angle and sink rate. The case when a pilot uses some manipulators (for example a control stick with two degrees of freedom) corresponds to the multi-channel system.

In flight, a pilot can transfer from a single to a multichannel system. For this reason the addition of the secondary task can be considered as a task variable in the investigation of a single loop system. For the case where a pilot perceives and reacts in several modalities (for example visual and motion cues) the multimodality of the pilot-vehicle system takes place.

Each piloting task corresponds to its specific display and type of system. The majority of them are the compensatory tasks. Examples are air-to-air tracking, refueling, instrument landing. This type of system will be investigated later.

1.1.4 Input Signal $i(t)$ or $d(t)$

The analysis of different tasks demonstrates that each piloting tracking task is characterized by the specific input signal $i(t)$ (for command tracking task) and $d(t)$ (for stabilization task). Examples of the input power spectral densities for several piloting tasks are shown in table 1.3.

1.2 THE PILOT'S VARIABLES

In addition to the task variables, there are the variables connected with a pilot which are discussed below. All of them have influence on the pilot-vehicle system characteristics.

Environmental Variables (ϵ)

These variables includes accelerations, weightlessness, temperature, noise, etc.

In some cases some of these variables make it impossible to fulfill the task. Considering accelerations for example, the maximum possible duration of flight T_{\max} in atmospheric turbulence depends on the mean square of acceleration σ_{n_z} according to the following equation [10].

$$T_{\max} = 10^{2.8-4.2\sigma_{n_y}}$$

Extended exposure to sinusoidal accelerations leads to significant discomfort [1]. The maximum amplitude of such accelerations depends on the frequency. However, some values of environmental variables don't lead to the inability of carrying out the task.

The Procedure Variables (P)

These variables include such aspects of experimental research, as a training program, order of presentation of variables, pilot's instructions, or criteria which he has to meet. As an example it is possible to give instructions to keep the error signal near zero or in the permissible interval $\pm d$.

Pilot-Centered Variables (σ)

These are variables such as motivation, level of training, and tiredness.

The division of pilot's variables into separate types is rather arbitrary, because of the coupling between some of the variables. For example, there is coupling between motivation and instruction (or criteria).

In the current PIO tendency research, the influence of one of the pilot's variables on a wide range of tasks was investigated. The last one was a criterion which can be given to the pilot or motivated by himself - to keep the error in the given permissible interval, d . The influence of this variable on PIO tendency is considerable as shown later.

Table 1.3 INPUT SIGNAL

Task	S_{ii}	S_{dd}
Pitch Angle Control		$\left \frac{M_\alpha}{(j\omega^2 + 2\xi_{SP}\omega_{SP}j\omega + \omega_{sp}^2)} \right ^2 S_{W_g}$
Air-to-Ground Weapon Delivery		$\left \frac{j\omega - M_q}{(j\omega^2 + 2\xi_{SP}\omega_{SP}j\omega + \omega_{sp}^2)} \right ^2 S_{W_g}$
Terrain Following	$\frac{k}{[\omega^2 + (0.12 \div 0.16)^2]}$ $\sigma_h = 50 \div 150m (H < 700m)$	$\left \frac{H}{W_g} \right ^2 S_{W_g}$
Air-to-Air Combat	$\frac{k}{(\omega^2 + (0.33)^2)} \left \frac{H_a}{W_g} \right ^2$	$\left \frac{\varepsilon_Z}{W_g} \right ^2 S_{W_g}$
Glide Tracking (longitudinal)	$\frac{(0.4)^2}{\omega^2 + (0.25)^2} \left[m^2 \right]$ (H=30m)	$\left \frac{d}{W_g} \right ^2 S_{W_g}$
Glide Tracking (lateral)	$\frac{0.48(\omega^2 + 1.5^2)}{[\omega^2 + (0.35)^2][\omega^2 + 10^2]}$ (H=30m)	$\left \frac{Y}{W_g} \right ^2 S_{W_g}$

2.0 ANALYSIS OF THE REASONS FOR PIO TENDENCY IN MODERN AIRCRAFT

The increase of PIO tendency is accompanied by the decrease of the amplitude and phase margin up to the loss of stability. That is why we need to investigate the PIO tendency from the frequency analysis point of view. For the stationary conditions of flight, the closed- and open-loop pilot-vehicle system parameters can be evaluated in experimental research of variances, frequency and spectral characteristics of the system by using the Fourier coefficient method. These parameters can be investigated by mathematical modeling based on a structural approach or modern control theory.

A brief description of the method and algorithm used for the measurement of pilot-vehicle system characteristics based on the unified Fourier coefficient method are given in Appendix A. A description of the algorithms used for mathematical modeling for both above mentioned approaches is given in Chapter 4. In the case of sudden origin change of the unstationary process arising from a change of task variables, the pilot-vehicle system can lose stability. It takes place when a pilot doesn't have time to adapt to the new conditions, and the system has small stability margins in its initial state. This can result in a sharp change of the pilot's parameters. The appearance of unstable processes can be evaluated by using the criteria of stability. Chapter 4 discusses the criteria of stability for the pilot-vehicle system used in this work. In the case where the unstable processes develop rapidly, it is not correct to use the Fourier coefficient method because of the existence of the stationary processes.

However, if the considered unstable processes arise periodically, disappearing in some conditions and existing for a limited time in the general duration of the run, the measurement of frequency and spectral characteristics in principle allows us to evaluate the influence of investigated conditions on the development of PIO tendency. The unstable processes developing periodically lead to the change of pilot parameters because of his attempts to transform the system into stable conditions. It increases the level of remnant power spectral density, and as a consequence, decreases the accuracy of estimation and reliability of the calculated frequency response characteristics. Therefore, the procedure has to be developed to evaluate the possibility of frequency analysis of the pilot-vehicle system before investigating its characteristics by means of this analysis. It is a known fact [1] that the accuracy in estimation of frequency response characteristics depends on the ratio (p^*) of spectral density correlated with the input signal to the spectral density defined by the remnant. For the error signal $p^* = S_{e_i e_i} / S_{e_n e_n}$ It is obvious that, if $S_{e_n e_n} > S_{e_i e_i}$ in some frequency range, the features of the system are defined here by the unstationary, nonlinear processes. The existence of the resonance peak in spectral density $S_{e_n e_n}$ shows the oscillations in the system defined by the nonlinear processes. The opposite ratio of these spectral densities ($S_{e_i e_i} > S_{e_n e_n}$) demonstrates that the systems are defined basically by the linear processes and can be investigated by the frequency analysis method. This rule was used in checking the results of the experimental research. It was revealed in the majority of experiments, that analysis of the pilot-vehicle system characteristics can be fulfilled only on the basis of its frequency response characteristic considerations. In some cases the analysis of the spectral densities demonstrates the strong nonlinear effects.

For the majority of the possible reasons for PIO tendency, most of the known research was dedicated to the influence of control element dynamics or manipulator characteristics on this phenomena.

Because pilot-vehicle system characteristics depend on other factors too, there is a range of variables in this work. It allowed us to carry out research on the following questions:

1. The influence of some dynamics peculiarities on attitude longitudinal motion of superaugmented vehicles.
2. The influence of different task variables.
3. The influence of the criteria used by the pilot in fulfillment of the tracking task.

Such division of the factors is conditional and reflects the volume of fulfilled work. Although in some of the cases investigated, the combination of variables and the detailed study of their mutual influence, for the typical missions considered, requires additional research. In the investigations mentioned above, configuration 2.10 was used as a basis. Because each investigation was carried out separately, the slight difference in results for configuration 2.10 can be seen from tables and figures, in spite of the same conditions for experiments.

MAI's Pilot Vehicle Laboratory experiments were carried out on a workstation for manual control tasks (see appendix C) and on a 3 degrees of freedom moving-base simulator (fig. 2.1). Some experiments at TSAGI and LII were conducted with participation of MAI's specialists. The MAI software for data reduction was transformed for use in these institutes. The methodology of experiments was also developed at MAI.

The preliminary stage of detailed experimental investigation was fulfilled in MAI with all LAHOS configurations. The analysis of results allowed us to choose two configurations, 2.10 and 1.4 for further research at MAI, TSAGI, and LII. Because these configurations had to be realized on the Tu-154 in-flight simulator, it was decided to investigate the pilot-vehicle system characteristics for Tu-154. This aircraft doesn't have any additional filters in the basic configuration except for the actuator dynamics. The frequency response characteristic of this aircraft is shown in fig. 2.10. The mathematical model of in-flight simulator and filters used for transforming its dynamics into LAHOS configurations was received from LII. Fig. 2.2 and all other similar figures, show part of the calculated characteristics. The description of characteristics demonstrated in these figures is given in appendix C (see fig. C.1).

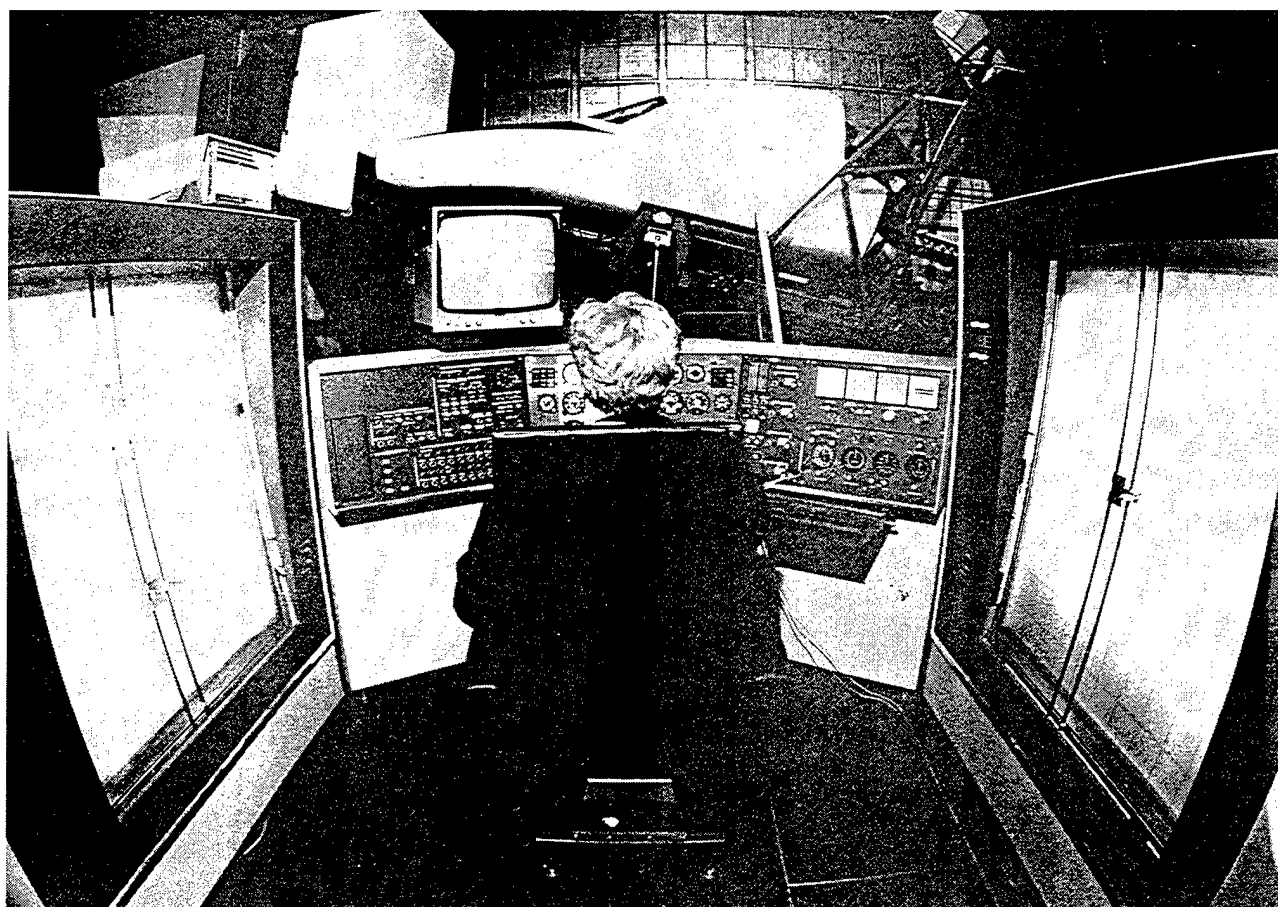
2.1 THE INFLUENCE OF SOME DYNAMICS PECULIARITIES IN ATTITUDE LONGITUDINAL MOTION OF SUPERAUGMENTED VEHICLES.

a) The Influence of the Flight Control System.

This question is considered in detail in Chapter 3. Here we'll discuss briefly the influence of additional filter dynamics in the FCS. Their installation leads to additional phase delay which can be taken into account by the element $e^{-s\tau}$. In this case the transfer function of highly-augmented aircraft in attitude control can be represented by the equation $W_c = W_c^* e^{-s\tau}$ where W_c^* is the transfer function of the aircraft described with the help of a second order equation. The influence of time delay was investigated in different works (see, for example [1]), where it was shown that an increase of τ leads to an increase of pilot lead, resonance peak of the closed-loop system, and remnant spectral density. The investigations carried out in this work allowed us to add these results and demonstrate that the effect of additional filters depends on the value of W_c^* .



Fig. 2.1. MAI's facilities used for experiments :
the workstation and moving-based simulator



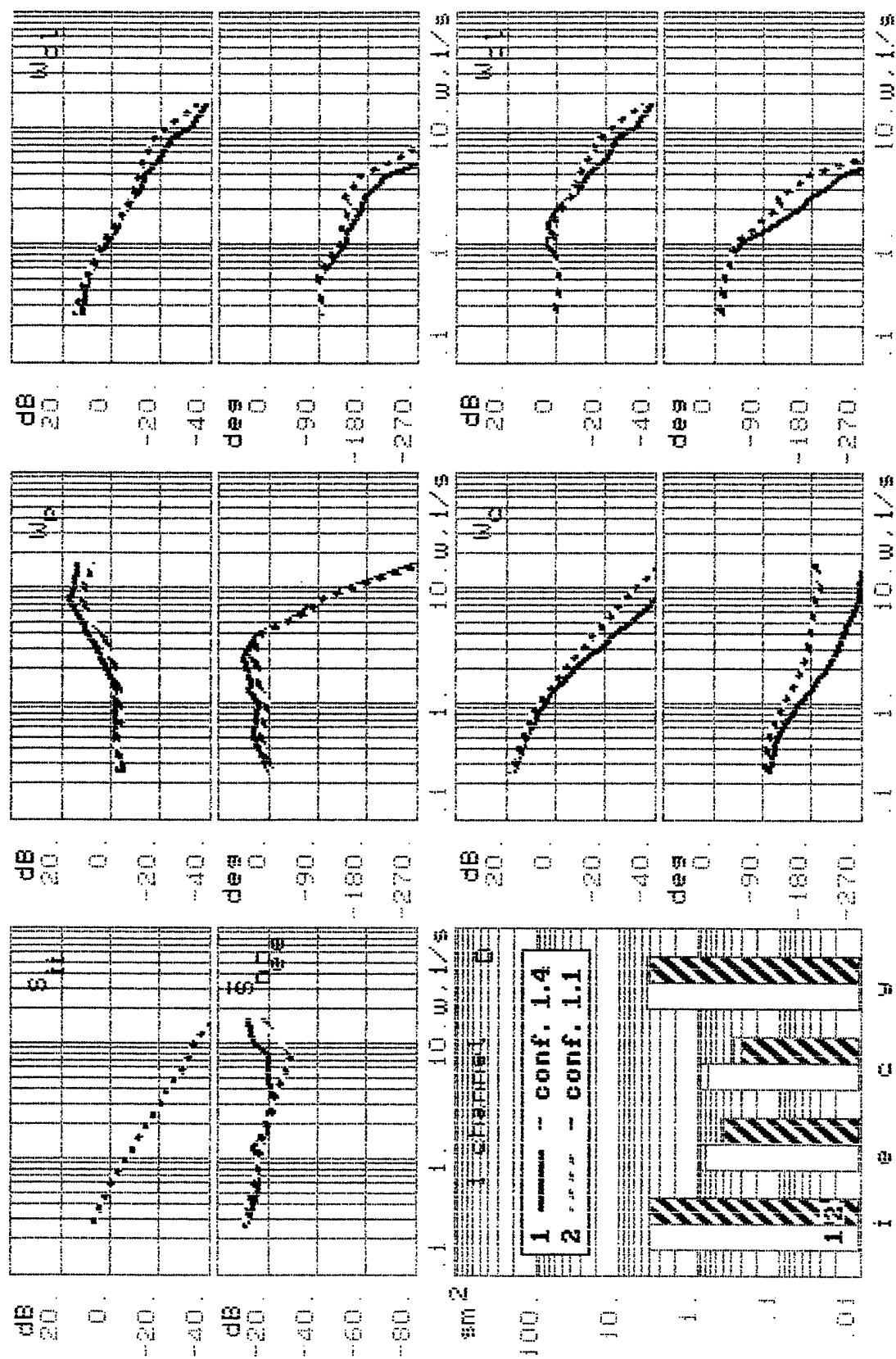


Fig. 2.2. The comparison of experimental results

It can be demonstrated in the research configurations 1.4 and 2.10, and LAHOS configurations 1.1 and 2.1. The last pair of configurations are the basic configurations for 1.4 and 2.10 accordingly, which don't have the additional filters. The pilot's task was to keep the signal error in the permissible interval $d=\pm 1$ cm. In the case of low short period frequency, W_c^* was close to the transfer function $W_c^* \cong k/s(Ts + 1)$ (the case close to configuration 1.4). The resonance peak (r) corresponding to this case takes place at the frequency close to the crossover frequency, ω_c , defined by the phase margin $\Delta\varphi$ (fig. 2.2). A pilot develops a considerable lead time in this case. Taking into account the connection between open- (W_{OL}) and close-loop (W_{CL}) system frequency response characteristics, it is easy to get the following equation for "r":

$$r = 20 \lg |W_{CL}| = 20 \lg \frac{1}{2 \sin \Delta\varphi / 2}.$$

Although the value of the peak for configuration 1.4 is relatively low, $r = 4$ dB (for configuration 1.1, r was equal to 2.2 dB only), it was reached by inducing high lead adaptation. The necessity of this lead is obvious because the aircraft phase characteristic for configuration 1.4 is close to zero at the crossover frequency. Thus, if a pilot decreases his lead or does not induce it at all in some intervals, then the resonance peak will increase significantly, or the system will lose stability. Because the spectral density of the input signal is considerable at the crossover frequency $\omega_c \cong 1$ rad/sec, the small resonance peaks here lead to considerable oscillation.

The increase of remnant power spectral density $S_{n_e n_e} = \bar{S}_{n_e n_e} \sigma_e^2$ for this configuration demonstrates the increase of variability of the pilot's parameters and consequently the probability of PIO tendency. The phase characteristics of configuration 1.1 is less than -180° . For this reason, the system doesn't lose the stability in the case where the pilot doesn't induce lead. Thus, the installation of additional filtering forces a pilot to keep the lead constant to maintain stability.

For high values of short period frequency ω_{sp} (configuration 2.10), the zero slope of $|W_c(j\omega)|$ in the middle frequency range is evident in fig. 2.3. This requires a pilot to realize rather complex lag-lead adaptation. The phase margin for this case is defined by the aircraft phase frequency response characteristic.

For the basic configuration (configuration 2.1) there are the same conclusions. The possible change in pilot lead adaptation does not lead to the loss of stability. As for pilot adaptation induced in the frequency range $\omega > \omega_c$, it decreases the amplitude margin under high phase margin. The resonance peak of the closed-loop system for such a configuration takes place at frequency $\omega|_{\varphi=-180^\circ}$ and corresponds to the amplitude margin ΔL . It can be defined from the

equation for closed-loop system $W_{CL}(j\omega) = \frac{W_{OL}}{1 + W_{OL}(j\omega)}$.

where

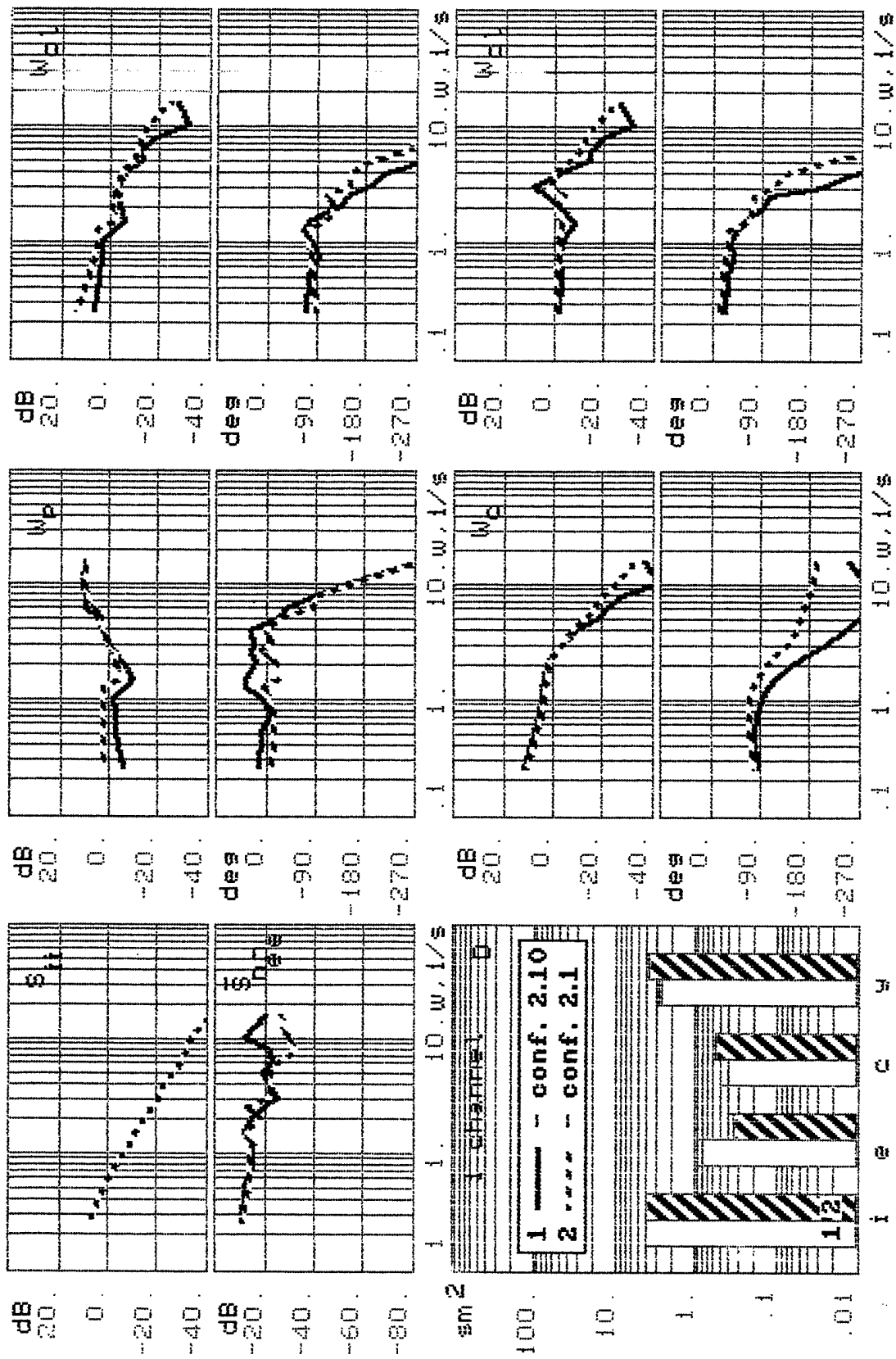


Fig. 2.3. The comparison of experimental results

$$W_{OL}(\omega)_{-180^\circ} = K = 1 - \Delta L \text{ and } \Delta L = 20 \lg |W_{OL}(\omega)_{-180^\circ}|$$

Then

$$R = \frac{K}{1-K} \text{ or } r = 20 \lg R \text{ [dB]}.$$

The last function is shown in fig. 2.4.

Under high values of R , (or r) the unessential change in the open-loop gain frequency response characteristic leads to considerable increase in the resonance peak. The operation of such a plant is accompanied by the increased oscillatory features.

Based on this analysis, it is possible to conclude that additional filters complicate the pilot behavior and increase the resonance peak. The resulting pilot ratings using the Cooper-Harper and PIOR scales are shown in table 2.1. For comparison in table 2.1, the ratings from [5] is shown.

Table 2.1

Configuration	2.10	2.1	1.4	1.1
PR(PR[5])	8(10)	4(2)	8.5(10)	5(4)
PIOR(PIOR[5])	4(4)	2.5(1)	4(4)	2(2)
r	8.3	3	4	2.2
φ_P^+, φ_P^-	$+38^\circ$	$-24^\circ ; +16^\circ$	$+46^\circ$	$+32^\circ$

This is why the parameters of pilot phase adaptation and resonance peak can be considered as characteristics defining the PIO tendency.

b. The influence of nonlinearities in FCS on PIO tendency

Two kinds of nonlinearities are considered below:

- The limitation on maximum velocity of control surfaces deflection $\dot{\delta}_{MAX}$.
- Nonlinear filter in FCS.

The influence of the limitation on maximum velocity of control surfaces deflection was investigated by considering the block-scheme in fig. 2.5. This scheme corresponds to the way of realization of configuration 2.10 on the Tu-154 in-flight simulator. The influence was investigated using MAI's PVL workstation with different values of limitation on $\dot{\delta}_{MAX}$: $\dot{\delta}_{MAX} = 126, 26$ and, $15^\circ/\text{sec}$. The value of $126^\circ/\text{sec}$ corresponds to a case of essentially no limitation. The value of $26^\circ/\text{sec}$ corresponds to the Tu-154 limitation on $\dot{\delta}_{MAX}$ and the value of $15^\circ/\text{sec}$ was used specially to increase the investigated effect. The results of the averaged experiments repeated many times are shown on fig. 2.6. The analysis demonstrates that decreasing $\dot{\delta}_{MAX}$ under high values of feedback coefficients leads to considerable change of the aircraft describing

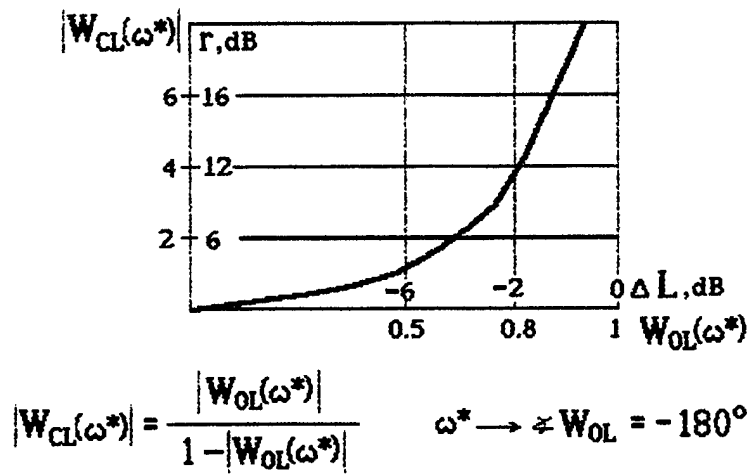


Fig. 2.4. The connection of amplitude margin and resonance peak

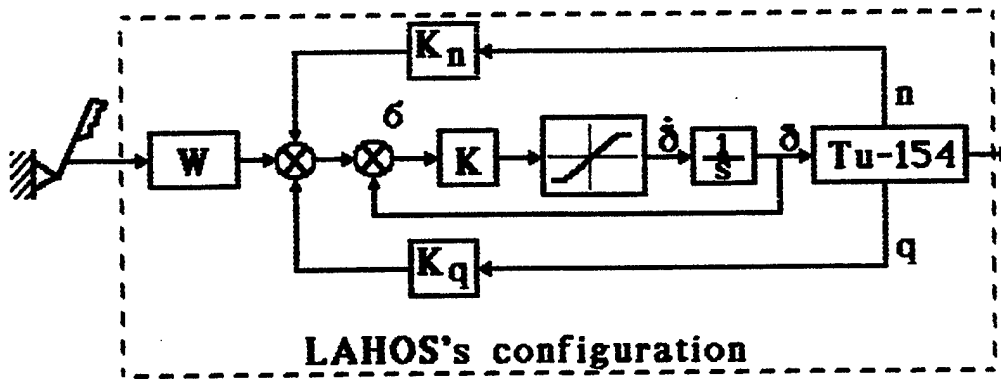


Fig. 2.5. The realization of LAHOS's configuration on in-flight simulator Tu-154

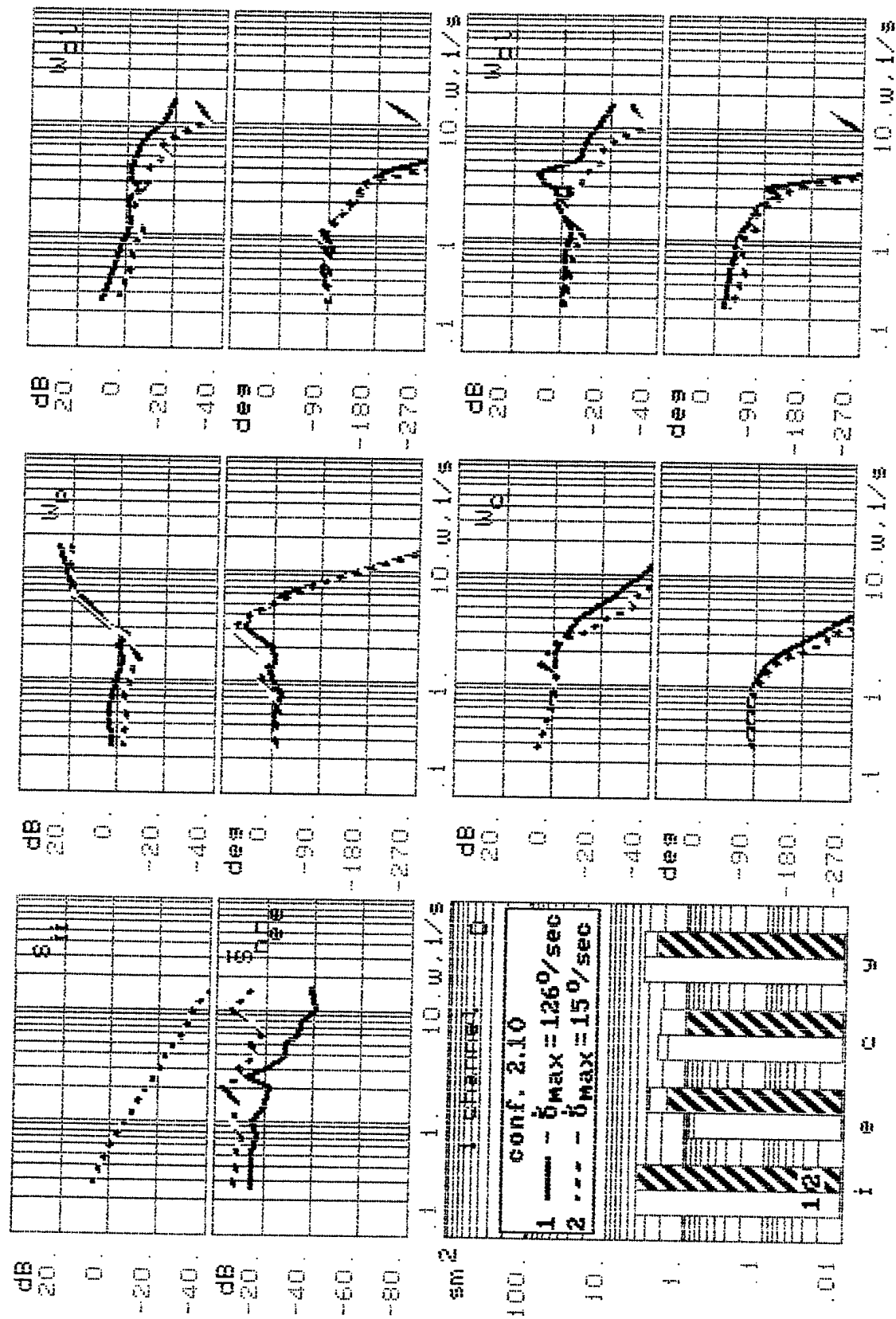


Fig. 2.6. The comparison of experimental results

function. Its damping ratio, delay of phase, and the slope in high frequency range decrease. All these effects decrease the pilot gain coefficient to realize more complex adaptation in the middle frequency range with the goal of decreasing the effect of low damping ratio $|W_C|$, to increase the phase lead in open-loop frequency response characteristics. For example, the maximum positive magnitude of pilot phase characteristic increases up to 30° when $\dot{\delta}_{MAX}$ decreases from $126^\circ/\text{sec}$ to $15^\circ/\text{sec}$. The characteristic features are a decrease of crossover frequency and a drop in closed-loop gain frequency response. The resonance peak, which is a characteristic feature of PIO tendency for linear system, practically disappears. The distinctive feature of investigated influence is an increase of the normalized spectral density level, which shows on development of nonstationary and nonlinear processes under a decrease of $\dot{\delta}_{MAX}$. For low values of $\dot{\delta}_{MAX}$, the spectral density of error signal correlated with remnant ($S_{e_n e_n}$) is much higher than the spectrum of its other component ($S_{e_{ii}}$) shown in fig. 2.7. Besides, $S_{e_n e_n}$ has a considerable peak in the frequency range $\omega \cong 2 \text{ rad/sec}$. This fact is the obvious indication of the oscillation process. All these results indicate the existence of nonlinear features in the system and connected with pilot induced oscillations with frequency $\omega_{PIO} \cong 2 \text{ rad/sec}$.

Thus the decrease of maximum velocity $\dot{\delta}_{MAX}$ under high values of feedback coefficients leads to appearance of PIO in the case of the absence of special means for suppression of oscillations.

Nonlinear filter in the FCS. In chapter 1 the use of nonlinear filters installed in the "Buran" FCS was mentioned. Fig. 2.8 shows the results of the experiments that demonstrated the dependence of the describing function on the value of stick deflection and its velocity, in increasing the PIO tendency. In this case, the change from considerable to small stick deflection leads to an increase in aircraft gain frequency response $|W_C(j\omega)|$; and because of the obvious pilot delay in change of his coefficient, such sudden increase of aircraft gain will lead to decrease of amplitude margin. As a consequence the resonance peak increases which indicates the PIO tendency increase.

2.2 THE INFLUENCE OF DIFFERENT TASK VARIABLES

The piloting process can be represented as a set of tasks (or missions) characterized by a different set of variables considered in part 1. A battery of experiments with the goal of determining their influence on pilot-vehicle system characteristics was carried out. Except for pitch control, the pilot fulfills the other tasks in the piloting process. Two of them are considered below: air-to-air tracking and altitude control in longitudinal motion.

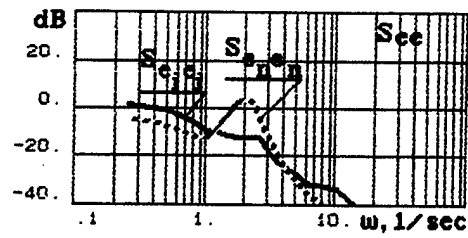


Fig. 2.7. Correlated and uncorrelated with input parts of power spectral density of error

$$W = \frac{1}{Tj\omega + 1}, \quad T = \frac{1}{K \operatorname{erf}\left(\frac{a}{\sqrt{2}\sigma}\right)}$$

$$\sigma_1 > \sigma_2$$

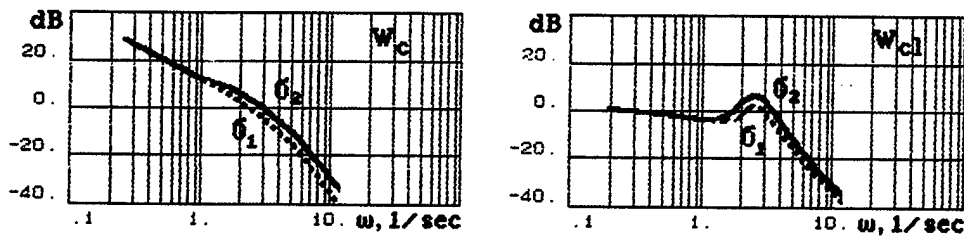


Fig. 2.8. The influence of FCS nonlinear filter on closed-loop system characteristic

1. The Influence of Specific Dynamics in Each Piloting Task.

a) Angle of Sight Control. In this task the pilot controls an angle $\varepsilon = \theta + \frac{H}{L}$, where L is the distance between airplane and another point (other airplane, a point on the ground, etc.). It takes place in an air-to-air tracking task and in an inner loop hovering task [1]. It can arise in some part of the final stage of landing, when a pilot has the goal of touching down in a definite place on a runway accurately. Experiments of this task were carried out on MAI's PVL simulator for conditions: of $L=150\text{m}$ and $V=150\text{m/sec}$ for two configurations: 2.10 (LAHOS configuration) and the Tu-154 in-flight simulator. The input signal was the same as for the pitch tracking task and a pilot had to keep the error signal within the permissible interval, $d = \pm 1^\circ$. The results are given in figs. 2.9 and 2.10. In comparison with the pitch tracking task, the investigated case is accompanied by increased pilot lead, resonance peak (from 5 dB up to 7.4 dB for the Tu-154 in-flight simulator dynamics, and from 9.5 dB up to 15 dB for configuration 2.10 (see table 2.2). The peculiarity of the investigated case is the appearance of an additional resonance peak in the low frequency range. The last is very notable in tracking process and reflects the oscillatory process in path motion. The pilot rating for the angle of sight $\varepsilon = \theta + \frac{H}{L}$ control task increases in comparison with pitch tracking task (see table 2.2).

Table 2.2

Task Parameters	Configuration			
	2.10		Tu-154	
	θ	ε	θ	ε
PR	8	9	4	6.5
r_{\max}	9.5	15	5	7.4
$r_{\text{low frequency}}^*$	-	7	-	4.4
φ_P^+, φ_P^-	$+13.7^\circ$	$+8^\circ$	$+18^\circ ; -27^\circ$	$+19^\circ ; -5^\circ$

These results raised the question of the possibility of using Neal-Smith ranges: resonance peak (r) and pilot phase compensation $\Delta\varphi_P = \varphi_P(\omega_{BW}) - \tau\omega_{BW}$, received from the investigation of the pitch tracking task for development of requirements for aircraft handling qualities in an angle of sight tracking task. Let's suppose that the resonance peak defined in ranges (r , $\Delta\varphi_P$) is the maximum peak in all frequency intervals. Comparison of the received results with ranges shown on fig. 3.5 shows that the parameters r , Dv move to the third level of pilot rating. This corresponds to the PR received in the experiments. This analysis demonstrates that ranges of r and $\Delta\varphi_P$ can be used for preliminary evaluation of handling qualities in an angle of sight task. This conclusion has to be checked additionally, to determine the influence of the low frequency peak on pilot rating. It is also possible to formulate other preliminary conclusion. The

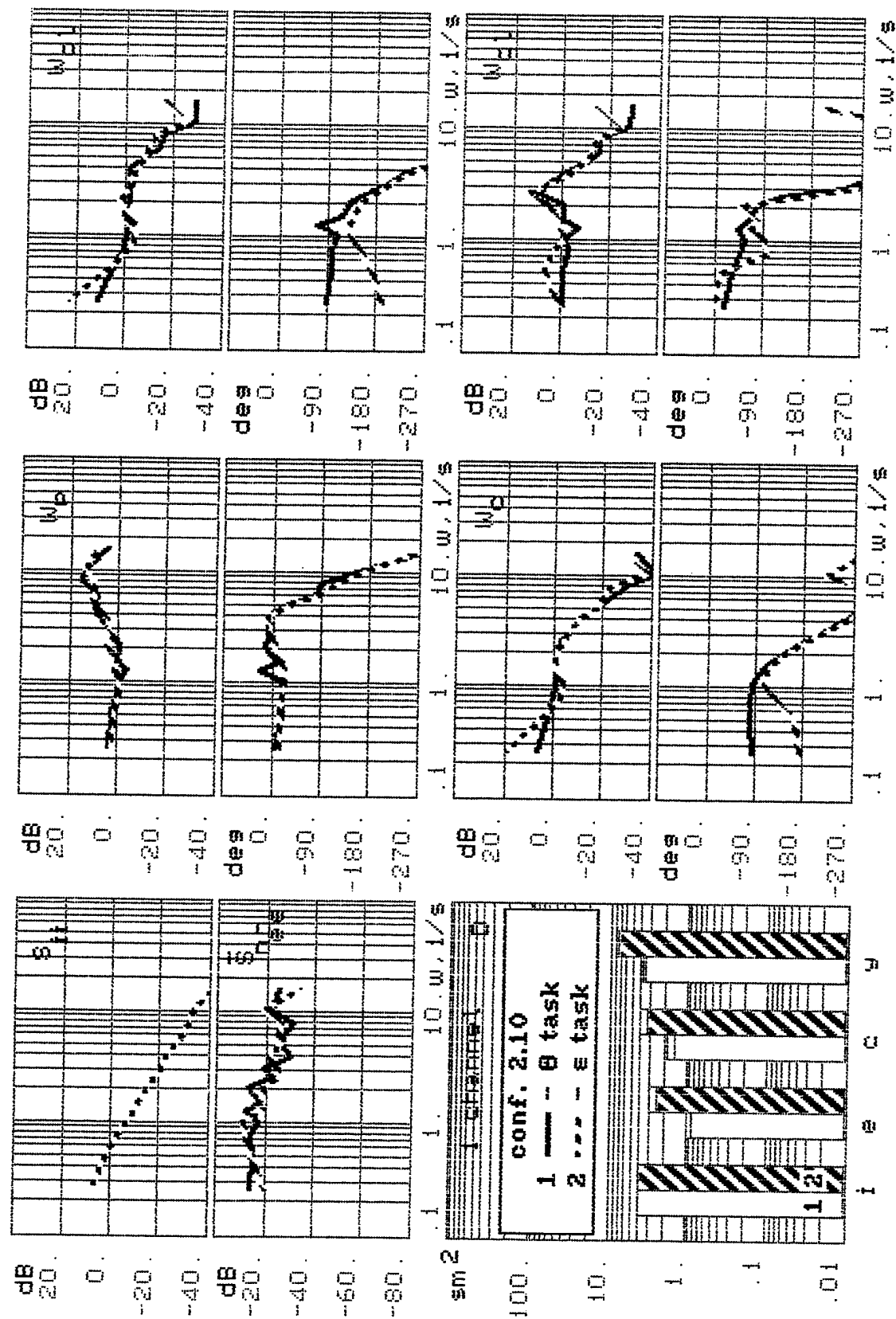


Fig. 2.9. The comparison of experimental results

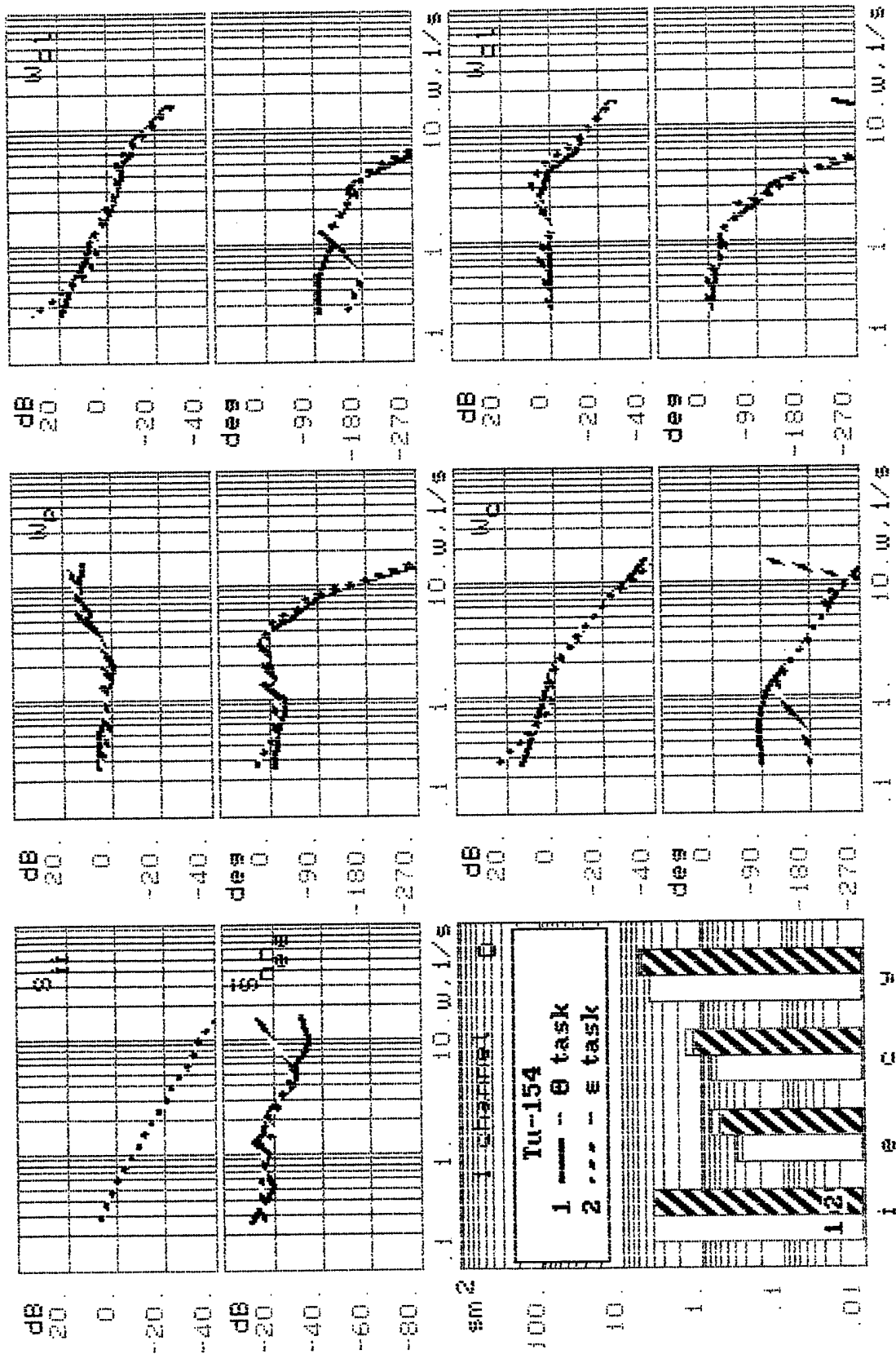


Fig. 2.10. The comparison of experimental results

requirements for handling qualities in a pitch tracking task has to correspond to pilot rating PR=1 to 2 (in any case less than 3.5). In this case, the transfer to the angle of sight task will not be accompanied by the considerable degradation in PR. The necessary pilot rating can be kept and by changing the aircraft handling qualities for each mission. In principle such an approach is considered in [1]. The improvement of PR can be achieved by changing the permissible (desired) level of accuracy in error tracking, d . This is considered in part 2.3 of this report.

b) Altitude Control Task. This path control task takes place in many aircraft missions. One of them is flare which occurs the final stage of landing. As a rule a pilot-vehicle system for that case can be interpreted with the help of a dual-loop system where pitch angle control is carried out in an inner loop. In fig. 2.11, the dual-loop system with a parallel type of loop closure corresponds to the series of loop closure. Here W_p is represented by the following: $W_p = \bar{W}_p W_p$ where W_p and W_p , the pilot describing functions, reflects his adaptation in outer and inner loops. The characteristics of such a system are defined so the aircraft dynamics in the inner loop W_{c_2} and the transfer function W_{c_1} couple the output signal $H_p(S)$ with the pitch angle $\theta(S)$. In chapter 1, it was shown that the aircraft with an elevator or the "flying wing" configurations have increased phase delay in the frequency response characteristics $H_p(j\omega)/\theta(j\omega)$. The influence of this factor on stability of the closed-loop system was investigated below. Two aircraft, the Space Shuttle and the Tu-154, are considered which have close characteristics in pitch control (table 2.3) and considerable differences, because of the difference in aerodynamic configurations, in path and angular coupling motion W_{c_2} .

The pitch angle frequency response characteristics for both aircraft are approximated by the equation $W_c = \frac{K}{S(TS + 1)} e^{\tau_c S}$

Table 2.3

Aircraft	W_{c_1}	W_{c_2}
Space Shuttle	$\frac{21.8 + 0.46S - S^2}{S(0.72 + S)}$	$\frac{4.}{S(1+0.7S)} e^{-0.15S}$
TU-154	$\frac{6.04 + 0.769S + S^2}{S(0.72 + S)}$	$\frac{4.}{S(1+0.7S)} e^{-0.08S}$

with approximately the same time constant $T \cong 0.7$ sec. The Space Shuttle time delay $\tau_c = 0.152$ sec [7]. As for Tu-154 its τ_c is equal to 0.08 sec. The assumption was that the pilot tries to realize the crossover model in the inner loop. To accomplish that he has to compensate the control element dynamics time constant T . This means that he tries to keep $T_L \cong T$ where T_L is the pilot lead time. Shown in [13], pilot actions in the outer loop are a proportional type ($W_p \cong \bar{K}_p$) in the case of a series scheme of the loop closure. Considering this, the equivalence

of the parallel scheme of closure and the series scheme can be reached when $W_{P_1} = K_{P_1}(T_{L_2} + 1)$, where $K_{P_1} = \bar{K}_{P_1} K_{P_2}$.

The pilot time delay and parameters of neuromuscular dynamics designated in chapter 4 as $W_{AA} = \frac{1}{(T_N S + 1)(T_I S + 1)}$ were chosen the same and equal accordingly $\tau = 0.2$ sec, $T_N = 0.1$ sec, and $T_I = 0.01$ sec. For simplicity it was assumed that the fraction of attention the pilot shared between loops are the same $f_1 = f_2 = 0.5$.

The calculation of ranges of possible values of pilot gain coefficients K_{P_1} and K_{P_2} was carried out according to $\sigma_{1,2}$ - criteria (see chapter 4). They are given in fig. 2.12 for $W_{D_1} = W_{D_2} = 1$. Except for the basic configuration of the Tu-154 in-flight simulator, the calculations were fulfilled for the Tu-154 with $\tau_c = 0.152$ sec. It allows us to reach an equivalence of Tu-154 and Space Shuttle dynamics in the inner loop and to investigate the influence of an instantaneous center of rotation (ICR) on stability. Analysis of results allows us to conclude that the location of ICR in front of the pilot leads to considerable decrease in the range of pilot gain coefficients in comparison with the basic Tu-154 configuration. It leads to tighter requirements on variability of pilot gains, which can be interpreted as an increase of tendency to PIO, see fig. 2.12. The change in time delay for the Tu-154 configuration leads to the change of K_{P_2} , but practically doesn't change the form of the lower part of curve defined by the boundary $\sigma_2 > 0$. However, it leads to a decrease in the maximum value of K_{P_1} . Thus the decrease of time delay in the inner loop, leads to an increase of the stability problems in the both loops. In fig. 2.13, the range of parameters received from Hurwitz criteria are plotted. Their comparison with the range calculated from σ_2 criteria, demonstrates that the last is considerably more narrow.

2. The Influence of Additional Tasks.

The additional task, such as control in the other channel, can be considered as a task variable in analysis of the single-loop pilot-vehicle system. The control of unstable first-order plant ($W_{C_2} = \frac{\lambda}{S - \lambda}$) was included as an additional task. Such a secondary task was considered in several research efforts for evaluation of pilot workload [1,18]. In the experiments configuration 2.10 and the Tu154 were investigated as the main task under the value of a divergent pole $\lambda = 0.5$; 1 sec. All runs were carried out under instructions to keep the error signal in the main loop in the interval ± 0.5 sm for $K_D = 0.5$ sm/deg and $\sigma_i = 1$ sm. As for the secondary task, the pilot tried to keep the horizontal motion error in the interval ± 3.5 sm. The results shown in figs. 2.14a,b and table 2.4 demonstrate that the addition of the secondary task leads to an increase of pilot ratings and resonance peaks.

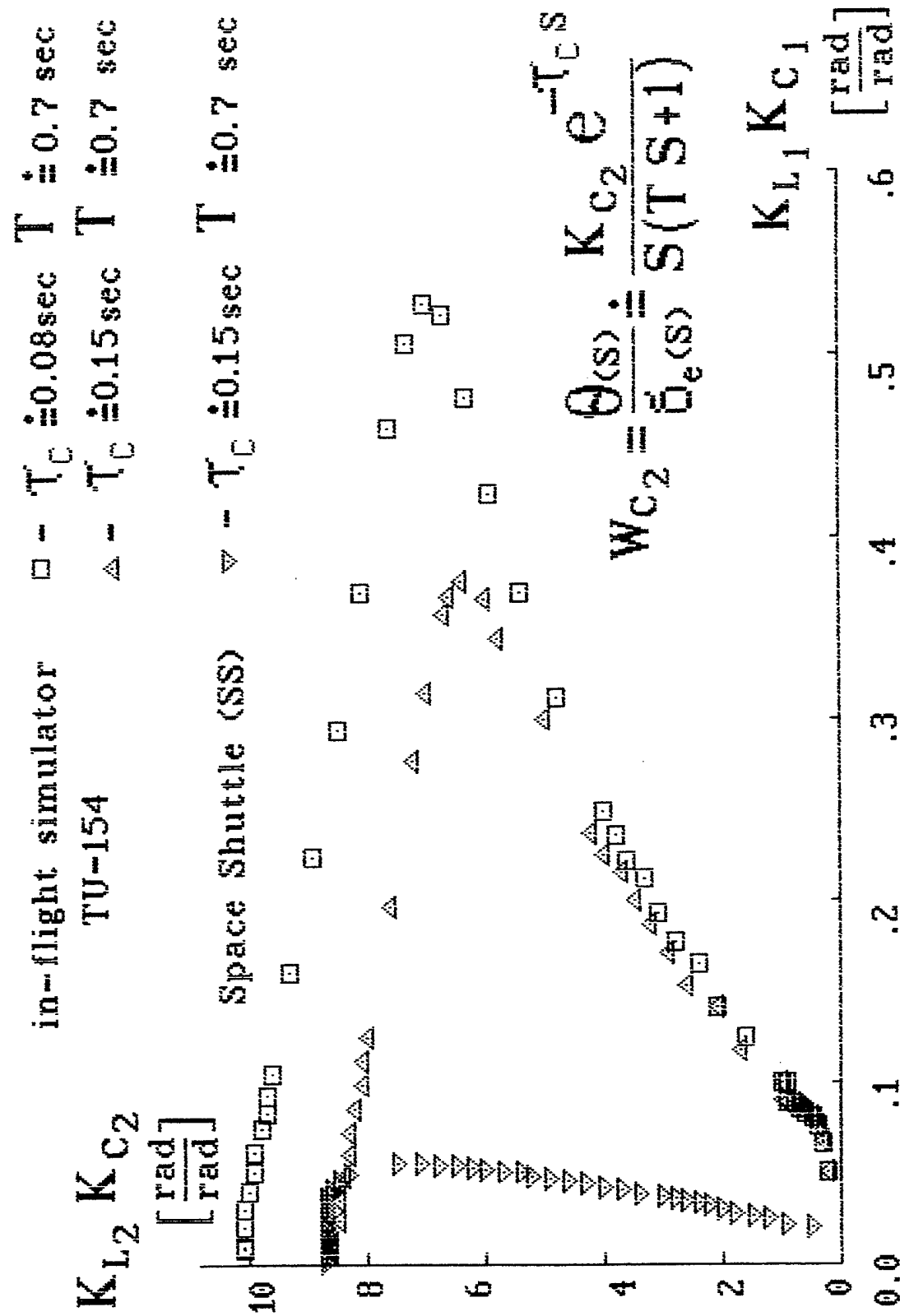


Fig. 2.12. Ranges of stability

Space Shuttle (SS)

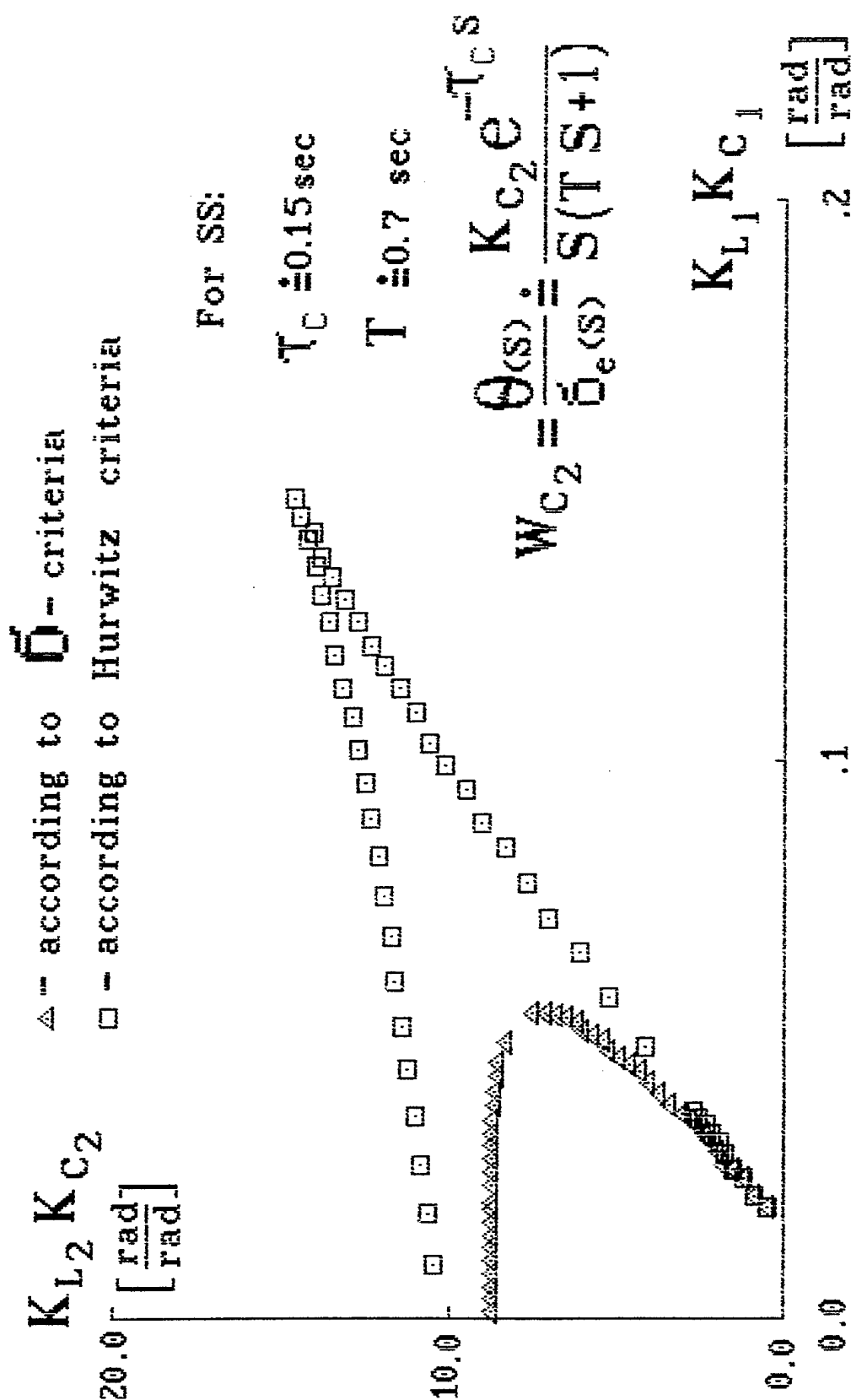


Fig. 2.13. The comparison of results received by different criteria

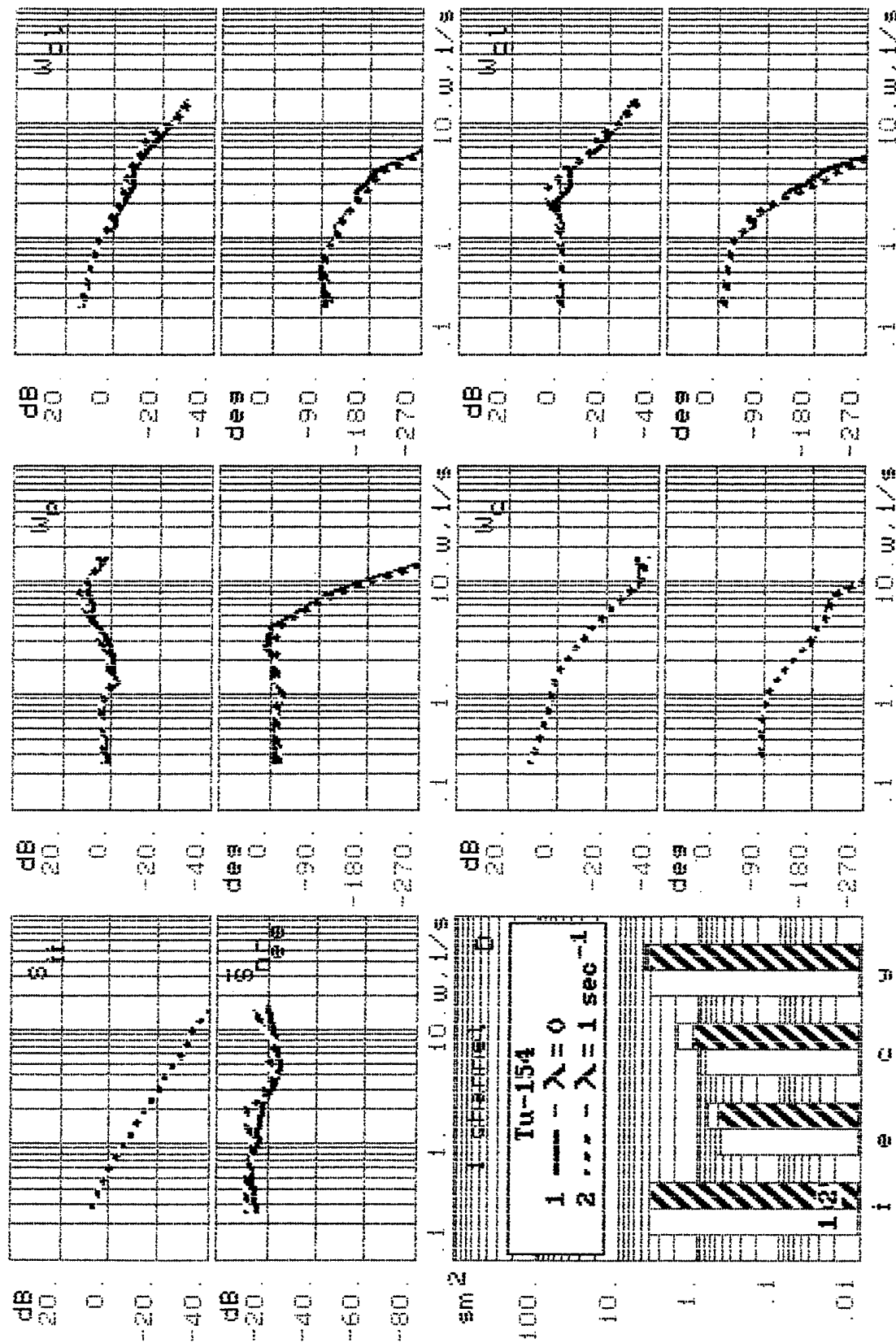


Fig. 2.14b. The comparison of experimental results

Table 2.4

Configuration		PR	r	φ_p^+, φ_p^-
2.10	$\lambda=0$	8	7.14	$\begin{smallmatrix} 0 \\ +19 \end{smallmatrix}$
	$\lambda=1$	9	14.5	$\begin{smallmatrix} 0 \\ +6 \end{smallmatrix}$
Tu-154	$\lambda=0$	4	2.5	$\begin{smallmatrix} 0 \\ +9 \end{smallmatrix}$
	$\lambda=1$	6	6.25	$\begin{smallmatrix} 0 \\ -11 \end{smallmatrix}$

Because the pilot acts in several channels simultaneously, in reality from the received results we can conclude that the probability of PIO tendency in real flight is higher than in single loop system experiments.

3. The influence of the Type of Piloting Task and Motion Cues.

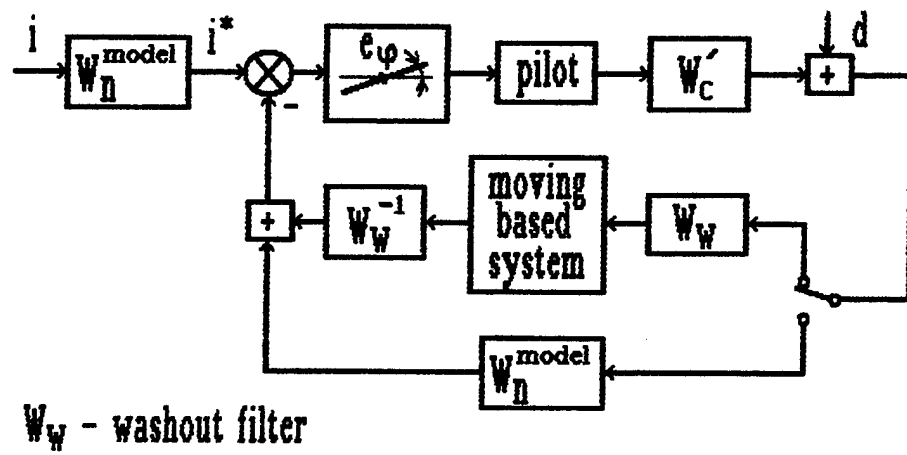
All piloting tasks can be divided on two types: a tracking of command input signal $i(t)$ and stabilization when the disturbance $d(t)$ is an input. When the spectral density of $i(t)$ and $d(t)$ are the same, the difference in pilot and pilot-vehicle system characteristics takes place only because of motion cues. This can be shown from the scheme in fig. 2.15. It reflects the experiments on attitude control for the both tasks on the moving-based simulator where the motion cues are simulated by rotation only. The pilot actions can be represented here with the help of two describing functions: W_p^{VIS} and W_p^{VEST} which define his reaction to visual and motion cues accordingly. By neglecting the moving-based system and washout filter dynamics, it is easy to see that the equivalent pilot describing function defines pilot reaction to visual cue taking into account the existence of an additional loop as follows:

$$W_{p_i}^e = \frac{W_p^{VIS}}{1 + W_C W_p^{VEST}} \quad \text{- for the tracking task,}$$

$$W_{p_d}^e = W_p^{VIS} + W_p^{VEST} \quad \text{- for the stabilization task.}$$

Because of the difference in the right parts of these equations, it is also possible to get the difference in the influence of motion cues on equivalent pilot describing functions and other pilot-vehicle system characteristics. It can be shown qualitatively that $W_p^{VEST} = K_{p_1} s e^{-s\tau}$, where "s" is the simplified model of semicircular canal for the case when input signal is an angle change, $W_p^{VIS} = K_{p_2} (1 + T_L s) e^{-s\tau}$ and $W_C = K_C / (TS + 1) S$.

If we suppose that the crossover model for the open-loop system is correct in both cases, the model for W_p^{VIS} is the following: $W_p^{VIS} = K_{p_2} e^{-s\tau}$. It is quite enough to get the required equivalent pilot describing function $W_{p_d}^e = K_{p_2} (1 + T_L s) e^{-s\tau}$, $T_L = K_{p_1} / K_{p_2}$ applied to the crossover model. In the second task, the crossover model can be achieved when the pilot induces a lead in his reaction to the visual cue $W_p^{VIS} = K_{p_2} (1 + T_L s) e^{-s\tau}$, even when he will not react to the motion cue.



$$W'_C = W_C W_n^{-1}$$

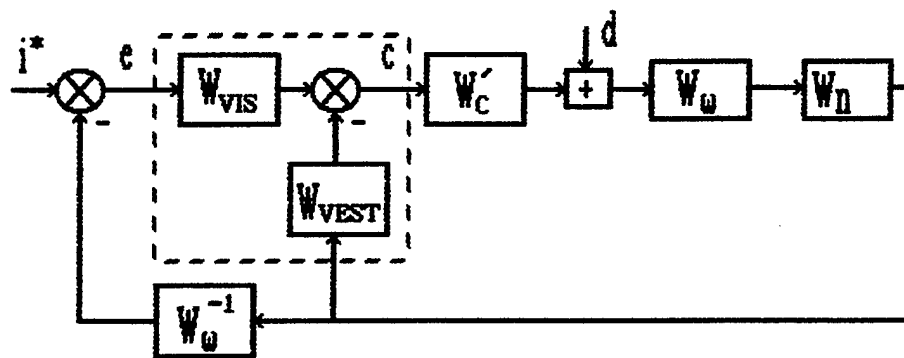


Fig. 2.15. The block-scheme of experiment

This is why it is possible to suppose that in the stabilization task, the motion cue will be used actively. As for the tracking task, the motion cue doesn't allow simplified pilot actions to the visual cue. This tells us that in a tracking task, the motion cues should be useless information. With goal to check the results of this analysis and to get the estimations of motion cues on PIO tendency, experiments were carried out on MAI's PVL moving-based simulator. The block-scheme corresponding to the technique of the experiment is shown in fig. 2.15. The controlled element frequency response characteristics modeled on the computer was $W_C' = W_C / W_n$, where W_n the mathematical model of the motion mechanism was defined preliminarily. The controlled element dynamics W_C corresponded to the LAHOS's configuration 4.1. The results shown in figs. 2.16a,b demonstrate that in the stabilization task the motion cue leads to an increase of crossover frequency up to 1 rad/sec and pilot gain coefficient (3 times), to a decreased lag in pilot reaction. Besides it leads to a decrease of closed-loop system resonance peak (r) taking place at higher frequency, to an increase of bandwidth frequency up to 1 rad/sec. All these results allow us to suppose that PIO tendency decreases for a stabilization task. The opposite tendency occurred in the tracking task. The motion cue here leads to a decrease of pilot gain coefficient and accuracy in the low frequency range. As for the resonance peak, it is slightly increased. These results allowed us to conclude that the motion cue only slightly increases the PIO tendency in the tracking task and leads to a considerable decrease in this tendency in stabilization task. That is why the tracking task was recommended for the further investigations on the in-flight simulator. The above results had a limitation because of the motion cues were simulated here by rotation of the cabin. That is why these results were checked on TSAGI's six-degree-of-freedom moving-based simulator. The test was worked out for the tracking task only and the results had the same tendency as in experiments fulfilled in MAI's PVL three-degree-of-freedom moving-based simulator. The quantitative difference was connected with the decreased value of control element and display gain coefficients (times two for both variables) in TSAGI's experiments compared with MAI's experiments.

4. The Influence of Display Gain Coefficient.

As noticed above, the visual flight or HUD from one side and HDD or instruments from the other side are characterized by the different gain coefficient K_D . For the first case it is defined by the distance (L) from pilot to the windshield glass. When $L = 57.3$ sm, $K_D = 1$ sm/deg. In the second type of indicator, the designers have to decrease the gain. For example, the ordinary attitude instruments or HUD installed in flight simulators have a gain coefficient $K_D = 0.1$ sm/grad. The increase of K_D leads to a decrease of the perceived error signal. When the last becomes too small the effects of thresholds appear. One of them is the decrease of resonance peak in the higher frequency range. The experiments carried out with a constant value of $d = \pm 1$ sm demonstrate (fig. 2.17) that for the gain coefficient $K_D = 0.5$, the resonance peak begins to decrease (in comparison with $K_D = 1$) and for $K_D \leq 0.3$ it disappeared. The decrease of K_D is accompanied by decrease of pilot gain coefficient and his lead.

According to the results in chapter 4, it was shown that in the precise tracking task the crossover frequency is close to its maximum value ω_C^* defined by the stability of the system. Thus the sudden change of display gain coefficient leads to significant increase of crossover frequency

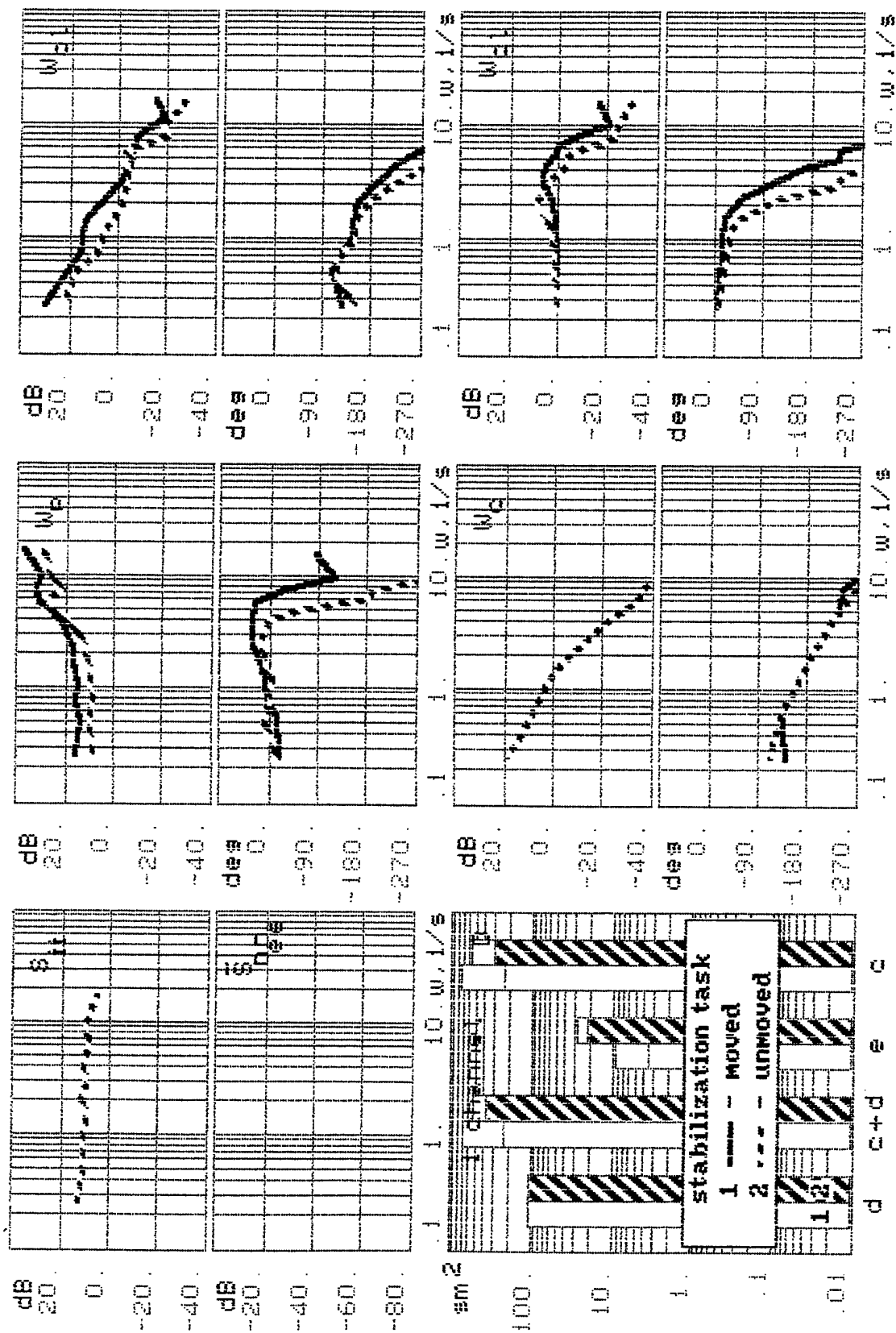


Fig. 2.16a. The comparison of experimental results

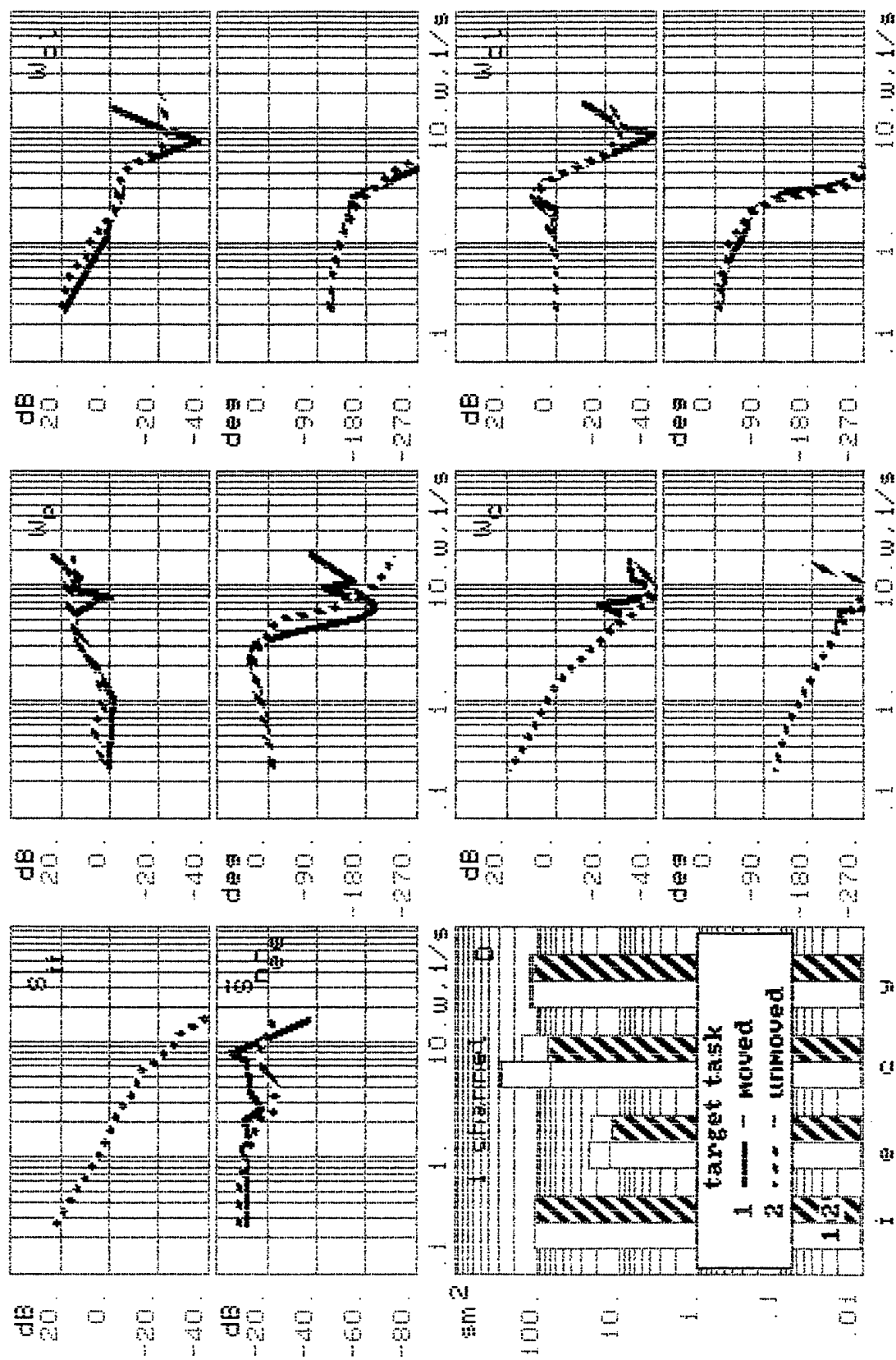


Fig. 2.16b. The comparison of experimental results

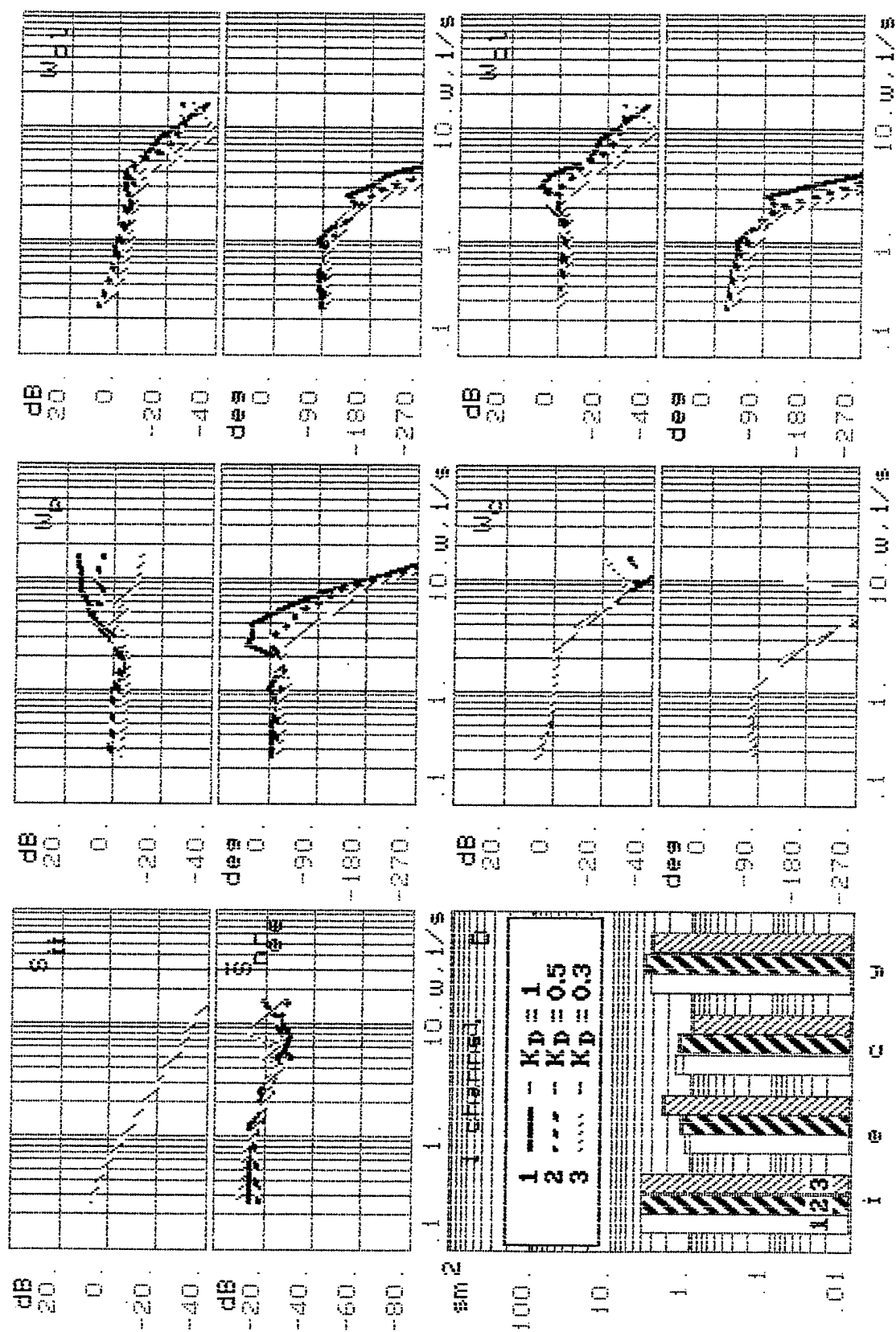


Fig. 2.17. The comparison of experimental results

because of a lag in change of pilot gain coefficient. This change can occur when his look transfer from HDD to HUD. As a consequence it leads to development of instability. Thus visual flight or use of the HUD characterized by the highest values of display gain coefficient have the increased tendency to PIO. That is why further investigation of PIO tendency with the HUD was recommended for the experiment on the in-flight simulator.

5. The Influence of Input Signal Characteristics.

Each piloting task is characterized by its own power spectral density, which influences the parameters of the pilot-vehicle system. These parameters can vary for different reasons. For example, the well-known Dryden turbulence model used for generation of disturbance signal $d(t)$ and characterized by the parameter L/V (where L is the so-called scale of turbulence) is different for different velocities, V . In the refueling task, the variance of command input signal depends on the distance between the airplanes. It is possible to give other examples of variability in input signal spectral density parameters. In the current research, two such parameters were investigated: the variance of input signal σ_e^2 and frequency ω , defined the following spectral density model $S_{ii}(\omega) = K^2 / (\omega_i^2 + \omega^2)^2$. The influence of these parameters was investigated partially in [1], where the pilot's goal was to keep an error signal at the zero position. It was shown here that a decrease of variance of input signal leads to an increase of nonlinear effect in perception: ratio σ_e^2 / σ_i^2 becomes the function σ_i^2 , as the normalized remnant power spectral density S_{n,n_e} increases. The experiments carried out in this work demonstrated that a change of σ_i in interval $\sigma_i = 1$ to 3 sm practically didn't lead to the change of pilot and pilot-vehicle system frequency response characteristics for the same pilot's instruction. In the case where the pilot tried to keep the error signal in the desired interval $d = \pm 1$ sm, the frequency response characteristics were considerably different. The decrease of σ_i leads to the decrease of phase lead in pilot frequency response characteristics and resonance peak of closed loop system (table 2.5 shows the results received for the 2.10 configuration, $K_D = 1$).

Table 2.5

σ_i , sm	1	3
r , sm	5.5	8.3
$\varphi_{p,max}$, deg	+15°	+38°

This and other research was carried out under conditions where a pilot had the possibility of choosing the best control element gain coefficient K_C . Analysis of the results demonstrates that an increase in σ_i arouses a pilot's wish for proportional increase of K_C . However, if this condition was not maintained, the results will not change considerably.

The investigation of the influence of frequency ω_i demonstrates that the effect depends considerably on the value of parameter "d". For small values of d ($d = \pm 0.25$ sm), increase of ω_i from 0.25 to 0.5 rad/sec leads to some decrease of resonance peak and phase lead (see fig. 2.18). The further decrease of ω_i up to 1 rad/sec leads to the disappearance of the resonance peak and a

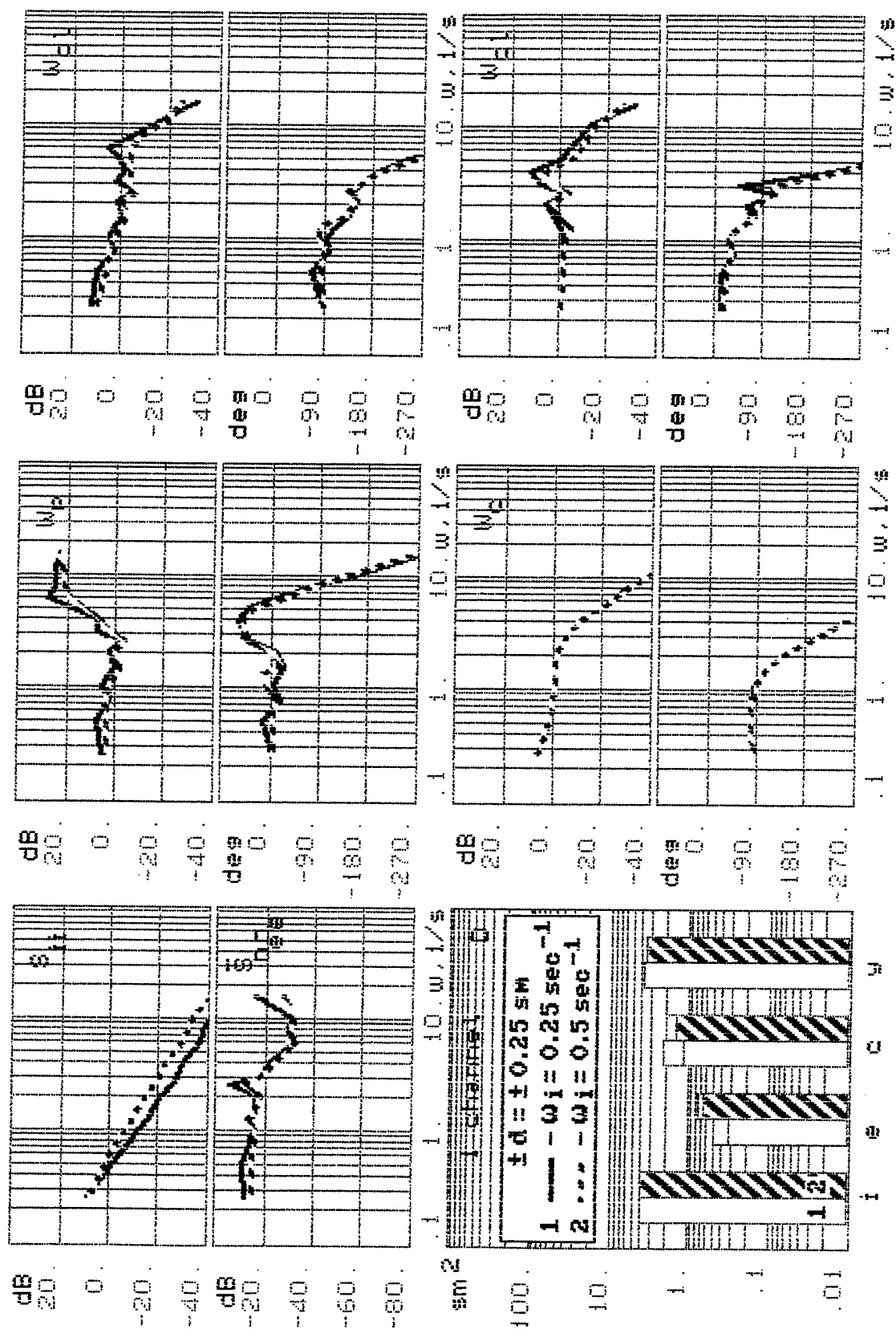


Fig. 2.18. The comparison of experimental results

sharp decrease of pilot phase frequency response characteristics. These results are analogous to a so-called crossover frequency regression [14]. For small values of ω_i , this effect can be explained by investigating configuration 2.10 characterized by unsatisfactory handling qualities and low crossover frequency of 1.2 rad/sec. The experiments carried out for higher values of "d" demonstrated the opposite effects. The increase of ω_i from 0.25 to 0.5 rad/sec in that case leads to the increase of a resonance peak and pilot lead (fig.2.19). This result takes place because an increase of "d" is equivalent to an increase of threshold influence on remnant and on pilot-vehicle system characteristics. Because the remnant defines the spectral density of signal $e_n(j\omega) = W_{CL}(j\omega)n_e(j\omega)$, the decrease of resonance peak is logical and is defined by the pilot's goal to decrease the variance of error. The further increase in ω_i ($\omega_i \geq 1$) is accompanied by the crossover frequency regression, decrease of the resonance peak, and pilot's lead. All these results lead to the conclusion that under conditions $\sigma_i^2 \approx 4sm^2$ and $\omega_i \approx 0.5$ rad/sec the resonance peak and pilot workload are considerable. That is a reason why these values were recommended to TSAGI and LII for further research.

2.3 THE INFLUENCE OF PILOT VARIABLES (π, σ).

From the majority of pilot variables (π, σ, ε), only one was considered: instruction or pilot's motivation to keep the error signal in the permissible (desired) interval $\pm d$. This interval can be different for different piloting tasks. It can be supposed that in air-to-air tracking tasks, it is considerably smaller than in the approach phase of landing. It can be different for different conditions of the same task. For example, it has to be less for the landing task under additional requirement to carry out touchdown in a definite point on the runway, than without it. This effect can be taken into account in mathematical modeling in two ways. One is the increase of threshold causing the decrease of describing function gain threshold N_e and N_i . In modeling it was supposed that $N_e = N_i = N$. The second is the addition of residual remnant $S_{n_{\infty}} = \pi\sigma_{\infty}^2$ to remnant power spectral density. Both ways are described in detail in chapter 4. Correlation of mathematical modeling and experimental results achieved in the first method (see fig. 4.1) allows us to further recommend it with due regard for the effect of permissible interval $\pm d$ for modeling based on the structural approach.

The exposed results of mathematical modeling and the first experiments demonstrated the increase of resonance peak and pilot workload in the case of a decrease of $\pm d$. It leads to the necessity to investigate this factor in experiments in detail. The experiments were carried out for two control element dynamics (configuration 2.10 and the Tu-154 in-flight simulator) for different intervals (see table 2.6). The results shown in figs. 2.20, 2.21 demonstrate that for both configurations an increase of "d" leads to a decrease of resonance peak and pilot lead compensation. For configuration 2.10, this tendency begins from a value of $d = \pm 1$ sm and the resonance peak practically disappears when $d = \pm 2$ sm. In this case the pilot's phase frequency $\varphi_P(\omega_{\varphi=-180^\circ})$ decreases from $+50^\circ$ to 0° . For the in-flight simulator, this tendency takes place practically in all interval of d and for $d \approx 1.5$ si, the resonance peak practically disappears. The comparison of results for these configurations demonstrates that the measured characteristics

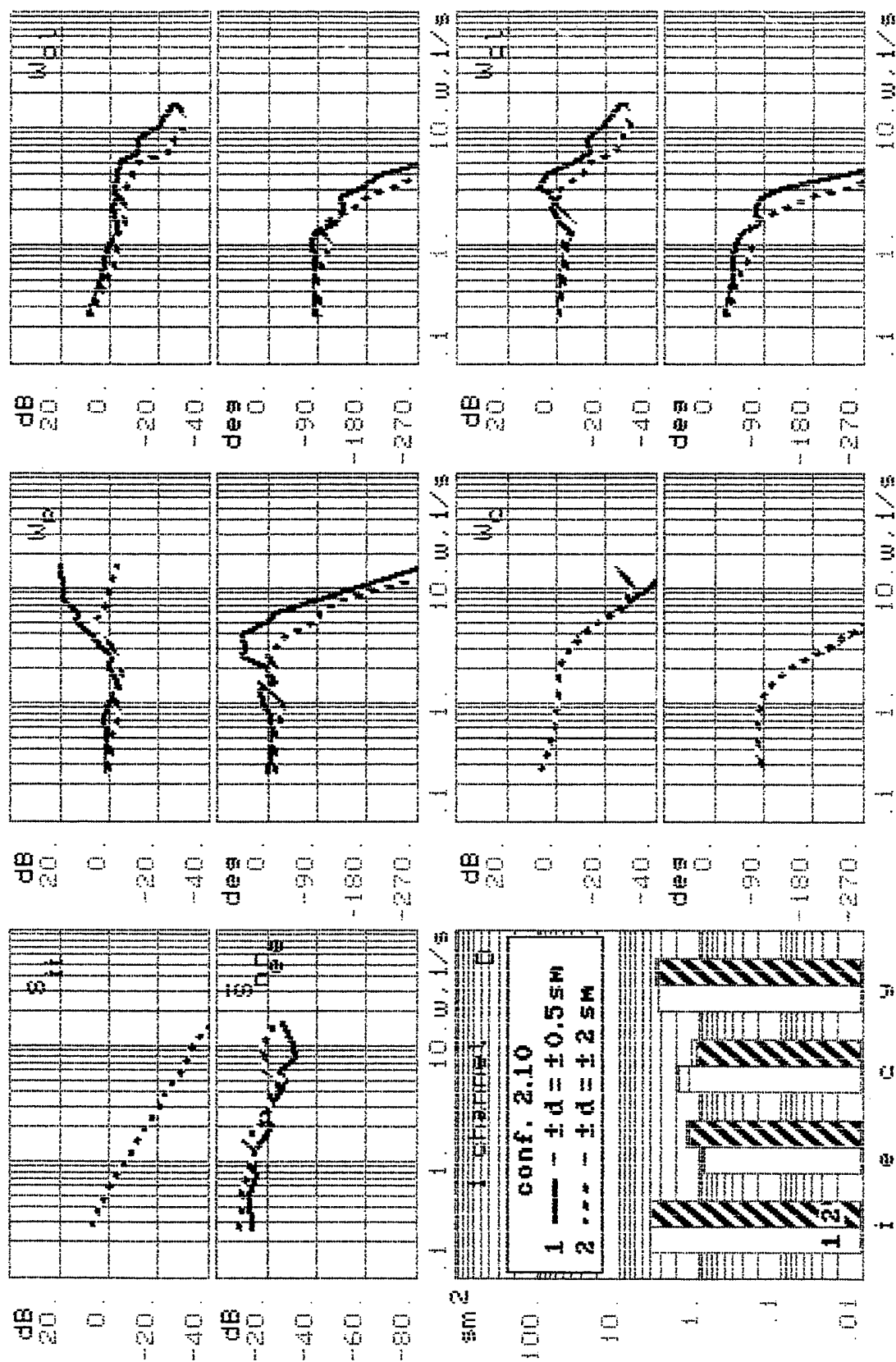


Fig. 2.20. The comparison of experimental results

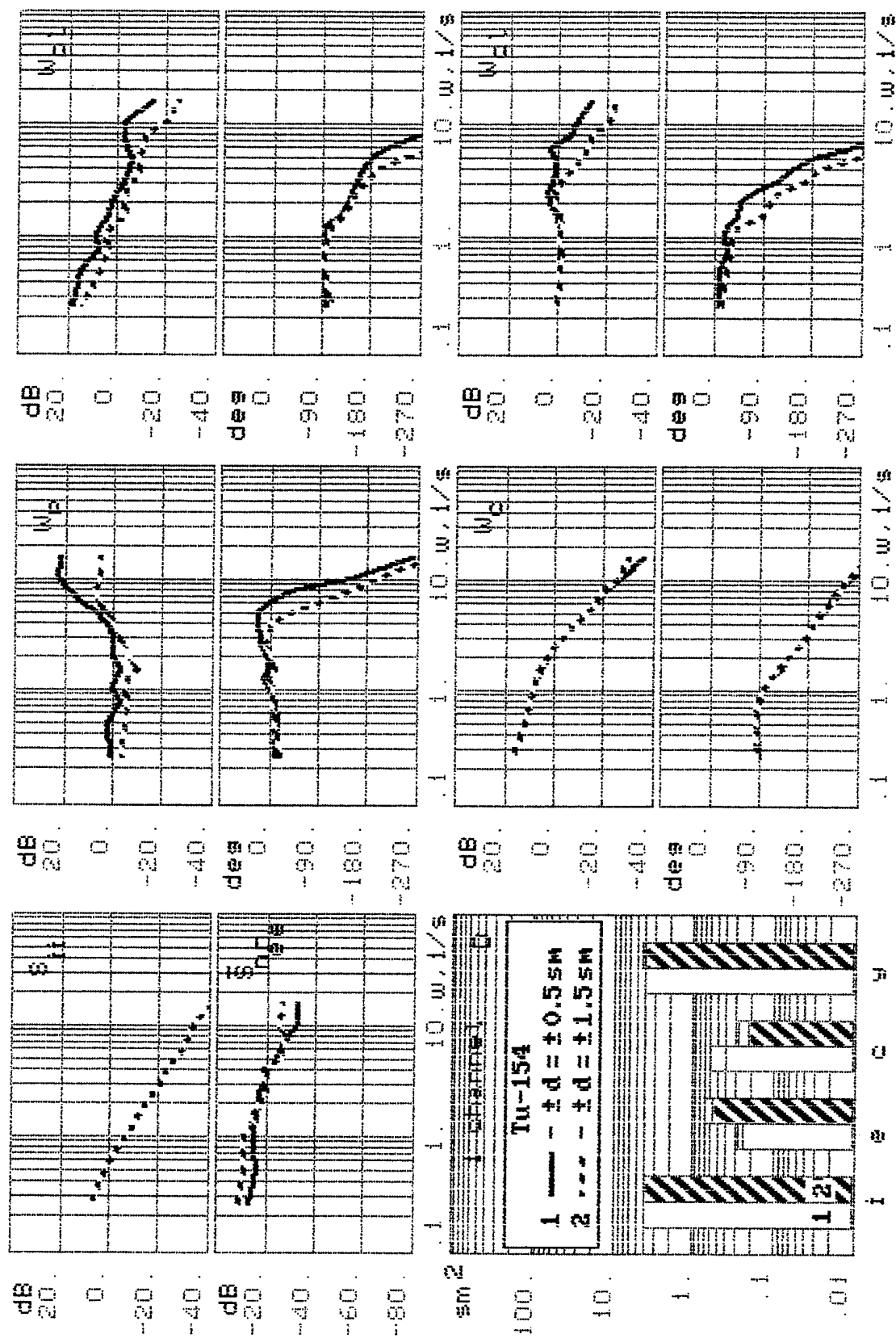


Fig. 2.21. The comparison of experimental results

corresponding to the different configurations are close to each other for the different values of d . For configuration 2.10 it takes place for $d \approx 1.5$ to 1.75 sm, and for the Tu-154 for $d \approx 0.5$ sm.

Table 2.6

TU-154/2.10	d[sm]			
	0.5	1	1.5	2
r, dB	4.2/8.15	3.85/7.53	-/6.3	-/2.1
$\varphi_P(\omega_{\varphi=-180^\circ})$, deg	+25/+45	+18/+40	-/+26	-/-1
PR	6/8.5	4/8	3.5/6	2.5/3.5

These results allows us to conclude that a change of requirements to permissible accuracy can influence the pilot-vehicle system characteristics considerably. It means that the same aircraft can be evaluated differently under a different requirement ($\pm d$), transforming aircraft with satisfactory to unsatisfactory handling qualities. In addition, the decrease of interval $\pm d$ increases the PIO tendency of the investigated aircraft. Because of such considerable influence on PIO tendency this variable was recommended for the further investigation at TSAGI and LII.

The effect of interval $\pm d$ depends on the display gain coefficient K_D and the variance of input signal σ_i^2 . The analysis showed that close results can be received for different sets of these parameters. The decrease of K_D leads to the same tendency in the system characteristics as a decrease of σ_i^2 or increase $\pm d$. This conclusion leads to the task of defining such criteria combining K_D , σ_i^2 , and d whose constant value guarantees the invariability of pilot-vehicle system characteristics under change of K_D , σ_i^2 , and d . This criteria called μ -criteria was found from the Weber - Fehner law. According to it the change of sensation dE is connected with the change of stimulus dJ in the following way

$$dE = K \frac{dJ}{J_0} \quad (2.1)$$

where J_0 - value of threshold,

K - constant coefficient, depended on the type of stimulus.

Because $dJ = J - J_0$, and supposing that the stimulus $J = K_D e$ and $J_0 = d$ in the equation (2.1) can be rewritten as

$$dE = K \left\{ \frac{K_D e}{d} - 1 \right\}.$$

Because "e" is a random signal and taking into account that the mean square error is proportional to σ_i ($\sigma_e = K_i \sigma_i$), where K_i is the function depending on the pilot vehicle system characteristics and input spectral density parameters, it is easy to get the following equation for mean square $\sigma_{\Delta E}$

$$\sigma_{\Delta E} = KK_1\mu, \text{ where} \quad (2.2)$$

$$\mu = \frac{\sigma_i K_D}{d} \quad (2.3)$$

which defines a level of pilot sensation.

It is possible to suppose that for a different set of σ_i , K_D , and d , under condition that for all of them, μ is a constant, the pilot frequency response characteristics has to be the same. In that connection " μ " can be considered as a criteria for adequacy of perception for different conditions of experiments.

This suggestion was checked and the results of experiments are shown in fig. 2.22, 2.23 for the different set of variable values supplied $\mu=1,2$ (see table 2.7). Their analysis demonstrates that experiments corresponding to the same μ -criteria value have approximately the same frequency response characteristics of the pilot-vehicle system. These circumstances allow us to be sure of the results received in MAI, where $K_D=1$ and $d=2.0$ sm and in TSAGI and LII where $K_D=0.5$ and $d=1.0$ sm under research of LAHOS configurations.

Table 2.7

μ	$\sigma_w, \text{ sm}$	$K_D, \text{ sm/deg}$	$d, \text{ sm}$
1 (fig. 2.22)	2	0.5	1
	2	0.25	0.5
	1	1	1
	1	0.5	0.5
2 (fig. 2.23)	2	2	2
	2	1	1
	2	0.5	0.5
	1	2	1
	1	1	0.5

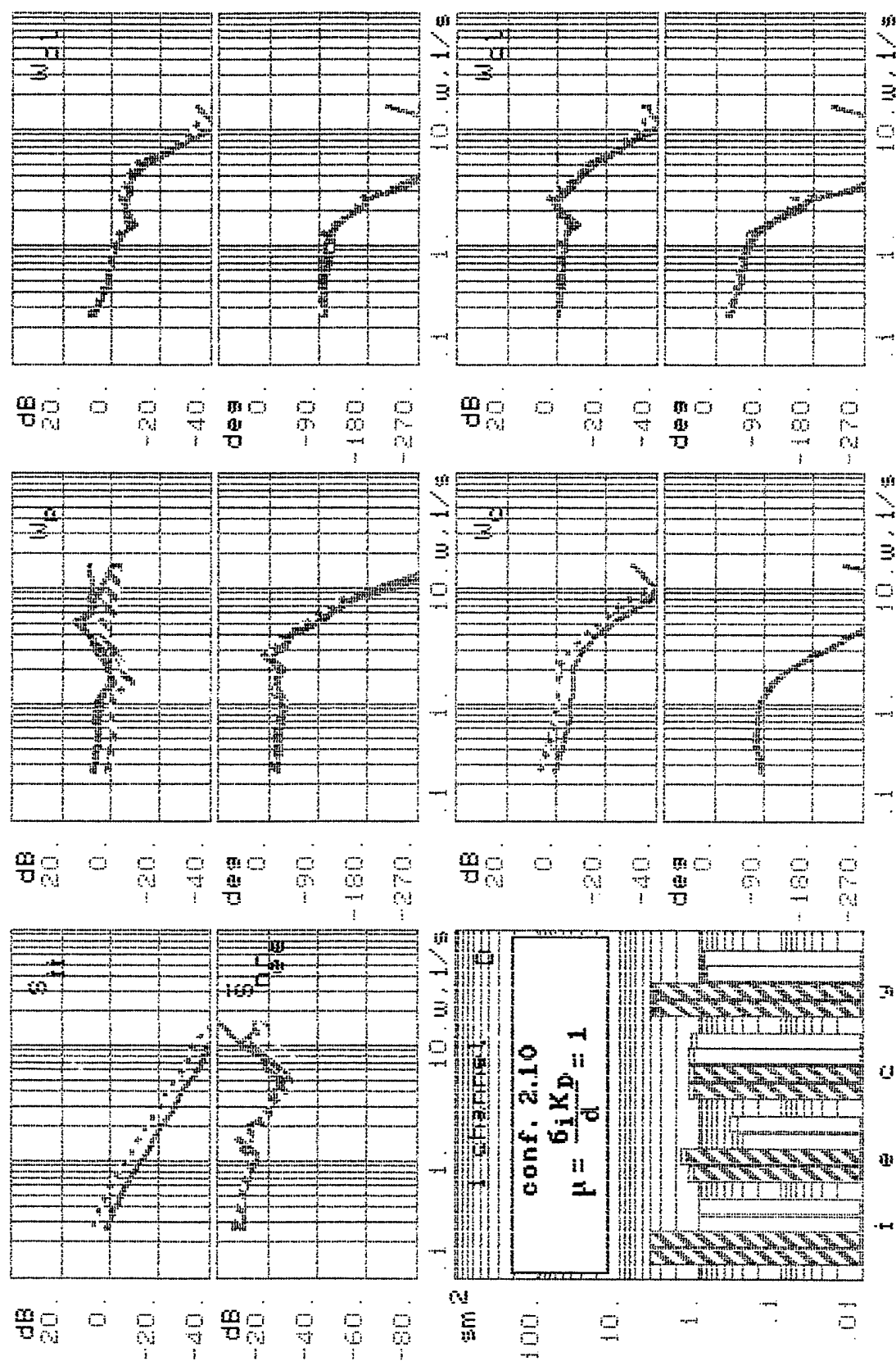


Fig. 2.22. The comparison of experimental results

3.0 DEVELOPMENT OF CRITERIA FOR HANDLING QUALITIES RESULTING FROM EXPERIMENTAL RESEARCH ON PILOT-VEHICLE SYSTEM CHARACTERISTICS

The results described in chapter 2 were used as a basis for development of handling qualities. This criteria was developed in the experimental research allowed the pilot-vehicle system characteristics to be obtained directly. The comparison of the frequency response parameters with measured pilot ratings helped to avoid inaccuracy in definition of handling qualities requirements.

3.1 THE TASK OF EXPERIMENTAL RESEARCH

In the first stage of development of criteria for handling qualities, the dynamic configurations investigated by Neal and Smith [4] were used. The same parameters of pilot-vehicle system (resonance peak of closed-loop system and pilot phase compensation) as in [4] were chosen. These parameters are quite well correlated with pilot ratings [see chapter 2]. In comparison with Neal-Smith research, the resonance peak of the closed-loop system and pilots phase compensation parameters were measured directly in the experiments. One of the problems was in the definition of experimental conditions that guaranteed the possibility of measuring three levels of pilot rating for the majority of investigated configurations. The analysis of Neal-Smith results [4] demonstrated that he managed to find such conditions. Therefore, the first step of our research was the definition of adequate conditions for experiments. These main conditions are input signal and motivation which can be defined as a level of permissible error d . Because of the absence of data about the input signal parameters in [4], a suggestion was made about the accordance of the input signals used in [5] and [15].

In the last work the discrete signal was used (fig 3.1). This required us to find its polygarmonic equivalent used in the Fourier coefficient method (see Appendix A) to receive the accurate results. Thus we found the power spectral density of equivalent stationary random process $S_{ii}(\omega)$ by use of Fast Fourier Transform and averaging of results. The calculation of the characteristics gave the following equation for $S_{ii}(\omega)$

$$S_{ii} = \frac{K_i^2}{(\omega^2 + \omega_i^2)^2}, \quad (3.1)$$

where $\omega_i = 0.5$ rad/sec, K_i corresponds to the mean square $\sigma_i^2 = 2^\circ$ (or sm). Almost the same parameters of input signal were received in [15] where we attempted to modify Neal-Smith criteria. The equation (3.1) was used for design of the poligarmonic signal according to the technique described in Appendix A.

The second major factor in creating conditions adequate to Neal-Smith investigations is the definition of interval "d" which determined the level of pilot motivation. This level corresponding to the desired level of task performance is a key factor in determination of pilot

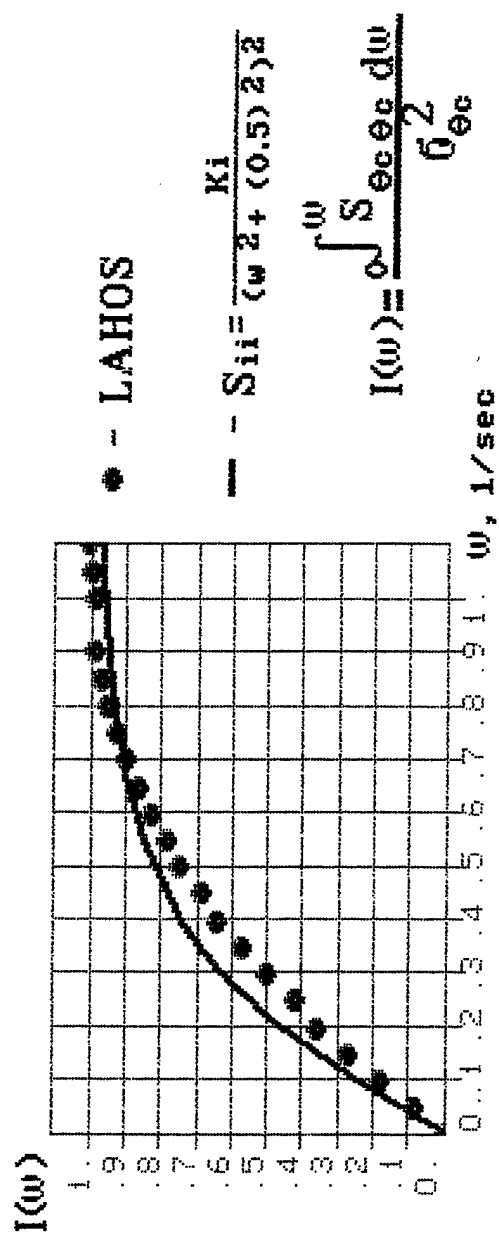
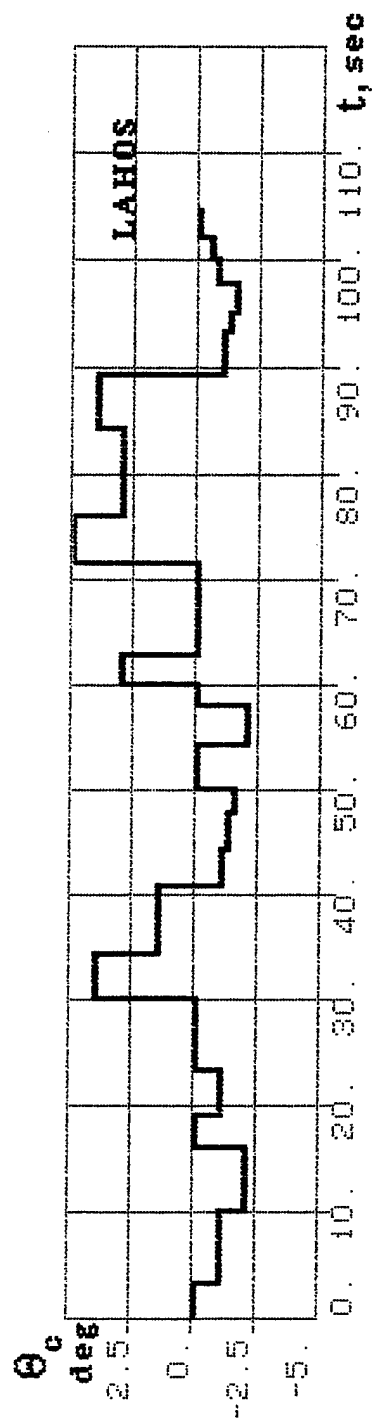


Fig. 3.1. The approximation of LAHOS input signal

rating according to the Cooper-Harper scale because of the border between the first and second levels of pilot ratings corresponds to PR=3.5 and is defined by the concrete value of desired accuracy (interval "d"). The determination of this level allows us to define then the pilot ratings.

The problem was decided by the special investigation of Neal-Smith configuration 2D corresponding to the best rating (PR=2.5) from all those investigated in [4] configurations. Then the interval $\pm d$ was defined for which the pilot rated the configuration with PR=2.5. The received level was equal 0.85^0 . This one and all other experiments were carried out for display gain coefficient $K_d = 1$. Further investigation of 23 Neal-Smith configurations (see table 3.1) was carried out under chosen parameters of input power spectral density and interval d . In the experiments a wide set of spectral, frequency, and integral characteristics of the pilot-vehicle system for four operators were measured. This knowledge allows us to get the parameters defining the pilot rating (PR): the resonance peak $r = \left| \theta / \theta_C \right|_{\max}$, bandwidth ω_{BW} , crossover frequency ω_C , and the pilot phase adaptation $\Delta\varphi_P$. The last parameters were calculated here as a difference between the pilot phase frequency response characteristic received for each configuration and the pilot phase characteristics received in experiments with the optimal aircraft dynamics. The dynamics corresponding to the simplest type of human behavior was received by use of the Wiener approach and is described in [1]. It is given briefly in Appendix B. The experiments with optimal aircraft dynamics were carried out for two operators.

The results demonstrated in fig. 3.2 show that pilot frequency response characteristics are close to the gain coefficient with time delay practically in all frequency range. The offered way in the determination of time delay allowed us to avoid the uncertainty in setting its value. In the considered experimental approach the pilot phase frequency response for the optimal dynamics

φ_P^{opt} keeps all the information about such limitation as delay in pilot reaction. Thus, the

calculation of the difference between the φ_P and φ_P^{opt} is the parameter

$\Delta\varphi_P = \varphi_P - \varphi_P^{opt}$ which defines the pilot workload.

3.2 ANALYSIS OF RESULTS

It is necessary to note that the use of the experimental approach for definition of criteria allows us to carry out the analysis of the calculated closed-loop system and pilot workload parameters not only at one frequency, but for the pilot-vehicle system the frequency range. This

range is the interval from the crossover frequency ω_C up to the frequency $\omega \Big|_{\varphi=-180^\circ}$

corresponding to the open-loop system phase $\varphi_{OL} = -180^\circ$. The frequencies ω_C and

Table 3.1

Configuration	$1 / \tau_1$	$1 / \tau_{\theta_2}$	$1 / \tau_2$	$\omega_{\varphi} / \xi_{\varphi}$	ω_3 / ξ_3
1A	0.5	1.25	2	2.2/0.69	63/0.7
1B	2.0	1.25	5.0	2.2/0.69	63/0.7
1C	2.0	1.25	5.0	2.2/0.69	16.0/0.7
1D	∞	1.25	∞	2.2/0.69	75/0.7
1E	∞	1.25	5.0	2.2/0.69	63/0.7
1F	∞	1.25	2.0	2.2/0.69	63/0.7
1G	∞	1.25	0.5	2.2/0.69	63/0.7
2A	2.0	1.25	5.0	4.9/0.70	63/0.7
2B	2.0	1.25	5.0	4.9/0.70	16.0/0.7
2C	5.0	1.25	12.0	4.9/0.70	63/0.7
2D	∞	1.25	∞	4.9/0.70	75/0.7
2E	∞	1.25	12.0	4.9/0.70	63/0.7
2F	∞	1.25	5.0	4.9/0.70	63/0.7
2G	∞	1.25	5.0	4.9/0.70	16.0/0.75
2H	∞	1.25	2.0	4.9/0.70	63/0.7
2I	∞	1.25	2.0	4.9/0.70	16.0/0.7
2J	∞	1.25	0.5	4.9/0.70	63/0.7
3A	∞	1.25	∞	9.7/0.63	75/0.7
4A	∞	1.25	∞	5.0/0.28	75/0.7
5A	∞	1.25	∞	5.1/0.18	75/0.7
6C	∞	2.4	∞	3.4/0.67	75/0.7
7C	∞	2.4	∞	7.3/0.73	75/0.7
8A	∞	2.4	∞	16.5/0.69	75/0.7

$\omega|_{\varphi=-180^\circ}$ define the amplitude and phase margins. The determination of ω_C ,

$\omega|_{\varphi=-180^\circ}$, and ω_{BW} indirectly, as it was done in other approaches, is inaccurate and

depends on the level of pilot mathematical model completeness. The experimental approach doesn't have such shortcomings.

The pilot behavior is defined in different frequency ranges with the goals pursued in fulfillment of a task. It is known a fact, that the pilot adapts his actions to correct the aircraft dynamics in low, middle, and high frequency ranges. These ranges corresponds to intervals

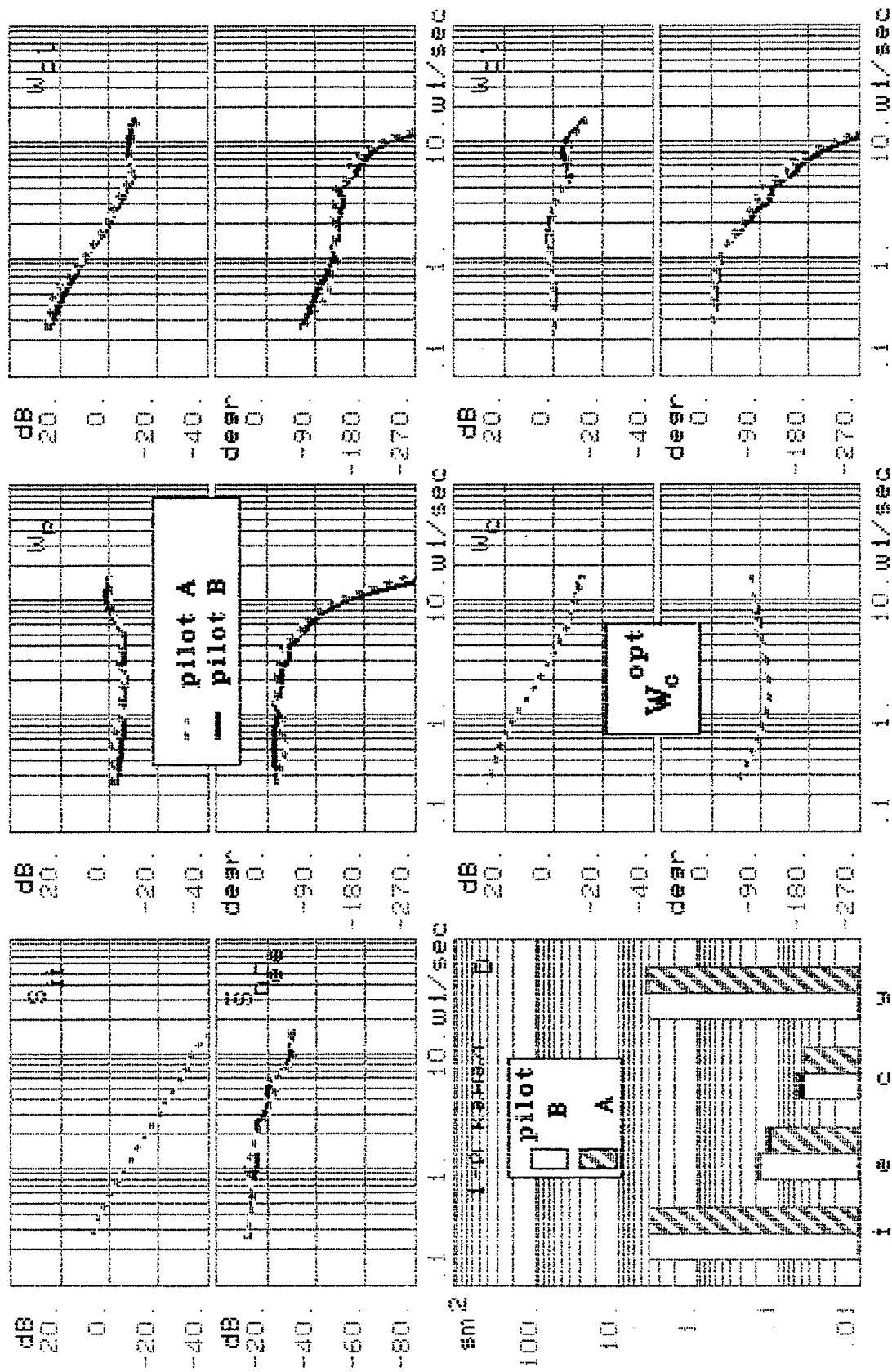


Fig. 3.2. The pilot frequency response characteristics for the optimal control dynamics

$\omega < \omega_C - \Delta\omega_1$, $\omega_C - \Delta\omega_1 < \omega < \omega_C + \Delta\omega_2$, and $\omega > \omega_C + \Delta\omega_2$ consequently.

The values ω_C , $\Delta\omega_1$, and $\Delta\omega_2$ depend on the task variables. In the low frequency range, the pilot induces the compensation to minimize an error, defined by the input spectrum. Because of this circumstance, a pilot tries to make $|W_{OL}| \gg 1$ in this frequency range.

In the middle (or crossover) frequency range, the pilot tries to reach the necessary margins and consequently the stability of system and task performance. In this range, including the frequency $\omega|_{\varphi=-180^\circ}$, the pilot aspires to satisfy the requirements of roughness in the closed-loop system and minimum error defined by the remnant. The last system requirement he tries to realize and in the high frequency range. The value of pilot compensation induced in all these subintervals defines the level of pilot workload. This compensation has to be analyzed in the development of criteria. The boundaries of the handling qualities were defined taking into account these considerations.

The results of the experiments demonstrated that there can be different values and signs of the pilot phase compensation parameter $\Delta\varphi_P$, mentioned in the above frequency subintervals.

In fig. 3.3 two typical cases are shown. The values of $\Delta\varphi_P^+$ and $\Delta\varphi_P^-$ can be changed in wide ranges depending on the aircraft dynamic configuration. The results of analysis of pilot, pilot-vehicle system characteristics, and pilot ratings received for one operator in the experimental research for 23 Neal-Smith configurations (see table 3.1) are shown in fig.3.4.

The determination of pilot workload parameter $\Delta\varphi_P$ was required to develop the set of procedures. In the beginning, values of $\Delta\varphi_P$ in the all frequency intervals were analyzed. For cases where a configuration had two maximum values $\Delta\varphi_P^+$ and $\Delta\varphi_P^-$, both of them were plotted on the fig. 3.4. After that the boundaries of pilot ratings levels were drawn and the pilot workload parameter $\Delta\varphi_P$ was analyzed. When the both values of $\Delta\varphi_P$ lie inside the range corresponding to experimental PR, then both values are the pilot workload parameters have to be stayed in the plan. In the case where one of the values $\Delta\varphi_P$ lies in the range of parameters not corresponding to the experimental PR, it has to be disregarded. These values are crossed in fig. 3.4. The boundaries of r and $\Delta\varphi_P$ were defined corresponding to equal levels of pilot ratings on precise pitch control tracking task. The proposed approach allowed all configurations rated up

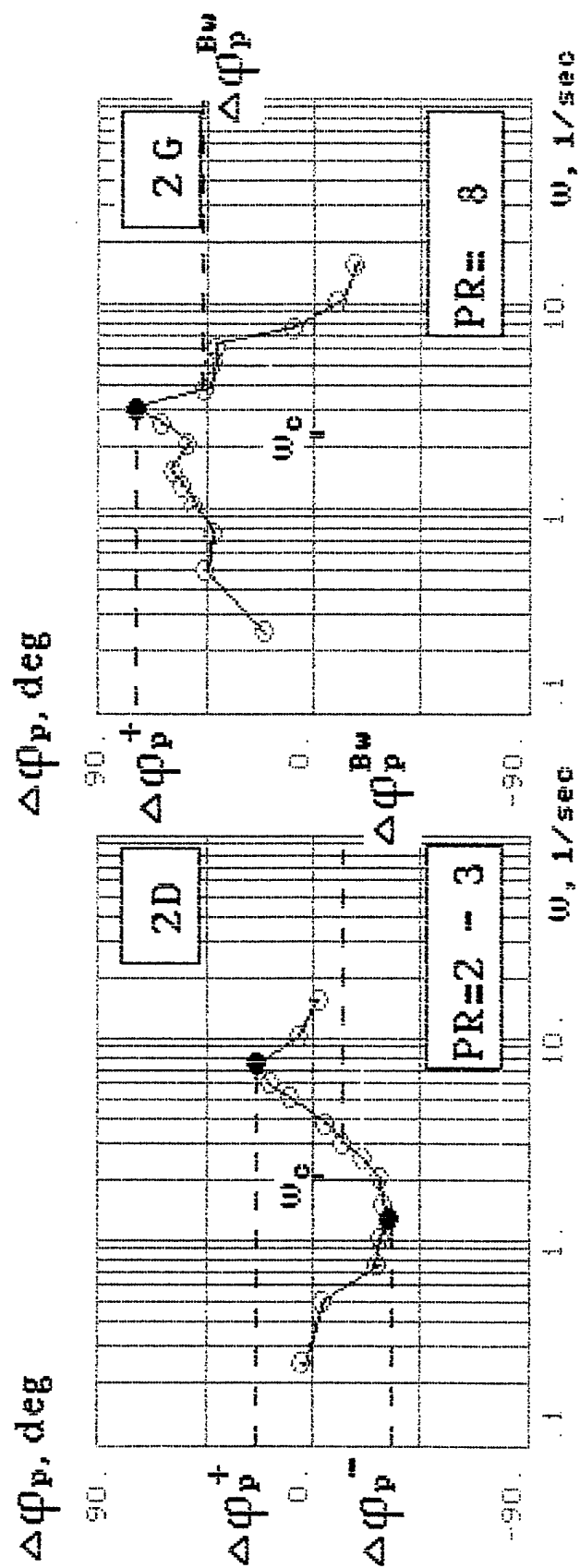


Fig. 3.3. The pilot phase compensation and workload parameters for 2D and 2G configuration

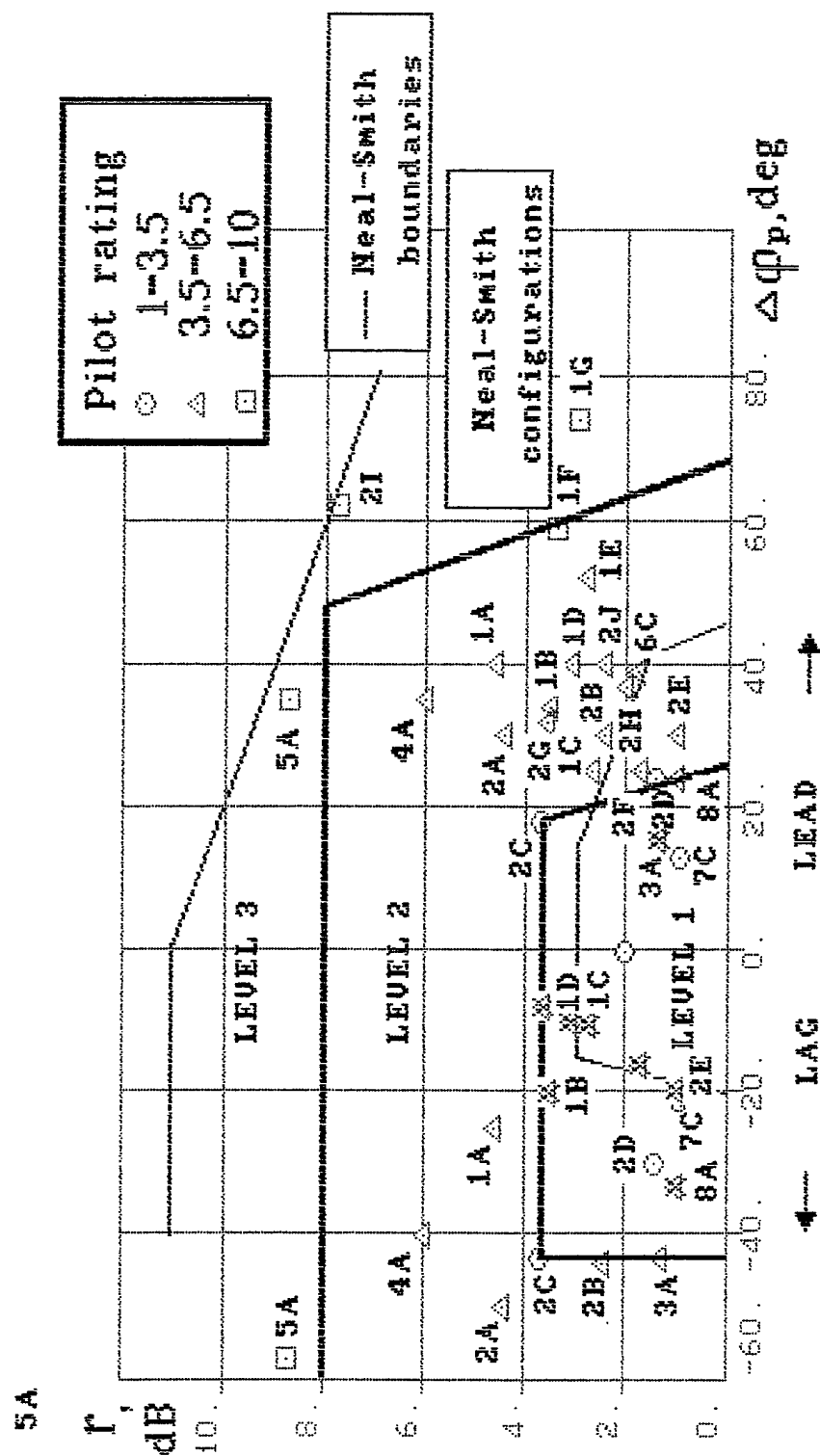


Fig.3.4 The levels of handling qualities

to $PR=1 - 3.5$ to be put into defined boundaries of r and $\Delta\phi_D$ parameters. The same result was received for configurations corresponding to the second level of pilot rating.

Twenty-five configurations were also investigated (see table 3.2) corresponding to LAHOS program. The results of these experiments fulfilled in accordance with Neal-Smith condition ($d = \pm 0.85$) are shown in fig. 3.5. These results were received for an operator who didn't participate in the preliminary stage of experiments described in chapter 2. For this reason, insignificant difference exist in the values of measured parameters. From fig. 3.5 it is seen that all the results correspond to the second and even third level and the location of some of them (configurations 2.1 and 2.C for example) do not correspond to pilot ratings defined in the flight test [5]. The attentive study of conditions for the flight tasks carried out in the LAHOS program [5] allowed us to expose the discrepancy in display gain coefficient used the LAHOS research. In LAHOS it was two times less ($K_D = 0.5$) than in the MAI research. This circumstance required us to repeat the research on the LAHOS configuration. After that, the all points moved to the ranges corresponding to the pilot ratings received in the LAHOS program. For example, the points 2.1 and 2.C were moved into the range corresponding to the first level of pilot ratings. Thus, the accordance in display gain coefficients allowed us to get good accordance with the LAHOS pilot ratings too.

The experimental data analysis in fig. 3.6 shows where the workload parameter $\Delta\phi_P$ was defined by bandwidth frequency ω_{BW} . Such a parameter was used in the Neal-Smith criteria. The levels defined by this are shown in fig. 3.6. They differ considerably from the ranges shown on fig. 3.4, however, these results were received under removal of uncertainty in setting of ω_{BW} . Analysis of known works [4,15] shows that uncertainty is one of the major factors limiting the use of Neal-Smith criteria.

The analysis of dependence $\Delta\phi_P(\omega)$ in the considered frequency range demonstrated that the parameter $\Delta\phi_P$ reaches the maximum value at frequencies close to ω_C and $\omega \Big|_{\varphi=-180^\circ}$. The frequency corresponding to the bandwidth lies between ω_C and $\omega \Big|_{\varphi=-180^\circ}$ and for some configurations $\Delta\phi_P(\omega_{BW})$ can be close to zero which does not reflect the pilot workload. The lower values of $\Delta\phi_P(\omega_{BW})$ in comparison with

Table 3.2

Configuration	τ_1	τ_{θ_2}	τ_2	$\omega_{\infty} / \xi_{\infty}$	ω_3 / ξ_3	ω_4 / ξ_4
1-A	0.4	1.4	0.1	1.0/0.74	-	-
1-B	0.3	1.4	0.1	1.0/0.74	-	-
1-C	0.2	1.4	0.1	1.0/0.74	-	-
1-1	0	1.4	0	1.0/0.74	-	-
1-2	0	1.4	0	1.0/0.74	-	-
1-4	0	1.4	0.5	1.0/0.74	-	-
1-11	0	1.4	0	1.0/0.74	16/0.93	16/0.38
2-C	0.2	1.4	0.1	2.3/0.57	-	-
2-1	0	1.4	0	2.3/0.57	-	-
2-2	0	1.4	0.1	2.3/0.57	-	-
2-3	0	1.4	0.25	2.3/0.57	-	-
2-4	0	1.4	0.5	2.3/0.57	-	-
2-9	0	1.4	0	2.3/0.57	6/0.7	-
2-10	0	1.4	0	2.3/0.57	4/0.7	-
3-C	0.2	1.4	0.1	2.2/0.25	-	-
3-1	0	1.4	0	2.2/0.25	-	-
3-3	0	1.4	0.25	2.2/0.25	-	-
3-7	0	1.4	0	2.2/0.25	12/0.7	-
4-1	0	1.4	0	2.0/1.06	-	-
4-7	0	1.4	0	2.0/1.06	12/0.7	-
4-10	0	1.4	0	2.0/1.06	4/0.7	-
4-11	0	1.4	0	2.0/1.06	16/0.93	16/0.38
5-4	0	1.4	0.5	3.9/0.54	-	-
5-6	0	1.4	0	3.9/0.54	6/0.7	-
5-11	0	1.4	0	3.9/0.54	16/0.93	16/0.38

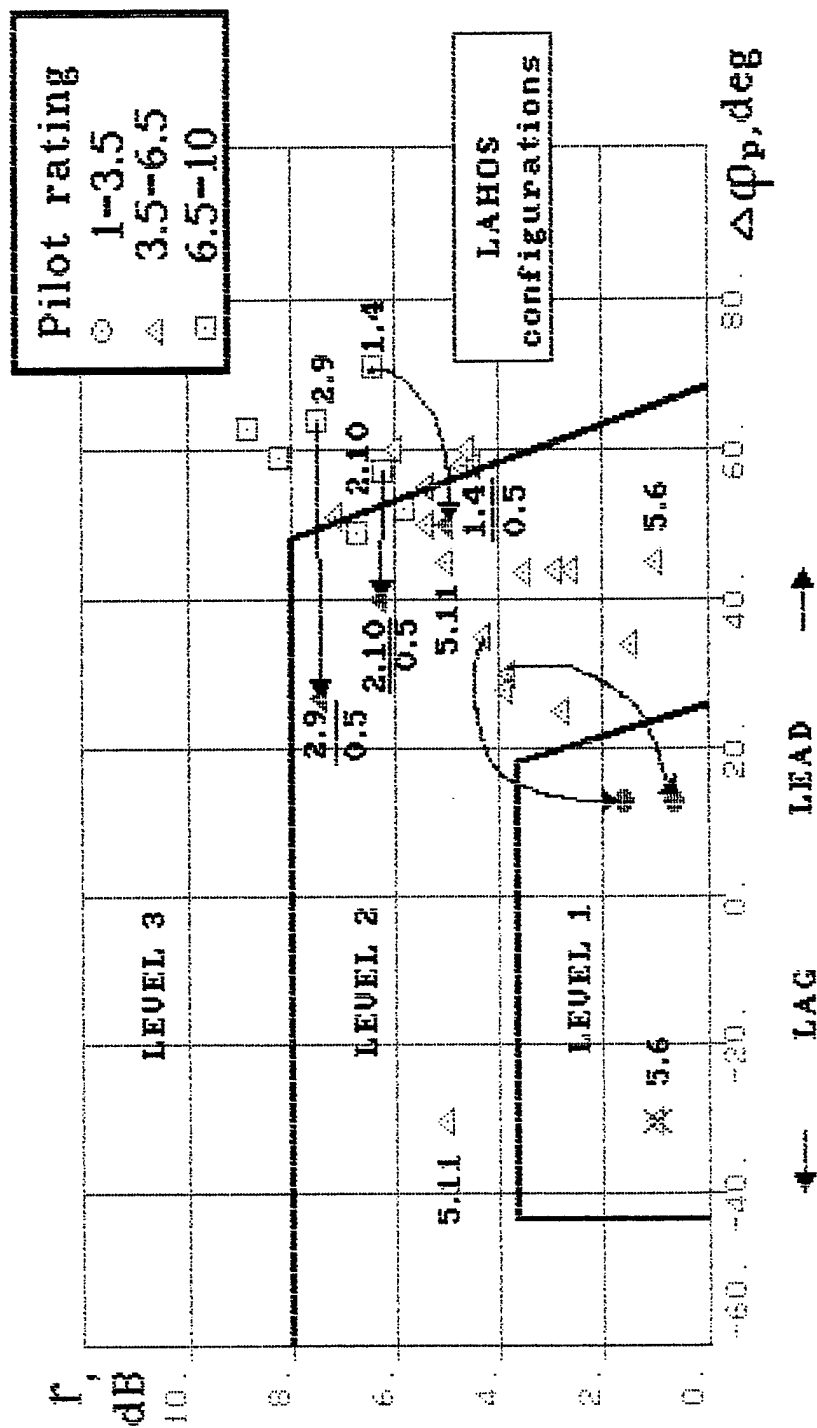


Fig. 3.5. The correlation of closed loop parameters with developed criteria

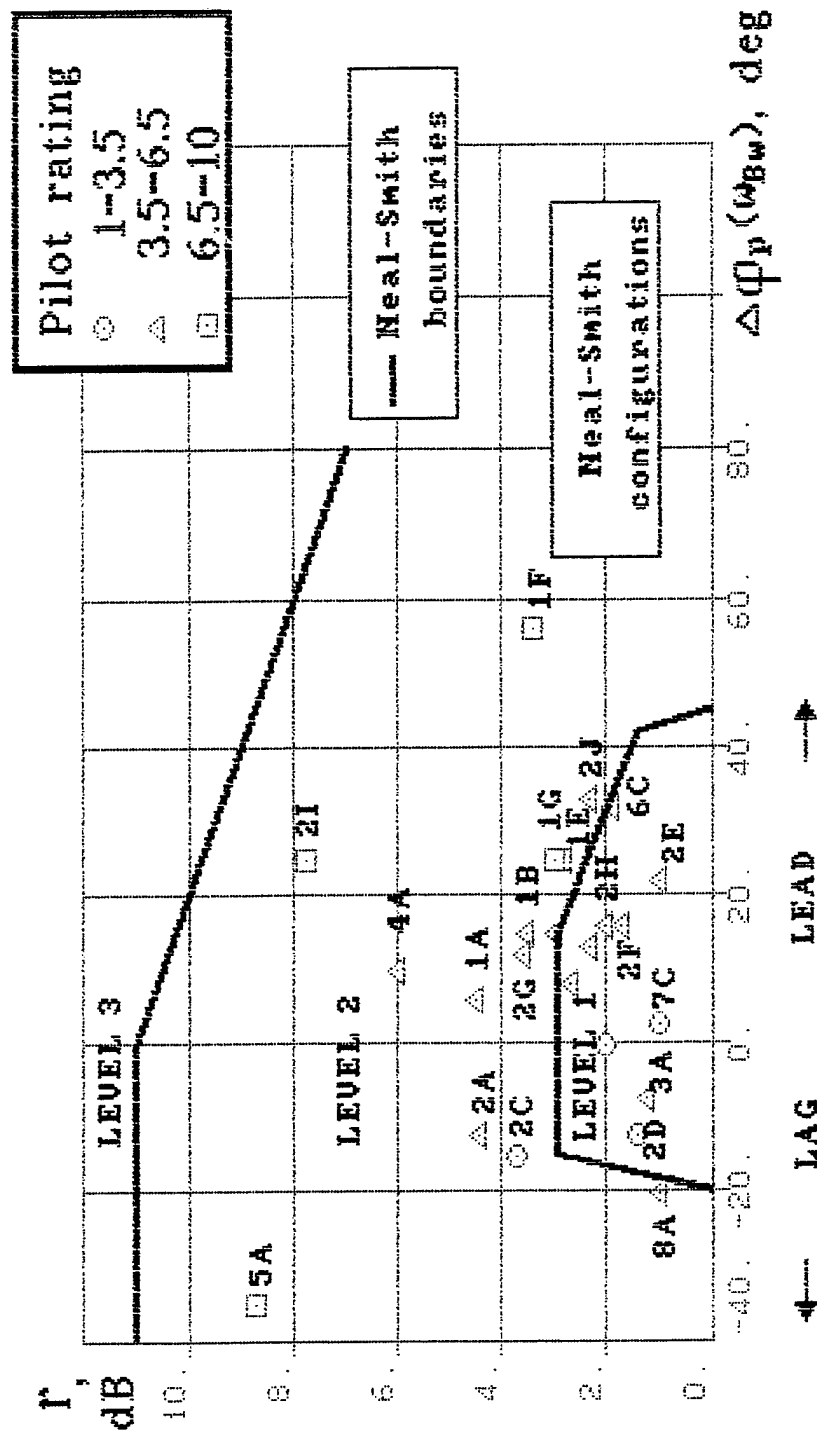


Fig. 3.6. The correlation of closed loop parameters with PR (for the case when pilot phase compensation is defined on $\omega = \omega_{BW}$).

$\omega \left| \varphi = -180^\circ \right.$ lead to variability of results especially for the second level of pilot ratings. And,

what is more, the configurations leads to results that a considerable part of configurations are moved out of the second level of handling qualities and donot correspond to the experimental data.

The evaluation of PIOR scales was carried out in all experiments in parallel with use of the Cooper Harper scale (PR). The comparison of the PIOR and PR ratings shown on fig. 3.7 demonstrates good correlation between the ratings. The boundary of the first level (PR=3.5) corresponds to rating PIOR=2, and the boundary of the second level PR=6.5 corresponds to rating PIOR=3-4 (3.5 in average). These results are close to the LAHOS results taken from [5] and shown on fig. 3.8. The boundaries of parameters r , $\Delta\varphi_P$ corresponding to the PIOR rating are shown in fig. 3.9. Their usage allowed us to predict PIO tendency. The excellent accordance between the ranges of equal ratings and parameters r and $\Delta\varphi_P$ measured for all 23 Neal-Smith configurations and all 25 LAHOS configurations was received owing to the following rules for determining the pilot workload parameter $\Delta\varphi_P$:

1. The pilot phase characteristics have to be evaluated for investigated configuration and for optimal aircraft dynamics (φ_P and φ_P^{opt} consequently).

2. The difference $\Delta\varphi_P = \varphi_P - \varphi_P^{opt}$ in frequency range $\omega_C + \omega \left| \varphi = -180^\circ \right.$ had to be analyzed to define the maximum value of $\Delta\varphi_P$. In general, it can be $\Delta\varphi_P$ of different sign: $\Delta\varphi_P^+$ and $\Delta\varphi_P^-$.

3. Both values $\Delta\varphi_P^+$ and $\Delta\varphi_P^-$ are considered as workload parameters.

4. If these values belong to the ranges of different pilot rating levels, it has to remain at the value corresponding to the level of worse pilot rating.

This rule can be recommended for experimental research in determining of requirements for handling qualities.

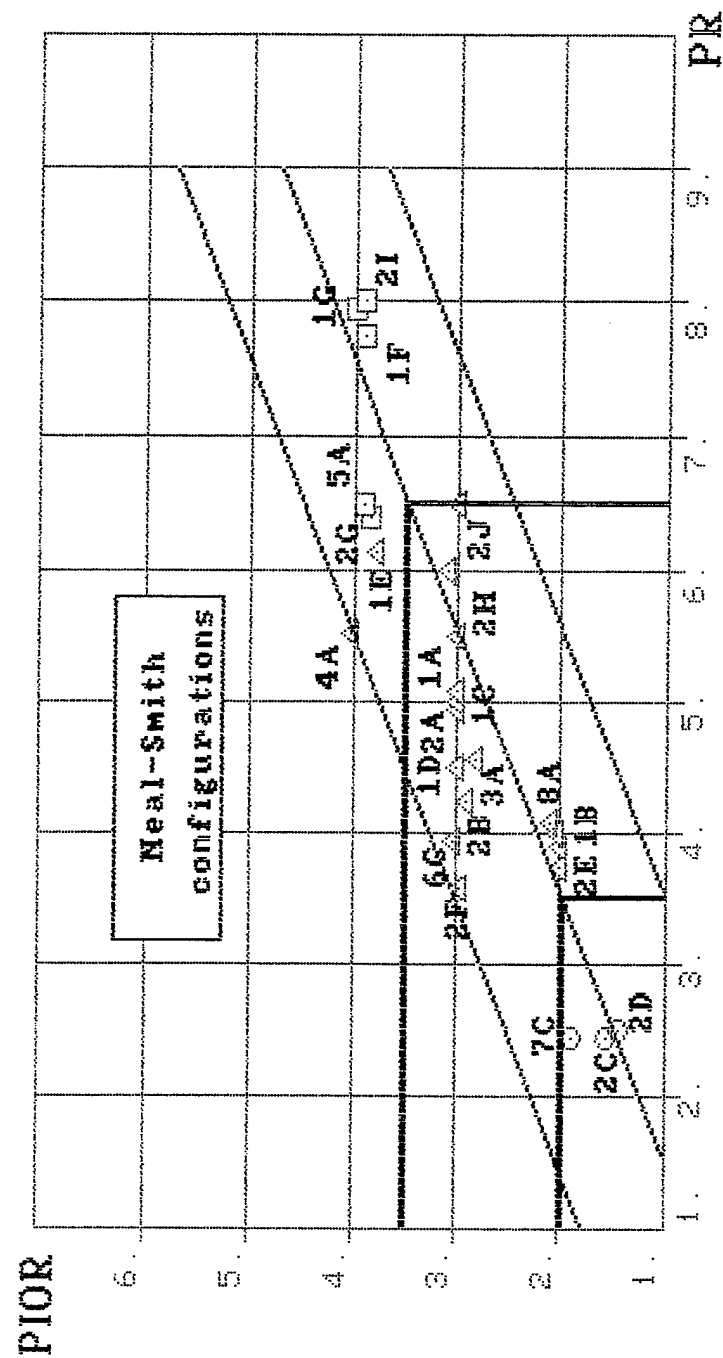


Fig.3.7 The correlation between PIOR and PR

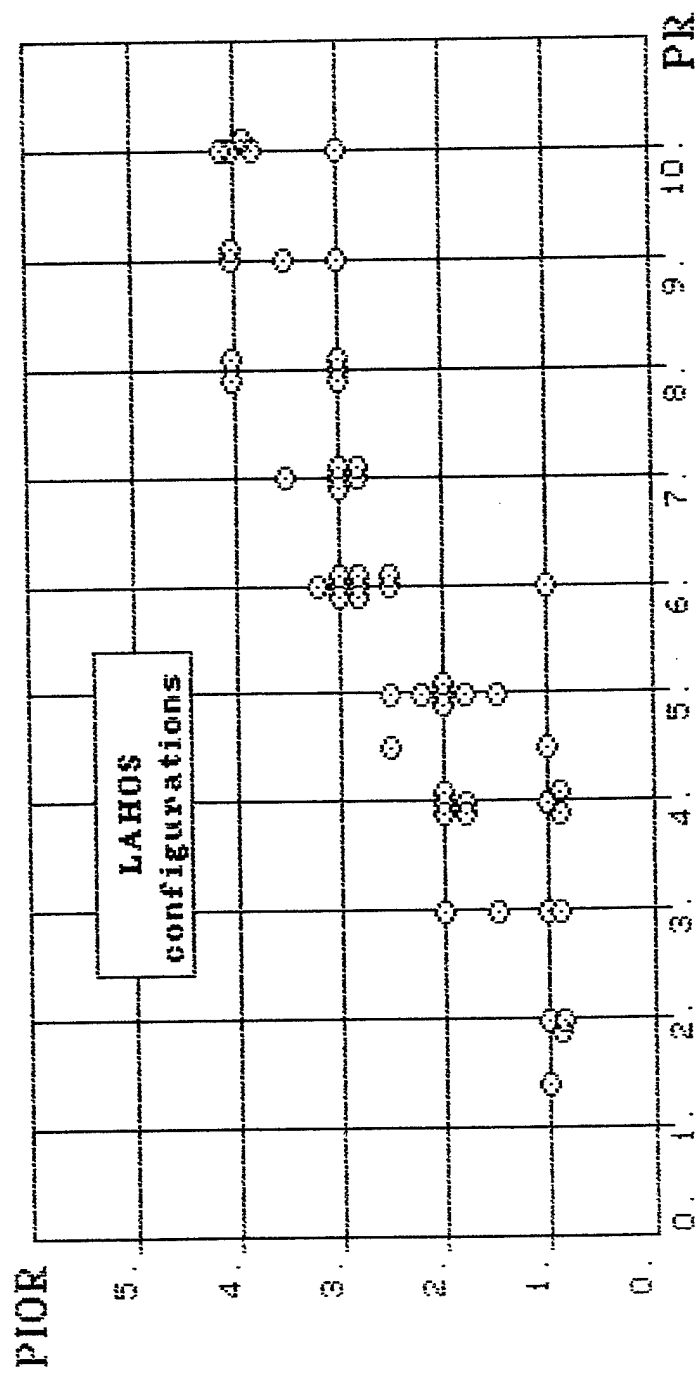


Fig. 3.8. The correlation between PIOR and PR (from [5]).

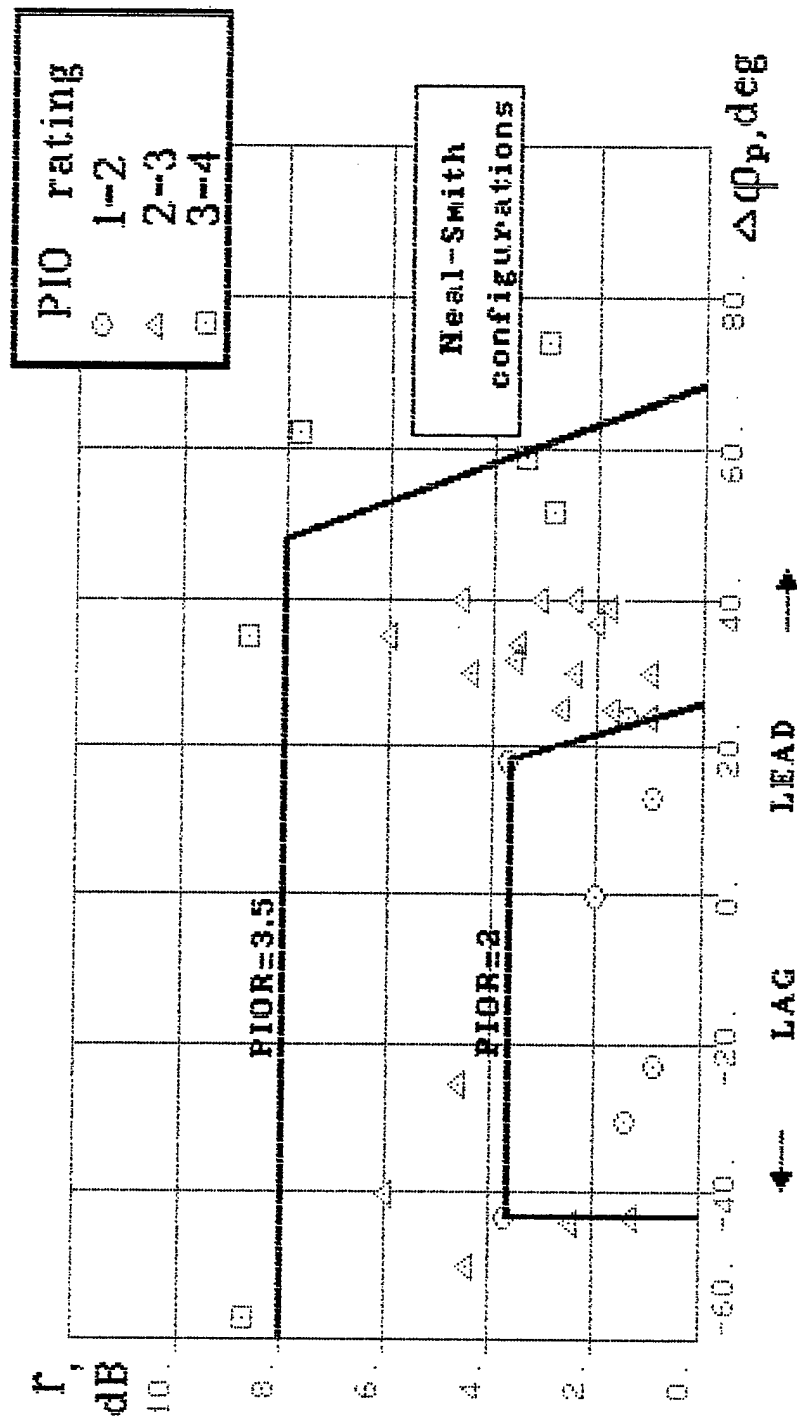


Fig. 3.9. The criteria for PIO tendency.

4.0 THE DEVELOPMENT OF CRITERIA FOR PREDICTION OF PIO TENDENCY

The experimental research discussed in chapter 3 allowed us to measure directly the resonance peak, pilot phase correction parameter $\Delta\varphi_P$, and use them to define the ranges of parameters "r" and " $\Delta\varphi_P$ " corresponding to the levels of pilot rating. Availability of such criteria allows us to evaluate handling qualities at least for the pitch tracking task for the conditions close to the conditions used in the considered research

$$(d = \pm 0.85 \text{ sm}; S_{ii}(\omega) = \frac{K^2}{(\omega^2 + \omega_i^2)^2}; \omega_i = 0.5 \text{ rad/sec}; \sigma_i = 2 \text{ deg}).$$

The possibility of using the criteria for any piloting task requires investigating the influence of the input spectral density parameters and controlled element dynamics corresponding to the investigated task on the boundary of criteria ranges. The results of such investigation will allow us to find the more general decision of the handling qualities requirement task.

Except for the boundaries of parameters r and $\Delta\varphi_P$, a criteria requires that the procedure for their determination was defined. In chapter 3 the experimental approach to the determination of these parameters was demonstrated. It includes the developed MAI PVL methods, algorithms, and software for analysis of pilot and pilot-vehicle closed-loop system characteristics using the workstation, ground-based, and in-flight simulators.

The second way is determining criteria parameters r, $\Delta\varphi_P$ based on mathematical modeling of pilot characteristics. One of the versions was offered by Neal and Smith [4]. They used the crossover model of pilot describing function, proposed several requirements on standard characteristics of closed-loop system parameters (frequency ω_{BW} and droop in its amplitude ratio), on pilot describing function $W_P = K_P e^{-0.3j\omega}$, and finally developed the specific procedure for calculation of parameters r and $\Delta\varphi_P = \varphi_P - 0.3\tau\omega$. The parameters φ_P and $\Delta\varphi_P$ are calculated at the frequency ω_{BW} . The comparison of this approach and experimental results demonstrates the significant discrepancy in defined parameters and boundaries of handling qualities (especially for the boundary corresponding to the second level of pilot ratings). It is connected with the limited possibilities of the model used and is not allow to predict the influence of other variables except the controlled element dynamics. This brought about the task of developing the procedure which has good predictable potentialities. Therefore, the MAI PVL developed structural approach and approach based on the well-known pilot optimal control model were offered for use.

4.1 THE PREDICTION OF PIO TENDENCY AND REQUIREMENTS FOR HANDLING QUALITIES BASED ON THE STRUCTURAL APPROACH

In mathematical modeling based on the structural approach, the models of pilot response characteristics and remnant whose parameters are defined by the special rules are given. In the MAI PVL the procedure was developed for optimization of pilot characteristic models based on minimization of variance of error (σ_e^2). This procedure allows us to use the different levels of complexity of pilot describing function. One of them is the simplest crossover model

$$W_p = K_p \frac{T_L j\omega + 1}{T_I j\omega + 1} e^{-j\omega\tau} \quad (4.1)$$

The choice of K_p, T_L, T_I can be made by optimization of the variance error. This procedure requires one to induce the remnant power spectral density. For its definition, perception of error and its derivative are accompanied by the noises \tilde{n}_e and $\tilde{n}_{\dot{e}}$ having the multiplicative nature.

Their spectral densities are equal:

$$S_{\tilde{n}_e \tilde{n}_e} = \pi K_{n_e} \sigma_e^2 \text{ and } S_{\tilde{n}_{\dot{e}} \tilde{n}_{\dot{e}}} = \pi K_{n_{\dot{e}}} \sigma_{\dot{e}}^2.$$

An effect of distribution of pilot's attention between the different tasks or indicators can be considered with the help of coefficient f_i - which is called the fraction of attention. In that case

$$K_{n_e} = K_{n_{ex}} \frac{P_O}{f_i} \text{ and the equation for remnant spectral density } S_{n_e n_e} \text{ is the}$$

following:

$$S_{n_e n_e} = \frac{\pi P_O}{f} \frac{\sigma_e^2 + \sigma_{\dot{e}}^2 T_L^2}{1 + T_L^2 \omega^2} \quad (4.2)$$

It corresponds to the equation received in [20] and considers the factor of distribution of attention. The effect of threshold or permissible interval for error, d can be taken into account by a different way. This is done in [21] with help of the equivalent coefficient:

$$N = 1 - \text{erf}(z), \text{ where} \quad (4.3)$$

$$\text{erf}(z) = \frac{2}{\sqrt{\pi}} \int_0^z e^{-y^2} dy, \quad z = \frac{a_e}{\sqrt{2}\sigma_e},$$

a_e is the threshold. When the permissible interval of error exists, $a_e \cong d$. This method of modeling the permissible level of error leads to the following equation of model for remnant spectral density

$$S_{n_e n_e} = \frac{\pi P_o}{f} \frac{\sigma_e^2 / N_e^2 + \frac{\sigma_{\dot{e}}^2}{N_e^2} T_L^2}{1 + T_L^2 \omega^2} \quad (4.4)$$

The considered factor can be modeled another way, by inducing the "residual" remnant $S_{\tilde{n}_e \tilde{n}_e}^* = K_{n_e} \pi \sigma_{e_o}^2$ and $S_{\tilde{n}_e \tilde{n}_e} = K_{n_e} \pi \sigma_{e_o}^2$. It leads to the following transformation of equation (4.2):

$$S_{n_e n_e} = K_{n_e} \pi \frac{\sigma_e^2 + T_L^2 \sigma_{\dot{e}}^2}{1 + T_L^2 \omega^2} + K_{n_e} \pi \frac{\sigma_{e_o}^2 + \sigma_{e_o}^2 T_L}{1 + T_L^2 \omega^2} \quad (4.5)$$

In that case the variance $\sigma_{e_o}^2$ is defined by interval d , $\sigma_{e_o}^2 = d^2$

Peculiarity in calculating equations (4.4) and (4.5) is their dependence from variance of errors (σ_e^2 and $\sigma_{\dot{e}}^2$) which are unknown beforehand. This problem can be decided by some transformation in (4.4) and (4.5). These transformations were carried out below for cases

$N_e = N_{\dot{e}}$ and when $\sigma_{e_o}^2 = 0$. For single-loop systems

$$\sigma_e^2 = \sigma_{e_i}^2 + \sigma_{e_n}^2, \text{ where} \quad (4.6)$$

$\sigma_{e_i}^2$ is a variance of error signal correlated with input signal

$$\sigma_{e_i}^2 = \frac{1}{2\pi} \int_0^\infty S_{ii}(\omega) \left| \frac{1}{1 + W_{OL}} \right|^2 d\omega,$$

and $\sigma_{e_n}^2$ is a variance of error signal correlated with remnant

$$\sigma_{e_n}^2 = \frac{1}{2\pi} \int_0^\infty S_{n_e n_e} \left| \frac{W_{OL}}{1 + W_{OL}} \right|^2 d\omega.$$

In the general case, the effects of threshold and residual remnant can be combined. For the considered case, the equation for remnant power spectral density is the following:

$$S_{n_e n_e} = \frac{K^2}{1 + T_L^2 \omega^2}.$$

The coefficient K^2 here is the following:

$$K^2 = \frac{K_{n_e}}{N_e^2} \left[\sigma_{e_i}^2 + T_L^2 \sigma_{e_i}^2 + \sigma_{e_n}^2 + T_L^2 \sigma_{e_n}^2 + \sigma_{e_o}^2 \right],$$

and after transformations

$$K^2 = \frac{\sigma_{e_i}^2 + T_L^2 \sigma_{e_i}^2 + \sigma_{e_o}^2 K_{n_e} \int_0^\infty |W_{CL}|^2 d\omega}{1/K_{n_e} N_e^2 - \int_0^\infty |W_{CL}|^2 d\omega}$$

Taking into consideration the equation (4.6) has the form

$$\begin{aligned} \sigma_e^2 = \sigma_{e_i}^2 + & \left[\frac{1 + T_L^2 (\sigma_{e_i}^2 / \sigma_{e_i}^2) + (\sigma_{e_o}^2 / \sigma_{e_i}^2) K_{n_e} \int_0^\infty |W_{CL}|^2 d\omega}{1/K_{n_e} N_e^2 - \int_0^\infty |W_{CL}|^2 d\omega} + \right. \\ & \left. + \sigma_{e_o}^2 K_{n_e} \int_0^\infty \left| \frac{W_{CL}}{1 + T_L \omega^2} \right|^2 d\omega \right] \end{aligned} \quad (4.7)$$

The right item of this equation is a variance σ_e^2 . Because it has to be less than infinity $\sigma_{e_n}^2 < \infty$, the following condition has to take place:

$$1/K_{n_e} N_e^2 - \int_0^\infty |W_{CL}|^2 d\omega > 0, \quad (4.8)$$

The last is called σ_1 -criteria [1] defined the permissible range of parameters supplying the stability of the single loop pilot-vehicle system. For the case where $W_{OL} = \frac{\omega_c}{j\omega} e^{-j\omega\tau}$ and

using the first order Pade approximation for $e^{-j\omega\tau}$ it is possible to get the following equation

for maximum $\omega_{\tilde{H}}^*$:

$$\begin{aligned} \omega_c^* &= -(\bar{r} + 1) + \sqrt{4\bar{r} + (\bar{r} + 1)^2} \\ \omega_c^* &= \omega_c \tau, \bar{r} = r / K_{n_e} N_e^2 \pi. \end{aligned} \quad (4.9)$$

It is easy to show that ω_c^* is less than 2, where "2" is the maximum value defined by the stability of the system according to Hurwitz criteria. Analysis of parameters defined in equation (4.9) allows us to conclude that an increase of τ, K_{n_e} (for example because of sharing of attention or effect of threshold) leads to a decrease of crossover frequency ω_c . It is also possible to get σ_1

- criteria for multiloop systems. For this case equation (4.6) transforms to the following matrix equation:

$$D_e = D_{e_i} + D_{e_n},$$

where D_{e_i} is a diagonal matrix with elements which are the integrals from the elements of matrix $[\Phi_e S_{ii} \Phi_e^T]$,

D_{e_n} is a diagonal matrix with elements defined by the integrals from the elements of matrix $[\Phi S_{n_e n_e} \Phi^T]$,

where S_{ii} and $S_{n_e n_e}$ are diagonal matrixes of input and remnant power spectral densities,

Φ and Φ_e are matrixes with elements W_{CL} and $\frac{1}{1+W_{CL}}$ consequently.

Taking it into consideration, this equation has the following matrix form:

$$D_e = D_{e_i} + A_1 D_e + B_1 D_{\dot{e}}, \quad (4.10)$$

where A_1 is a diagonal matrix with elements defined the integrals from elements of matrix $[\Phi W_{n_e} \Phi^T]$,

B_1 is a diagonal matrix with elements defined by the integrals from elements of matrix $[\Phi T_L W_{n_e} T_L^T \Phi^T]$,

where W_{n_e} is a diagonal matrix with elements

$$W_{n_e}^m = \frac{P_O \pi}{f_m} \frac{1}{1 + \omega^2 T_{Lm}^2},$$

m is the number of loop,

T_L is a vector whose elements are the pilot lead time T_{Lm} in each loop.

The equation for the diagonal matrix $D_{\dot{e}}$ whose elements are the variances of the error derivatives is the following:

$$D_{\dot{e}} = D_{\dot{e}_i} + A_2 D_e + B_2 D_{\dot{e}}, \quad (4.11)$$

where $D_{\dot{e}}$ is a diagonal matrix whose elements are the integrals from elements of matrix

$$[\omega \Phi_e S_{ii} \Phi_e^T \omega^T],$$

ω is a vector $[\omega 0]^T$,

A_2 is a matrix whose elements are the integrals from elements of matrix

$$[\omega \Phi W_{ne} \Phi^T \omega^T],$$

B_2 is a matrix whose elements are the integrals from elements of matrix

$$[\omega \Phi T_L W_{ne} T_L^T \Phi^T \omega^T].$$

Combining equations (4.10) and (4.11) gives the following matrix equation for determination elements of matrixes D_e and $D_{\dot{e}}$

$$\begin{vmatrix} E - A_1 & -B_1 \\ -A_2 & E - B_2 \end{vmatrix} \begin{vmatrix} D_e \\ D_{\dot{e}} \end{vmatrix} = \begin{vmatrix} D_{e_i} \\ D_{\dot{e}_i} \end{vmatrix}, \quad (4.12)$$

where E is a unit matrix.

The requirement defining the stability of the multiloop system is the following:

$$\sigma_1 = \begin{vmatrix} E - A_1 & -B_1 \\ -A_2 & E - B_2 \end{vmatrix} > 0 \quad (4.13)$$

It is σ_2 -criteria for the multiloop case which allows us to define the permissible range of pilot-vehicle system parameters which guarantee its stability.

For dual-loop pilot-vehicle system (fig. 2.11) it is assumed that the equation for models of pilot and pilot-vehicle describing functions and remnant power spectral densities are the same:

$$S_{n_{e1(2)}} n_{e1(2)} = \frac{0.01\pi}{f_{1(2)}} \frac{\sigma_{\dot{e}1(2)}^2 + \sigma_{\dot{e}1(2)}^2 T_{L1(2)}^2}{1 + T_{L1(2)}^2 \omega^2},$$

$$W_{p_{1,2}} = W_{p_{1(2)}} W_{AA},$$

$$W_{p_{1(2)}} = K_{p_{1(2)}} \frac{T_{L1(2)}^{j\omega+1}}{T_{I1(2)}^{j\omega+1}},$$

$$W_{AA} = \frac{1}{(1 + j\omega T_i)(1 + j\omega T_n)};$$

$$f_1 = f, f_2 = 1 - f_1,$$

1,2 - number of loop.

The equation (4.13) in this case transforms into the following:

$$\sigma_2 > 1 - (A_1 + B_2 + C_3 + D_4)$$

where

$$A_1 = \frac{1}{f} 0.01 \int_0^\infty \left| \frac{N_{L_1} K_{D_1} N_{AA} N_1 N_2 D_{L_1}}{D_{ne_1} A^*} \right|^2 d\omega$$

$$B_2 = \frac{1}{f} T_{L_2}^2 0.01 \int_0^\infty \left| \frac{N_{L_1} K_{D_1} N_{AA} N_1 N_2 D_{L_2}}{D_{ne_1} A^*} j\omega \right|^2 d\omega,$$

$$C_3 = \frac{1}{1-f} 0.01 \int_0^\infty \left| \frac{N_{L_2} K_{D_2} N_{AA} N_2 D_{c_1} D_{L_1}}{D_{ne_2} A^*} \right|^2 d\omega,$$

$$D_4 = \frac{1}{1-f} T_{L_2}^2 0.01 \int_0^\infty \left| \frac{N_{L_2} K_{D_2} N_2 N_{AA} D_{c_1} D_{L_2}}{D_{ne_2} A^*} j\omega \right|^2 d\omega,$$

$$A^* = D_{L_1} D_{L_2} D_{AA} D_{c_1} D_{c_2} + K_{D_1} N_{L_1} N_{AA} N_{c_1} N_{c_2} D_{L_2} + \\ + K_{D_2} N_{L_2} N_{AA} N_{c_2} D_{L_1} D_{c_1}$$

$N(\cdot)$ and $D(\cdot)$ are a numerator and a denominator of corresponding frequency response

$$\text{characteristic } W(\cdot) = \frac{N(\cdot)}{D(\cdot)}.$$

$D_{ne_{1,2}}$ - the equation for denominator of the filter for remnant spectral density. In our case

$$D_{ne_{1,2}} = 1 + T_L j\omega.$$

K_{D_1} and K_{D_2} - display gain coefficients in inner and outer loops.

Application of Structural Approach to the Evaluation of Handling Qualities.

The algorithms for mathematical modeling of pilot control response characteristics combined with the procedure of parameter optimization according to criteria minimum variance σ_e^2 are allowed to choose the pilot's model parameters and to be used for evaluation of handling qualities. This was done for some Neal-Smith configurations. The mathematical modeling was carried out for pitch tracking tasks for both ways of calculation of the permissible interval "d". As an example, shown are the results of modeling for $d = \pm 1.8$ sm in figs. 4.1, 4.2. They demonstrate that the modeling of the permissible interval "d" by increase of equivalent gain coefficient N_e allows us to get the tendency in change of frequency response characteristics corresponding to the experimental results (fig. 4.1). The other way of modeling the investigated factor was not in accordance with experimental results. For example the change of interval "d" did not lead to the change of pilot describing function (fig. 4.2) which doesn't correspond to experiments. As for quantitative accordance with experiments, we need to continue research in developing mathematical models of pilot control response characteristics by using Hess's pilot model [22]. In future investigations this suggestion will be checked.

4.2 APPLICATION OF THE OPTIMAL PILOT BEHAVIOR MODEL FOR PREDICTION OF PIO TENDENCY.

The core of the Optimal Control Model (OCM) for the human operator is the assumption that a highly-trained human operator acts as an optimal controller within psychophysiological limitations [24]. OCM is widely used in many research efforts for different manual control tasks. In particular OCM was used for design of display systems [25], for estimation pilot workload [21], and for predicting pilot rating [26]. OCM was used for investigation PIO tendency also [15]. However, absence of experimental data didn't allow the development of mathematical modeling with well-grounded parameters.

In the current work the use of experimental data, described in chapter 3, gave the possibility of getting necessary OCM parameters. It was used for calculating pilot and pilot-vehicle system parameters (resonance peaks, pilot phase compensation, variances of signals, etc.), with goal to define the potential of the model in predicting pilot-vehicle system characteristics. OCM is based on modern control theory and its computer implementation requires extensive use of numerical methods.

4.2.1 The Structure of OCM and Description of it's Computer Implementation

OCM assumes that the system dynamics can be described in following form:

$$\dot{X} = AX + BU + E\varpi, \text{ where:}$$

X - is the vector described the state of vehicle;

U - the vector of pilot control inputs;

ϖ - a vector of white driving noise processes with intensity V_{ϖ} .

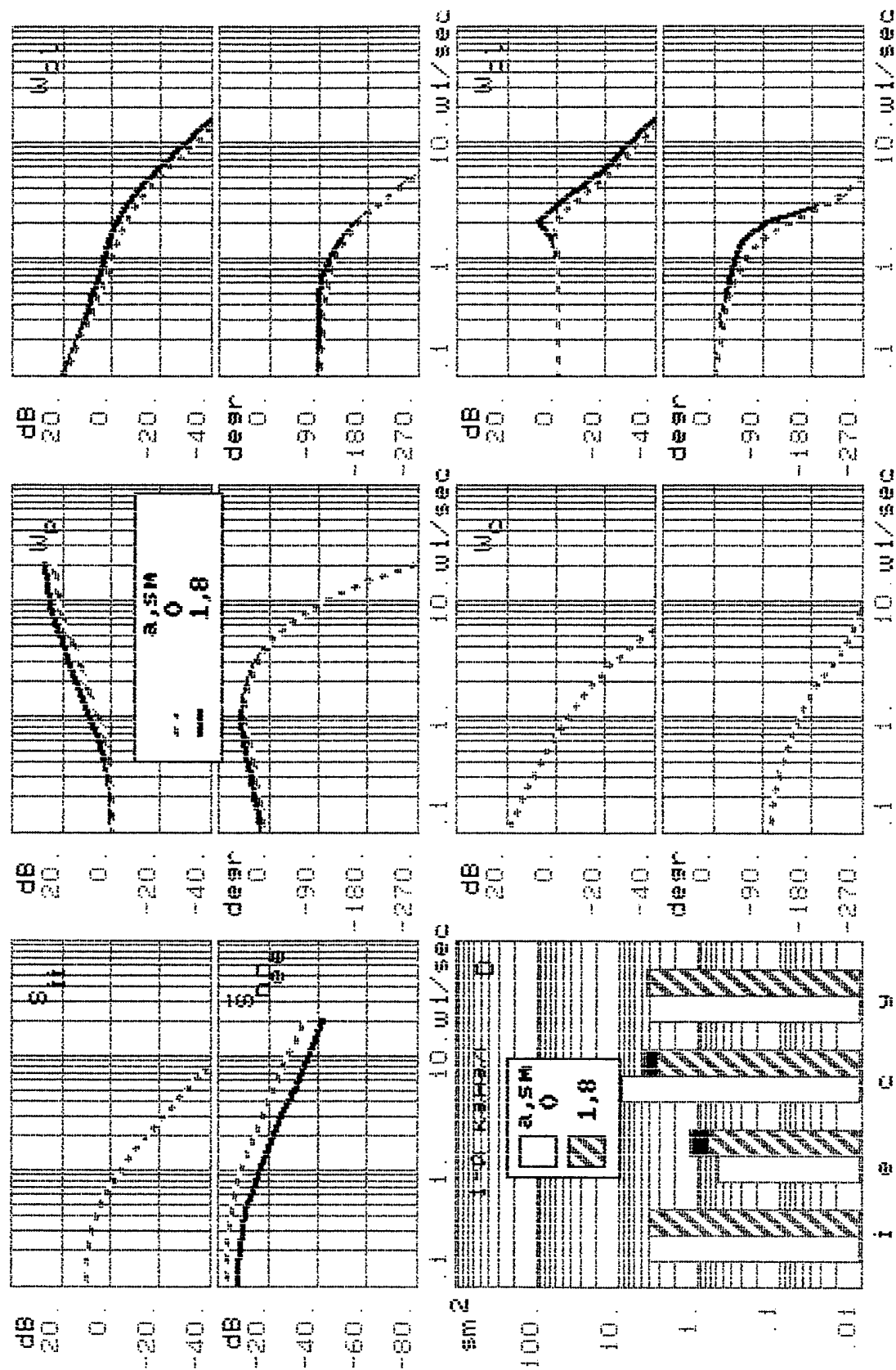


Fig. 4.1. The modeling of effect of permissible interval d by the threshold $a=d$.

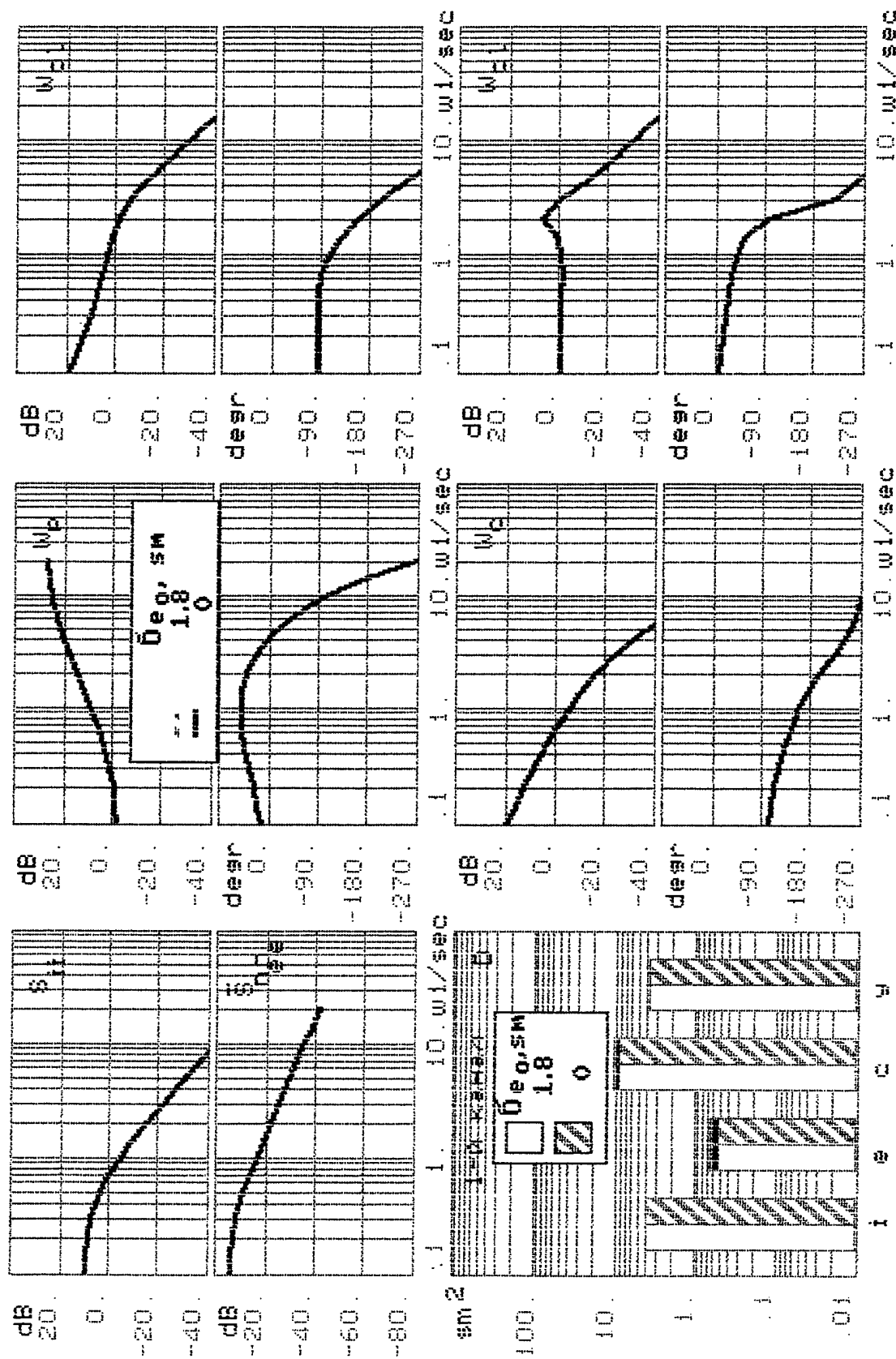


Fig. 4.2. The modeling of effect of permissible interval d by the residual remnant.

The command signal has been used as an input disturbance signal. It was modeled as a random Gaussian white noise process $\overline{w}(t)$ with intensity $V_{\overline{w}} = 0.647$, passed through the second order shaping filter with transfer function $W_f = \frac{K}{(s + \omega_i)^2}$ and with parameters

$\omega_i = 0.5 \text{ rad/sec}, \sigma_i^2 = 4 \text{ sm}^2$. The dynamics of this filter is included in matrices A.

It is assumed that the pilot controls the vehicle to get the minimum of the following cost functional:

$$J = \lim_{T \rightarrow \infty} \left\{ \frac{1}{T} \int_0^T (Q_y \sigma_y^2 + Q_u \sigma_u^2 + g \sigma_{\dot{u}}^2) dt \right\}$$

where Q_y, Q_u, g - weighting coefficients. The weighting coefficient Q_y is the vector: $Q_y \begin{bmatrix} Q_{\theta_e}, Q_{\theta_{\dot{e}}} \end{bmatrix}$, and Q_u, g are the scalars.

The display variables are assumed to be linear combinations of the state and control variables and are given by the "display vector":

$$Y(t) = CX(t) + DU(t)$$

The pilot perceptual model transfers displayed variables Y into delayed "noisy" perceived variables Y_p . It is described by following equation:

$$Y_p = Y(t - \tau) + V_y(t - \tau), \text{ where}$$

τ - is a delay in perception;

V_y - is an observation noise vector.

The observation noise was modeled by a white noise source $\vartheta_y(t)$ with intensity V_{y_i} where

$$V_{y_1} = \frac{\rho_{y_1}}{f_1} \frac{\sigma_{y_1}^2}{N_{y_1}}, \text{ where}$$

ρ_{y_1} - observation noise ratio;

f_i - the fraction of attention shared to the considered task

$$0 \leq f_i \leq 1;$$

N_y - function modeled the pilot perceptual threshold.

The resulting controller action is modeled by a combination of three elements: Kalman Bucy Filter (KBF), a Linear Predictor (LP), and Linear Quadratic Regulator (LQR).

The LQR problem is solved by augmentating the input with an integrator $X_0 = \begin{pmatrix} X \\ U \end{pmatrix}$:

$$\dot{X}_0 = A_0 X_0 + B_0 \mu, \text{ where}$$

$$\mu = \dot{u}$$

$$X_0 = \begin{pmatrix} X \\ U \end{pmatrix}; A_0 = \begin{pmatrix} A & B \\ 0 & 0 \end{pmatrix}; B_0 = \begin{pmatrix} 0 \\ I \end{pmatrix}.$$

The solution is $\mu = -L X_0$

$$L = g^{-1} B_0' K_0,$$

K_0 - solution of the Riccati equation

$$A_0' K_0 + K_0 A_0 + Q_0 - K_0 B_0 g^{-1} B_0' K_0 = 0.$$

The weighting coefficient g depends on neuromotor lag T_n . It is chosen to satisfy the expression $L_2 = T_n^{-1}$, where

$$L = (L_1, L_2).$$

The KBF/predictor problem can be solved if vector X will be augmented by control variable U :

$$X_0 = \begin{pmatrix} X \\ U \end{pmatrix} \quad \dot{X}_0 = A_1 X_0 + B_1 U_a + \omega_1,$$

$$\omega_1 = \begin{pmatrix} \omega \\ \vartheta_{Ua} \end{pmatrix}; A_1 = \begin{pmatrix} A & B \\ 0 & -L_2 \end{pmatrix}; B_1 = \begin{pmatrix} 0 \\ L_2 \end{pmatrix}; C_1 = (CD)$$

$$W_1 = \begin{pmatrix} EV\omega E' & 0 \\ 0 & L_2 V_{Ua} L_2' \end{pmatrix}.$$

The white noise source $\omega_1(t)$ with intensity W_1 includes the motor noise $\vartheta_{Ua}(t)$.

The motor noise is modeled as a white noise source with intensity $V_{Ua} = \rho_{ou} \sigma_{ua}$ and is added to output signal U_a before lag $1/(T_n p + 1)$ described the neuro-muscular system.

The Kalman filter generates a least mean-squared estimate, $p(t)$ of the vector $X_0(t - \tau)$:

$$\dot{p}(t) = A_1 p(t) + H_1 [Y(t) - C_1(t)] + B_1 U_a$$

$$H_1 = \Sigma_1 C_1^1 V_y^{-1}$$

The error covariance matrix Σ_1 satisfies

$$A_1 \Sigma_1 + \Sigma_1 A_1^1 + N_1 - \Sigma_1 C_1^1 V_y^{-1} C_1 \Sigma_1 = 0.$$

The predictor generates the best estimation of the current delayed system state by:

$$\dot{\xi}(t) = A_1 \xi(t) + B_1 U_a(t), \hat{X}_0 = \xi(t) + e^{A_1 \tau} [p(t) - \xi(t - \tau)].$$

$$U_a = -L^* \hat{X}_0, L^* = (L_2^{-1} L_1 0)$$

Fig. 4.3 shows the full structure diagram of optimal model.

The OCM allows us to get the following pilot-vehicle system characteristics: mean square errors of any state, control and display variables, value of performance index J , and open- and closed-loop frequency performance. In the current work all these characteristics were calculated by the computer program "OC.MODEL", developed in the MAI PVL - implementation of optimal pilot behavior model. "OC.MODEL" is a complex of 60 computer subroutines; each of which solves its own numerical task. The low level numerical routines which are required for the "OC.MODEL" are:

- block matrix manipulations; - matrix exponential;
- Lyapunov and Riccati equation;
- "erfc" function.

Part of the programs were developed in MAI PVL and part of them are taken from the international computer library's IMSL and SSP. The "OC.MODEL" was tested by using the examples investigated in other research. One such tests studied in [24] is shown below. Here, the control element and driving noise dynamics are:

$$W_c = 1/s; \quad W_f = 3/(s+2);$$

$$Y_e = W_c [U + W_f \omega].$$

The model parameters from [24] are presented in table 4.1. The same parameters were used in the "OC.MODEL".

Table 4.1

$V\omega$	τ	T_N	ρ_{oy_1}	ρ_{oy_2}	ρ_{ou}	f	a_{θ_e}	$a_{\dot{\theta}_e}$
1	0.15	0.1	0.01	0.01	0.003	1	0	0

The "OC.MODEL" results and data from [24] are presented in table 4.2. Their comparison demonstrates good accordance of results.

Table 4.2

	σ_e^2	$\sigma_{\dot{e}}^2$	σ_u^2	J	$\sigma_{u\dot{e}}$	σ_{ua}^2
Current Research	0.11796	3.0927	3.8628	0.1591	0.0017	4.78
Data from work[24]	0.11803	3.0830	3.8633	0.1592	0.0017	4.8

4.2.2 OCM Application to PIO Tendency Investigation

This was considered the compensatory task with the pitch angle command signal θ_n . So the display vector Y consists of two variables: error and its derivative

$$Y = [\theta_e, \dot{\theta}_e], \text{ where } \theta_e = \theta_c - \theta$$

The goals of investigation were:

1. The evaluation of potential of OCM for PIO tendency prediction.
2. Assessment OCM sensitivity to the task variables and, in particular, to permissible error value " $\pm d$ ".

1. The OCM parameters used in investigation are given in table 4.3.

Table 4.3

a_{θ_e} deg	$a_{\dot{\theta}_e}$ deg	f	ρ_{oy_1}	ρ_{oy_2}	ρ_{ou}	τ , sec	T_N , sec	Q_{θ_e}	$Q_{\dot{\theta}_e}$
0	0	1	0.01	0.01	0.003	0.25	0.1	1	0

where a_{θ_e} and $a_{\dot{\theta}_e}$ - observation thresholds for an error and its derivative;

f - fraction of attention;

ρ_{oy_1}, ρ_{oy_2} - observation noise ratios;

ρ_{ou} - motor noise ratio;
 τ - observation delay;
 T_N - neuromuscular lag;
 $Q_{\theta_e}, Q_{\dot{\theta}_e}$ - weighting coefficient for error and its derivative.

Observation and motor noise ratios $\rho_{oy_1}, \rho_{oy_2}, \rho_{ou}$ were chosen to achieve the best in accordance with experimental data. The chosen values correspond to the widely accepted values for these parameters.

The weighting coefficient Q_u is usually taken as zero, but in the current work it was stated that the better coincidence is achieved when Q_u is not equal to 0. The values of Q_u for each Neal-Smith and LAHOS investigated configuration are given in table 4.4. The weighting coefficient Q_u was chosen to achieve the best in accordance with experimental variance σ_u^2 .

As mentioned above, the weighting coefficient g was chosen in accordance with parameter T_n . As a result of mathematical modeling by means of the developed software, the frequency performance of the pilot-vehicle system and its parameters, in particular, resonance peak r , and the pilot phase compensation $\Delta\phi_p$, defined in chapter 3, were obtained. The resonance peak was

determined as a maximum amplitude value of closed loop frequency response: $r = \left| \frac{\theta}{\theta_c} \right|_{\max}$. The

standard pilot phase frequency response (SPPFR) corresponding to the optimal control dynamics (see Appendix B) was used to get the parameter $\Delta\phi_p$. The SPPFR was obtained in mathematical modeling and presented in fig. 4.4. Also shown are the experimental data. This figure shows good agreement between experimental results and modeling. The necessary pilot phase compensation, for each investigated configuration, was defined as a maximum deviation phase frequency response for this configuration from SPPFR.

Table 4.4

Configuration	1A	1B	1C	1D	1E	1F	1G
$Q_u, 1/sm^2$	0.06	0.03	0.26	0.57	0.27	0.14	0.1

Configuration	2A	2B	2C	2D	2E	2F	2G
$Q_u, 1/sm^2$	0.05	0.15	0	0.4	0.15	0.18	1.5

Configuration	2H	2I	2J	3A	4A	5A	6C
$Q_u, 1/sm^2$	0.3	0.05	0.15	0.3	1.15	0.06	0.51

Configuration	7C	8A	LAHOS	LAHOS
$Q_u, 1/sm^2$	0.75	0.51	0.0001	0.2

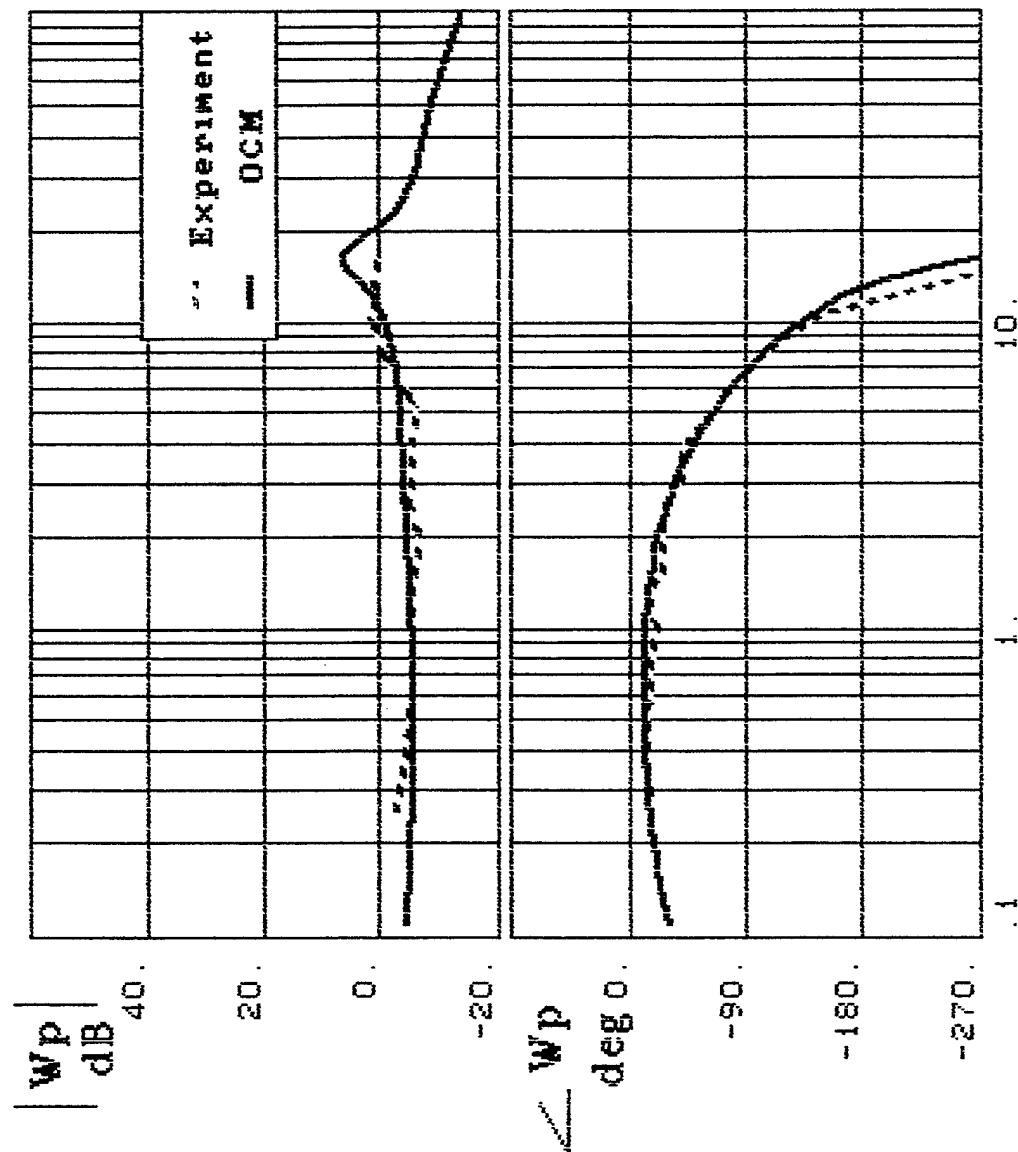


Fig. 4.4. Comparison of mathematical modeling and experimental results. Pilot frequency response corresponding to the optimal control dynamics.

The resonance peak values and pilot phase compensations for each of Neal-Smith and LAHOS configuration are presented in table 4.5.

The frequency characteristics of configuration 1B, 1D, 1E, 1F, 1G, 6C, LAHOS 1.4 are presented in figs. 4.5 - 4.11. They also demonstrate the accordance with experimental data presented here. The mathematical modeling results $r(\Delta\phi_p)$ are plotted in fig. 4.12. Also shown are the boundaries of PR levels obtained in chapter 3. This figure demonstrates good agreement between parameters r and $\Delta\phi_p$ received in experiments and in modeling except configuration 2C, 2G (figs. 4.13, 4.14).

It may be assumed that this disagreement was caused by the fact that not all OCM parameters correspond to the experimental data. Also, it leads to disagreement of integral characteristics. In particular, the data shown in table 4.6 demonstrate that the error and pilot's output signals variances received from modeling are very close to experimental.

Table 4.5

Configuration	1A	1B	1C	1D	1E	1F	1G
$\Delta\phi_p$, deg	47	41	47	34	53	64	70
r , dB	4.96	4.78	3.63	2.04	2.87	2.97	2.49

Configuration	2A	2B	2C	2D	2E	2F	2G
$\Delta\phi_p$, deg	-65	-55	-54	-37	48	56	78
r , dB	2.91	3.05	3.48	2.01	3.07	2.14	4.2

Configuration	2H	2I	2J	3A	4A	5A	6C
$\Delta\phi_p$, deg	49	85	47	-58	-51	72 (-68)	31
r , dB	3.03	4.68	1.06	1.7	-0.14	2.11	2.06

Configuration	7C	8A	LAHOS 1.4	LAHOS2.1 0
$\Delta\phi_p$, deg	-20	-45	103	97
r , dB	-0.26	1.4	5.4	4.4

Table 4.6

Configuration	Experiment				Model			
	σ_e	σ_{ω}	σ_u	σ_{ω}	σ_e	σ_{ω}	σ_u	σ_{ω}
2C	0.109	0.628	0.318	0.503	0.132	1.923	0.231	4.390
2G	0.363	0.943	0.372	0.788	0.267	1.63	0.378	9.78

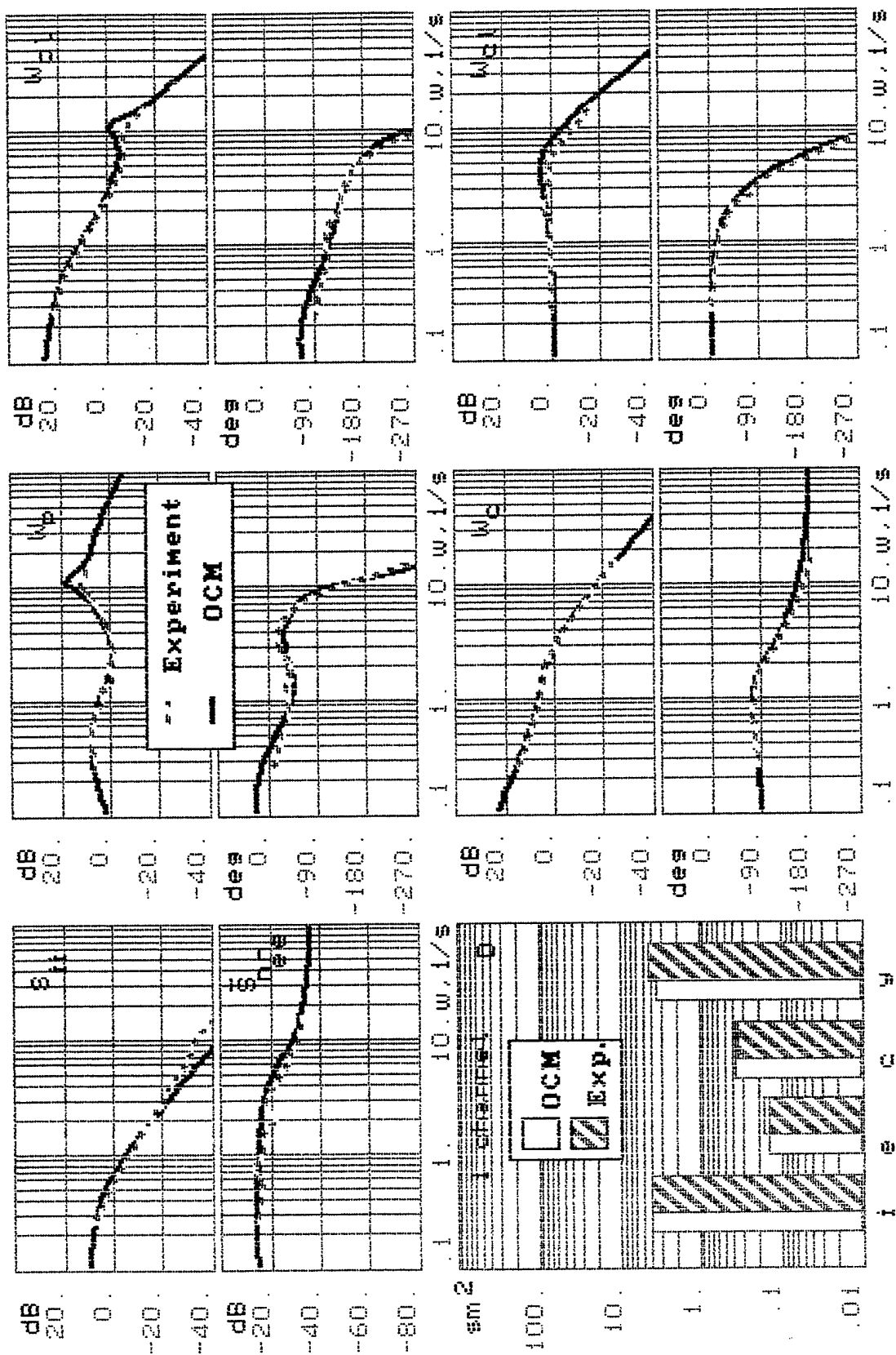


Fig. 4.5. Comparison of mathematical modeling and experimental result (conf. 1B).

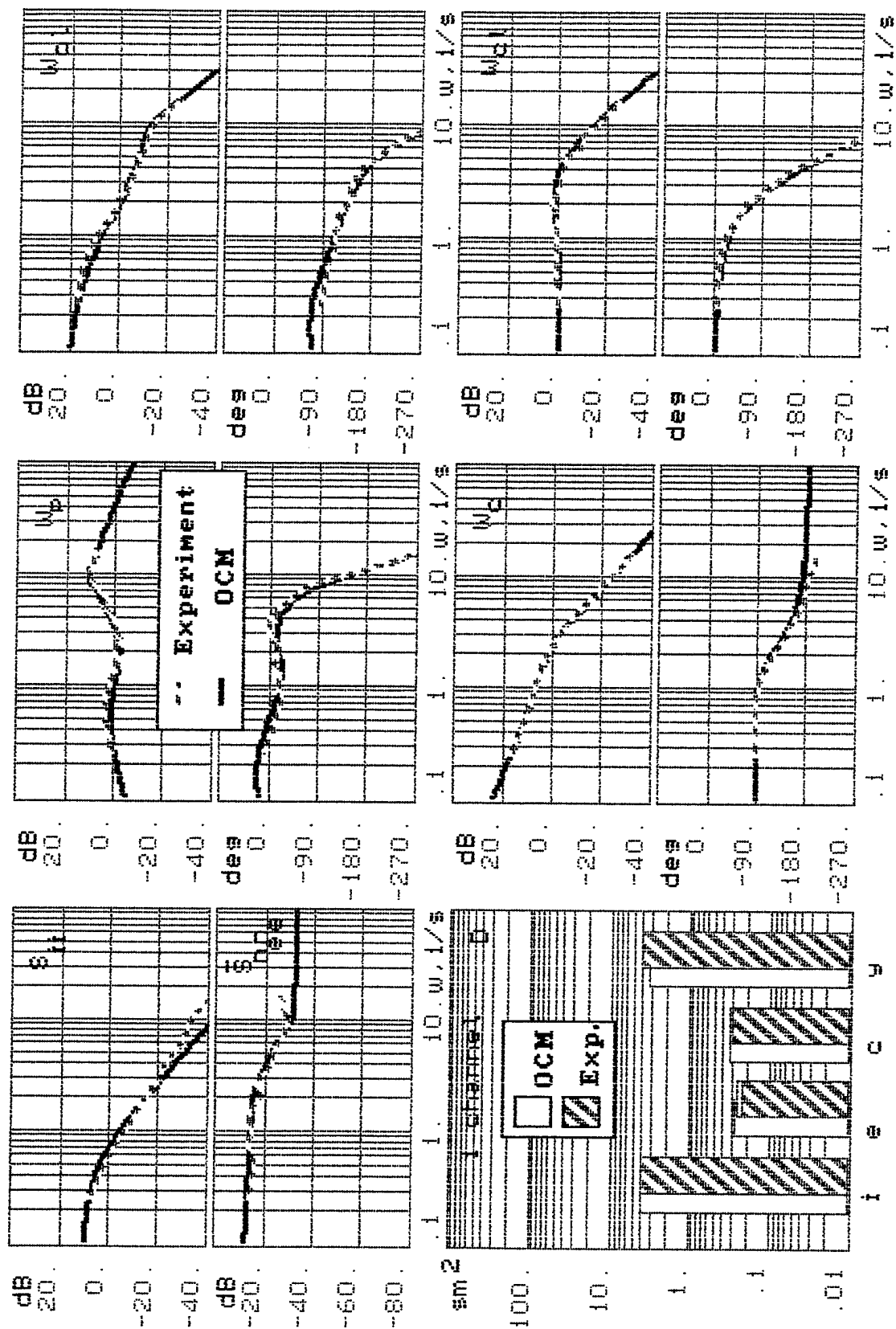


Fig. 4.6. Comparison of mathematical modeling and experimental result (conf. 1D).

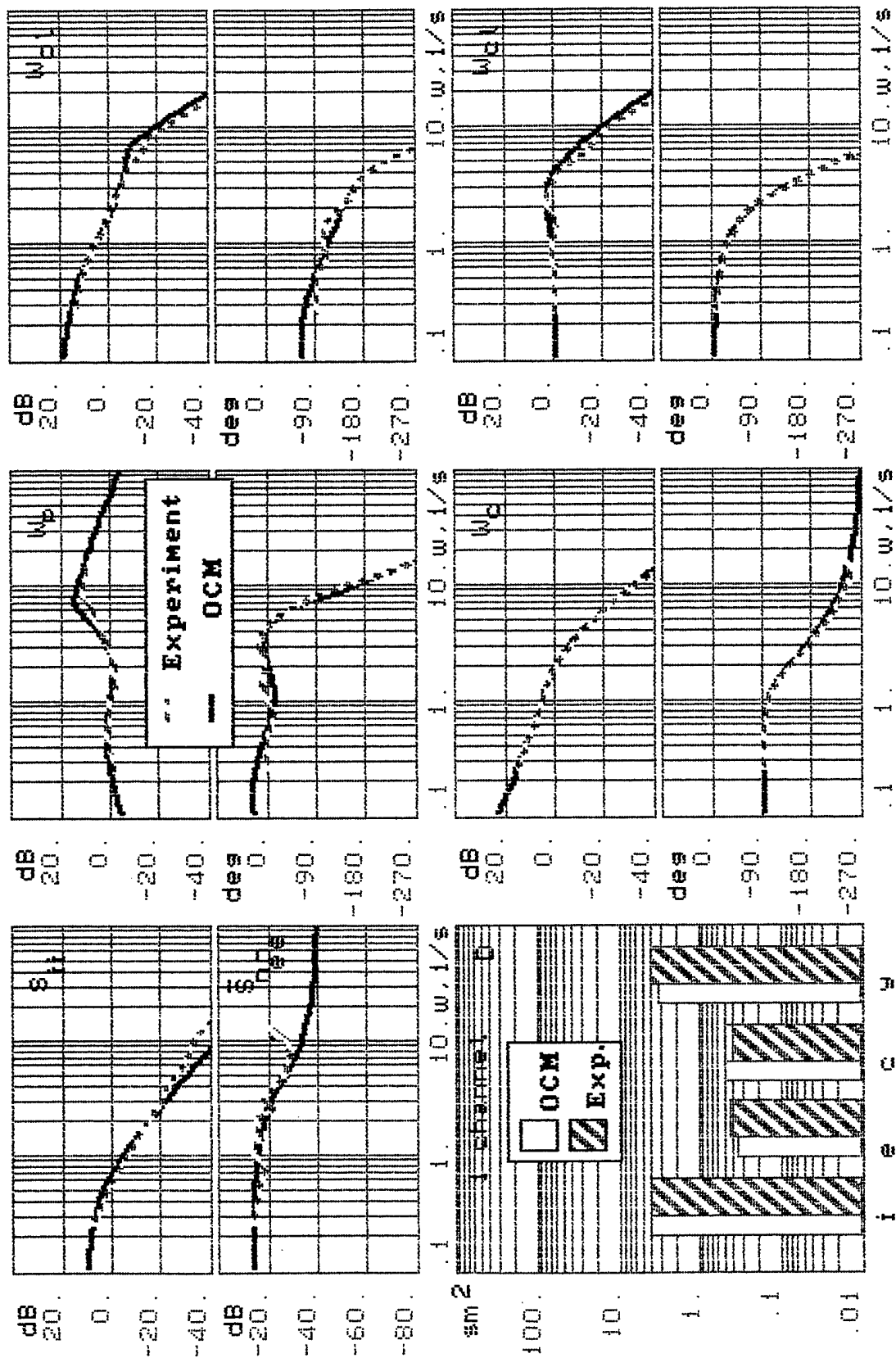


Fig. 4.7. Comparison of mathematical modeling and experimental result (conf. 1E).

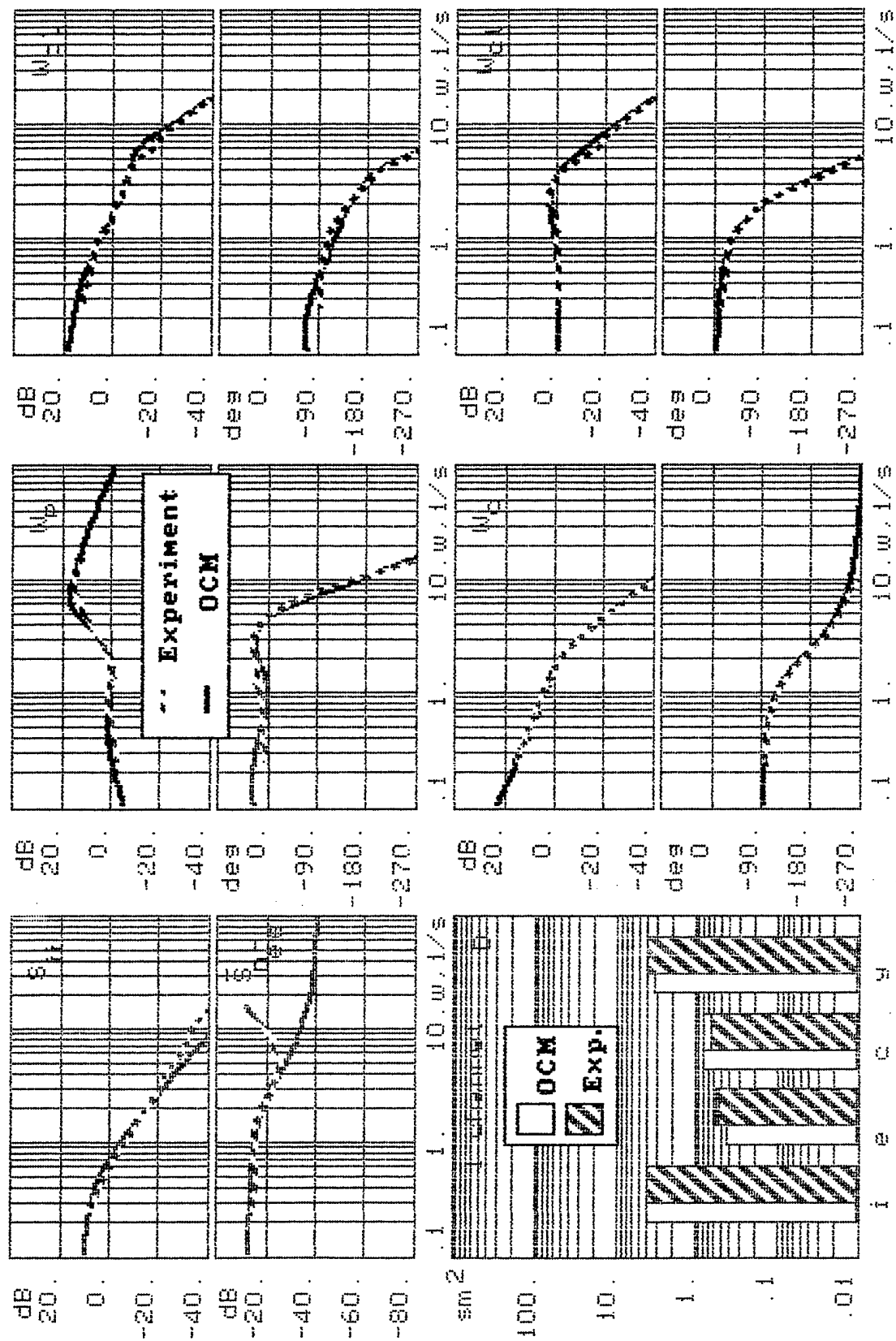


Fig. 4.8. Comparison of mathematical modeling and experimental result (conf. 1F).

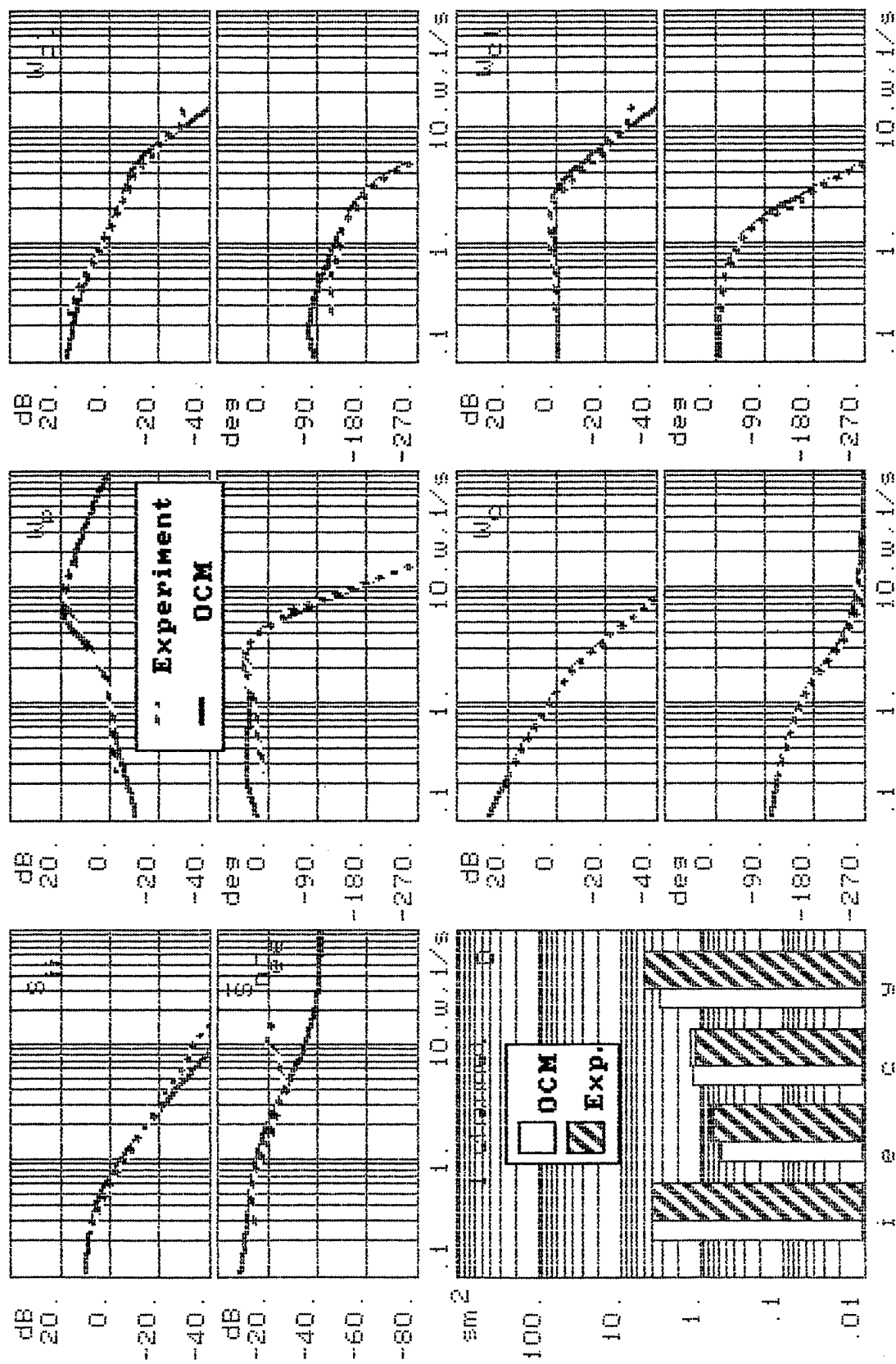


Fig. 4.9. Comparison of mathematical modeling and experimental result (conf. 1G).

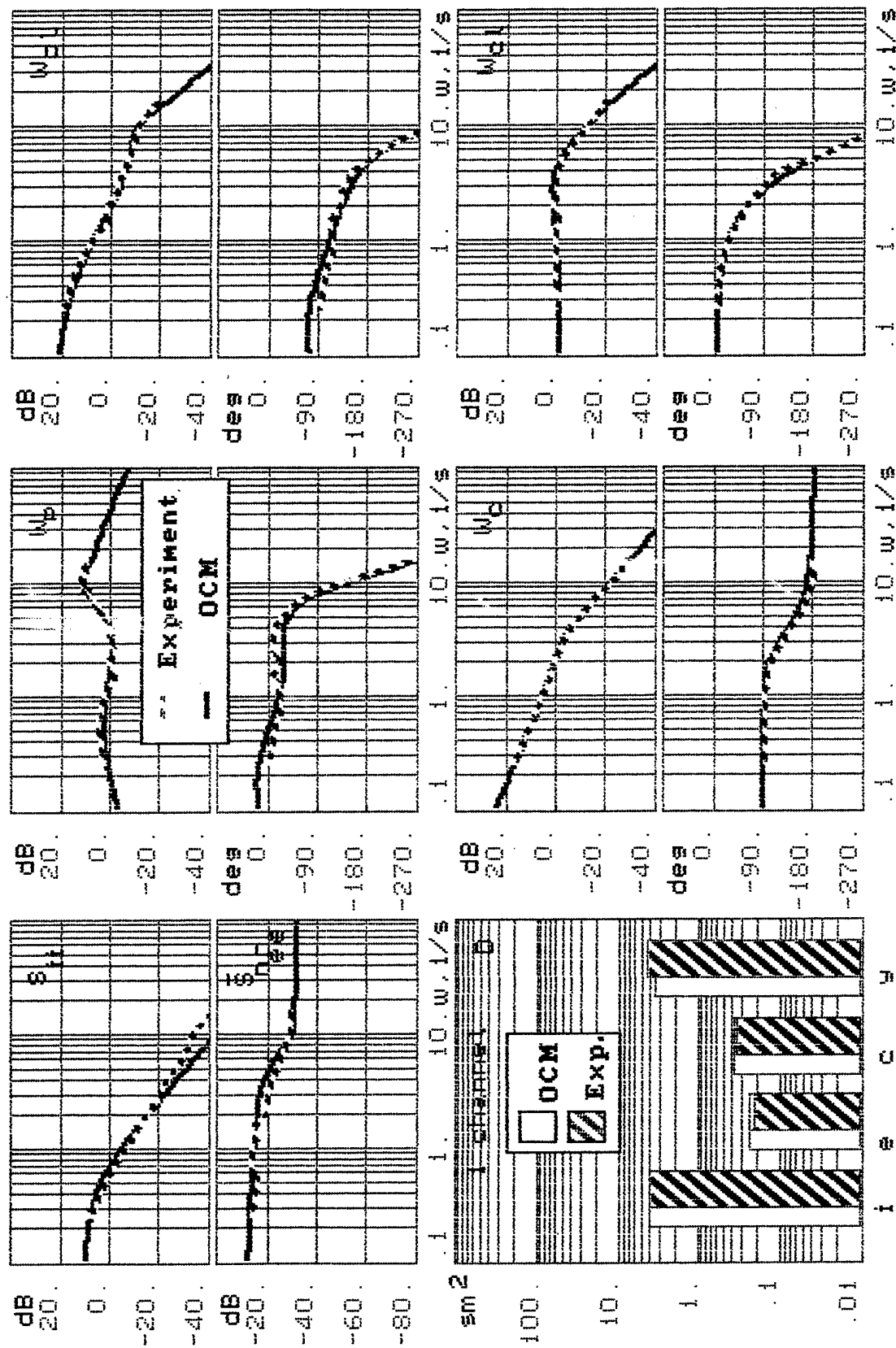


Fig.4.10. Comparison of mathematical modeling and experimental result (conf. 60).

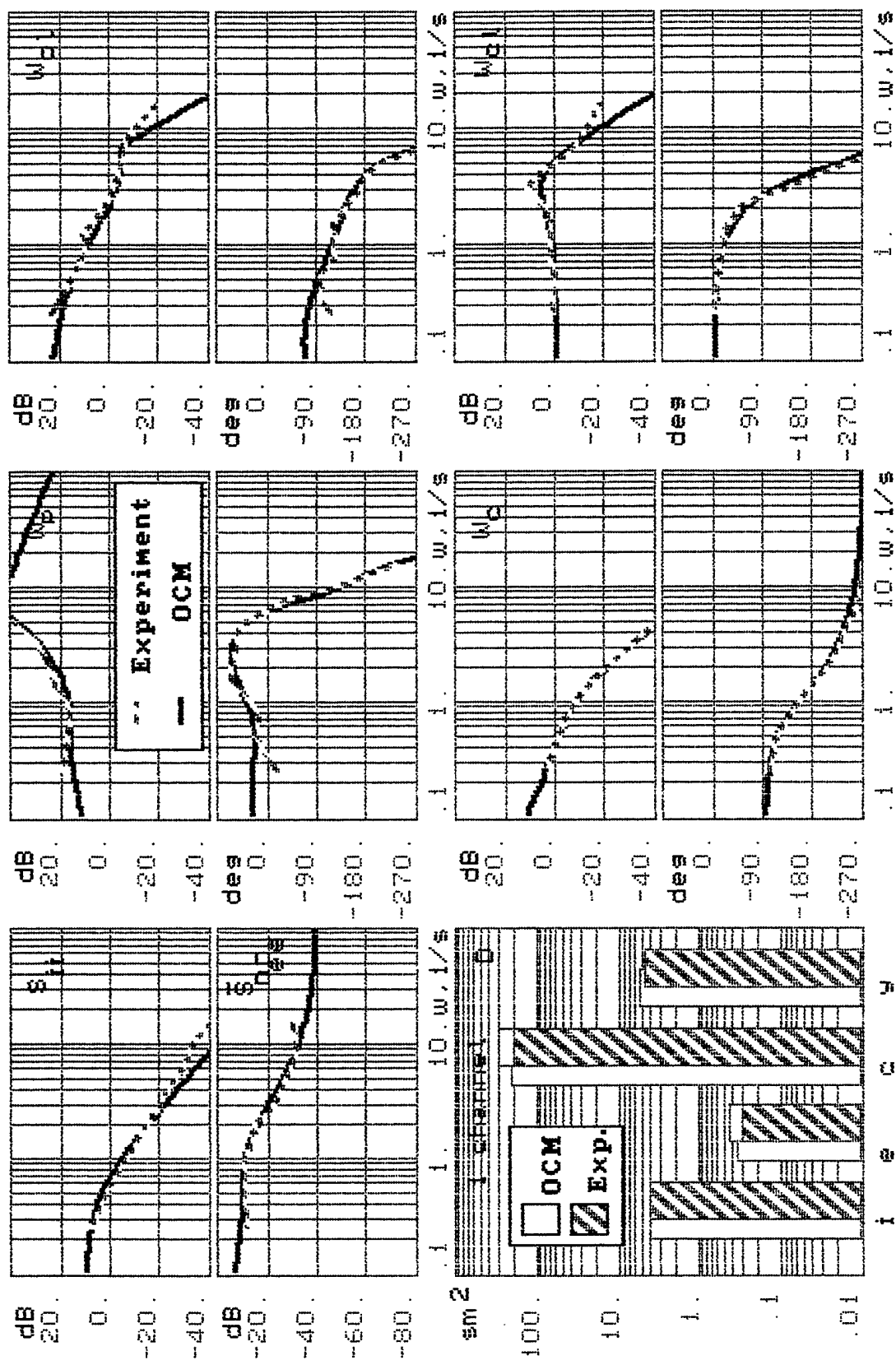


Fig. 4.11. Comparison of mathematical modeling and experimental result
(conf. LAHOS 1.4).

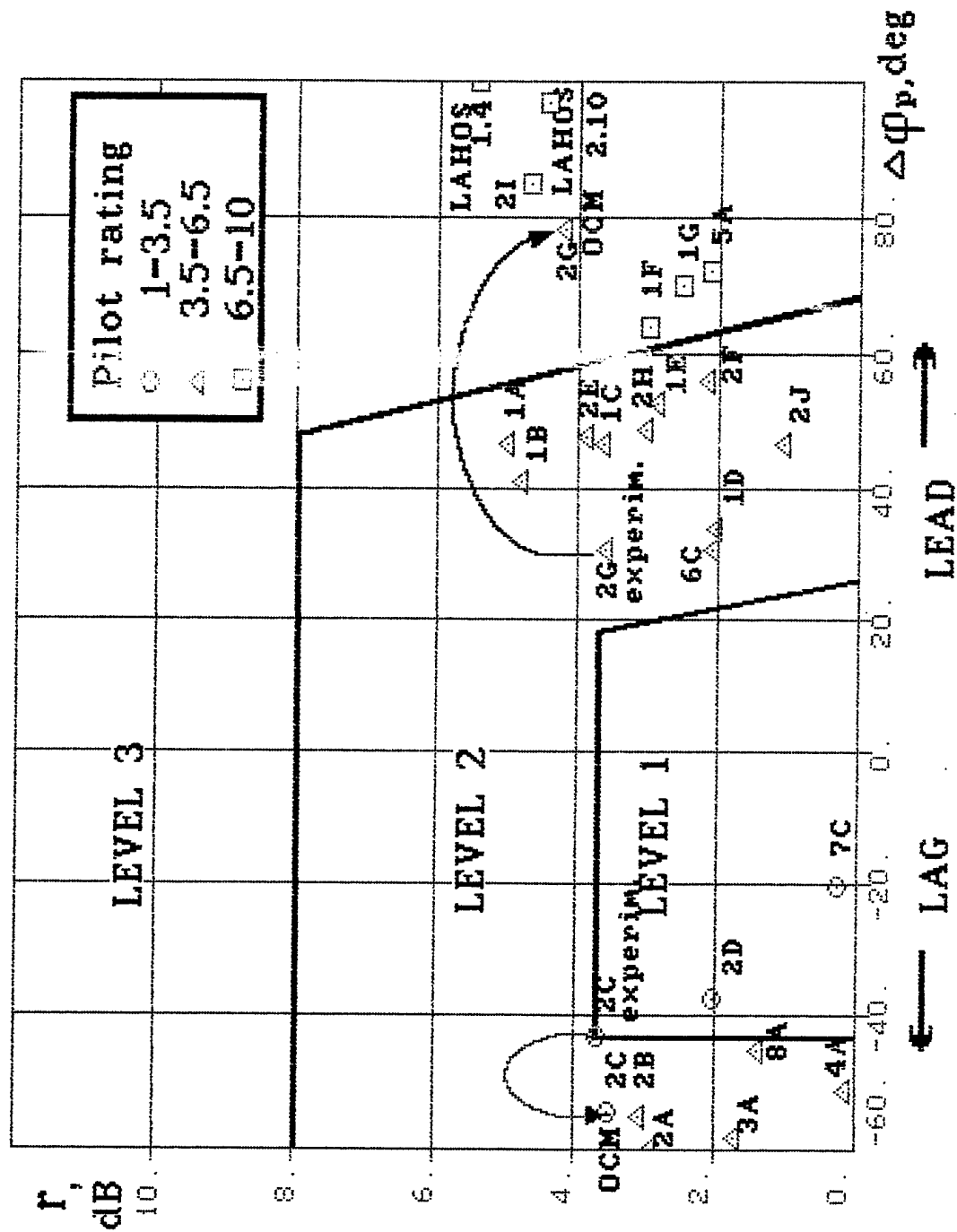


Fig. 4.12. Results of optimal control analysis.

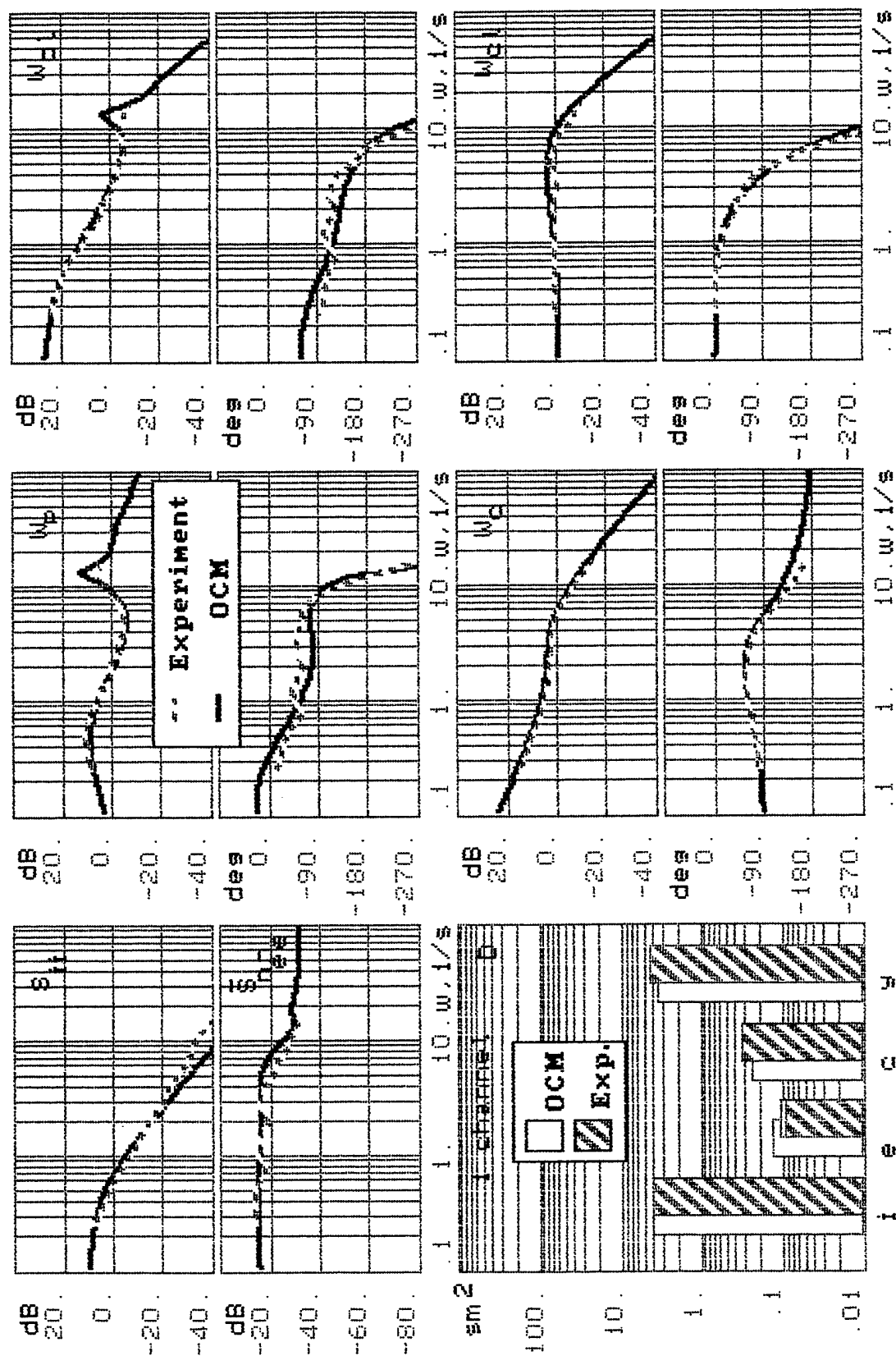


Fig.4.13. Comparison of mathematical modeling and experimental result (conf. 2C).

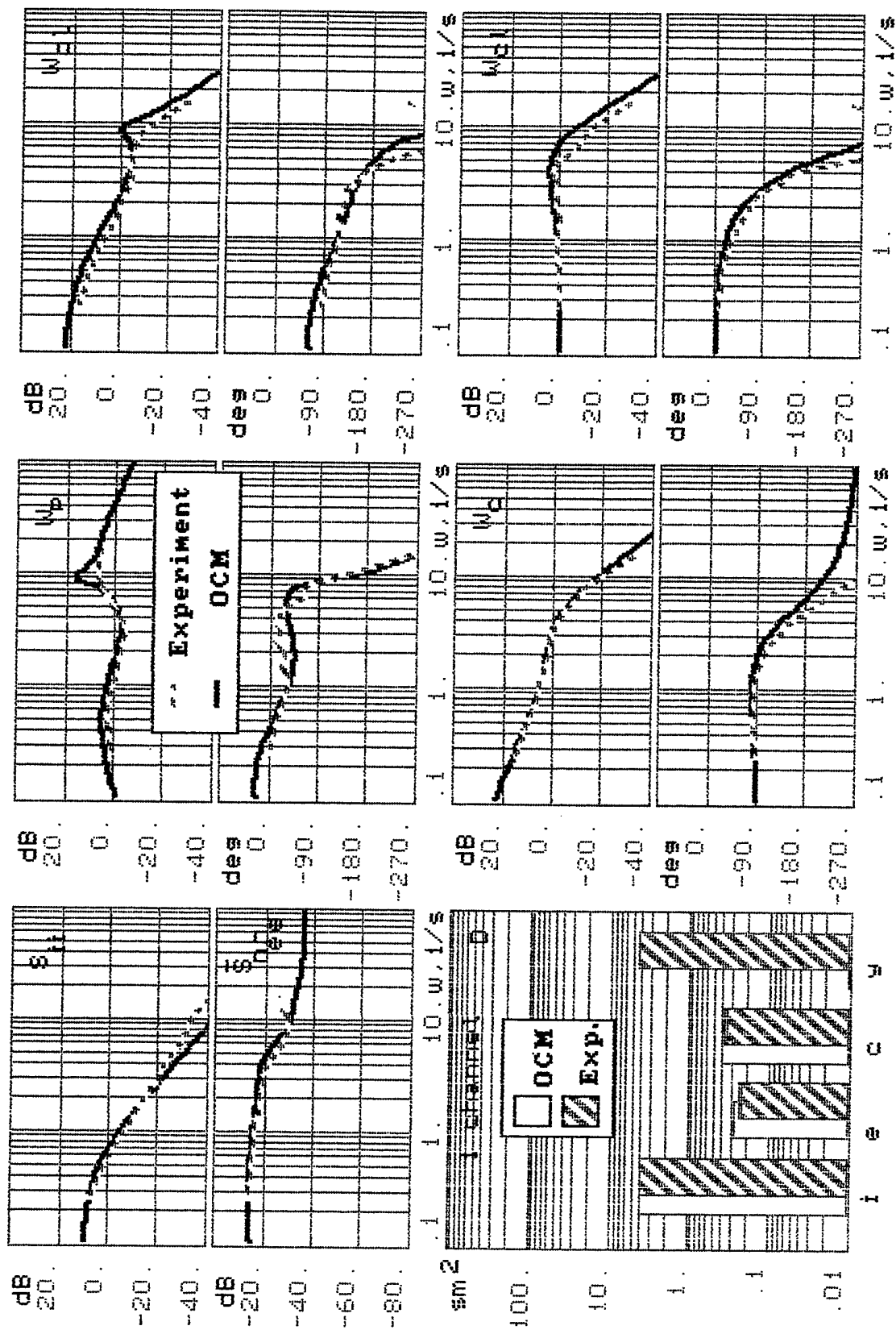


Fig.4.14. Comparison of mathematical modeling and experimental result (conf. 2G).

As for the variances of the pilot's output derivative and error derivative signal, they differ from experimental data. The preliminary research demonstrated that improvement of accordance can be reached by the increase of T_n and weighting coefficient $Q_{\dot{\theta}_e}$. The determination of ways of improvement of the OCM requires additional fundamental research.

2. The results of experimental work showed the dependence of close loop characteristics and pilot workload on interval " $\pm d$ ". For modeling this influence the OCM parameters were changed i.e.: observation noise ratio ρ_{oy_1}, ρ_{oy_2} and fraction of attention which the pilot paid to the error signal observation were changed:

- the weighting coefficient Q_{θ_e} was decreased;
- the weighting coefficient Q_u was increased.

These changes are expected to result in the increase of error signal variance, the decrease of resonance peak and the other changes of corresponding experimental data.

The attempt of modeling the interval " $\pm d$ " only by means of observation noise ratio (with the help of residual remnant σ_o^2 when $V_{y_i} = \frac{\rho_{oy_i}}{f_i N_y} (\sigma_{\theta_e}^2 + \sigma_o^2)$ or by increasing observation thresholds) didn't lead to good results.

The improved coincidence with the experiments was achieved by means of both increasing observation noise ratios and changing weighting coefficients. The change of weighting coefficient corresponds to the change of the task's goal. For example, the decrease of weighting coefficient Q_{θ_e} reflects the operator's motivation to control the vehicle with a increased error value and vice versa.

In table 4.7 are shown the OCM parameters for the 1E configuration for three values of " $\pm d$ ":

1. $d = 0$
2. $d = 0.75$ sm
3. $d = 2$ sm

The results of modeling in comparison with experimental data are presented in fig. 4.15-4.17. These figures show that modeling correctly reflects the change of system characteristics demonstrated in chapter 3.

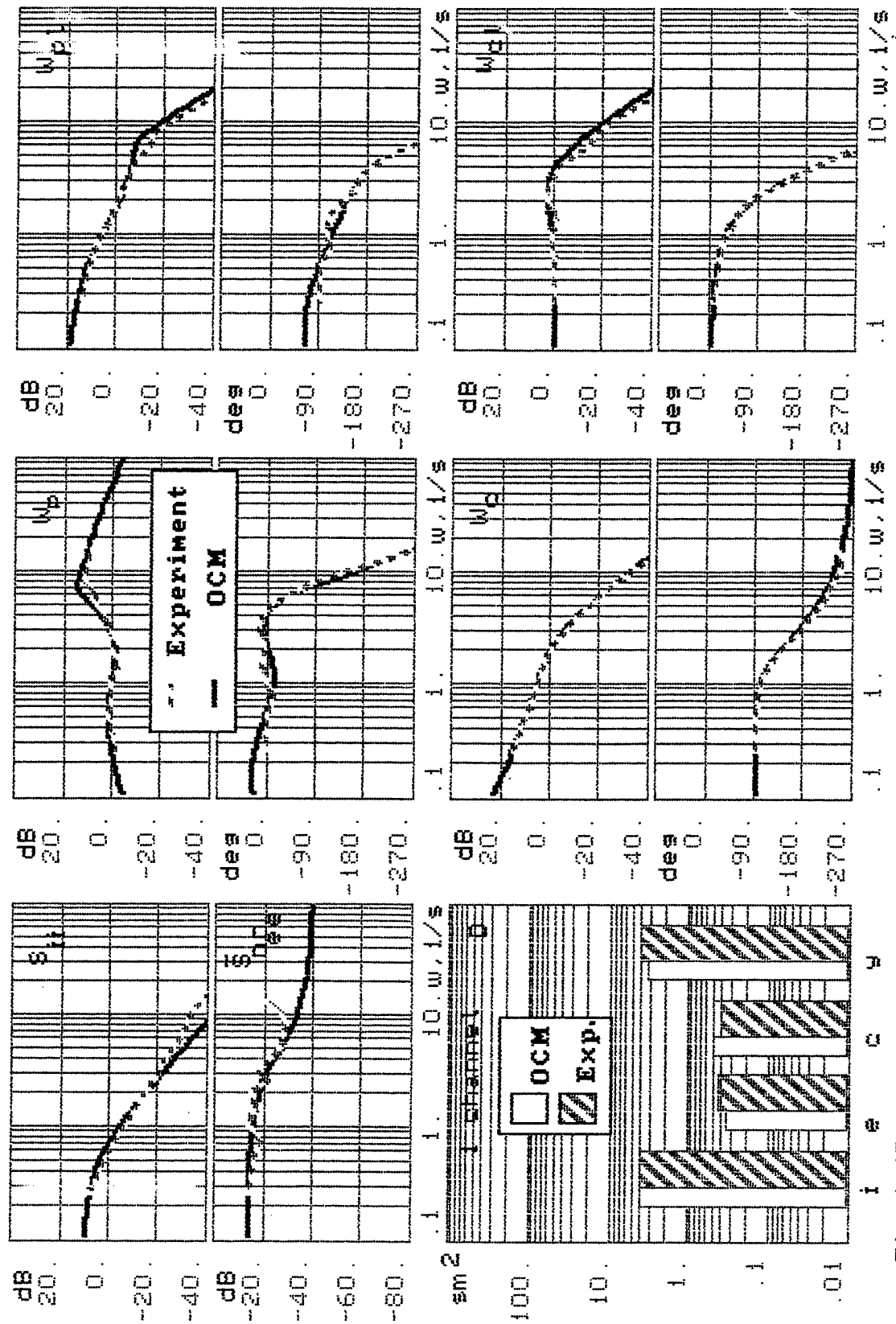


Fig. 4.15. Comparison of mathematical modeling and experimental result (conf. 1E, d=0 sm).

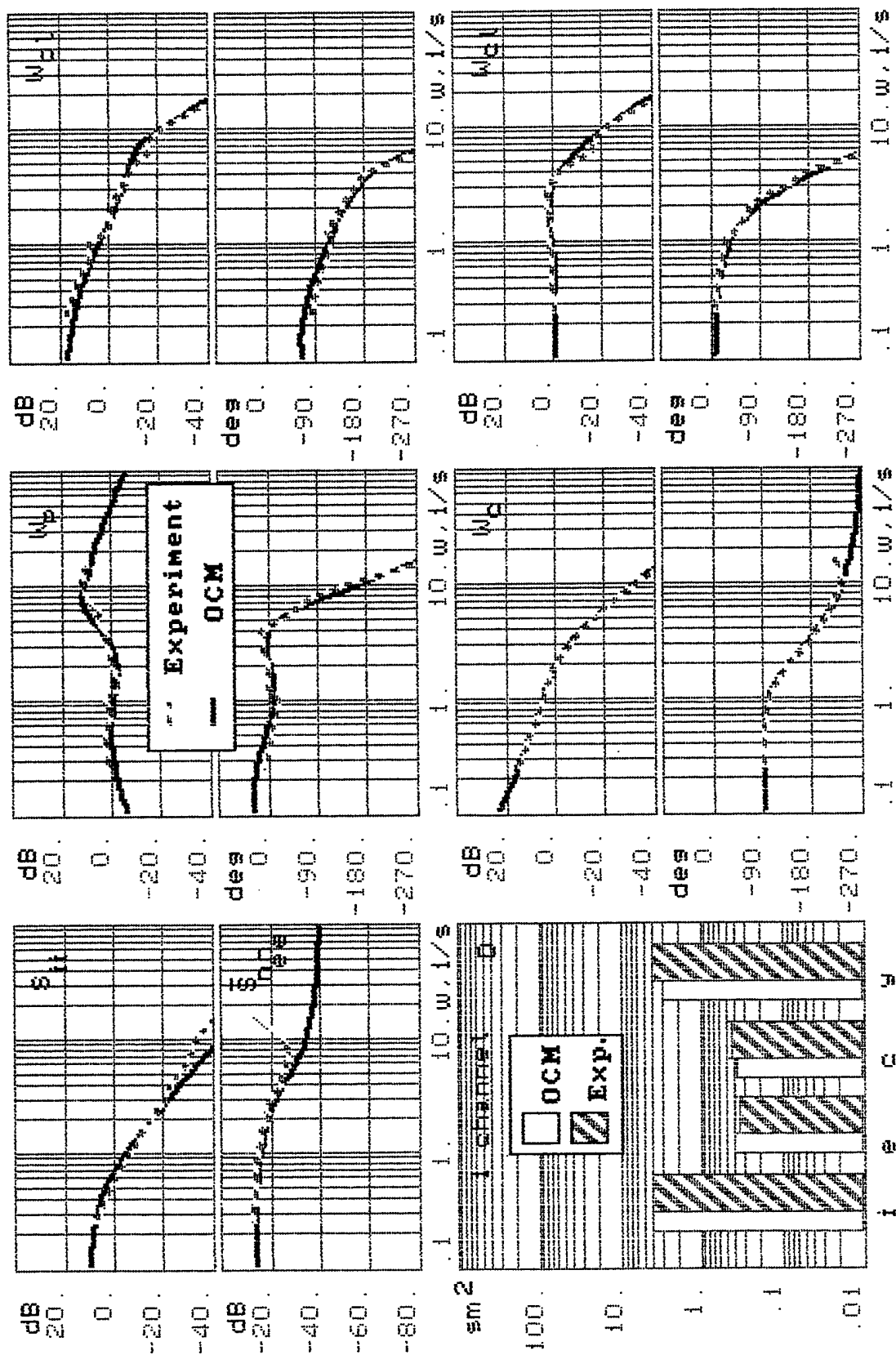


Fig. 4.16. Comparison of mathematical modeling and experimental result (conf. 1E, $d=0.85$ sm).

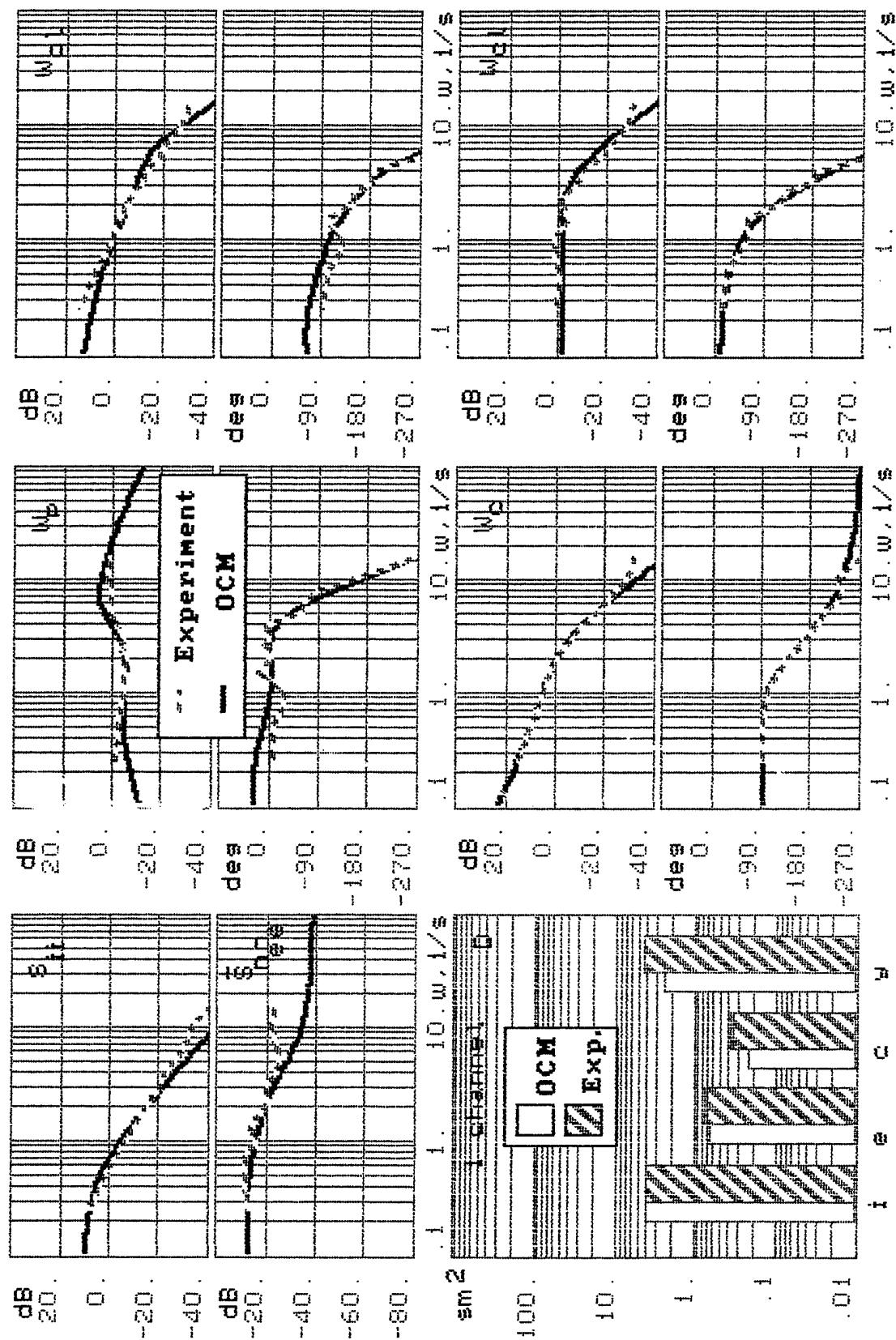


Fig. 4.17. Comparison of mathematical modeling and experimental result
(conf. 1E, $d=2$ sm).

Table 4.7

OCM Parameters (sm)	ρ_{oy_1}	ρ_{oy_2}	f	Q_e	Q_u
0	0.006	0.006	1	1	0.05
0.75	0.01	0.01	1	0.5	0.27
2	0.01	0.01	0.66	0.2	0.4

Thus, the received results allowed us to give the preliminary conclusion that the OCM is able to predict PIO tendency and to consider the influence of interval " $\pm d$ ". The accordance of the OCM parameters to experimental data can be increased by a corresponding choice of weighting coefficient. For this purpose, it was necessary to develop a special automated procedure for model parameters choice. It will increase potentialities in prediction of results in the solution of applied manual control tasks. This work requires additional research.

GENERAL CONCLUSIONS AND RECOMMENDATIONS

A. General Conclusions

In this report the following research areas on Pilot Induced Oscillation tendency are fulfilled:

- analysis of the reasons of PIO tendency for the modern aircraft;
- definition of the main factors causing increased PIO tendency and recommendations for the further investigation on ground and in-flight simulators;
- fulfillment of experimental research on measurements of pilot and pilot-vehicle system characteristics;
- development of criteria for prediction of PIO tendency.

The study of PIO tendency was carried out from the system approach point of view based on in-depth investigation of pilot control response and pilot-vehicle system characteristics and definition of their connection with the pilot-vehicle system variables.

The parameters characterizing the PIO tendency were defined:

- For insignificant nonlinear effects in controlled element dynamics, the characteristics are a resonance peak of closed-loop system and pilot workload parameter $\Delta\varphi$. The last one corresponds to the maximums, positive ($\Delta\varphi^+$) and negative ($\Delta\varphi^-$) of the difference between the pilot phase for the investigated configuration and pilot phase for the aircraft dynamics not requiring phase compensation (the optimal aircraft dynamics). The parameter $\Delta\omega$ is defined in the frequency range from the crossover frequency up to the frequency corresponding to the amplitude margin.
- For evident nonlinear effects in control element dynamics, parameters r and $\Delta\varphi$ are not indicators of PIO tendency in many cases. In these cases the tendency can be defined by consideration of the ratio of spectral densities $S_{e_{\alpha}} : S_{e_{\beta}}$: in the case where this ratio is more than 1 in the pilot-vehicle system, the oscillations are evident at the frequency corresponding to the maximum value of this ratio.

The influence of different pilot-vehicle system variables on PIO tendency was studied and shows that:

- Installation of additional filters accompanied by the additional phase lag typical for highly augmented aircraft leads to a considerable increase of PIO tendency: increase of PR and PIOR, pilot lead compensation, and resonance peak, - in comparison with the configurations corresponding to the lower level of augmentation.
- Decrease of maximum velocities of control surface deflection under high value of gain coefficients of FCS filters, typical for highly augmented aircraft, leads to extreme increase of PIO tendency.

- PIO tendency can arise in visual flight or use of the HUD. In the case of instruments or HDD flight the tendency decrease considerably.
- In disturbance tasks, PIO tendency decreases in comparison with target tasks.
- The necessity to control in additional channels with the requirement to maintain a given accuracy, leads to an increase of PIO tendency (increase of resonance peak and PR) in comparison with the single loop task.
- The different piloting tasks are characterized by the different PIO tendency types. For example in the flare the oscillation processes can arise in angular and path motions for specific aerodynamic configurations (aircraft with elevator or flying wing).

The similar processes are noticeable in angle of sight tracking control tasks. There are additional low frequency resonance peaks and increased middle frequency resonance peaks in closed-loop systems compared to pitch tracking tasks. The first peak is characterized by the oscillation process in path motion. Except for these features, the angle of sight task is accompanied by increased pilot rating.

- The decrease of permissible level of error increased the PIO tendency considerably. This is the major factor in the pilot evaluation of flying qualities. It was shown that agreement of the permissible level of error (value of desired task performance) with the aircraft dynamics decreases PIO tendency up to its complete disappearance.
- Perception of stimulus depends on the set of variables: display gain, permissible level of error, and mean square of input signal. The μ -criteria combined these variables. The constant value of this criteria guaranteed the invariant condition of perception and pilot-vehicle system frequency response characteristics.

Investigated were 23 Neal-Smith and 25 LAHOS configurations. The pilot and pilot-vehicle system characteristics were measured for each of them. The results of this research are the following:

- The ranges of resonance peak (r) and pilot workload parameters corresponding to the equal levels of pilot ratings were determined. These ranges differ considerably from the well-known ranges received by Neal-Smith.
- The rules were developed for determining the pilot workload parameter $\Delta\phi$, which guaranteed the accordance of predicted levels of PR to the experimental PR for all investigated configurations.
- The connection was defined between the pilot rating (PR) on the Cooper Harper scale and PIOR on the pilot induced oscillation scale. This makes it possible to get the criteria for prediction PIO tendency.

The following variables and their values were selected and recommended for the further investigation in TSAGI and LII:

- Controlled element dynamic configurations (2.10, 1.4, 4.10 LAHOS configurations);
- Target manual control task;
- The characterized frequency of input spectral density $\omega_i = 0.5$ rad/sec;

- Values of display gain coefficient, mean square of input signal, and permissible interval of error corresponding to μ -criteria equal to 1 and 2.

The research on creating the technique of prediction of PR and parameters r and $\Delta\varphi$ by the mathematical modeling were carried out.

- The human operator optimal control model technique gave good results in accordance with experimental results practically for all except two investigated configurations.
- The results received from use of the structural approach demonstrated the possibility of predicting the influence of the variables on PIO qualitatively.

B. Recommendations

All these results demonstrate the necessity of the following further research:

- The detailed study of the influence of the different piloting tasks on PIO tendency and development of an approach to the design of flying qualities based on consideration of all these tasks.
- Investigation of PIO tendency in lateral motion. The influence of lateral and longitudinal motion on PIO tendency.
- Development of a technique for the choice of handling qualities taking into account the influence of permissible value of error.
- The further development of criteria and techniques for prediction of flying qualities and PIO tendency by experimental research and mathematical modeling.

REFERENCES

1. Efremov, A. V., Ogloblin, A. V., Predtechensky, A. N., Rodchenko, V. V. Pilot as a Dynamic System. Moscow, Mashinostroenie, 1992, 331 pp.
2. Parrag, M. L. Pilot Evaluations in a Ground Simulator of the Effects of Elevator Control System Dynamics in Fighter Aircraft. Technical Report AFFDL-TR-67-19, September 1967.
3. DiFranko, D. A. Flight Investigation of Longitudinal Short Period Frequency Requirements and PIO Tendencies. Technical Report AFFDL-TR-66-163, June 1967.
4. Neal, T. P., Smith, R. E. A Flying Qualities Criterion for the Design of Fighter Flight-Control Systems. J. Aircraft, vol.8, N 10, October 1971.
5. Smith, R. E. Effects of Control System Dynamics on Fighter Approach and Landing Longitudinal Flying Qualities, v.1, AFFDL-TR-78-122, 1978.
6. Bjorkman, E. A., Silverthorn, J.T., Calicp, R.A. Flight Test Evaluation of Techniques to Predict Longitudinal Pilot Induced Oscillations, AIAA Paper 86-2253.
7. Myers, T. T., Johnston, D. E., McRuer, D. T. Space Shuttle Flying Qualities and Criteria Assessment. NASA Contractor Report 4049, 1987.
8. Powers, B. An Adaptive Stick-Gain to Reduce Pilot-Induced Oscillation Tendencies. J. Guidance vol.5, N 2, April 1982.
9. Efremov, A. V., Ogloblin, A. V., Koshelenko, A. V. Development and Application of Methods for Pilot-Vehicle Researches in the Safety of Flight Tasks. Aircraft Flight Safety International Conference Proceedings, pp.529-533. Zhukovsky, Russia, 31 August - 5 September 1993.
10. Efremov, A. V. Dynamics in Low Altitude Flight in Atmosphere Turbulence. Proceedings of the research fulfilled in Tashkent Polytechnical Institute in 1972-1973 N 137 Tachkent 1974.
11. Hess, R. The effects of Time Delays on Systems Subject to Manual Control. J. Guidance, Control and Dynamics 1984, vol.7, pp.165-174.
12. Efremov, A. V., Ogloblin, A. V., Alexandrov, V. V. Experimental Research of Pilot-Vehicle Compensatory System for One Input Signal. In the book "The Questions of Flight Control. Moscow, MAI, 1993", pp.37-44.
13. Starleford, R. L., Craig, S. J., Tennant, J. Measurement of Pilot Describing Functions in Single Controller Multiloop Tasks. NASA-CR-1239, 1968.

14. McRuer, D., Graham, D., Krendel, E., Reisener, W. Jr. Human Pilot Dynamics in Compensatory Systems Theory, Models and Experiments with Controlled Element and Forcing Function Variations. AFFDL-TR-65-15.
15. Bacon, B. J., Schmidt, D. K. An Optimal Control Approach to Pilot/Vehicle Analysis and the Neal-Smith Criteria. J. Guidance, vol.6, N 5, Sept.-Oct. 1983.
16. Shirley, R. S., "Application of a Modified Fast Fourier Transform to Calculate Human Operator Describing Functions", IEEE Trans. Vol. MMS-10, No.4, Pt.1, Dec.1969, pp.21-47.
17. Guskov, J. P., Zagainov, G. I. Flight Control. Moscow Mashinostroyenie, 1980.
18. Jex, H. R., McDonnell, J. D., and Phatak, A. V. A "Critical" Tracking Task for Man-Machine Research Related to the Operator's Effective Delay Time. Part I: Theory and Experiments with a First-Order Divergent Controlled Element, NASA CR-616, Nov. 1966.
19. Efremov, A. V. The Peculiarities of Pilot Behavior in Control of Unstable Controlled Element Dynamics. In the book "Influence of Pilot Behavior on Man-Machine System Design". MAI, Moscow, 1983.
20. Levison, W. H., Baron, S., and Kleinman, D. L. "A Model for Controller Remnant", IEEE Trans. Vol. MMS-10, No.4, Dec. 1969, pp.101-108.
21. Baron, S., Levison, W. "An Optimal Control Methodology for Analyzing the Effects of Display Parameters on Performance and Workload in Manual Flight Control", IEEE, Trans. on Systems, Man and Cybernetics, vol. SMC-5, N 4, 1975.
22. Hess, R. A. Dual-Loop Model of the Human Controller. J. of Guidance and Control, vol.1, 1978.
23. Volgin, L. N. Optimal Discrete Control of Dynamic System. Moscow, Nauka, 1986.
24. Kleiman, D. L., Baron, S., Levison, W.H. "An Optimal Control Model of Human Response", Automatica, vol.6, pp.357-369,1970.
25. Hess, R. "Analytical Display Design for Flight Tasks Conducted Under Instrument Meteorological Conditions", IEEE Trans. on SMC, vol. SMC-7, N 6, 1977.
26. Hess, R. "Prediction of Pilot Opinion Ratings using an Optimal Pilot Model" IEEE Trans. on SMC, June 1977.

APPENDIX A. Method for Experimental Measurement of Pilot-Vehicle System Characteristics

The unified Fourier coefficient method was used for the experimental investigation of pilot-vehicle system characteristics [1]. This method allows three groups of characteristics to be obtained:

- frequency response characteristics of the pilot, open- and closed-loop system;
- spectral characteristics of the pilot's remnant and all signals;
- variances of all signals and their correlated and uncorrelated input components.

The algorithms for data reduction and the technique developed for choice of input signal are briefly discussed below.

A.1. The Unified Fourier Coefficient Method

The Definition of Frequency Response Characteristics.

The algorithms and software used in the research are based on the unified Fourier coefficient method. The basis of this method is the calculation of Fourier coefficients $\hat{a}_k(\cdot)$ and $\hat{b}_k(\cdot)$ (where (\cdot) - is analyzed signal) according the following equations:

$$\left. \begin{matrix} \hat{a}_k(\cdot) \\ \hat{b}_k(\cdot) \end{matrix} \right\} = \frac{2}{T} \int_0^T (\cdot) \begin{Bmatrix} \cos \omega_k t \\ \sin \omega_k t \end{Bmatrix} dt.$$

This knowledge enables finding the Fourier transform of the signal (\cdot) and frequency response characteristic on input frequency " ω_k ". For example the equation for pilot describing function is the following:

$$\hat{W}_p(j\omega) = \frac{\hat{C}(j\omega)}{\hat{E}(j\omega)} = \frac{a_k^e - jb_k^e}{a_k^e - jb_k^e}.$$

The accuracy in calculation of frequency response characteristics depends on [1]:

- the ratio of input and remnant signal levels of power;
- the time duration used for calculation of Fourier coefficients.

The use of poligarmonic signal $i(t)$

$$i(t) = \sum_{k=1}^N A_k \sin(\omega_k t + \varphi_k)$$

$$\omega_k = \frac{2\pi n_k}{T}, n_k - \text{integer number,}$$

increases the accuracy in determination of frequency response characteristics.

The use of Fast Fourier Transform (FFT) and its modified version [16] decreases the time for data reduction considerably. At the same time the use of FFT induces the additional requirement

$$\begin{cases} \omega_k = \frac{2\pi n_k}{\Delta t N}, \\ \frac{n_k}{N} = m_k, \end{cases}$$

where Δt - time of discretization ($N\Delta t = T$);
 n_k, m_k - integer numbers

For modified FFT used in the data reduction, procedure n_k has to be a number divisible by 4. That is connected with symmetry of sinusoid functions used in this method.

The Evaluation of Pilot Remnant and Different Signal's Power Spectral Densities.

Each signal (for example E) of the pilot-vehicle system consist of the two components defined by the different sources - input signal and remnant. In the case where the input signal is a sum of sinusoids these components have power spectral densities of a different nature: the discrete - for the component E_i correlated with input and continuous - for the component E_n correlated with remnant. The Fourier coefficients consist of these components too. The power of the discrete spectrum on frequency ω_k ($P_d(\omega_k)$) is defined by the amplitude of E_k of the same frequency

$$P_d = \frac{E_k^2}{2}.$$

The power of the continuous component P_c can be evaluated by the average level of spectral density $S_{e_n e_n}$ according to the following equation:

$$P_c(\omega) = S_{e_n e_n}(\omega) \frac{2\pi}{T}.$$

The summarized power of signal E corresponds to the equation

$$\frac{(a_k^e)^2 + (b_k^e)^2}{2} = \frac{E_k^2}{2} + S_{e_n e_n}(\omega_k) \frac{2\pi}{T}.$$

The analysis of this equation shows, that evaluation of Fourier coefficients for the different time duration T and T', where $T=QT'$, allows us to get the remnant component of signal E_n ;

$$S_{e_n e_n} = \frac{T}{2\pi(Q-1)} \left[\left(\frac{(a_k^e)^2 + (b_k^e)^2}{2} \right)' - \frac{(a_k^e)^2 + (b_k^e)^2}{2} \right], \text{ where}$$

$$P_{T'} = \left(\frac{(a_k^e)^2 + (b_k^e)^2}{2} \right)' - \text{the power of signal defined by time duration } T'$$

$$P_T = \left(\frac{(a_k^e)^2 + (b_k^e)^2}{2} \right) \text{ - the power of signal defined by time duration T.}$$

The knowledge of $S_{e_n e_n}$ defines remnant power spectral density:

$$S_{e_n e_n}(\omega_k) = \frac{S_{e_n e_n}(\omega_k)}{|W_{CL}(\omega_k)|^2}$$

Evaluation of Variances.

The evaluation of variances was carried out according to the equation:

$$\sigma^2(\cdot) = \frac{1}{T} \int_0^T (\cdot)^2 dt - \left(\frac{1}{T} \int_0^T (\cdot) dt \right)^2,$$

where $\frac{1}{T} \int_0^T (\cdot) dt$ - mean of the signal (\cdot) evaluated on interval T.

Fourier coefficient method measures the components of any signal correlated $(\sigma_i(\cdot))$ and uncorrelated $(\sigma_n(\cdot))$ with input according to the equations:

$$\sigma_i^2(\cdot) = \sum_k \left(\frac{a_k^2(\cdot) + b_k^2(\cdot)}{2} \right)$$

$$\sigma_n^2(\cdot) = \sigma^2(\cdot) - \sigma_i^2(\cdot)$$

A.2. The Input Signal Development

The amplitude of input signal has to be chosen from the condition of conformity the discrete spectrum characteristics to the continuous spectrum $S_{ii}(\omega)$. Such continuous spectrum can be characterized with the help of power spectral density or distribution of power function. The last is characterized with the help of equation:

$$I_{ii}(\omega) = \int_0^\omega S_{ii}(\omega) d\omega, \quad I_{ii}(\omega \rightarrow \infty) = \sigma_i^2.$$

The concept of spectral density is not correct for the input signal consisted from the sum of sinusoids because of its power is concentrated in the separate frequencies. The distribution of power $I_{ii}^{(d)}$ is a sum of powers of separate sinusoids

$$I_{ii}^{(d)}(\omega) = \sum_{k=1}^{\omega < \omega_k} \frac{A_k^2}{2}(\omega_k),$$

where $\frac{A_k^2}{2}$ - is a power of sinusoid characterized by frequency ω_k and amplitude A_k .

The task of guaranteeing the accordance of the signal consisting of the sum of sinusoids to signal with continuous power distribution requires the minimization of the difference between $I_{ii}(\omega)$ and $I_{ii}^{(d)}(\omega)$ (see fig. A.1.). For that purpose the quadratic criteria can be used and the requirement has to be kept that

$$I_{ii}(\omega \rightarrow \infty) = I_{ii}^{(d)}(\omega \Big|_{k=N}) = \sigma_i^2.$$

The concrete choice of amplitudes has to be fulfilled according to the following rules:

1. The following continuous power spectral density $S_{ii}(\omega)$ and distribution of power $I_{ii}(\omega)$ is induced corresponding to it:

$$S_{ii}(\omega) = \begin{cases} \frac{1}{\omega_k}, & \omega \leq \omega_k \\ 0, & \omega > \omega_k \end{cases}$$

$$I_{ii}(\omega) = \begin{cases} \frac{\omega}{\omega_k}, & \omega \leq \omega_k \\ 1, & \omega > \omega_k \end{cases}$$

The amplitudes of sinusoids $A(\omega_i)$ are chosen to approximate this spectrum. Their definition is carried out by minimization of the function

$$F = \int_0^{\omega_k} (I_{ii}^d(\omega) - I_{ii}(\omega))^2 d\omega$$

In this case $I_{ii}^d(\omega)$ can be defined by

$$I_{ii}^d(\omega_i) = \begin{cases} I_{ii}(\omega_k), & \omega > \omega_k \\ \frac{I_{ii}(\omega_i) + I_{ii}(\omega_{i+1})}{2}, & \omega_i < \omega < \omega_{i+1} \end{cases}$$

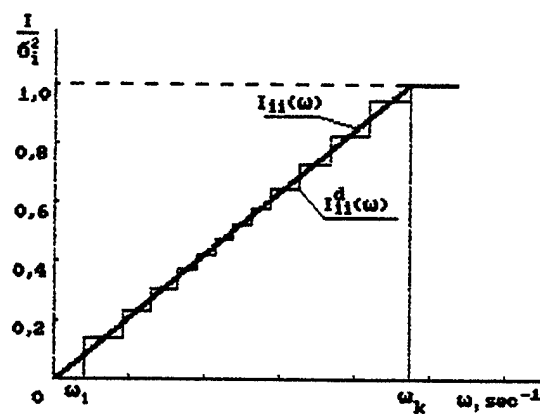


Fig. A.1. The distribution of power function

and consequently

$$A(\omega_i) = \sqrt{2(I_{ii}(\omega_{i+1}) - I_{ii}(\omega_i))}.$$

2. The calculation of the amplitudes of sinusoids is carried out for the given power spectral density $S_{ii}(\omega)$. For this purpose it has to be defined:

- the additional coefficients for amplitudes of sinusoids:

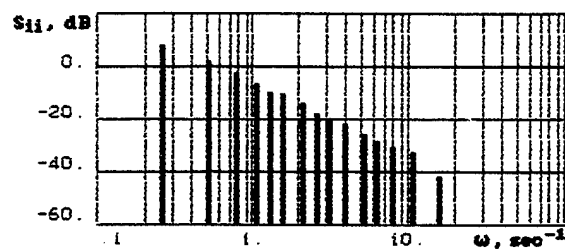
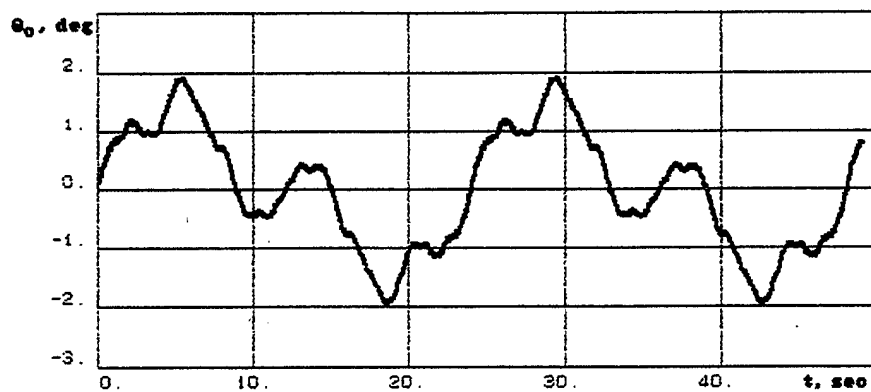
$$a_i = \sqrt{S_{ii}(\omega_i)};$$

- the final values of amplitudes of sinusoids:

$$A_i = a_i A(\omega_i).$$

The simplicity of this approach is connected with the fact that it is necessary to define the amplitudes for given frequencies of input signal only one time. The further transform of amplitudes for any power spectral density is not complex.

Fig. A.2. shows the input signal used in the research and its spectrum.



k	$\omega_k, \text{sec}^{-1}$	k	$\omega_k, \text{sec}^{-1}$	k	$\omega_k, \text{sec}^{-1}$
1	0.2618	6	1.571	11	5.236
2	0.5236	7	2.094	12	6.283
3	0.7854	8	2.618	13	7.854
4	1.047	9	3.142	14	10.47
5	1.309	10	3.927	15	15.71

Fig. A.2. The input signal

APPENDIX B. Standard Dynamics in Precise Tracking Tasks

Optimal aircraft dynamics W_c^{opt} can be defined based on the Wiener approach by minimization of error variance. As an additional requirement the pilot's behavior has to correspond to the simplest proportional type. This means that

$$W_p(j\omega) = K_p e^{-j\omega\tau},$$

$$S_{n_e n_e}(\omega) = K_{n_e} \pi [\sigma_e^2]_{opt}. \quad (B.1)$$

The model in fig. B.1 consists of the main limitations typical for proportional pilot's behavior. The time delay and remnant power spectral density is proportional to the variance of error only ($T_L = 0$). In fig. B.1 is shown the scheme of the optimal compensatory system. Here, the time delay t takes into account the pilot and control element dynamics. The pilot gain coefficient is included in aircraft dynamics. This task has two peculiarities in comparison with the traditional Wiener approach:

- it has a nonminimum phase element $e^{-p\tau}$. Further it is approximated with a first order Pade approximation:

$$e^{-p\tau} \approx \frac{2 - p\tau}{2 + p\tau} = W_o(s)$$

- the remnant spectral density depends on variance of error.

As for the first peculiarity it can be decided by inducing the requirement of roughness. This means that the given part $W_o(s)$ has to be included in the optimal closed-loop system transfer function W_{CL}^{opt} . Taking it into account the following equation was received in [1]:

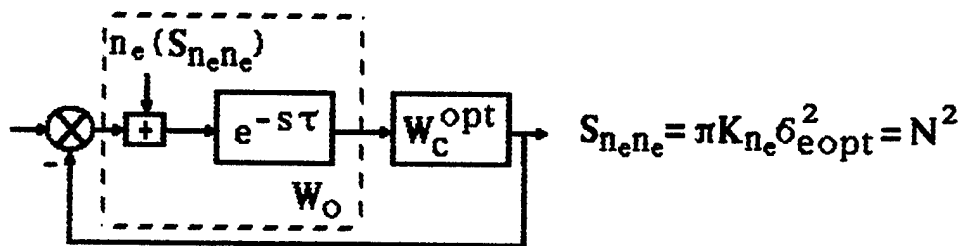
$$W_{CL}^{opt}(s) = W_o(s) \frac{M(s)}{A^+(s)D^+(s)} \quad (B.2)$$

where $M(s)$ is the solution of polynomial equation [23]:

$$P^-(s)M(s)A^-(s)D^-(s) + B^+(s)D^+(s)L(s) = C(s)B(s)\hat{P}^-(s) \quad (B.3)$$

Except for the unknown polynoms $L(s)$ and $M(s)$, the others are the results of factorization of input and remnant power spectral densities and the given part. The factored equations are as follows:

OPTIMAL AIRCRAFT DYNAMICS



Synthesis by using of Wiener approach

Fig. B.1. The optimal aircraft dynamics

- for input power spectral density:

$$S_{ii}(s) = \frac{C(s)}{D(s)} = \frac{C^+(s)C^-(s)}{D^+(s)D^-(s)}, \quad (\text{B.4})$$

- the sum consisted of remnant power spectral density and input power spectral density:

$$S(s) = S_{ii}(s) + S_{n_e n_e}(s) = \frac{A(s)}{B(s)} = \frac{A^+(s)A^-(s)}{B^+(s)B^-(s)}, \quad (\text{B.5})$$

- for the given part of a system:

$$W_o(s) = \frac{2-s\tau}{2+s\tau} = \frac{P^-(s)}{\hat{P}^-(s)} \quad (\text{B.6})$$

The polinoms with sign (+) and $\hat{P}^-(s)$ have the poles in the left part of complex space and polinoms with sign (-) and $P^-(s)$ in the right part. For the considered model $S_{n_e n_e}(\omega)$,

$B(s) = D(s)$. Equation (B.2) can be simplified by substitution $M(s) = D^+(s)M_o(s)$ and

$L(s) = D^-(s)L_o(s)$. The equations (B.1) and (B.2) are transformed to the following:

$$W_{CL}^{opt}(s) = \frac{P^-(s)M_o(s)}{\hat{P}^-(s)A^+(s)}, \quad (\text{B.7})$$

$$P^-(s)M_o(s)A^-(s) + B^+(s)L_o(s) = C(s)\hat{P}^-(s) \quad (\text{B.8})$$

These equations can be combined and

$$W_c^{opt}(s) = \frac{A^-(s)M_o(s)\hat{P}^-(s)}{D^+(s)[N^2 D^-(s)\hat{P}^-(s) - L_o(s)]} \quad (\text{B.9})$$

$$\text{where } N^2 = S_{n_e n_e}(\omega) = \frac{[\sigma_{e_i}^2]_{opt}}{\frac{1}{K_{n_e}} - \int_0^\infty \left| W_{CL}^{opt}(s) \right|^2 d\omega} \quad (\text{B.10})$$

Analysis of B.9 demonstrates that the number of poles here is more than number of poles in the input signal filter in distinction from the Wiener approach.

The second peculiarity of the task can be seen in consideration of B.9 and B.10, where N^2 depends on the W_{CL}^{opt} . This peculiarity requires developing an iterative procedure for a final solution. Fig. B.2 shows the optimal control element frequency response characteristics for the different parameters of input spectral density. The decrease of frequency ω_i leads to increase of distinction between $W_C^{opt}(s)$ and $W_C = \frac{k}{s}$ which is used in many research efforts as a standard characteristic.

The effect of ω_i, m :
$$S_{ii} = \frac{K_i^2}{(\omega^2 + \omega_i^2)^m}$$

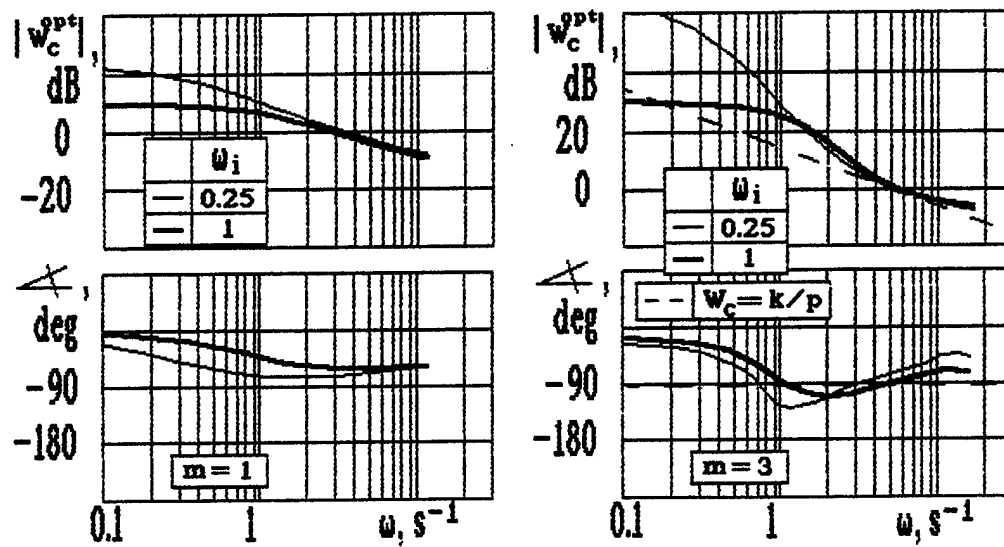


Fig. B.2. The frequency response of optimal aircraft dynamics

APPENDIX C. The Workstation for Manual Control Task Research

The workstation is intended for fulfillment of a wide range of investigations in the manual control field. It is based on IBM PC's usage.

The workstation can be used as:

1. A mini-simulator - for the preliminary stage of research (80-85% of all experiments).
2. An element (hardware and/or software) of a simulator's computer for the final ground stage of experiments.
3. An element (hardware and/or software) of ground or on-board computer used for flight test on an in-flight simulators.

The workstation consists of two main elements: hardware and software parts.

Hardware

1. The minimum set of PC and hardware configuration for the workstation usage.

- personal computer IBM PC (386/387 or later processor) or computer compatible with IBM PC;

- RAM no less 1 MB;

- color graphic display (no less 640 × 350);

- video graphic controller SVGA;

- A/D converter; - matrix printer.

2. A two-axis manipulator with characteristics close to the side stick.

Software

The software used in workstation is a package of support programs for personal computer (PPS PC) supplying the program support for preparation, realization, and data reduction of experiments.

PPS PC consists of the system part and supported modules.

The main parts of programs are written in "FORTRAN 77", and a part in the "MACRO assembler". PPS PC is oriented operational system use of MS DOS version 3.3 and later.

The workstation supplies the automation of the following processes:

- 1) Input of task variables: controlled element dynamics, input signal, additional variables (step of integration, number of runs and trials, etc.)
- 2) Realization of experiment in real time, records of data, calculations during the process of experiment, the generation of visual pictures (display, runway, director indicator, etc.) in real time.
- 3) Data reduction for calculation of pilot, pilot-control element dynamic open- and closed-loop describing functions; pilot remnant spectral density, and spectral density of all measured signals;

variances, and their correlated and uncorrelated parts of all signals; parameters of pilot open- and closed-loop describing functions; density of probability distribution for measured signal.

4) Representation of all results on the display screen or printer in the form convenient for analysis. Fig. C.1 shows an example of a typed picture which gives the interpretation of symbols. All figures showing the results of the experimental research are fulfilled in such a format.

The Description of Possibilities

PPS PC consists of some modules realizing the different functional possibilities. They allow us to realize the following possibilities:

- *to prepare* experimental research;
- *to carry out* the experimental research in real time;
- *to reduce* the data;
- *to draw* the results with help of graphic curves and set of figures on the display screen and matrix printer.

The module for preparation of experiments.

This Module gives the possibility for users to work with the interface for input of data (or variables) necessary for experimental research. There are following variables:

- characteristics of input signal: the form of input spectrum induced as a ratio of numerator to denominator of the forming filter and its power determined by the value of variance. This input signal can be recorded on the disk for its further usage;
- control element dynamic induced as a ratio of numerator to denominator of transfer function and time delay element. The new version allows inducing the nonlinear differential equations for the simulation. The control element dynamics can be recorded on disk for further usage;
- gain coefficients of display and controlled element dynamics;
- additional parameters necessary for fulfillment of experiments and data reduction;
- characteristics calculated by PPS PC, method of identification (Fourier Transform, Fast Fourier Transform), type of task (stationary, unstationary).

The following are additional variables:

- the step size of integration in modeling the control element dynamics in real time;
- the step size of recording (given in the steps of integration) determined by the frequency interval of input signal;
- the number of runs in one trial, determined by the quantity of the same type experiments, carried out in each trial and reduced together;
- the number of trials of experiments. After each trial, the data reduction of experiments is carried out and the results are drawn for current trial. After the end of the last trial, the functions for all trials are shown on one picture (for comparison). The difference in trials is determined by the pilot's variables: by operators taking part in the research, and by task variables (control element, dynamics, input spectrum, manipulator, etc.);

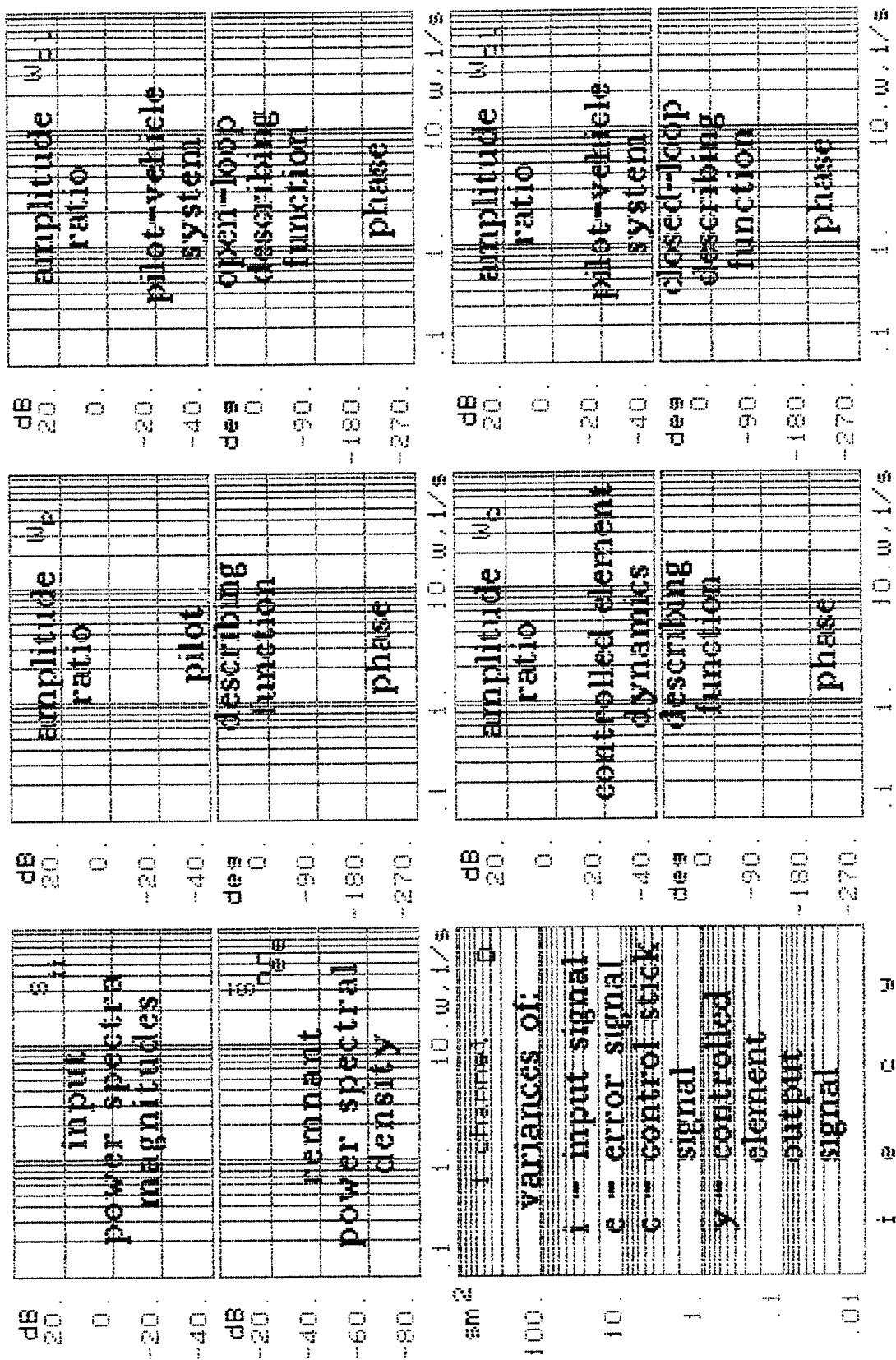


Fig. C.1. The graphical presentation of results

- the number of variable parameters which will be changed from trial to trial;
- a file's name which consist the way of access and a file's name of the results of data reduction.

The module for fulfillment of research.

This module organizes the realization of the current trial of experimental research in real time. It allows:

- to record the trial of runs on disk; and in real time;
- to generate the input signal;
- to form the results (functions) on the display screen;
- to read the values of manipulator deflections;
- to integrate the equation of control element dynamic;
- to synchronize the experimental process with real time;
- to keep the results of the current run.

The data reduction module.

This module allows to get the following:

- the frequency response characteristics of the control element dynamics, pilot, open-loop and closed-loop system;
- the power spectral densities and variances of all signals and their correlation and noncorrelation with input parts.
- the density of probability distribution for the measured signals.
- the parameters for frequency response characteristics of the open- and closed-loop system and parameters of pilot describing function.

The module for representation of results.

This module allows to get:

- the graphic representation of the current trial (each trial on a separate picture) and all trials together on the same picture (fig. C.1 shows the replacement of cues for the frequency response characteristics);
- output the results displayed on the screen or on the matrix printer.

SECTION 2

INVESTIGATION OF FEEL SYSTEM AND CONTROL SENSITIVITY CHARACTERISTICS INFLUENCING PIO OF UNMANEUVERABLE AIRCRAFT

Victor V. Rodchenko, PhD

Larisa E. Zaichik, PhD

Yury P Yashin, PhD

Victor V. Lyasnikov, PhD

Alexander M. Galyuchenko, PhD

Igor W. Rufov, PhD

CENTRAL AEROHYDRODYNAMIC INSTITUTE

ZHUKOVSKY, RUSSIA

CONTENTS

LIST OF FIGURES	141
NOMENCLATURE	144
INTRODUCTION	146
1.0 EXPERIMENTAL INVESTIGATION TECHNIQUE	148
1.1 FLIGHT SIMULATOR	148
1.2 THE TECHNIQUE OF PIO SIMULATION	148
1.2.1. Piloting Task and Other Experimental Conditions	148
1.2.2 An effect of Motion Cues on PIO	155
1.3 EXPERIMENTAL DATA PROCESSING	161
2.0 EFFECT OF FEEL-SYSTEM AND COMMAND SENSITIVITY CHARACTERISTICS ON LOW-FREQUENCY PIO	165
2.1 EFFECT OF COMMAND-RESPONSE GRADIENTS	165
2.2 EFFECT OF FEEL-SYSTEM CHARACTERISTICS	170
2.3 DESIGN CRITERIA FOR EVALUATION OF FEEL-SYSTEM AND COMMAND SENSITIVITY CHARACTERISTICS EFFECT ON PIO	177
3.0 INVESTIGATION OF LIMB-MANIPULATOR DYNAMIC INTERACTION WITH CONTROL OF "ELASTIC" AIRCRAFT	182
3.1 STATEMENT OF THE PROBLEM	182
3.2 UNMANEUVERABLE AIRCRAFT LATERAL MOTION MODEL COUPLED WITH ELASTIC MODES	186
3.3 EXPERIMENTAL RESULTS	191
3.4 ANALYSIS OF PILOT-AIRCRAFT SYSTEM CHARACTERISTICS	207
CONCLUSIONS	215
REFERENCES	217

LIST OF FIGURES

	Page
Figure 1.1 Flight Simulator FS-102	149
Figure 1.2 Cockpit Interior of Flight Simulator FS-102	149
Figure 1.3 Tracking Task Indicator	150
Figure 1.4 Tracking Task Scheme	150
Figure 1.5 Central Stick Feel System Characteristics	151
Figure 1.6 Side Stick Feel System Characteristics	152
Figure 1.7 Types of Indication for the Pitch Tracking Task	154
Figure 1.8 Forcing Function Spectral Densities	156
Figure 1.9 Motion Cues Influence on Roll Stabilization Precision	157
Figure 1.10 Motion Cues Influence on Roll Rate Magnitude of Roll Oscillations	157
Figure 1.11 Motion Cues Influence on Pilot Describing Function	158
Figure 1.12 Cockpit Motion Influence on High-Frequency Roll Oscillation of Elastic Aircraft	159
Figure 1.13 Diagram of Pilot-Aircraft System Including Closed-Loop Limb- Manipulator System	163
Figure 1.14 Pilot Closed-Loop Limb-Actuation With Feel System Dynamics	163
Figure 2.1 Command-Response Gradients Influence on Pilot Ratings (PR and PIOR) at Different Dynamic Performance for an Aircraft with a Central Stick	166
Figure 2.2 Lateral Command-Response Gradients Influence on Pilot Ratings (PR and PIOR) for Two Values of Roll Mode Time Constant for an Aircraft with Central Stick	167
Figure 2.3 Longitudinal Command-Response Gradient Influence on PIOR and PR	169

Figure 2.4 Limits of Pilot Ratings Worsening Variation PR at Command-Response Gradient Deflecting About Their Optimum Values	169
Figure 2.5 Pilot/Pilot-Aircraft Describing Function for Different Aircraft Gains	171
Figure 2.6 Longitudinal Feel System Gradient and Breakout Force Influence on PIOR and PR	172
Figure 2.7 Pitch and Roll Feel System Gradients Influence on PR	173
Figure 2.8 Influence of Feel System Gradients F^x and Command Response Gradients X_{nz} and X_p on Pilot Ratings	175
Figure 2.9 Pilot Ratings Deterioration Degree Due to PIO Tendency Increasing in the Case of Feel System (a) nad Control Sensitivity (b) Characteristics	176
Figure 2.10 Optimum Command-Response Gradients X_{nz} for 5 LAHOS Configurations for Landing Approach and Tracking Task	179
Figure 2.11 Roll Transfer Function Response for Optimal Control Sensitivity of Different Dynamic Configurations	180
Figure 2.12 Parameter A Depending on Gradient F^x of Central and Side Sticks	181
Figure 3.1 Time Histories for the Ratchet Case	183
Figure 3.2a Roll-Rate Transfer Function Response for the Aircraft with and without Airframe Elasticity	184
Figure 3.2b Lateral-Acceleration Transfer Function Response for the Aircraft with and without Airframe Dynamics	185
Figure 3.3 Block-Diagram of Aircraft Lateral Control System	189
Figure 3.4 Time Histories of Aircraft as Rigid Body	192
Figure 3.5 Time Histories of Elastic Aircraft ($A=1.0$) (roll, yaw, lateral)	193
Figure 3.6 Time Histories of Elastic Aircraft ($A=0.5$) (roll, yaw, lateral)	194
Figure 3.7 Time Histories of Elastic Aircraft ($A=0.25$) (roll, yaw, lateral)	195
Figure 3.8 Time Histories of Elastic Aircraft ($A=0.125$) (roll, yaw, lateral)	196

Figure 3.9 Elastic Mode Amplitude A Influence on Roll Rate and Lateral Acceleration Amplitudes	197
Figure 3.10 PIORs Depending on Elastic Mode Amplitude	197
Figure 3.11 Time Histories of Elastic Aircraft ($A = 1.0$) (roll motion) (central stick) (aircraft gain = 1.0)	198
Figure 3.12 Time Histories of Elastic Aircraft ($A = 1.0$) (no motion) (central stick) (aircraft gain = 1.0)	199
Figure 3.13 Time Histories of Elastic Aircraft ($A = 1.0$) (roll, yaw, lateral motion) (side stick) (aircraft gain = 1.0)	200
Figure 3.14a Time Histories of Elastic Aircraft ($A = 1.0$) (roll, yaw, lateral motion) (side stick) (aircraft gain = 0.5)	201
Figure 3.14b Time Histories of Elastic Aircraft ($A = 1.0$) (roll, yaw, lateral motion) (central stick) (aircraft gain = 0.5)	202
Figure 3.15 Time Histories of Elastic Aircraft ($A = 1.0$) (roll, yaw, lateral motion) (side stick) (aircraft gain = 2.0)	203
Figure 3.16 Lateral Control Sensitivities Influence on PIOR	204
Figure 3.17 Time Histories of Elastic Aircraft ($A = 1.0$) (roll motion) (central stick) (aircraft gain = 1.5)	206
Figure 3.18 Pilot/Pilot-Aircraft Describing Function ($T_R = 0.1s$)	208
Figure 3.19 Pilot/Pilot-Aircraft Describing Function ($T_R = 0.5s$)	209
Figure 3.20 Pilot/Pilot-Aircraft Describing Function ($T_R = 1.0 s$)	210
Figure 3.21 Pilot/Pilot-Aircraft Describing Function.....	211
Figure 3.22 Pilot/Pilot-Aircraft Describing Function (elastic aircraft)	213

NOMENCLATURE

- F, X - Manipulator force and displacement (kg, mm)
- F_{n_z}, X_{n_z} - Longitudinal command-response gradients (control sensitivity characteristics, kg/g, mm/g)
- F_p, X_p - Lateral command-response gradients (kg/deg/sec, mm/deg/sec)
- F^x, F_{br} - Feel system gradient and breakout force (kg/mm, kg)
- n_z, n_y - Normal and lateral accelerations
- n_{z_α} - Normal acceleration per unit angle of attack (g/rad)
- α, β - Angle of attack and sideslip angle (rad)
- θ, ϕ, ψ - Pitch, roll and yaw angles (rad)
- q, p, r - Pitch, roll, yaw rates (rad/sec)
- V - Flight velocity (m/sec)
- T_R - Roll mode time constant (sec)
- Y_p, Y_c - Transfer functions models of pilot and controlled element
- Y_{n_z} - $\frac{X}{n_z}$ - Transfer function
- Z, Y - Aerodynamic forces along z- and y- axes
- M, L, N - Pitching, rolling and yawing aerodynamic moments
- $\delta_a, \delta_e, \delta_r$ - Deflection of aileron, elevator and rudder (deg)

$Z_\alpha, \dots, Y_\beta, \dots, M_\alpha, \dots, L_\beta, \dots, N_\beta, \dots$ - Force and moment aerodynamic dimensionless derivatives

INTRODUCTION

Pilot-induced-oscillation phenomenon (PIO) has been a problem of considerable importance for modern aircraft. This problem crops up while developing almost every new aircraft. However, no effective design or experimental methods have yet been developed to predict a PIO tendency at an early stage of aircraft designing and tests. MIL-F-8785C for example, just states that an aircraft will not have a PIO tendency, but provides no guidance in the area of precluding PIO tendency by design ⁽¹⁾. So the great attention has been paid recently to investigation of this problem both in this country and abroad ⁽¹⁻¹⁶⁾.

A PIO tendency depends on aircraft dynamic performance, as well as on manipulator feel system characteristics and command - response gradients. The greater success was achieved in studying the effect of aircraft dynamic performance (time delay, actuator rate limiting, etc.) on the ordinary low-frequency, up to 1 Hz, PIO (works of D.McRuer, T.Neal, R.Smith, R.Hoh⁽⁴⁻⁷⁾, and others). For studying and precluding this type of PIO there are well developed and widely used methods based on a pilot-vehicle mathematical model; the methods allow a designer to estimate the dynamic performance admissible in terms of pilot-vehicle system stability. A number of criteria are developed to investigate the latent PIO causes due to abrupt changes in dynamic performance or in flying conditions (presence of a catalyst: failures, stress situations, switching from one control loop over to another, etc.). The common drawback of the approaches is that they do not take into account the effect of feel system and control sensitivity characteristics on PIO. These characteristics are usually considered to be optimum and, as a rule, they are considered optimum for a tracking task. However, neither the optimum values of the characteristics nor any methodology for their definition are ever shown. These drawbacks diminish considerably the approaches usefulness since in reality the feel system characteristics and command gradients can greatly differ from the optimum values.

Along with low-frequency PIO, high-frequency oscillations (about 1.5-3 Hz), named *ratchet*, have become possible. Especially great attention has been paid recently to the ratchet in the roll axis, discovered on quite a number of aircraft with small roll mode time constants. As it is shown in many publications (see ^(8,9) and others), ratchet, as well as low-frequency PIO, occurs as a result of pilot / aircraft interaction. The main cause of ratchet was peaking in amplitude of a limb-manipulator describing function in high frequencies region. The presence of the peaks, their values and frequencies, depend on manipulator feel system and command sensitivity characteristics. However, this dependence and a ratchet phenomenon as a whole have not been sufficiently studied yet. Special attention should be paid to ratchet coupling with structural modes of an airframe (CH-53, F-111, C-17 ⁽³⁾ and others), since there is a tendency in modern aircraft to diminish their structural stiffness that results in coupling of airframe structural modes and limb-manipulator dynamic performance.

A number of publications on an effect of manipulator feel system and command sensitivity characteristics on handling qualities ⁽¹⁷⁻²²⁾ have appeared recently. Nevertheless, this problem, in terms of PIO tendency especially, is insufficiently studied yet, and at present there are no methods to estimate the above mentioned effect.

While developing controllability criteria and theoretical methods of PIO tendency estimation, it is also important to improve the experimental methods of investigation. Complexity of PIO ground-based investigation is determined by the fact that aircraft oscillation tendency manifests itself irregularly and depends not only on aircraft characteristics, but on the piloting task and pilot physiological state. Therefore, it is necessary to improve methods of PIO modeling and experimental data processing to study both evident and latent causes of PIO.

The goals of the work are:

- development of PIO investigation methods on a ground-based simulator,
- studying the effect of manipulator feel system and command sensitivity characteristics on low-frequency PIO and creating the criterion of the effect estimation,
- studying the effect of limb-manipulator dynamic performance coupled with structural elastic modes on high-frequency oscillation aircraft, and the development of a technique to estimate the effect.

Besides, a few experiments in cooperation with MAI and FRI were conducted on TsAGI Flight Simulator FS-102 as a part of work under the contracts with Wright Laboratory. For those purposes, the Tu-154M in-flight simulator dynamics was modeled in FS-102, the tracking task indicator was modeled on the special "book-size" display, the flight test technique was worked out and in-flight simulator model parameters were selected, the test-pilots were trained. The results of this part of the work are not considered in the present report, since they are referred to in the reports of MAI and FRI.

1.0 EXPERIMENTAL INVESTIGATION TECHNIQUE

1.1 FLIGHT SIMULATOR

The experimental part of the work was conducted on flight simulator FS-102. The simulator is intended, mainly, for investigation of stability and controllability of unmaneuverable aircraft. This simulator was selected because its structure and system parameters give an opportunity to study, more completely, the effect of different flight factors on PIO: to reproduce linear and angular accelerations along all degrees of freedom, to change quickly manipulator types and their characteristics and the kinds of flight information displayed, and other flight conditions.

The photos of the simulator and its systems are presented in fig. 1.1-1.3. The simulator has following principal characteristics:

- Visual system: single-channel, optical collimating system, computer-generated image of a runway and its vicinity (fig. 1.2).
- Motion system (fig. 1.1): of synergetic type, 6DOF with the travel limits:
 - vertical ± 1.2 m, longitudinal and lateral directions ± 1.5 m;
 - roll ± 30 deg, pitch ± 40 deg, yaw ± 60 deg.
- Pilot cockpit (fig. 1.2): two seats, the equipment ordinary for unmaneuverable aircraft.
- Piloting displays (fig. 1.2): In the instrument desk there are the ordinary piloting indicators and two special displays installed. On the first of them, the right one, there are different indicators reproduced which display the current values of angle-of-attack, normal acceleration, airspeed, altitude, vertical speed. The left display (fig. 1.3) was used as an indicator for the tracking task simulation (fig. 1.4) while studying PIO phenomenon.
- Control manipulators: changeable. The spring central stick and electro-hydraulic side stick (fig. 1.3) were mostly used in the experiments (the characteristics are presented in fig. 1.5, 1.6). In several experiments the electro-hydraulic central stick with widely changeable characteristics was used. These manipulators were used because the simultaneous work being conducted by MAI and FRI using these types of manipulators.

1.2 THE TECHNIQUE OF PIO SIMULATION

1.2.1 Piloting Task and Other Experimental Conditions

Piloting task. For experimental investigation of PIO the tracking task was used (the diagram is represented in fig. 1.4). This type of piloting task was selected due to its methodological advantages. First, only in the case of persistent handling under disturbance input conditions, can pilot describing functions be identified. It is impossible to develop theoretical

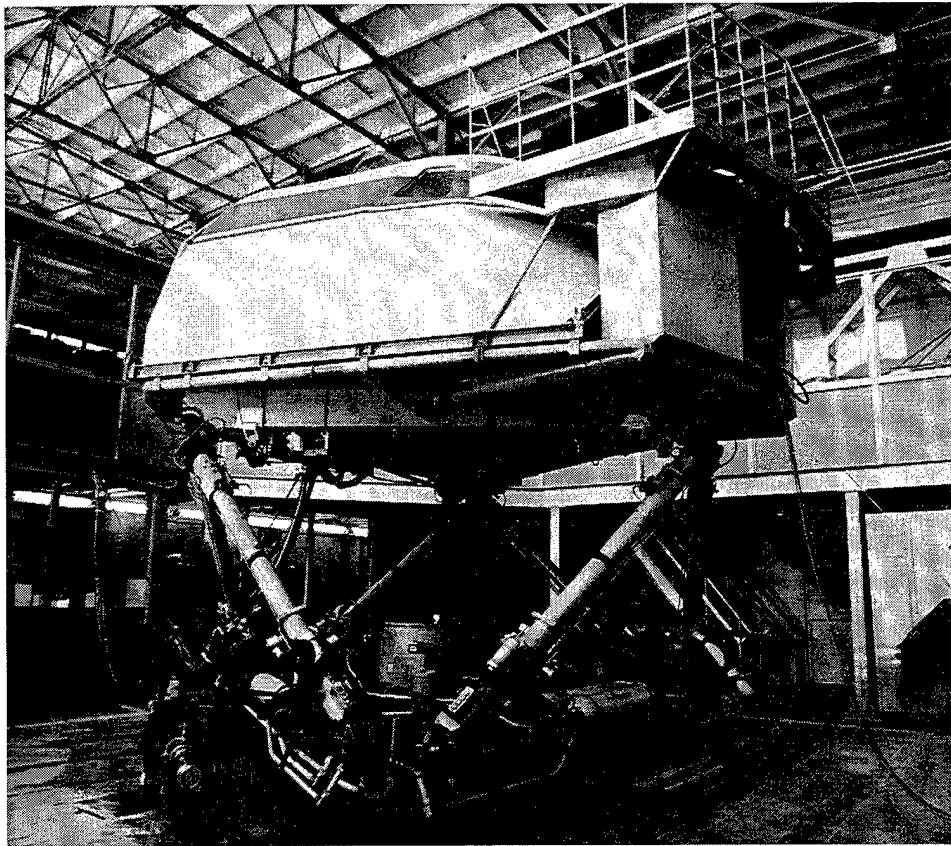


Fig.1.1. Flight Simulator FS-102

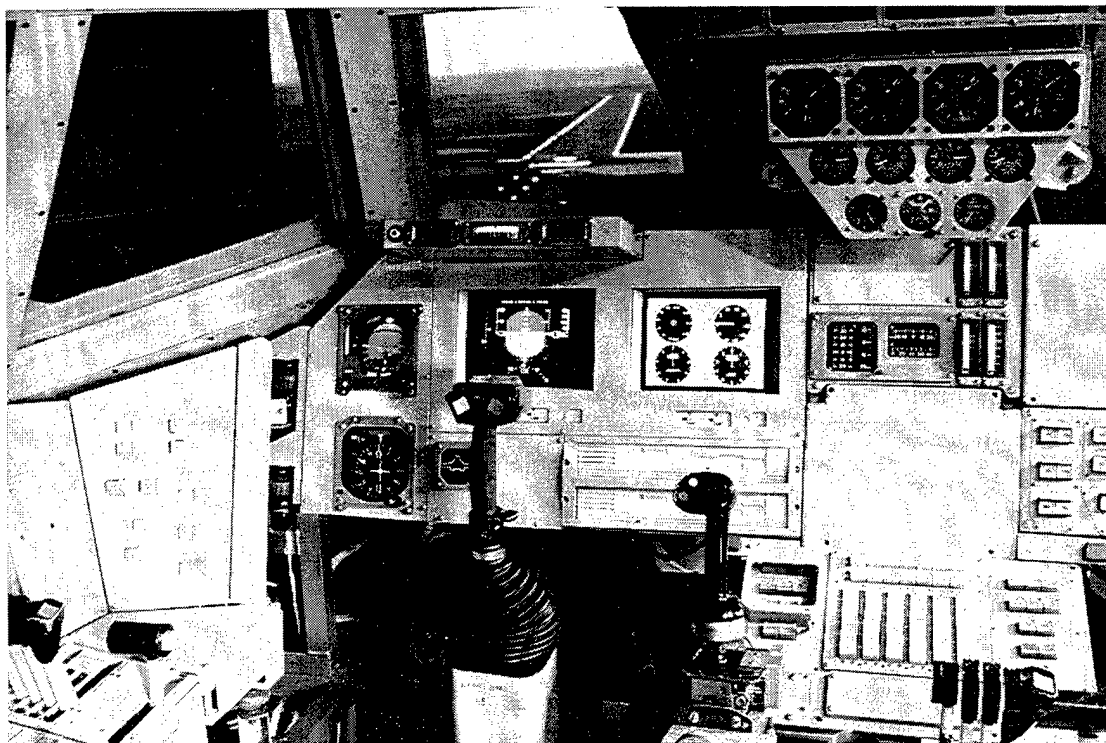


Fig.1.2. Cockpit Interior of Flight Simulator FS-102



Fig.1.3. Tracking Task Indicator

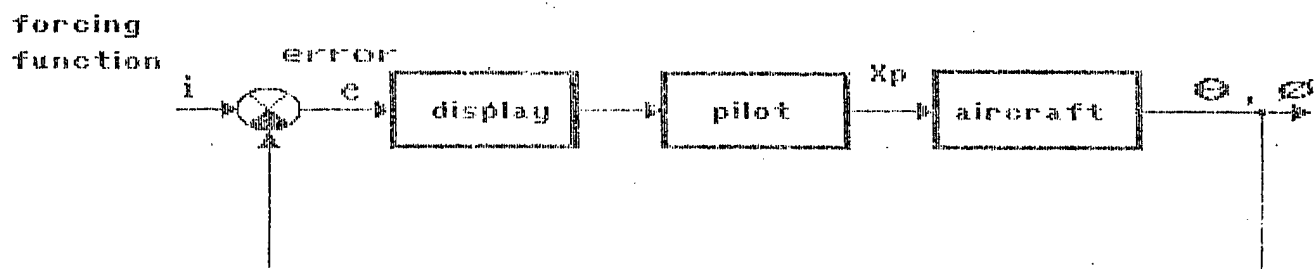


Fig. 1.4 Tracking task scheme.

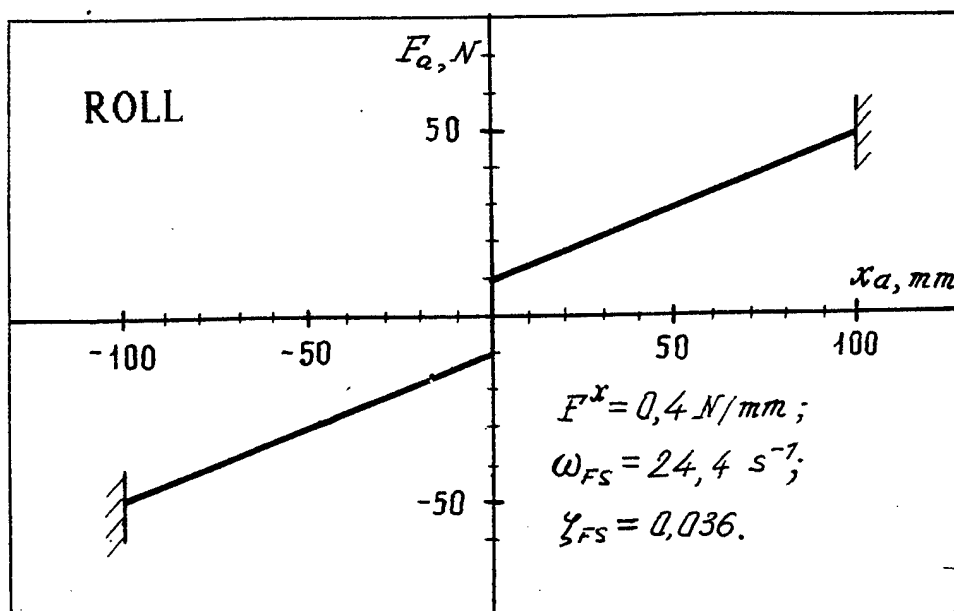
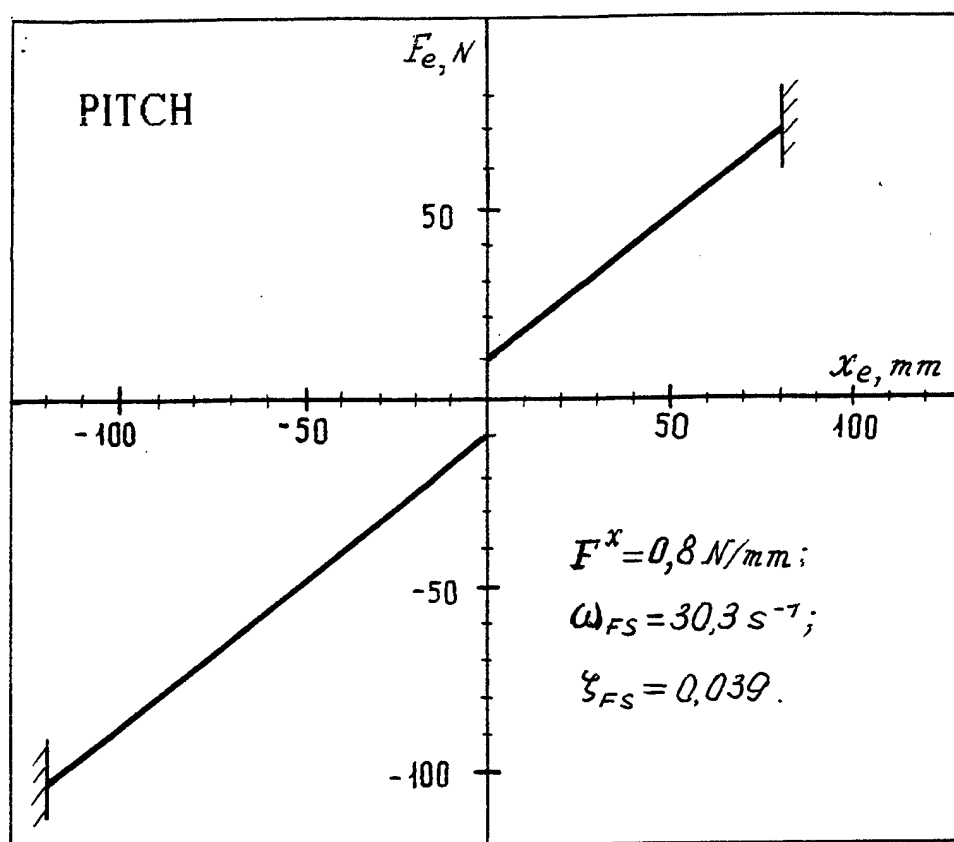


Fig.1.5. Central Stick Feel System Characteristics

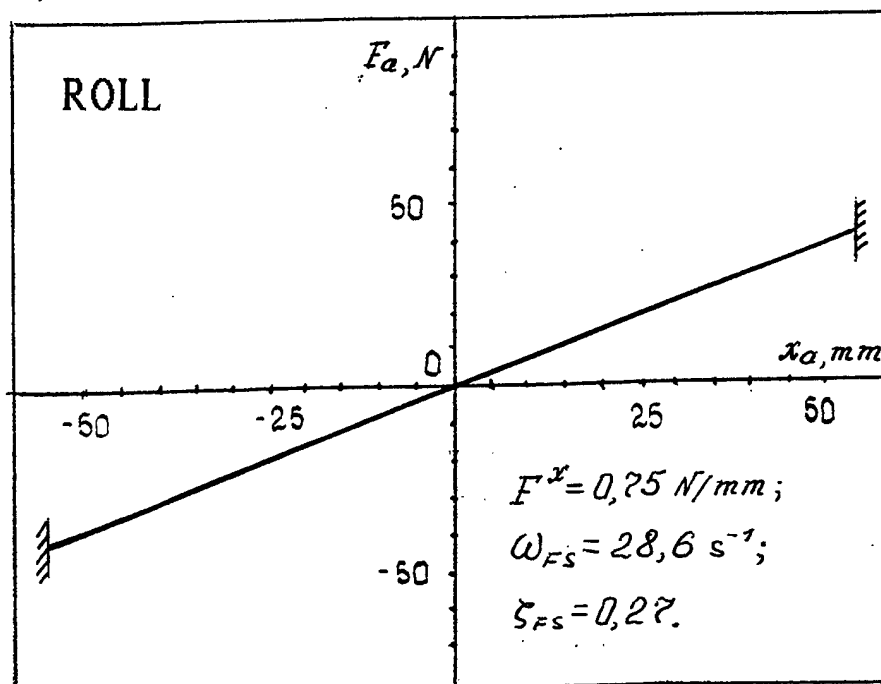
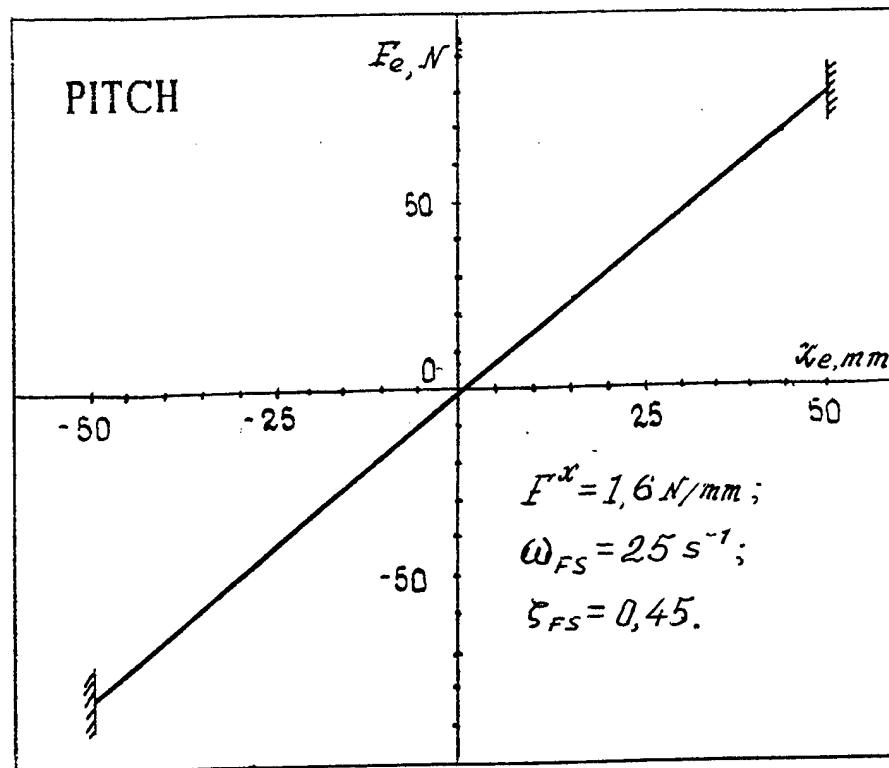


Fig.1.6. Side Stick Feel System Characteristics

methods of controllability or to investigate PIO problems without these functions. Second, it was this very piloting task that was used to develop a number of existing methods to study controllability as a whole and criteria for PIO tendency evaluation in particular. Therefore, when considering this piloting task, there is the possibility of comparing the results of theoretical and experimental investigations. It results in improving the theoretical methods of controllability investigation, on the one hand, and, on the other hand, in simplifying the experimental results analysis. Third, the tracking task is easy to simulate and it is easy for both pilots and operators to be trained. Its modeling does not require complex experimental equipment and experimental conditions; results obtained in different experiments, on flight simulators and flying conditions, are easy to reproduce and compare. Finally, the pilot-aircraft system responses defined for this piloting task can be a sort of basic standard for PIO tendency evaluating. This very task was used to conduct unique flight tests within different programs (LAHOS and others). In the present work this task was used as well for the joint experiments (TsAGI, MAI, FRI) carried out to develop a technique of PIO analyzing.

In addition to the tracking task, a landing approach was modeled in the course of experiments. The experimental conditions for a landing approach task correspond to those defined in the report ⁽²²⁾ and, therefore, are not referred to in this report.

Tracking task indication type. While performing a pitch tracking task, a pilot was instructed to keep the pitch tracking error e (i.e. the difference between the pitch predetermined by a certain disturbance input function i and the current pitch value θ) (fig. 1.4) within the limits represented in the indicator as lines. The lines were to be the permissible range of the tracking error. An indication of the lines and the tracking error were reproduced in the attitude indicator together with an indication of the current values of pitch, roll and yaw, altitude, vertical speed and others. Angles of pitch and roll were reproduced in full scale. The image of the attitude indicator was generated on a computer and then reproduced on a special "book-size" display (fig. 1.3), which was installed in the instrumentation panel of the simulator cockpit. Two types of indication were considered (fig. 1.7a,b). In the first case (fig. 1.7a) the mark of the tracking error moved while the lines were fixed. In the second case (fig. 1.7b) the error mark was fixed about the central line of the attitude indicator while the lines moved, i.e. were deflected in accordance with the pitch angle.

The investigation results showed that pilots adaptability was absolutely the same in both cases of error indication. Piloting accuracy does not depend on the type of indication either. However, for the operators, who participated in the experiments as well, the first type of indication seemed to be easier to comprehend and to use in practice. Therefore, the first indication type was chosen for further investigation (fig. 1.7a).

To simulate a roll tracking task, the roll error mark was presented on the display and the error was to be nulled by a pilot while performing the tracking. For this case no precision limits were displayed.

Disturbance input and aircraft dynamics. Pitch and roll force functions manifested themselves as sum of sines (SOS):

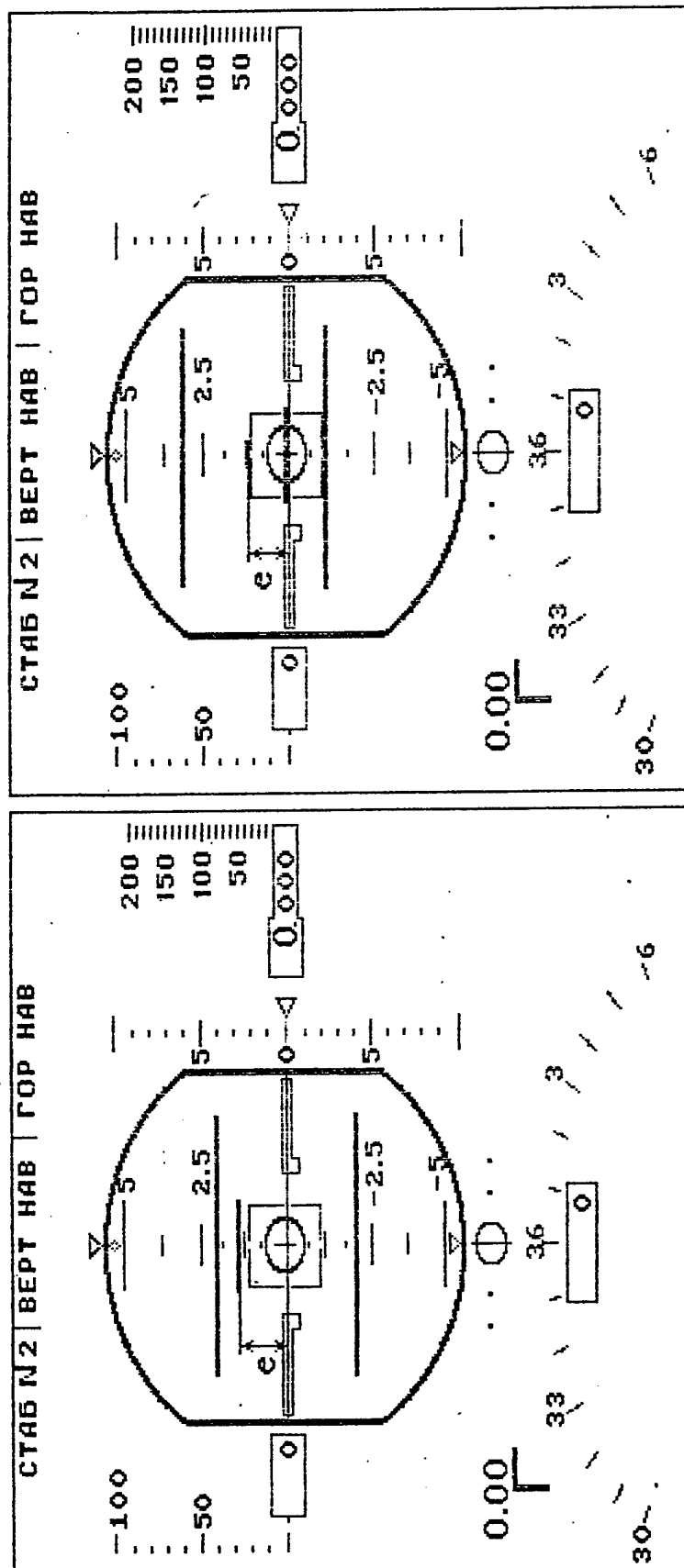


Fig. 1.7 Types of indication for the pitch tracking task.

$$F(t) = \sum_{i=1}^{i=15} A_i \sin \omega_i t$$

Magnitudes A_i and frequencies ω_i used in the pitch and roll loop correspond to those plotted in fig. 1.8. Higher force function frequencies for the roll in comparison with the pitch are accounted for by the fact that in the longitudinal channel low-frequency oscillations were studied, while in the lateral channel high-frequency oscillations were considered.

In a few experiments some LAHOS dynamic configurations were modeled for the results to be later compared with the results of MAI and FRI studies. In the present work LAHOS configurations 1-4, 2-1, 2-10, 3-3, 4-10 and others were considered.

In other experiments both longitudinal and lateral aircraft motion was modeled in accordance with the equations given in part 3.2.

Three test-pilots, one former military pilot and one operator participated in the experiments.

1.2.2 An Effect of Motion Cues on PIO

The conducted investigations of acceleration effect on PIO phenomenon and available publications as well, show, that motion cues play a significant role in PIO. The degree of this effect depends on quite a number of factors: control channel, aircraft performance, flying task and others.

Let us consider first the experimental results of motion cue effect on roll control, see fig. 1.9.-1.12. Fig. 1.9 illustrates roll damping influence ($1/T_R$) on roll tracking precision. It is seen that simulator motion diminishes a roll error considerably. The positive role of motion cueing is especially evident at low values of roll damping, where a PIO tendency is observed. In fig. 1.10 the data on roll rate magnitudes of the oscillations occurred at low negative roll damping values are shown. The data were obtained earlier on TsAGI's simulator with and without motion system for various fields of view ⁽¹¹⁾. It is seen that angular accelerations greatly influence PIO. Due to the simulator motion the roll rate oscillation magnitude decreases 3-5 times.

That positive effect of simulator motion on handling quality can be illustrated by the pilot describing function presented in fig. 1.11. The data show that in the case of both moving and unmoving simulator, the pilot behavior can be described quite well by the function

$$Y_p = K_p (T_1 s + 1) e^{-s\tau}.$$

However, as a simulator moves pilot pure time delay decreases (in this case, from $\tau = 0.26$ sec to $\tau = 0.19$ sec). Due to time delay decreasing a pilot-aircraft system stability margin increases, that allows a pilot to raise his gain (in our case from $K_p = 4.5$ to $K_p = 7.5$). For this

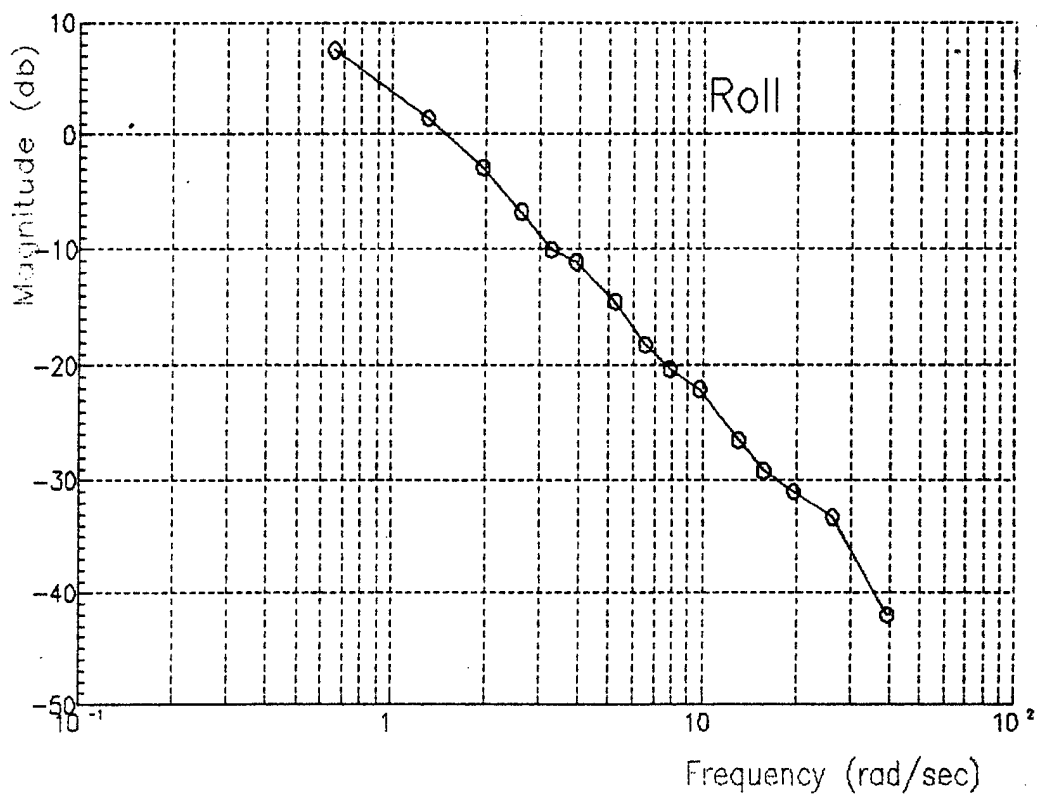
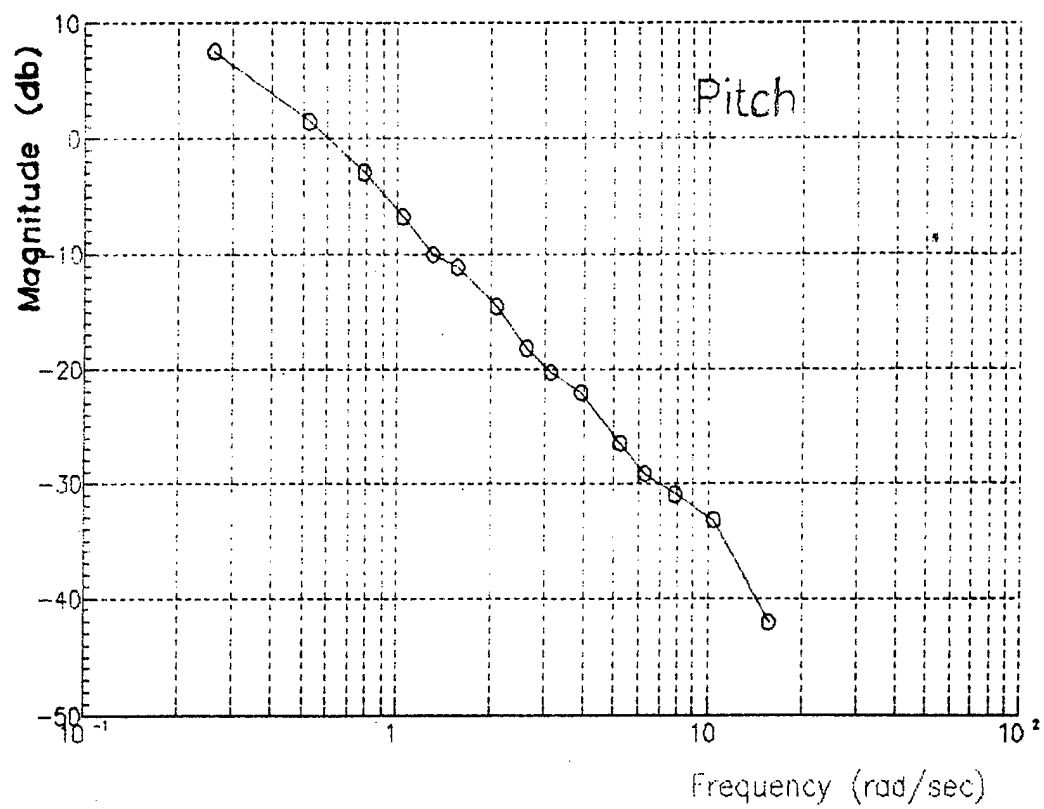


Fig.1.8 Forcing function spectral densities.

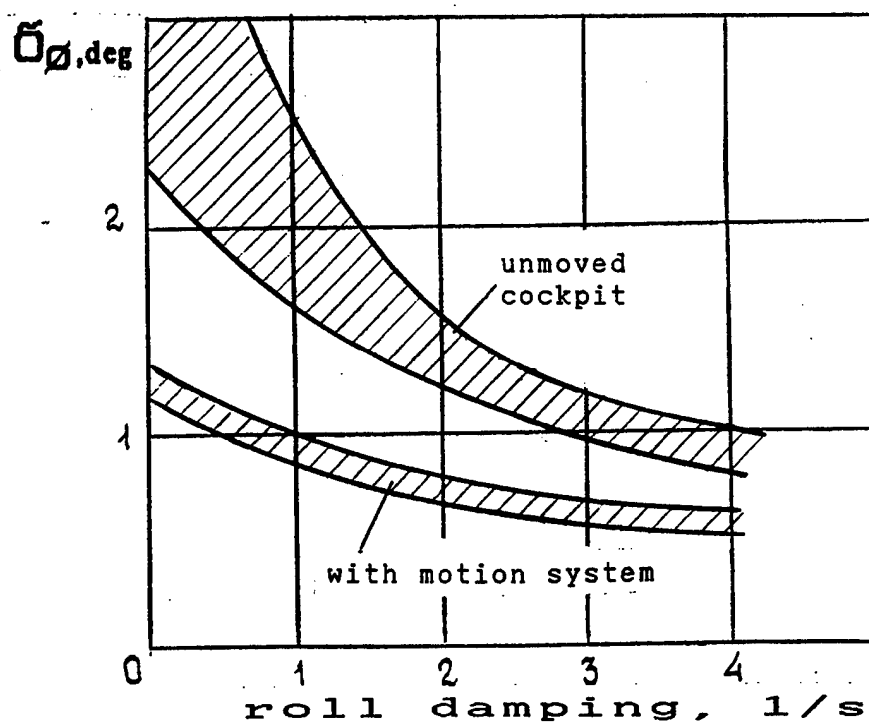


Fig.1.9. Motion Cues Influence on Roll Stabilization Precision

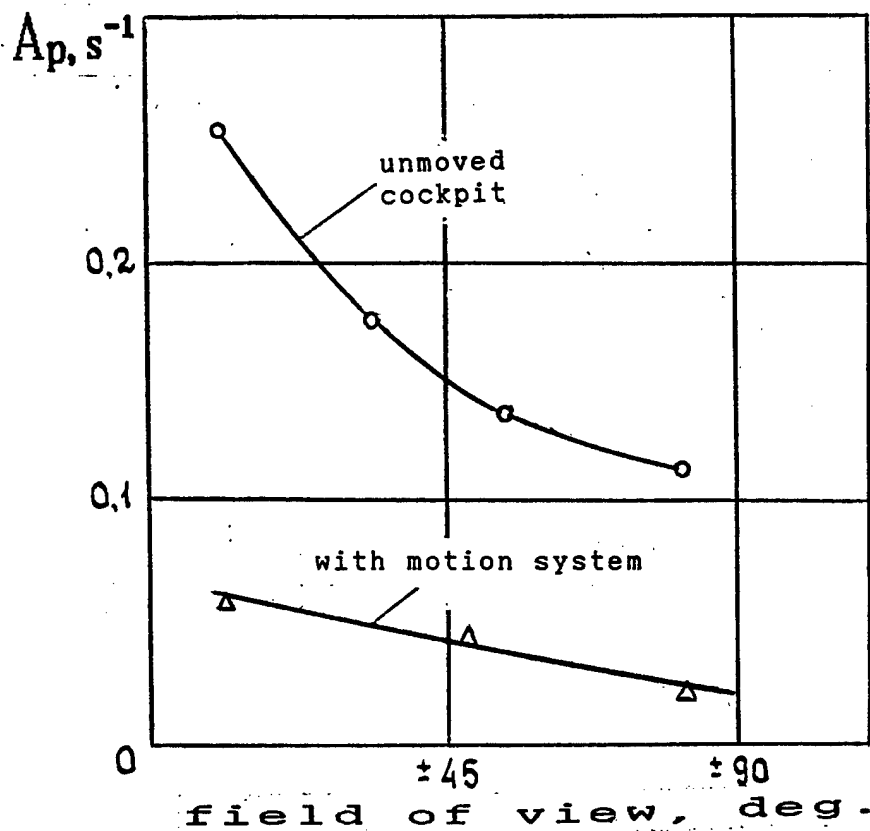


Fig.1.10. Motion Cues Influence on Roll Rate Magnitude of Roll Oscillations

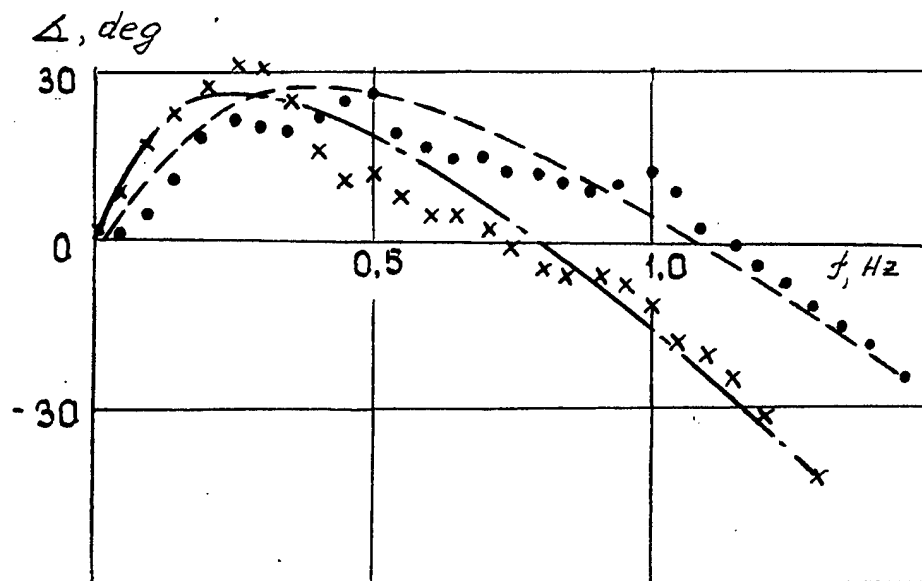
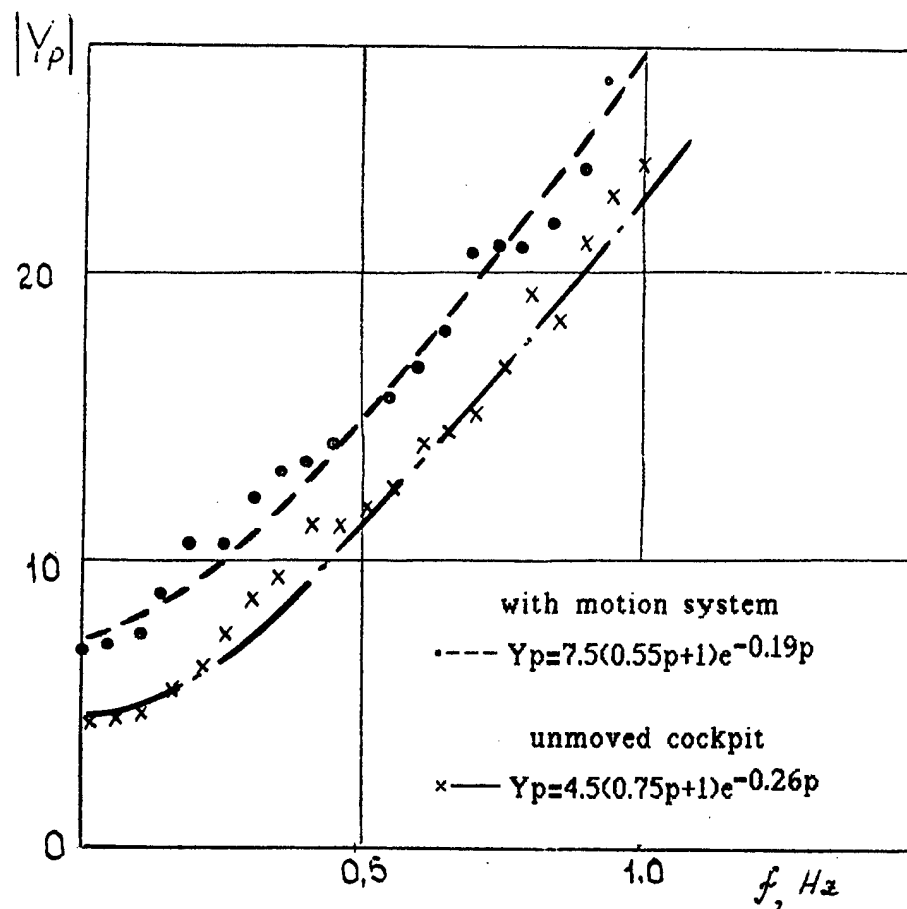


Fig.1.11. Motion Cues Influence
 on Pilot Describing Function

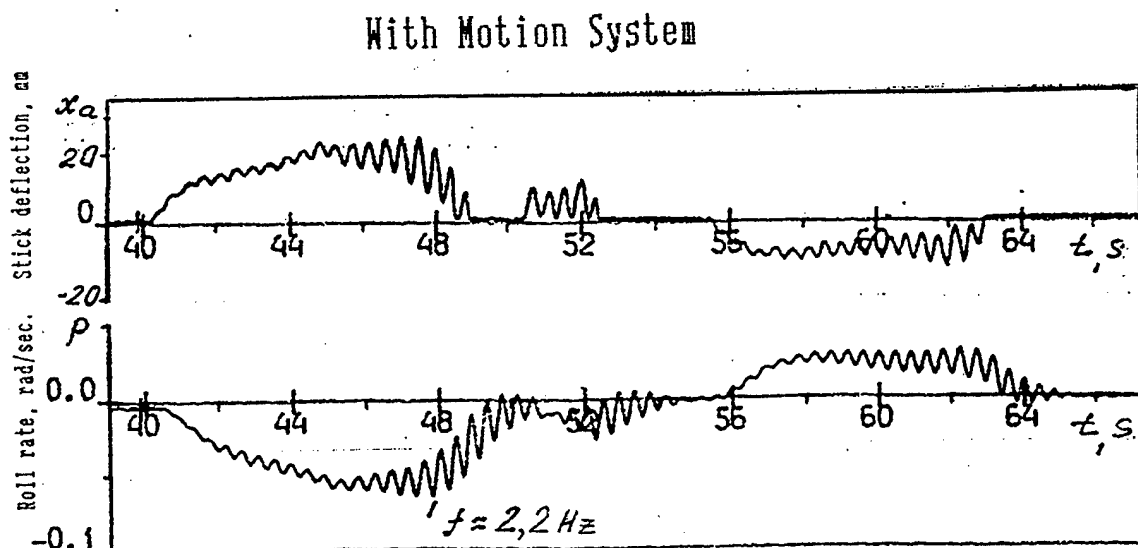
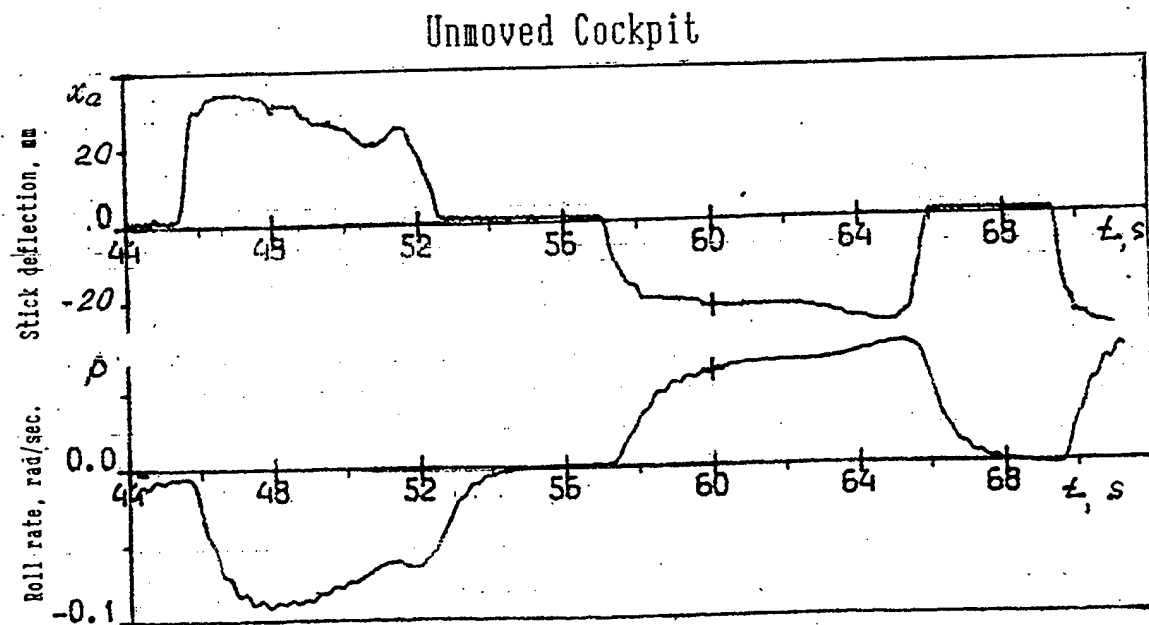


Fig.1.12. Cockpit Motion Influence on High-Frequency Roll Oscillation of Elastic Aircraft.

reason in the case of moving simulator roll error compensation improves and PIO probability decreases.

In some cases motion cues can, on the contrary, promote PIO. Roll high frequency oscillations can be an illustration of this effect. In fig. 1.12 time histories obtained on a moving/unmoving simulator for the aircraft model with certain elastic modes are shown. (The results of the experiments will be considered in detail in chapter 3.) It is seen, that oscillations appear only on a moving simulator. Neither in the previous investigations ⁽⁹⁾ nor in the present one the attempts to reproduce ratchet cases in real flight have been successful on unmoving simulators. This fact points out once more to the essential role of motion cues in high frequency oscillations phenomenon.

In the longitudinal channel an effect of motion cueing on piloting and a PIO tendency is not so evident. Nevertheless, according to the comments of the evaluation pilots, simulator motion makes simulation conditions seem more realistic. The pilots noted that in some cases motion cues intensify a PIO tendency, in others they do not influence the tendency or mitigate it. Motion cues influence piloting precision in the same way as they affect PIO.

A possibility of a negative effect of accelerations on PIO is consistent, for example, with R. Smith's criterion ⁽⁵⁾. In accordance with the criterion the frequency can exist at which the power spectral density of the pilot's normal acceleration due to pitch attitude tracking is sufficiently narrowband. If such a frequency exists, there is a high probability in high gain tracking task pilot will switch from tracking pitch to tracking the normal acceleration he feels at that frequency. If phase margin of the pilot-felt normal acceleration to stick force dynamics is less than zero, then the aircraft will have a tendency to PIO at that frequency.

The positive effect of cockpit motion on piloting is usually displayed while the accelerations are reproduced with regard to the distance between the cockpit position and center-of-gravity ($l \gg 0$) and especially while there is no PIO tendency observed.

The effect of cockpit motion on pitch tracking may disappear at $l = 0$, which can be attributed to the fact that motion cues do not give a pilot any additional information in comparison with visual ones. It has been shown that in the case of an aircraft of a traditional configuration, motion cues do not practically lead visual cues due to the inseparable connection of a normal acceleration and a pitch angle at pilot activity frequencies

$$\frac{n_z}{\theta} = \frac{n_z s}{s + \frac{n_z g}{V}}$$

and due to the fact that the acceleration in c.g. does not significantly lead a pitch angle. Pitch acceleration feeling and its using by a pilot are hampered due to the strong effect of normal accelerations acting in combination with a pitch acceleration.

In view of the distance between the pilot cockpit and c.g., the $\frac{n_z}{\theta}$ - transfer function takes the form

$$\frac{n_z}{\theta} = \frac{n_z s}{s + \frac{n_z g}{V}} + \frac{l}{g} s^2.$$

It is seen from this equation, that an acceleration leads a pitch angle, and therefore, motion cues can produce a favorable effect on controlling. If the aircraft tends to oscillate in pitch, simulating a normal acceleration can worsen these oscillations, as it was observed in several experiments.

Thus, the data considered above show that motion cues can influence piloting and a PIO tendency greatly. Three cases should be defined: motion cues producing a positive effect on piloting and mitigating a PIO tendency; motions cues producing no effect at all; motion cues intensifying a PIO tendency. At present there are no theoretical methods to estimate a degree of this effect for all possible cases. Therefore, experimental investigations of PIO should be conducted on moving-base flight simulators. It can be mentioned also, that a moving-base simulator has some methodological advantages in comparison with an in-flight simulator. For example, on a moving-base simulator, it is possible to change acceleration conditions (scaling, separate switching on different degrees of freedom, etc.) without changing other flying conditions, which is impossible in real flight due to the inseparable unity of motion and visual cues and other types of flying information. Therefore, for a study of motion cues effect on PIO phenomenon, a moving-base simulator is preferable to an in-flight simulator.

1.3 EXPERIMENTAL DATA PROCESSING

In the work both subjective and objective methods of experimental data processing were used.

Pilot rating scales used. in the work two pilot rating scales were used: PIO rating scale (PIOR) and Cooper-Harper's pilot rating scale (PR). The PIOR scale was used to illustrate that pilot ratings worsen due to PIO tendency intensification as command sensitivity increases or feel system gradients decrease in comparison with their optimum values. However, for the final rating the PR-scale was used, since it is a multipurpose scale adapted for evaluation of controllability in different flight conditions, including a PIO tendency. The scale is well known for experts in stability and controllability problems and pilots engaged in the experiments. It is important also that this scale is used for standardization of handling qualities in Specifications in different countries.

Each studied aircraft configuration was flown no less than 3 - 5 times. The ratings obtained were averaged. In accordance with the technique stated in ⁽¹³⁾, the confidence interval of rating arithmetic mean for 3-5 runs does not exceed PR = 0.7-1. For the aircraft configurations of Level 1, the confidence interval is about PR = 0.5.

The technique of pilot describing function identification. In the study the run-time histories processing was carried out according to the technique for a single-loop tracking task ⁽¹³⁾.

In this study, an attempt was made to develop an experimental technique to identify a pilot describing function as a whole and, in particular, its partial corresponding to the dynamics of a limb-manipulator system. The block diagram of the pilot-aircraft system for this case is shown in fig. 1.13. The model does not contradict the modern pilot behavior models, for example, the McRuer's model presented in fig. 1.14. In this diagram and further the following notations are applied:

- e - tracking error displayed on an indicator and observed by a pilot (command stimulus),
- i - disturbance input (sum-of-sines forcing function),
- θ, ϕ - current state variables (for example, pitch or roll angle),
- F - stick force, kg
- X - stick displacement, mm
- f - force disturbance generated in feel system,
- Y_{cns} - transfer function model of central nervous system,
- Y_{lm} - transfer function model of closed-loop limb-manipulator system,
- Y_{ns} - transfer function model of neuromuscular system,
- Y_p - pilot transfer function model ($Y_p = Y_{cns} \times Y_{lm}$),
- Y_{fs} - feel system transfer function model,
- Y_c - transfer function model of the controlled element (for example, stick displacement (X , mm) referred to pitch or roll (θ, ϕ , deg)),
- n_e - pilot remnant transferred to visual input,
- n_x - limb-manipulator system remnant transferred to force.

As seen in the diagram, a pilot-aircraft system incorporating a neuromuscular system is a two-loop model. To identify simultaneously two transfer functions in this system (Y_p and its partial Y_{lm}), the inputs i and f should be uncorrelated. Let us consider each of them to be Gaussian white noise passing through a linear filter. In accordance with the remnant definition given in ⁽¹³⁾, remnants n_e and n_x are considered uncorrelated with the inputs i and f .

To identify the transfer function models the Fourier transform algorithm was used. According to this algorithm, a stick displacement and a tracking error can be described as follows:

$$\begin{aligned} X(j\omega) &= X_i(j\omega) + X_{n_e}(j\omega) + X_f(j\omega) + X_{n_x}(j\omega) \\ E(j\omega) &= E_i(j\omega) + E_{n_e}(j\omega) + E_f(j\omega) + E_{n_x}(j\omega) \end{aligned} \quad (1.1)$$

Subscripts i, n_e, f, n_x here and further, refer to the processes in a closed-loop pilot-aircraft system, caused by $i(t), n_e(t), f(t), n_x(t)$. With the use of the transfer functions shown in figure 1.13, eq.(1.1) takes the following form (for the sake of brevity, $j\omega$ is omitted):

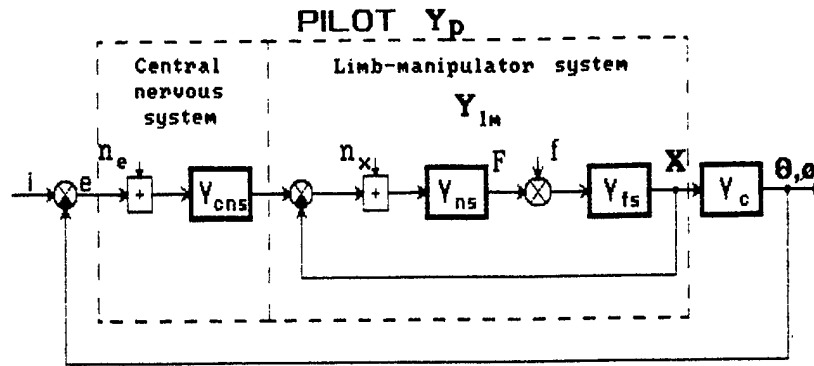


Fig.1.13 Diagram of pilot-aircraft system including closed loop limb-manipulator system.

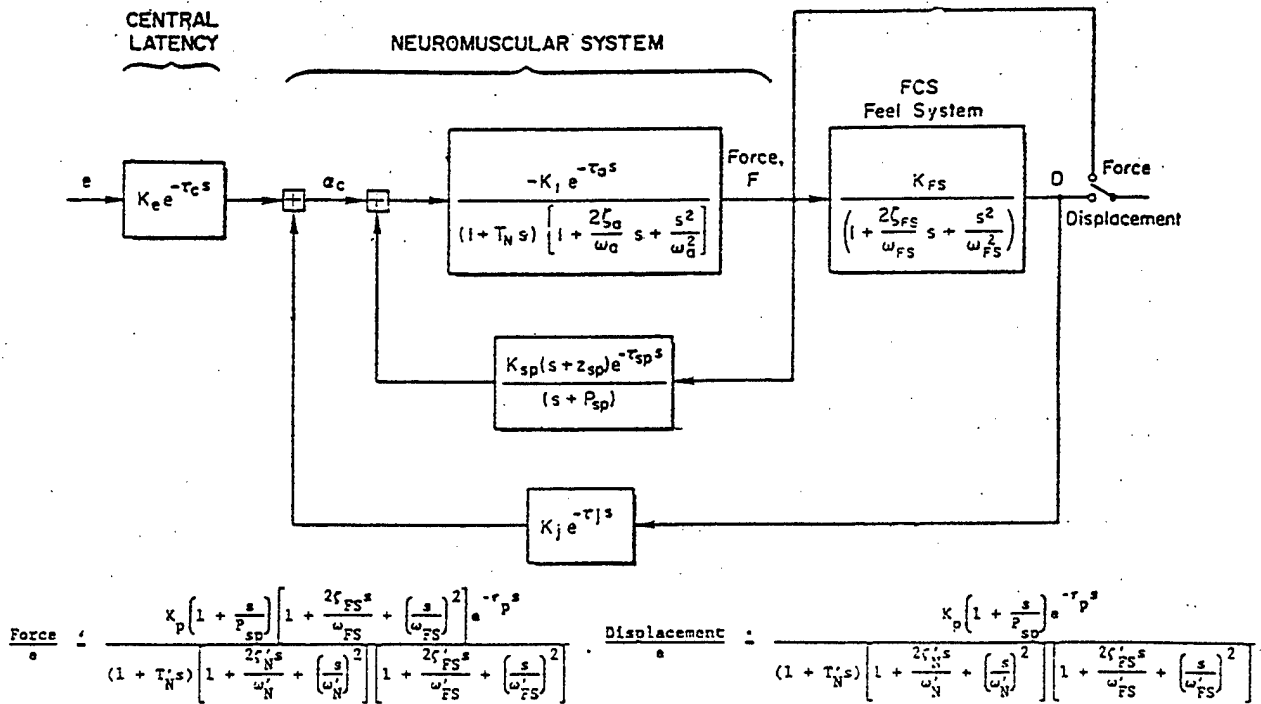


Fig.1.14. Pilot Closed-Loop Limb-Actuation With Feel System Dynamics

$$\begin{aligned} X &= \frac{Y_p}{\Delta} I + \frac{Y_p}{\Delta} N_e + \frac{Y_{fs}}{\Delta(1+Y_{ns}Y_{fs})} F + \frac{1}{1+Y_{ns}Y_{fs}} N_x \\ E &= \frac{1}{\Delta} I - \frac{Y_p Y_c}{\Delta} N_e - \frac{Y_{fs} Y_c}{(1+Y_{ns}Y_{fs})\Delta} F - \frac{Y_c}{(1+Y_{ns}Y_{fs})\Delta} N_x \end{aligned} \quad (1.2)$$

where $\Delta = 1 + Y_p Y_c$.

Now, taking into account that i, f, n_e, n_x are uncorrelated, one can obtain the following power spectra:

$$\begin{aligned} S_{xi} &= \frac{Y_p}{\Delta} S_{ii} \\ S_{ei} &= \frac{1}{\Delta} S_{ii} \\ S_{xf} &= \frac{Y_{fs}}{\Delta(1+Y_{ns}Y_{fs})} S_{ff} \end{aligned} \quad (1.3)$$

where $S_{ii}, S_{ff}, S_{cf}, S_{ef}$ - power spectra of inputs.

Having divided left and right hand parts of the first two equations, one has

$$Y_p(j\omega) = \frac{S_{xi}(j\omega)}{S_{ei}(j\omega)} \quad (1.4)$$

Taking into account that

$$\begin{aligned} \delta &= F + \bar{F}, \\ Y_{fs}(j\omega) &= \frac{S_{xi}}{S_{\delta i}}, \end{aligned}$$

from equations (1.3), it is easy to obtain

$$Y_{lm}(j\omega) = \frac{S_{xi} S_{ei} S_{ff} - S_{xf} S_{ii} S_{\delta i}}{S_{xi} S_{ei} S_{ff}}. \quad (1.5)$$

As it is shown in⁽¹³⁾, for a two-loop controlling task it is impossible to define separately the remnants n_e, n_x . It is possible to define their sum only. Let us consider that the remnant n_x as well as remnant n_e are transferred to command e . So, further we will consider only the sum of

remnant n_e , transferred to e . It can be shown that the power spectrum of the remnant can be calculated as

$$Se_n e_n(j\omega) = \frac{S_{ee}S_{ii}^2 - S_{ii}S_{ei}^2}{S_{xi}^2} \quad (1.6)$$

Thus, in the case of a two-loop controlling task, the describing functions Y_p, Y_{ln} and the pilot remnant $Se_n e_n$ can be determined by (1.4), (1.5), (1.6).

As to the practical application of the method, the following fact should be mentioned. A pilot describing function is identified more precisely when an input function manifests itself as sum of sines. However, in the case of a two-loop task, using two input functions leads to some difficulties in the identification process. These difficulties are accounted for by the difficulty in reproducing two uncorrelated input functions. Taking this into account, it has been proposed to produce one of the inputs as SOS, and another input as white noise passing through a linear filter.

The first experience in using the method has given hopeful results. However, the method requires further development.

2.0 EFFECT OF FEEL-SYSTEM AND COMMAND SENSITIVITY CHARACTERISTICS ON LOW-FREQUENCY PIO

Command sensitivity and feel system characteristics are the main factors affecting PIO phenomenon. This fact is mentioned in a number of publications. It is enough to say, that great attention is paid to this problem in specifications. It is for PIO precluding that the requirements for minimum values of these characteristics are specified in them. Nevertheless, the documents available show the effect of control sensitivity and feel system characteristics on PIO insufficiently and in kind only. It is known that complex interaction of such factors as dynamic performance, feel system characteristics and piloting task influences a degree of this effect considerably. However, reliable evaluation methods to show the effect have not yet been developed. One possible approach to this problem is considered in this chapter.

2.1 EFFECT OF COMMAND-RESPONSE GRADIENTS

In figs. 2.1, 2.2 the pilot ratings are plotted against the command-response gradients for longitudinal and lateral channels. The relations have been obtained for different dynamic performance for an aircraft with a central stick. The PIORs presented there together with the PRs show that pilot ratings deterioration in the case of command-response gradients decreasing is correlated with PIO tendency intensified. These and quite a number of other data available show that regularities of the effect of control sensitivity and feel system characteristics on handling qualities and PIO, being referred to their optimum value, are the same for different piloting conditions, aircraft classes, control channels, piloting tasks, dynamic performance and manipulator

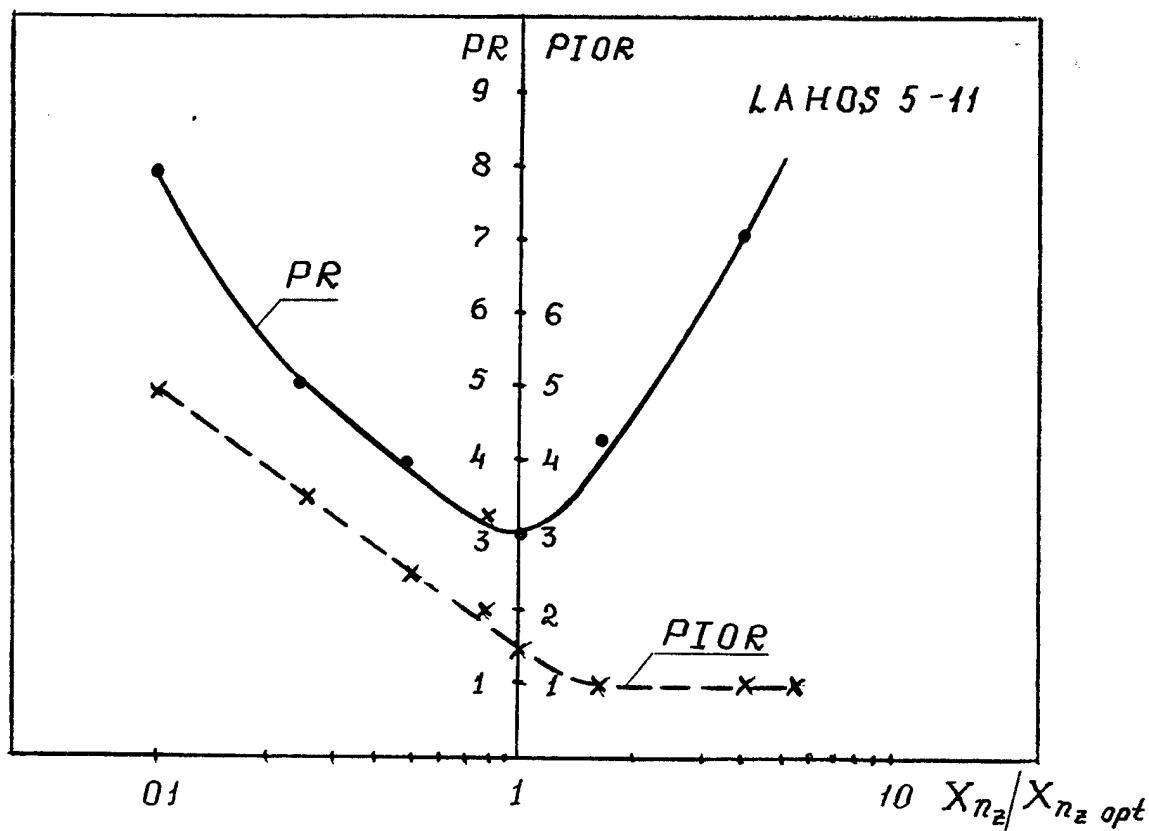
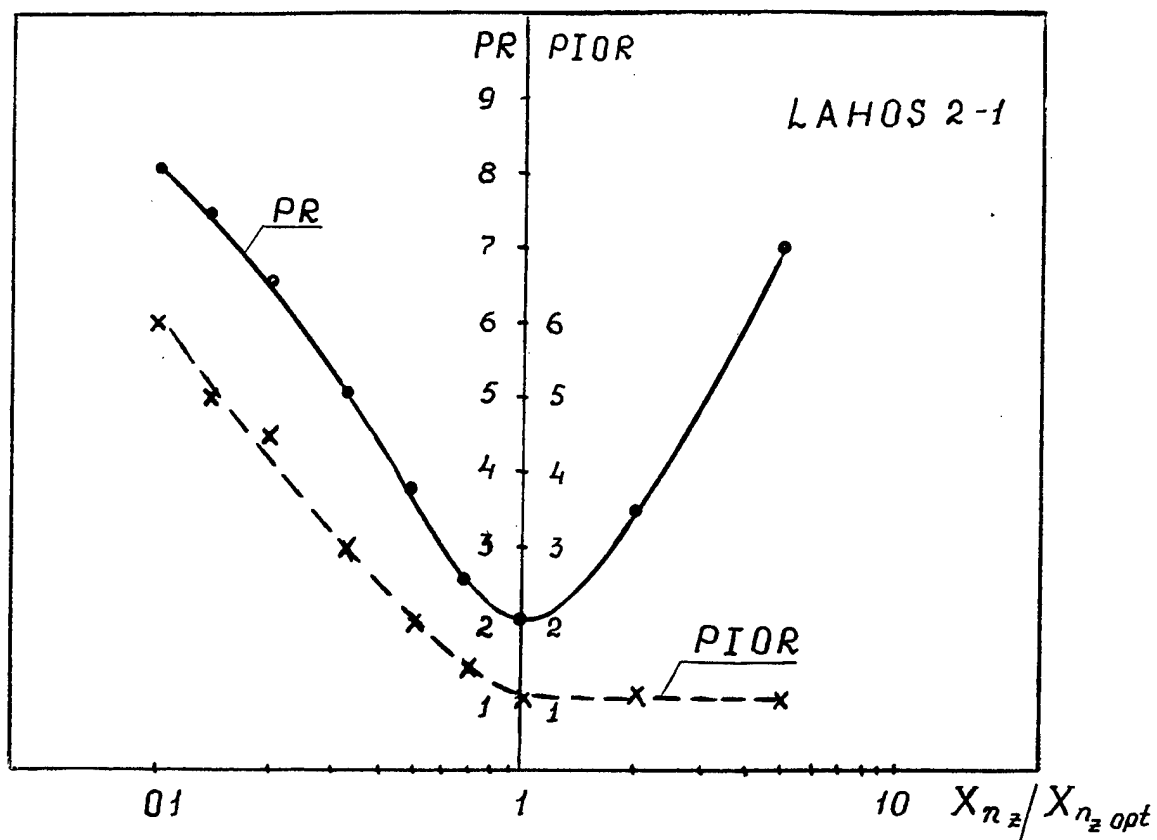


Fig.2.1. Command-Response Gradients Influence on Pilot Ratings (PR and PIOR) at different dynamic performance for an aircraft with a central stick.

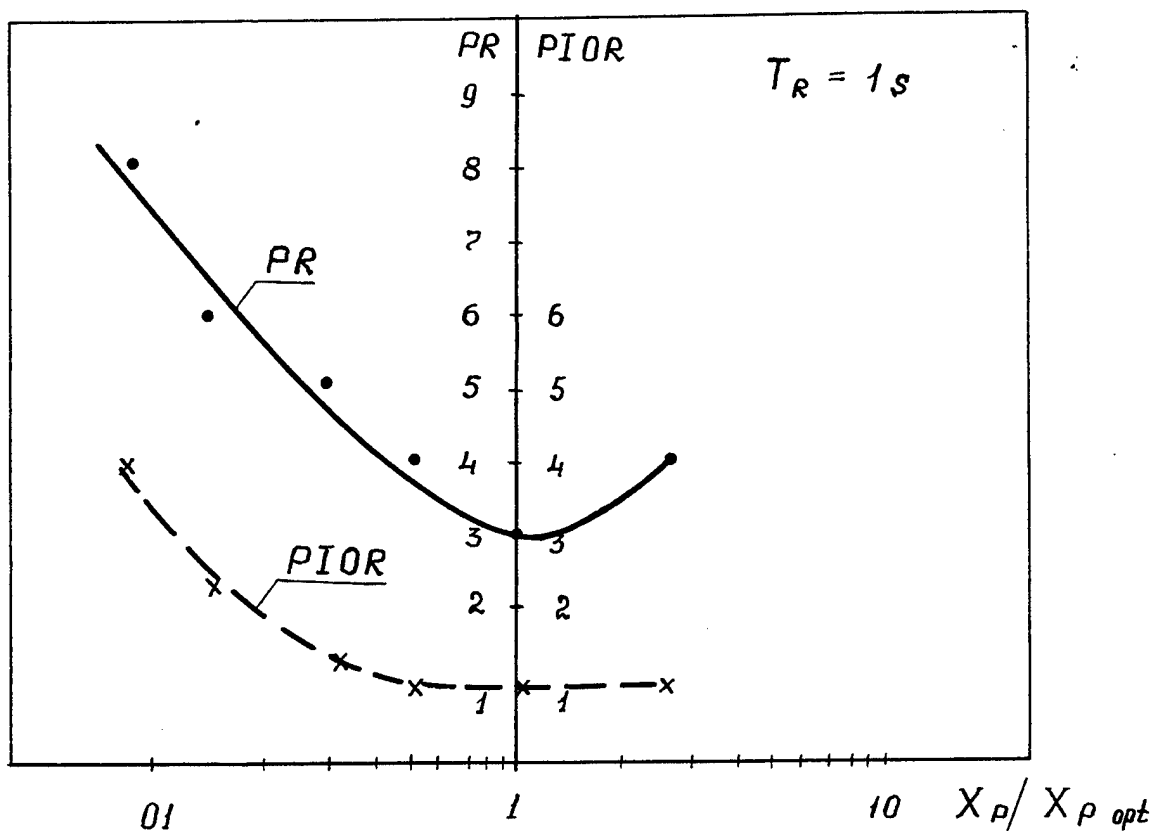
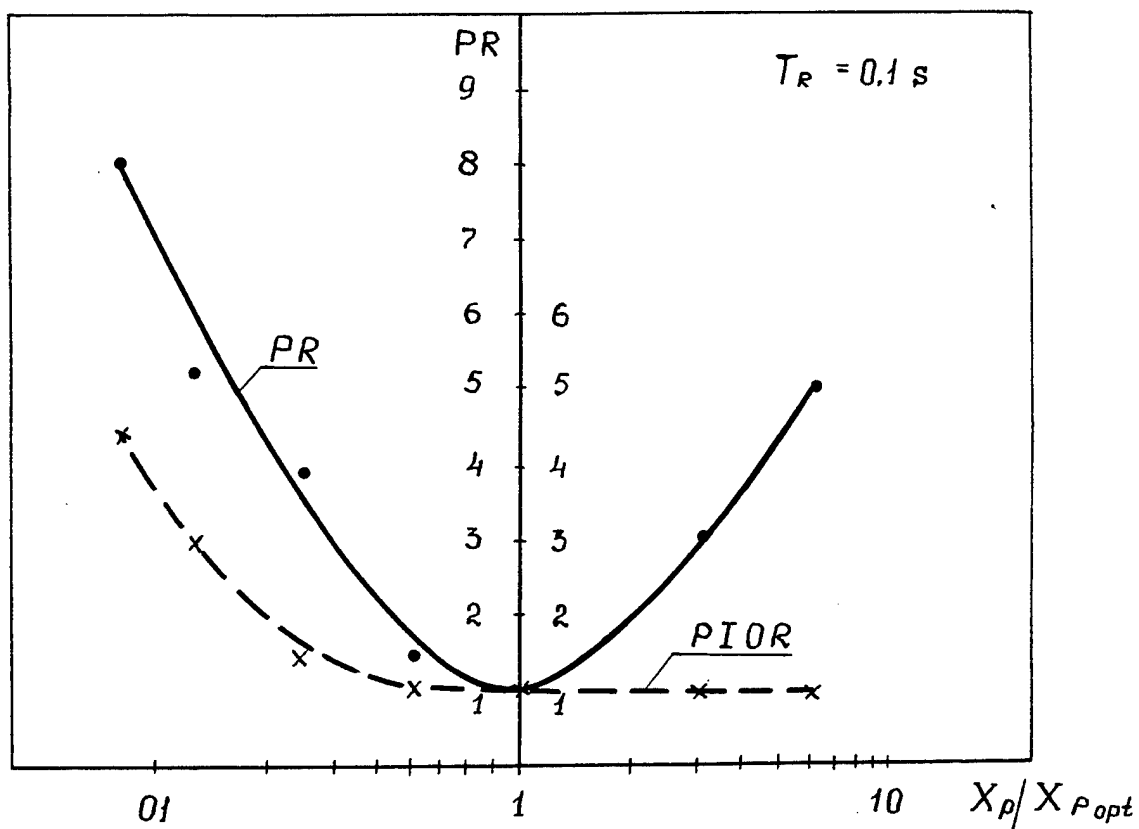


Fig.2.2. Lateral Command-Response Gradients Influence on Pilot Ratings (PR and PIOR) for two values of roll mode time constant for an aircraft with a central stick.

feel systems (fig. 2.3). (The above mentioned conditions affect only optimum values of command-response gradients. This effect will be considered in greater detail in part 2.3.)

As it is seen from the given data, an increase of control sensitivity (command-response gradients decrease) over optimum values, leads to PIO tendency arising. At small deviations from optimum values the tendency is slight. It becomes considerable if control sensitivity characteristics are more than 2 times greater in comparison with optimum values. For example, if sensitivity increase is 2 times the PRs and the PIORs deteriorate by 0.6. If sensitivity increase is 4 times the PR-ratings deteriorate by 2-2.5, the PIOR-ratings deteriorate by 2.

A dependence of pilot ratings on dimensionless command gradients ($F_{n_z}/F_{n_z}^{opt}, F_p/F_p^{opt}, \dots$) is approximately the same for different conditions not only in kind, but in degree as well. The degree of pilot ratings deterioration if the command-response gradients are below their optimum values, can be described by the relation (feel system characteristics are considered optimum):

for Cooper-Harper scale

$$\Delta PR = \begin{cases} -6 \lg \frac{F_r}{F_r^{opt}} - 1.5, & \text{at } \frac{F_r}{F_r^{opt}} \leq 0.5 \\ 6 \lg^2 \frac{F_r}{F_r^{opt}}, & \text{at } 0.5 \leq \frac{F_r}{F_r^{opt}} \leq 1.0 \end{cases}$$

For PIO scale

(2.1)

$$\Delta PIOR = \begin{cases} -4 \lg \frac{F_r}{F_r^{opt}} - 0.5, & \text{at } \frac{F_r}{F_r^{opt}} \leq 0.5 \\ 6 \lg^2 \frac{F_r}{F_r^{opt}}, & \text{at } 0.5 \leq \frac{F_r}{F_r^{opt}} \leq 1.0 \end{cases}$$

It should be mentioned also, that if dynamic performance causes no PIO tendency, control sensitivity decreasing (command gradient values increasing) causes only Cooper-Harper pilot ratings variation, while PIO ratings do not change. It is accounted for by the fact that command gradients increase over their optimum values does not result in PIO tendency intensification. Controllability worsening in this case is due to piloting precision deterioration and heavy controlling, but not to PIO tendency (fig. 2.1 - 2.3). If dynamic performance is a cause of PIO tendency, reducing control sensitivity can mitigate it.

It is evident, that eq.(2.1) describes growth of PIO tendency only approximately. In each particular case, PIO severity may differ from this empirical relation, as it is shown in fig. 2.4. This tendency could be evaluated more precisely studying pilot behavior models in terms of command gradients decrease. Unfortunately, the models and controllability criteria developed so far (McRuer, Neal-Smith, et al.) do not clarify this tendency peculiarities. In fact, they assume that as aircraft gain deviates from its optimum value, a pilot changes his gain in inverse proportion to it

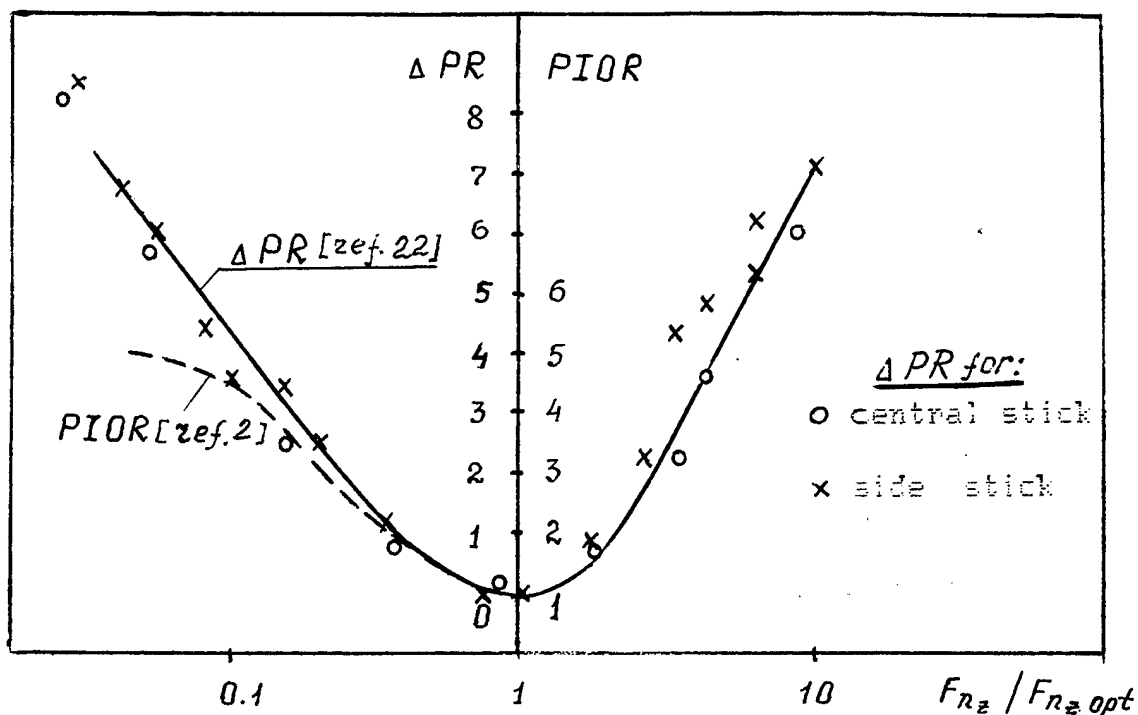


Fig.2.3. Longitudinal Command-Response Gradients Influence on PIORs and PR.

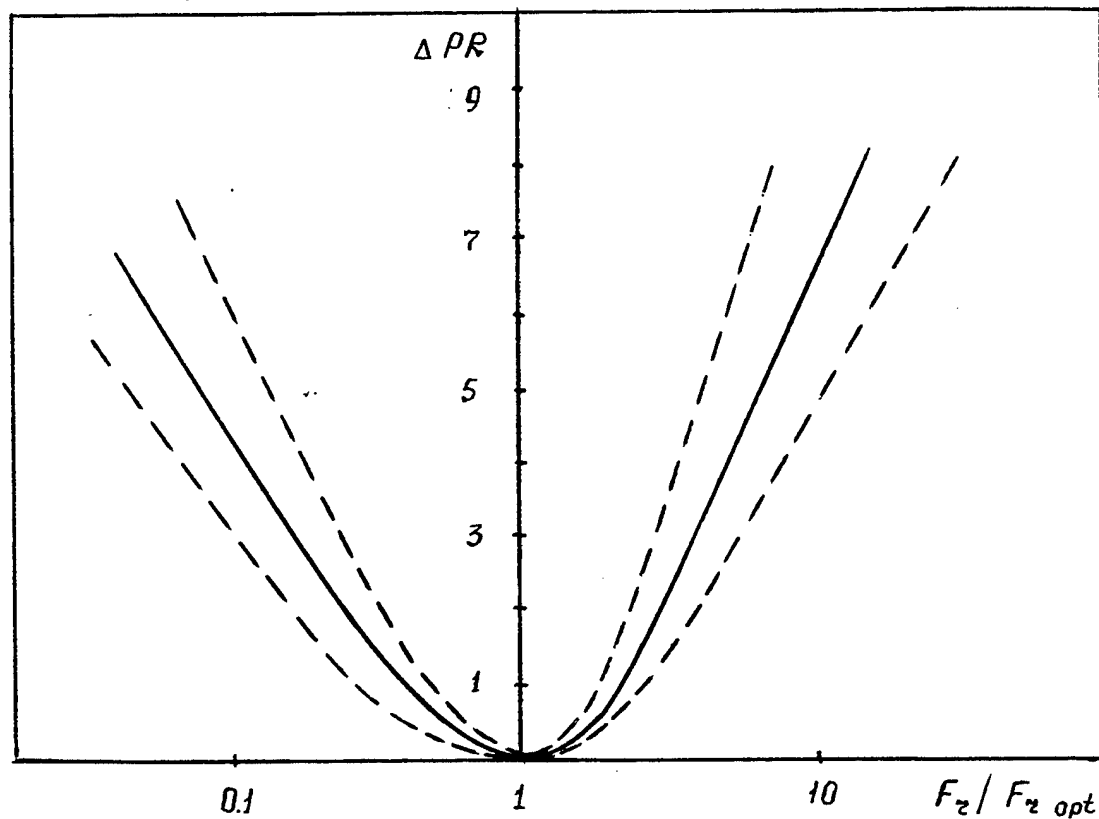


Fig.2.4. Limits of Pilot Ratings Worsening Variation PR at Command-Response Gradients Deflecting about their optimum values.

so, that $Y_p Y_c$ describing function remains unchanged. Therefore, models of this type do not consider the fact that as command sensitivity increases a pilot-aircraft system becomes more unstable. To define possible ways of eliminating this drawback of the modern pilot models, special investigations of pilot adaptability to a high aircraft gain were conducted in the present work.

Fig. 2.5 plots the pilot and pilot-aircraft describing functions obtained for the tracking task with various command sensitivity gradients. The analysis of these and other data obtained during the experiments, shows the following: if control sensitivity increase exceeds 2 times, a pilot-aircraft cut-off (crossover) frequency becomes somewhat higher, i.e. control sensitivity variation interferes with pilot adaptability. The interference becomes considerable at high frequencies. In fig. 2.5, at frequencies of 0.7-1.0 Hz, the magnitudes of pilot describing functions are practically the same in spite of the great difference in aircraft gains. The pilot phase remains equal over a wide frequency range for all aircraft gains.

This pilot peculiarity may be a result of different muscles of an arm being engaged in deflecting a certain manipulator and their having different dynamics and displacement ranges. Wide-ranged manipulator displacements, which are low-frequency as a rule, are produced mainly by a shoulder and a forearm. Due to this fact, pilot adaptability is higher at low frequencies. High-frequency deflections of manipulator are produced by muscles of a hand, having more narrow displacements limits. It is these limits that restrain the pilot high-frequency adaptability to aircraft gain variations.

Due to this human peculiarity noticeable changes take place in a closed-loop pilot-aircraft describing function. As shown in fig. 2.5, the amplitude peak increases. The peak is often used (Neal-Smith, et al.) as a standard of an aircraft tendency to PIO. Thus, an increase of control sensitivity leads to increasing a pilot-aircraft cut-off frequency and rising a pilot amplitude ratio in a high frequency band. This, in turn, leads to peaking in a pilot-aircraft system and, therefore, increasing the system instability. This is a possible if not a sole cause of PIO tendency arising under increased control sensitivity. Much more attention should be paid to this fact in the future.

2.2 EFFECT OF FEEL-SYSTEM CHARACTERISTICS

The main feel system parameters are manipulator gradient F^x and breakout force F_{br} . PIO determined by abrupt changes in force gradient values have been considered in a number of works (see ^(15,16)). An effect of force gradients and breakout on PIO is considered in the present work. Its regularities have not been sufficiently presented in publications yet, though these parameters are paid great attention to.

Figs. 2.6; 2.7 are plots of pilot ratings and force gradients for different force breakouts. The results presented were obtained for both central and side sticks for optimum aircraft control sensitivity characteristics. These and other data available brought us to the following results.

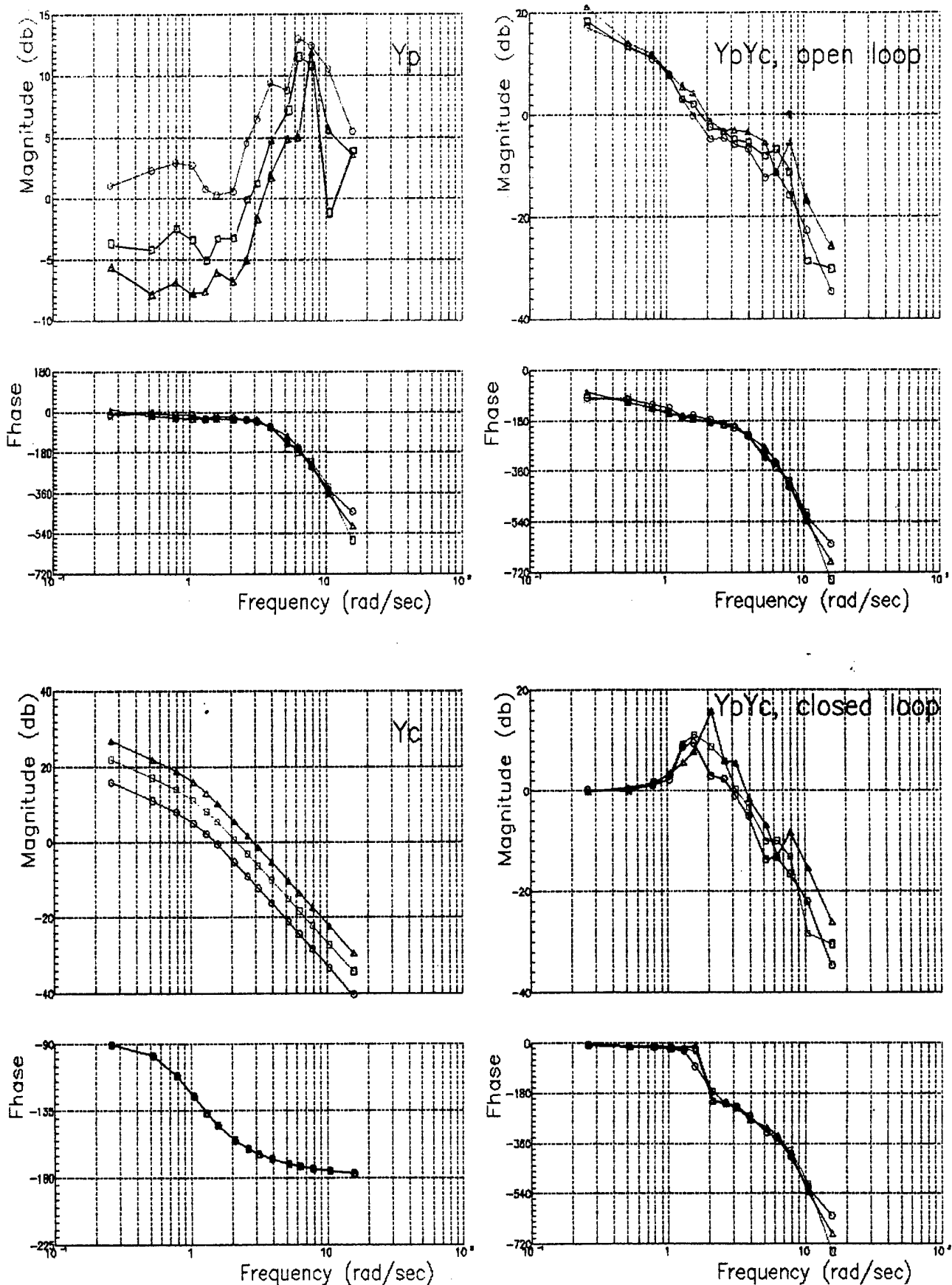


Fig.2.5 Pilot/Pilot-Aircraft describing functions for different aircraft gains /longitudinal channel '1-1' LAHOS/.

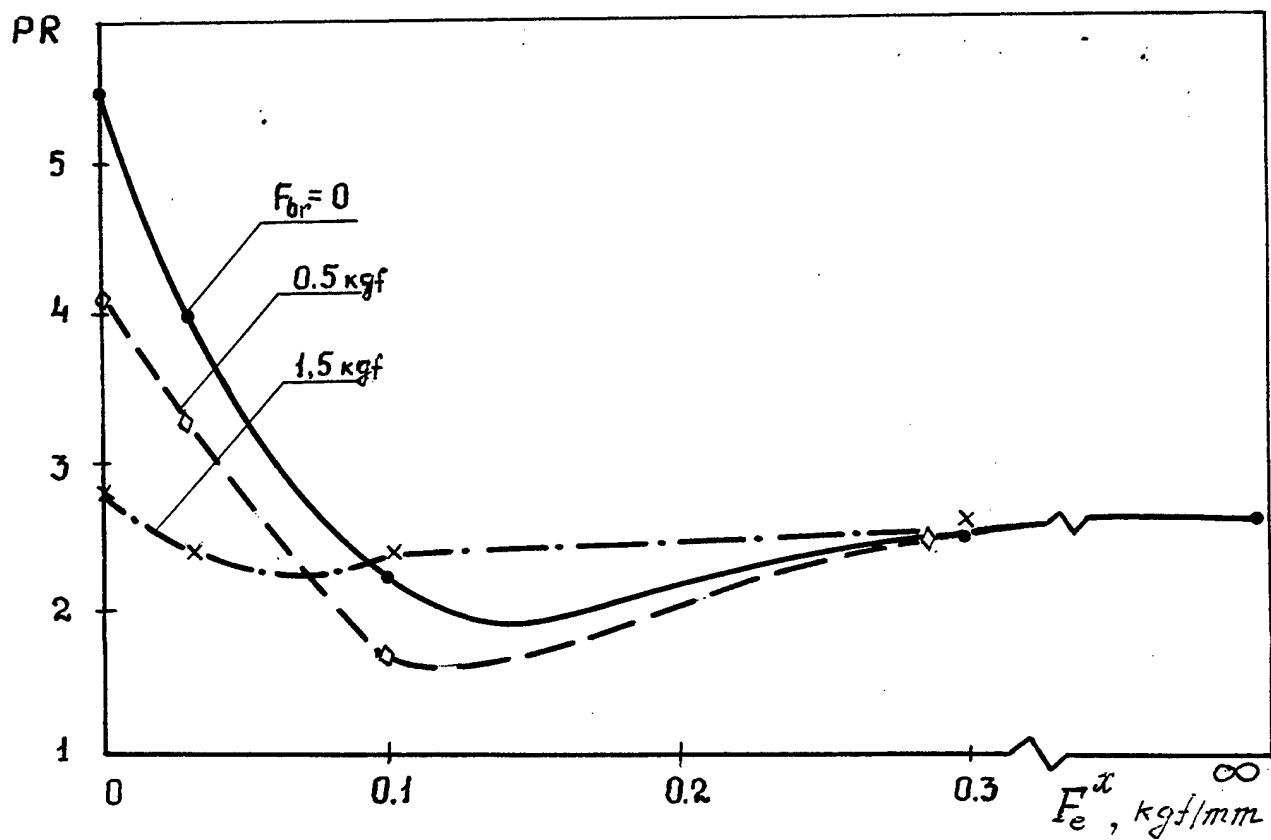
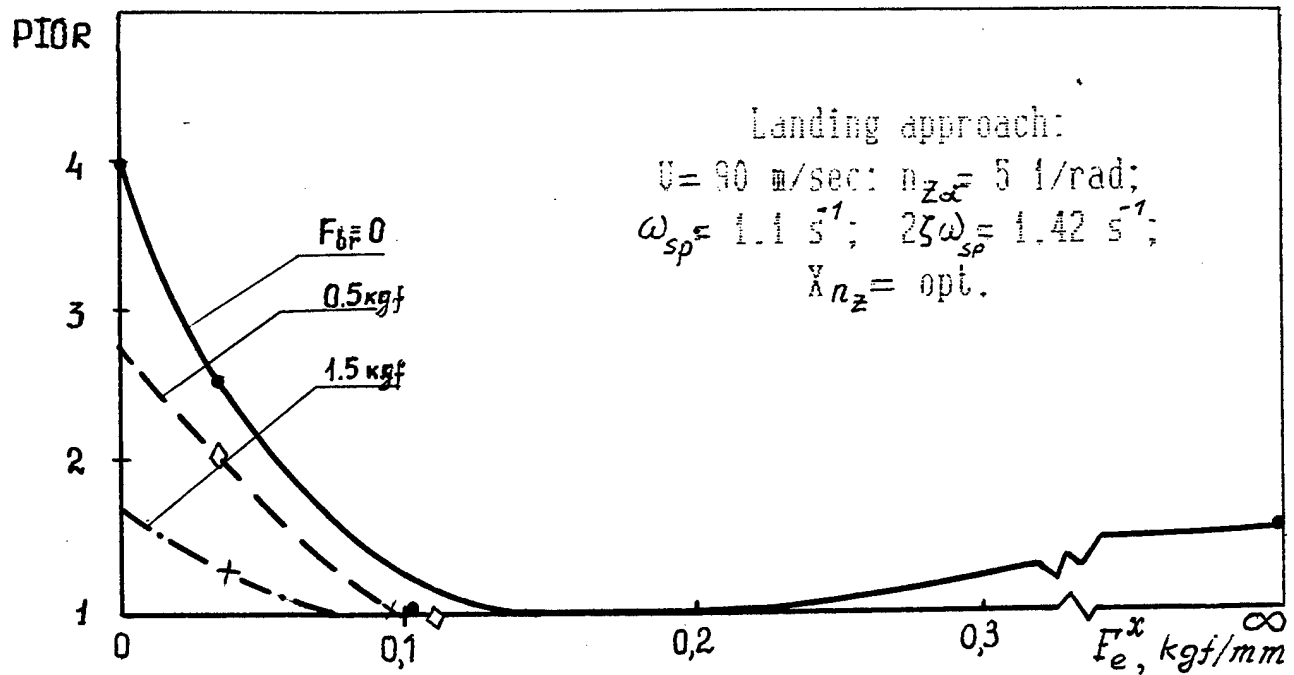


Fig.2.6. Longitudinal Feel System Gradient and Breakout Force Influence on PIOR and PR (central stick)

Landing Approach

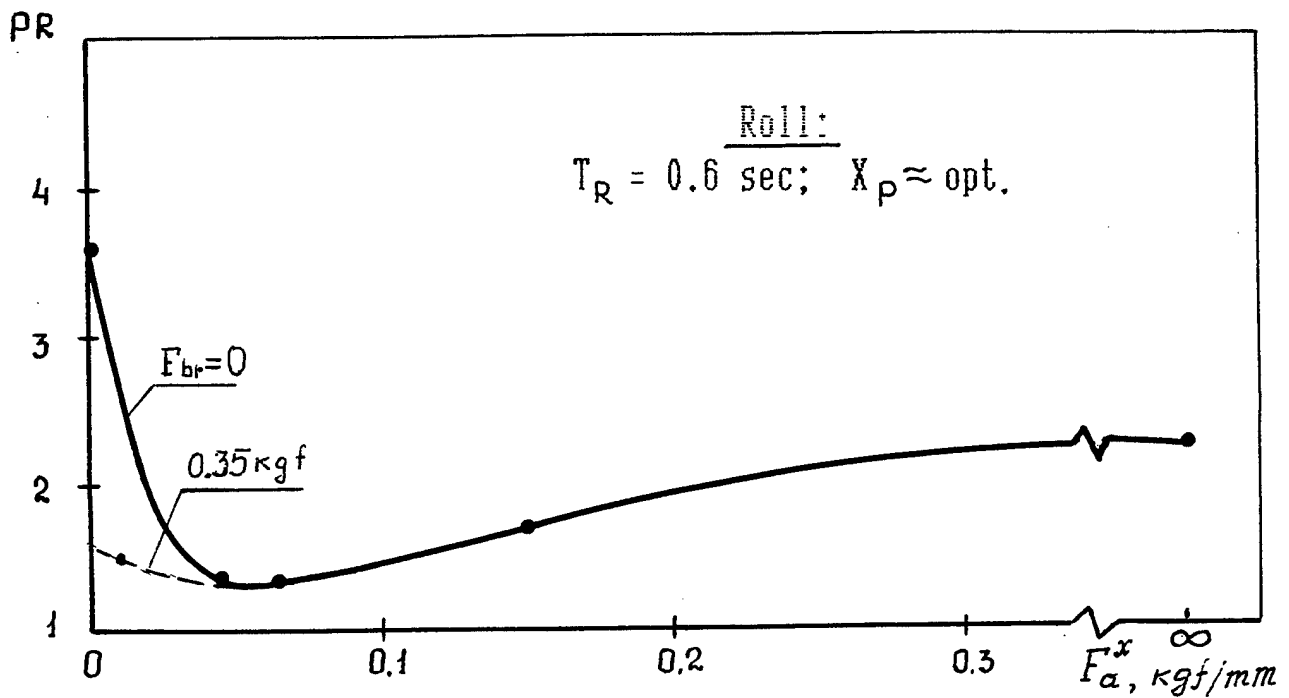
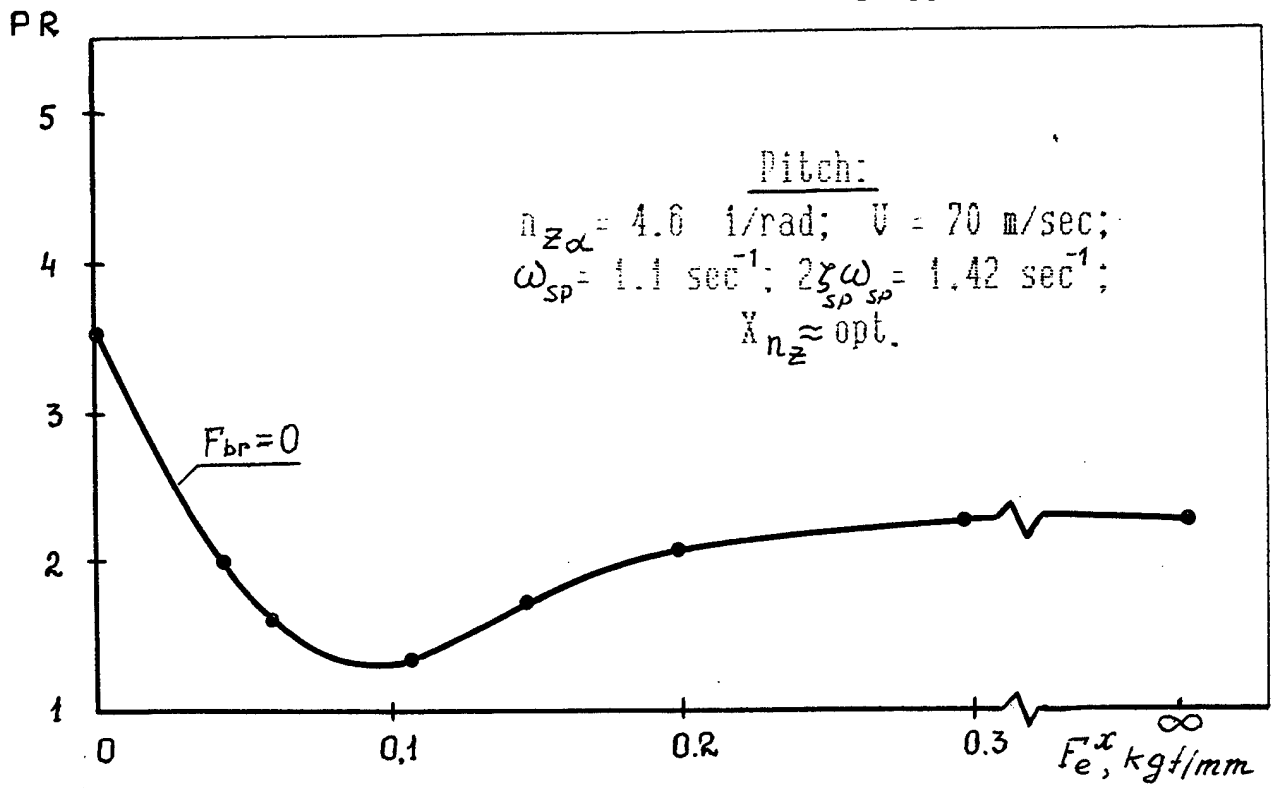


Fig.2.7. Pitch and Roll Feel System Gradients Influence on PR
(side stick)

Force gradient F^X and breakout force F_{br} qualitative influence on PIO is the same for different manipulators, aircraft dynamics and piloting tasks. There are certain optimum values of manipulator force gradients for each manipulator type and control channel. In the case of any deviations of force gradients from their optimum values the aircraft tends to oscillate and pilot ratings worsen; but it is force gradient values decreasing that plays a decisive role in PIO tendency severity and pilot ratings worsening. For low force gradient values a certain additional value of force breakout mitigates a PIO tendency and improves controllability, due to the fact that too low gradient values hamper pilot's measuring control forces. In this case the lack of control forces is compensated by some additional breakout.

We should mention that for low gradient values, an effect of control sensitivity characteristics on PIO is also greater; see the experiments, in fig. 2.8. This results in changing relation (2.1): for low gradient values, deviations of control sensitivity from its optimum value lead to more considerable pilot ratings worsening as compared to (2.1).

If gradients and breakouts are referred to their optimum values (fig. 2.9), the dependence of pilot ratings on these referred values is about the same in degree for different manipulators and control channels. The latter fact is determined by the theoretical approach to optimization of control sensitivity and feel system characteristics presented in ^[22]. According to the approach, for a pilot there exist certain desirable ranges of force F_* and displacement X_* for every control manipulator. The optimum gradient value (for $F_{br}=0$) is about

$$F_{opt}^X = F_* / X_* . \quad (2.2)$$

If pilot forces and displacements differ from their desirable values, controllability deterioration degree is determined by F/F_* and X/X_* . This dependence remains the same for different manipulators and control channels. For slight deviations of F/F_* and X/X_* from 1 the dependence can be described by the equation

$$\Delta PR = f \lg^2 F/F_* + g \lg^2 X/X_* , \quad (2.3)$$

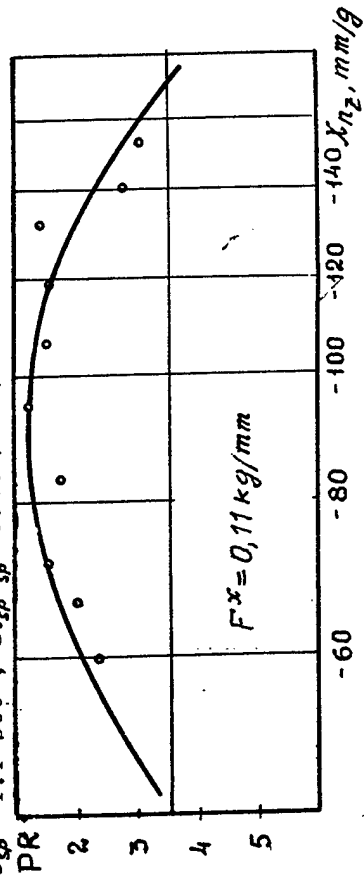
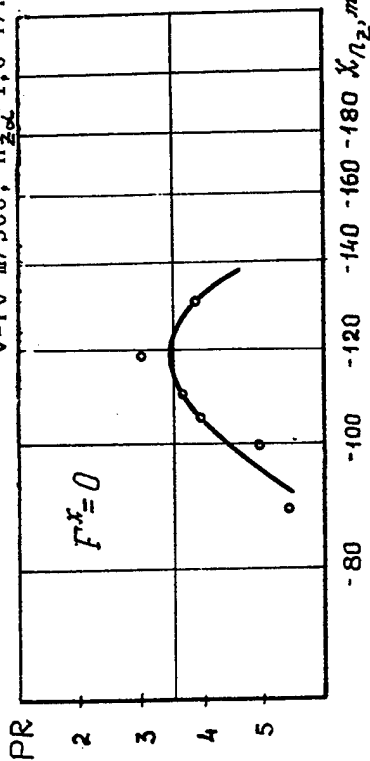
where f, g are constant for different manipulators.

For optimum control sensitivity and low values of gradient and breakout force, a manipulator displacement range does not depend greatly on F^X and F_{br} . So, it can be assumed that

$$X = X_* . \quad (2.4)$$

PITCH:

$U=70$ m/sec; $n_z=4,6$ 1/rad; $\omega_{\varphi}=1,1$ sec⁻¹; $2\zeta_{\varphi}\omega_{\varphi}=1,42$ sec⁻¹.



ROLL: $T_R = 0,6$ sec.

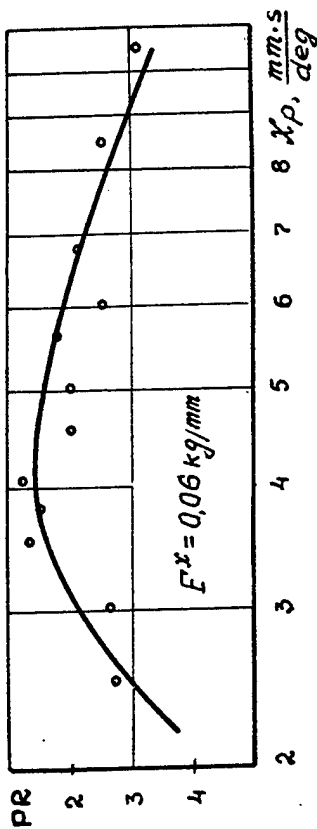
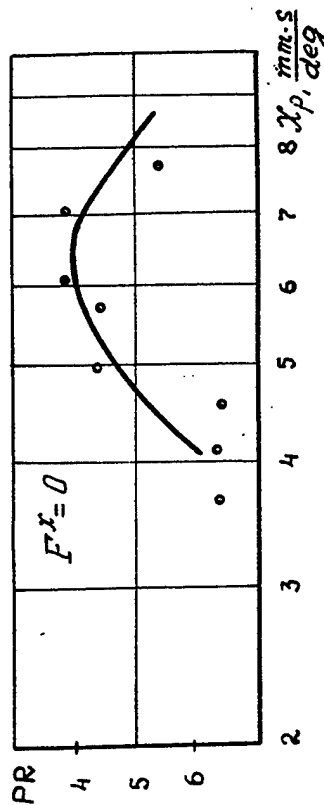


Fig.2.8 Influence of Feel System Gradients F^x and Command Response Gradients X_{n_z} and X_p on Pilot Ratings (side stick)

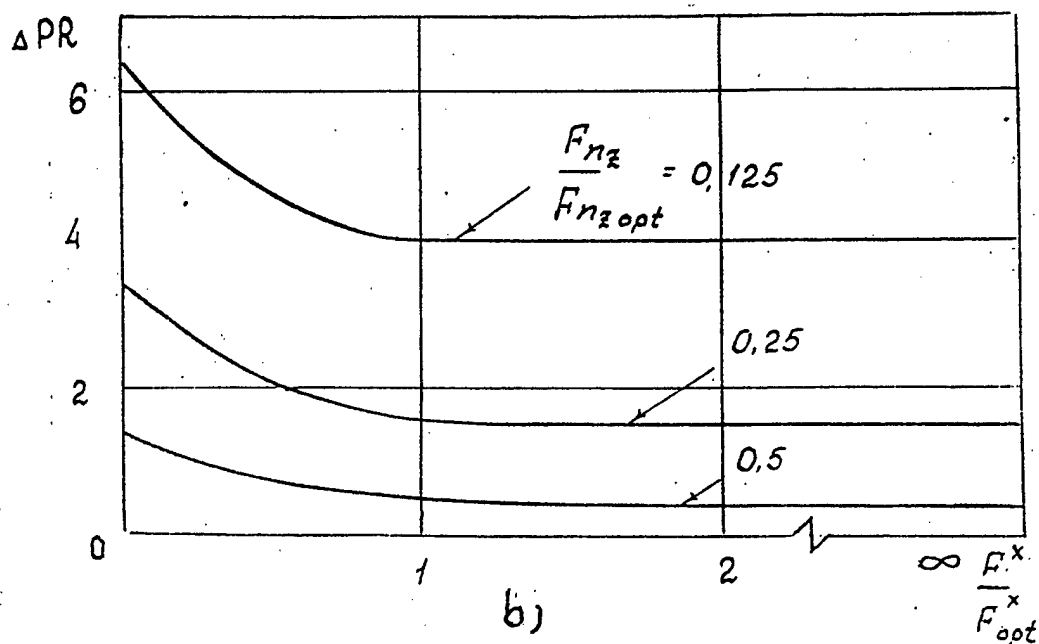
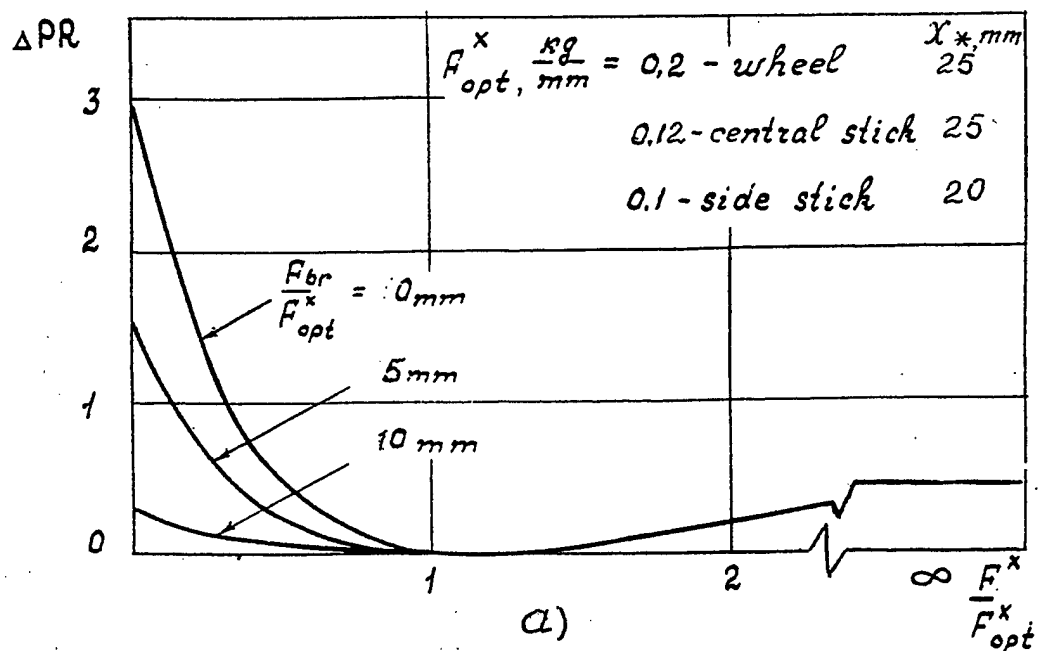


Fig.2.9 Pilot Ratings Deterioration Degree due to PIO Tendency Increasing in the case of Feel System (a) and Control Sensitivity (b) Characteristics Deviation from Their Optimum Values.

For optimum values of gradients and $F_{br} = 0$, the manipulator force range is close to desirable F_* . If gradient values decrease and breakout values increase, force range values change according to

$$F = \frac{F^X}{F_{opt}^X} \cdot F_* + F_{br}. \quad (2.5)$$

Having inserted (2.5) into (2.3) and considering (2.2) and (2.4), we have

$$\Delta PR = f \lg^2 \left(\frac{F^X}{F_{opt}^X} + \frac{F_{br}}{F_{opt}^X X_*} \right)$$

The equation shows that if gradients deviate from their optimum values, pilot ratings deterioration is determined by F^X / F_{opt}^X and $F_{br} / F_{opt}^X X_*$ only, regardless of breakout values and the manipulator type.

Thus, longitudinal PIO tendency severity due to deviations of feel system and control sensitivity characteristics from their optimum values can be evaluated with the function plotted in fig. 2.9. Optimum gradient values and X_* for different manipulator types are presented in the same figure.

2.3 DESIGN CRITERION FOR EVALUATION OF FEEL-SYSTEM AND COMMAND SENSITIVITY CHARACTERISTICS EFFECT ON PIO

An essence of the criterion proposed here is the following:

1. With the help of the criteria available (T. Neal, R. Smith, R. Hoh and others) severity of PIO tendency is evaluated for optimum values of feel system and control sensitivity characteristics.
2. In accordance with the technique stated below, the tracking task optimum values of control sensitivity characteristics are evaluated for given feel system characteristics and aircraft dynamic performance.
3. With the help of the function in fig. 2.9 the degree of PIO tendency increase is evaluated for control sensitivity and feel system characteristics deviating from their optimum values.

To develop the technique of optimum values selecting for control sensitivity characteristics, the investigations have been conducted to define the regularities of an effect of dynamic performance and feel system characteristics on optimum values of command-response

gradients for the tracking task conditions. The analysis of data obtained shows that the relation of optimum command-response gradients to aircraft dynamics and manipulator feel system characteristics is the same in its nature for the tracking task and for the ordinary flying task (landing approach and cruise). This relation for the main flying tasks was considered in great detail in⁽²²⁾ and, therefore, is not referred to in this work. To illustrate the relation of optimum command gradients to aircraft dynamic performance, fig. 2.10 presents the optimum command-response gradients X_{n_z} which have been obtained in the experiments for five different LAHOS configurations. Having compared configurations 2-1 and 5-11 which have approximately equal damping ratios, one could see that if natural short-period mode frequency increases, optimum command-response gradients X_{n_z} increase too. The comparison of configurations 2-1 and 3-3 shows that damping ratio increase results in increasing optimum X_{n_z} .

The experimental data obtained allow us to assume that optimum command-response gradients for a tracking task as well as for other piloting tasks can be defined by A-criterion⁽²²⁾. For the longitudinal channel the criterion takes the form:

$$\left[\left[1 + \frac{V_0}{n_{z\alpha} g} \sqrt{\omega_*^2 + \left(\frac{n_{z\alpha} g}{V} \right)^2} \right] \cdot \left| Y_{n_z}(\dot{\omega}_*, X_{n_z}^{opt}) \right| \right]^{-1} = A(F^X, F_{br}, \dots). \quad (2.6)$$

To show that A-criterion application is well-grounded for a tracking task as well as for landing approach, aircraft describing functions are plotted in fig. 2.11. These functions were defined for optimum values of X_{n_z} for the same LAHOS configurations as presented in fig. 2.10. It can be seen that in spite of different configurations dynamics, their transfer function amplitude ratio curves meet at about the same point demonstrating the physical nature of A-criterion (2.6).

But, quantitatively optimum values of command gradients depend on a piloting task. See, for example, fig. 2.10 where the optimum command gradients for some LAHOS configurations are shown for the tracking task and landing approach.

It is obvious that the difference in optimum values of command-response gradients for different piloting tasks can be considerable; quantitatively this difference depends on aircraft dynamic performance.

Relation (2.6) shows optimum command gradients values in kind and in degree, if the parameters in (2.6) are specified. The comparison of the calculated and experimental data has shown that the values of the parameters in (2.6), but for ω_* , do not depend on a piloting task. Also, as it has been shown in⁽²²⁾ the value of V_0 can be put equal to 140m/sec for all flight conditions of an unmaneuverable aircraft. The parameter A depends on a manipulator type and its feel system characteristics. The values of A for central and side sticks of an unmaneuverable aircraft are shown in fig. 2.12.

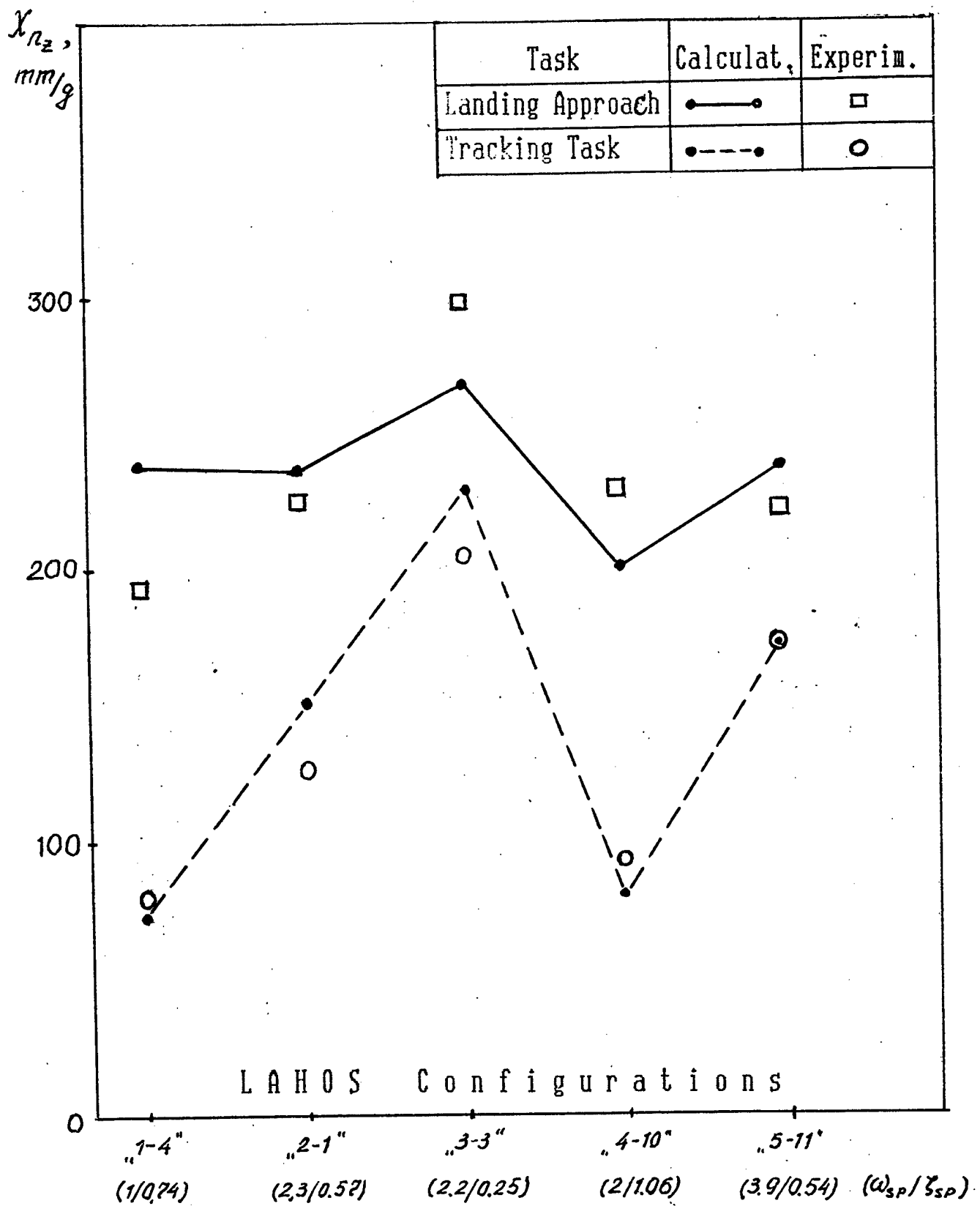


Fig.2.10 Optimum Command-Response Gradients χ_{n_z} for 5 LAHOS Configurations for Landing Approach and Tracking Task.

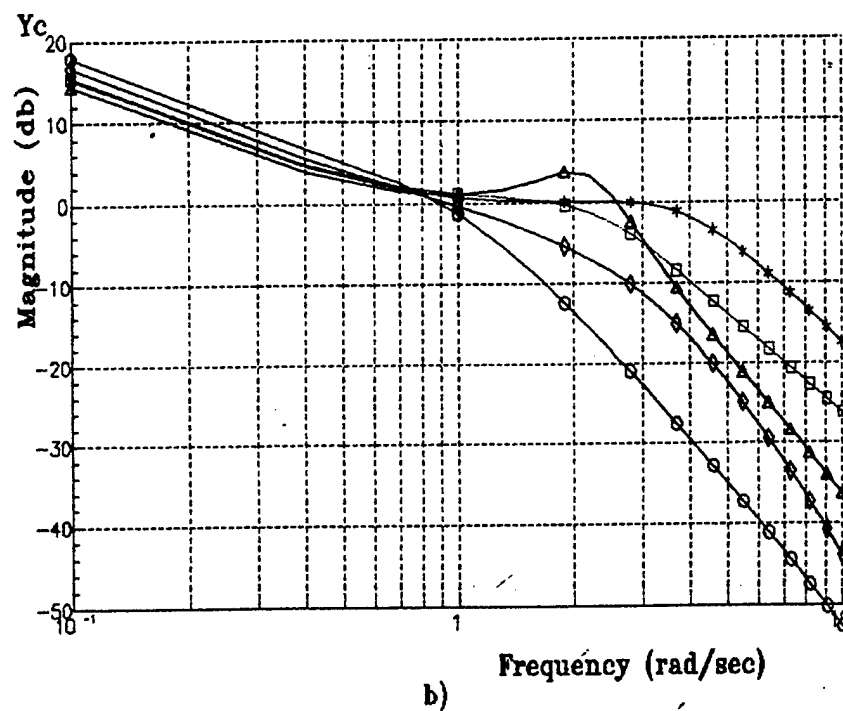
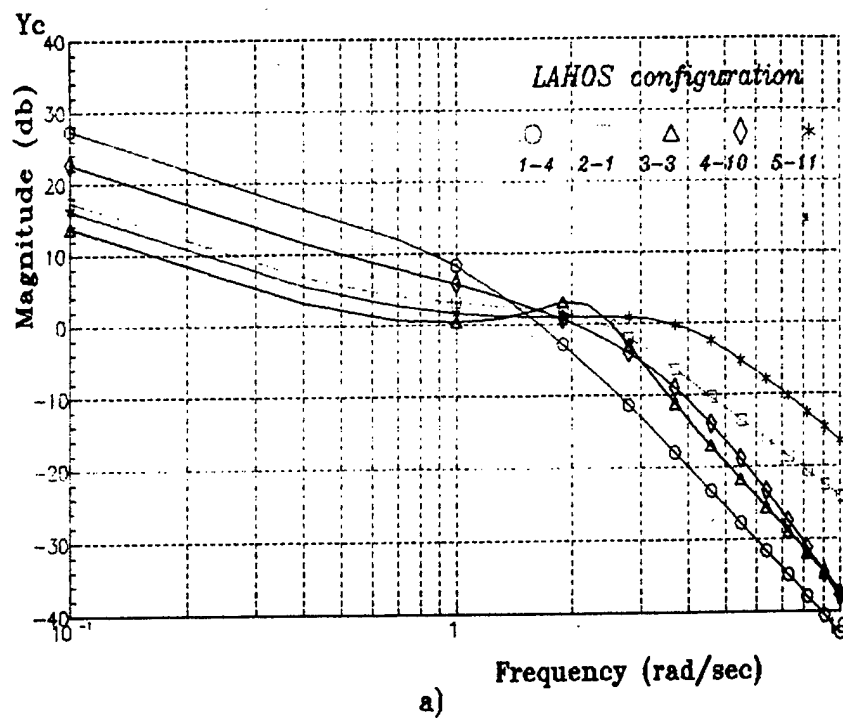


Fig.2.11 Roll transfer function responses for optimal control sensitivity of different dynamic configuration,
a) tracking task
b) landing approach.

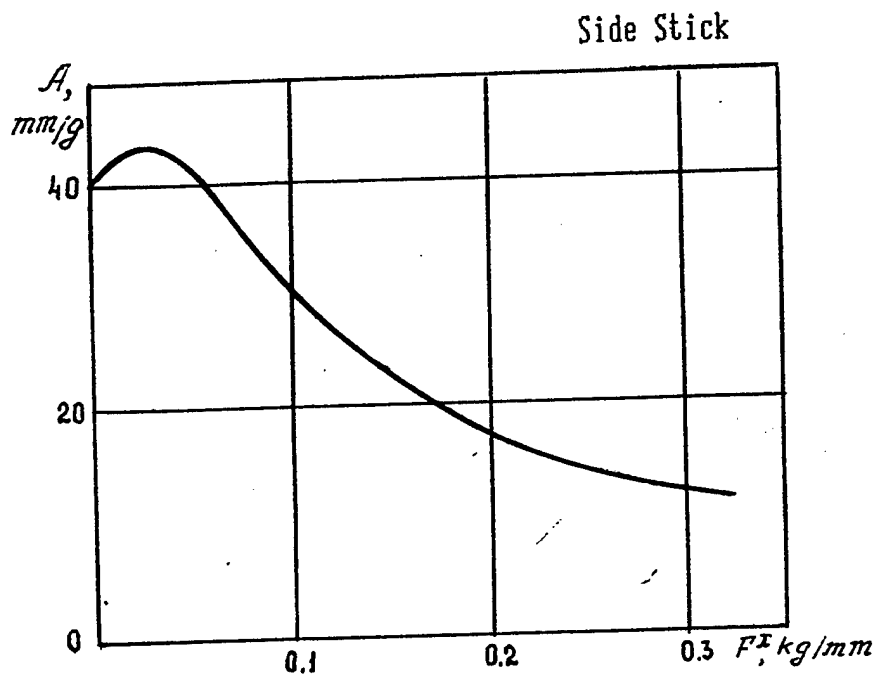
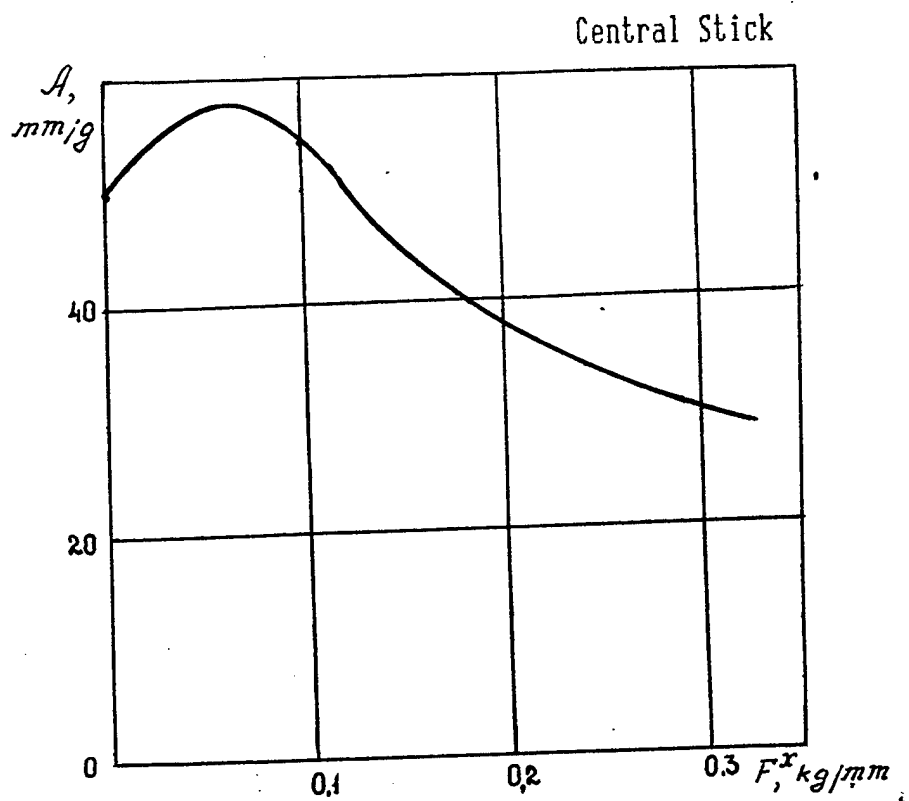


Fig.2.12 Parameter A Depending on Gradient F^x of Central and Side Sticks ($F_{br}=F_{fr}=F^{\ddot{x}}=0$)

The characteristic frequency ω_* depends only on a piloting task and an aircraft class. It is 1.2-1.5 rad/sec (or 0.7 rad/sec for a landing approach task), see fig. 2.11, for an unmaneuverable aircraft with the input disturbance shown in fig. 1.8.

Thus, optimum command-response gradients values for a tracking task on an unmaneuverable aircraft with central or side sticks can be calculated using (2.6), where A values correspond to those shown in fig. 2.12 and ω_* is about 1.2-1.5 rad/sec.

Some additional studies may clarify a relation of parameter A to manipulator feel system characteristics and specify the characteristic frequency ω_* in order to define optimum command gradient values for other control channels, manipulators and aircraft classes for a tracking task.

3.0 INVESTIGATION OF LIMB-MANIPULATOR DYNAMIC INTERACTION WITH ROLL CONTROL OF "ELASTIC" AIRCRAFT

3.1 STATEMENT OF THE PROBLEM

In view of change-over to fly-by-wire system on modern unmaneuverable aircraft a necessity disappeared for a pilot to apply great forces to move a control linkage. Therefore, small-inertia manipulators have come into use on unmaneuverable aircraft (small-mass wheels, mini-wheels, central and side sticks: Tu-204, A-320, A-340, etc.). For these types of manipulators high frequency resonant peaks (1-3 Hz) in limb-manipulator system describing function are typical. As to roll mode time constants, their low values are not characteristic of unmaneuverable aircraft. For unmaneuverable aircraft the values about $T_R = 0.5$ sec or more are typical. Therefore, for unmaneuverable aircraft, in contrast to maneuverable ones, high frequency peaking in limb-manipulator system and, consequently, *ratchet* phenomenon due to only unfavorable limb-manipulator system characteristics is hardly probable.

For a modern unmaneuverable aircraft noticeable peaking in aircraft describing function in a frequency band about 2-3 Hz is typical due to airframe elasticity. It is accounted for by the fact that attempts of reducing airframe weight, installing engines on a wing, increasing aircraft dimensions lead to a tendency of decreasing aircraft elastic mode frequency and increasing elastic mode amplitudes on modern and prospective aircraft. As a result, in peak frequencies aircraft dynamics differs from traditional ones, which could be described by roll mode only. In the 2-3 Hz frequency band a resonant peak appears in roll amplitude ratio; considerable lateral accelerations can arise while controlling roll. (It is seen from flight data given in fig. 3.1 and transfer function models responses shown in figs. 3.2a,b.) Due to this fact, high-frequency oscillations of ratchet type become possible on unmaneuverable aircraft as well, in spite of high roll mode constant values. These oscillations were observed, for example, in flight tests of one of Russian unmaneuverable aircraft (fig. 3.1).

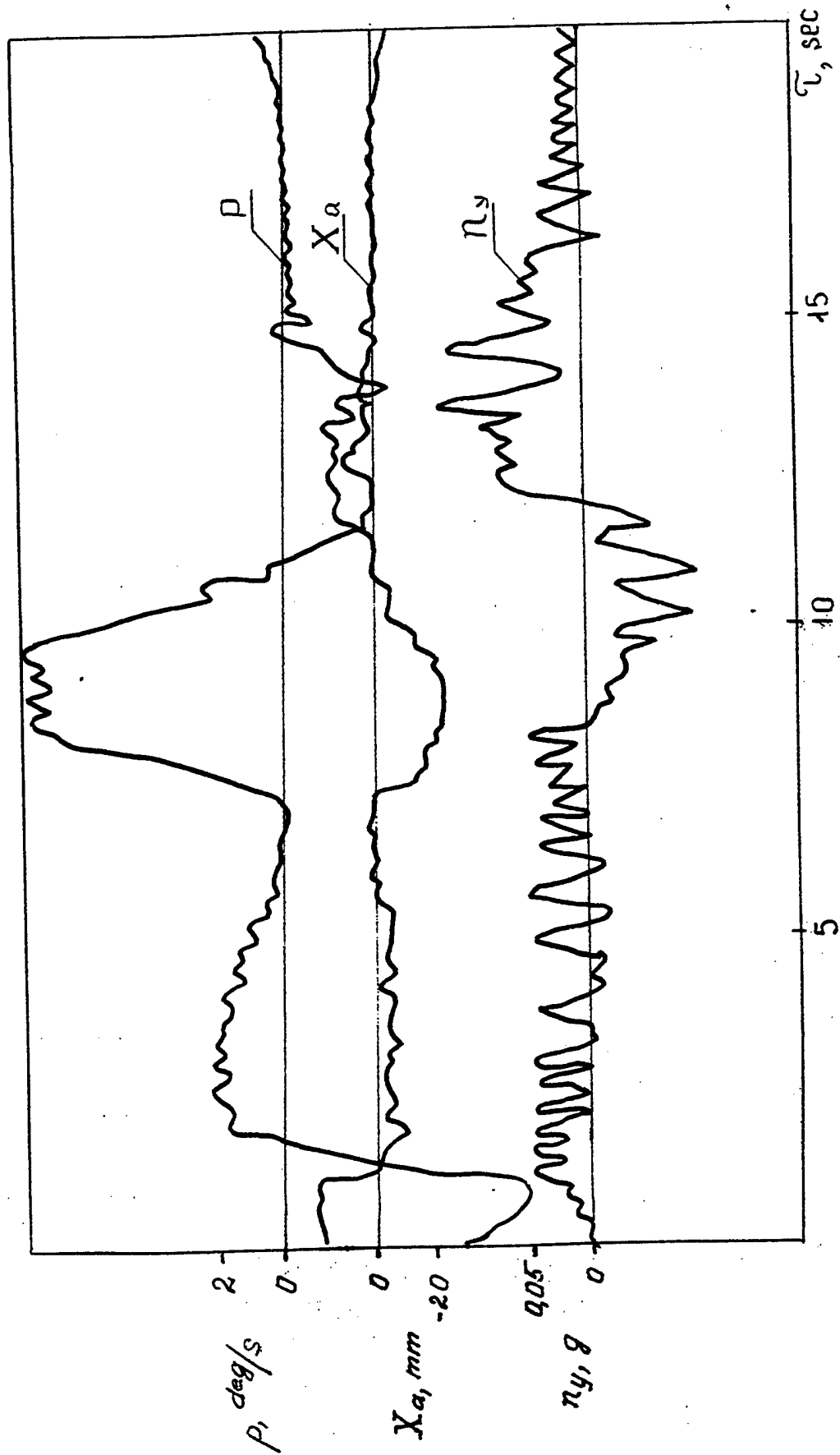


Fig. 3.1. Time Histories for the Ratchet Case.

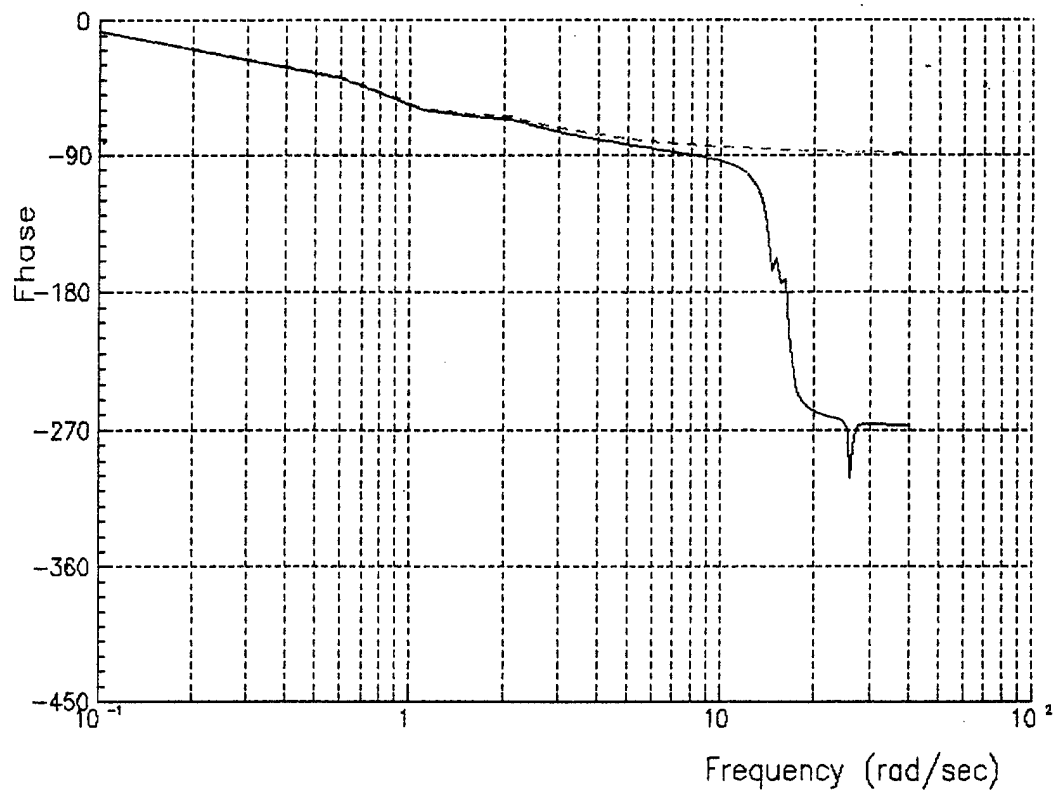
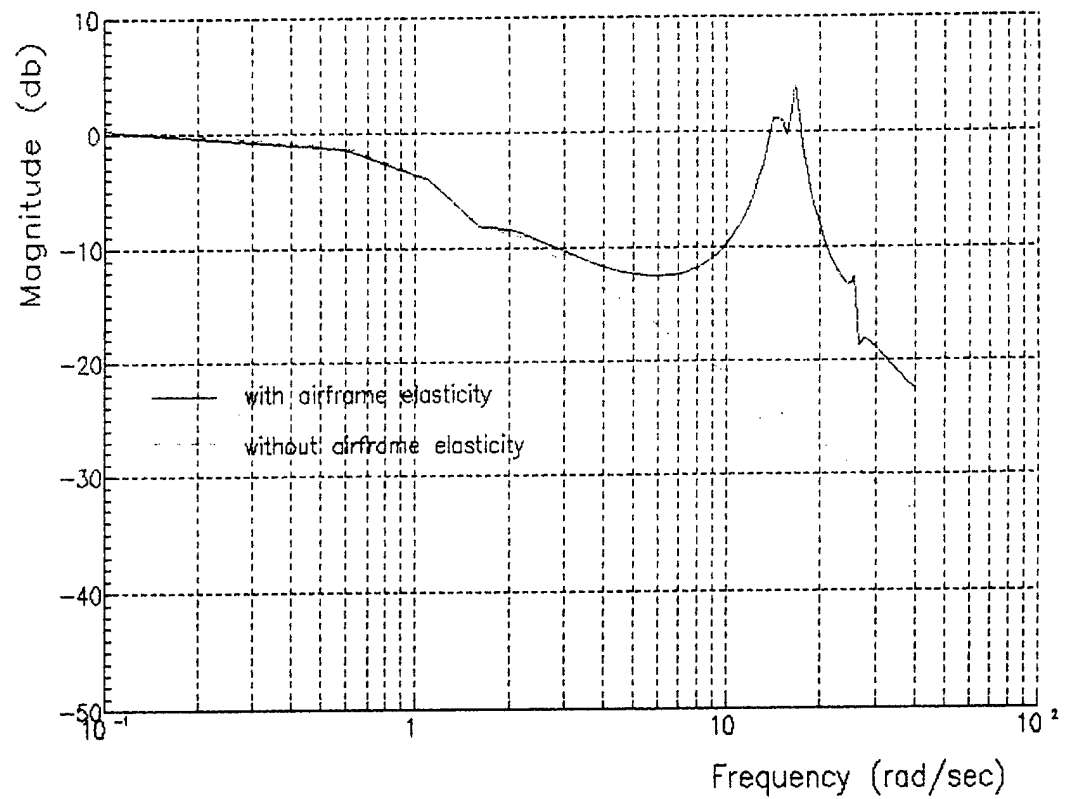


Fig.3.2a Roll-rate transfer function responses for the aircraft with and without airframe elasticity.

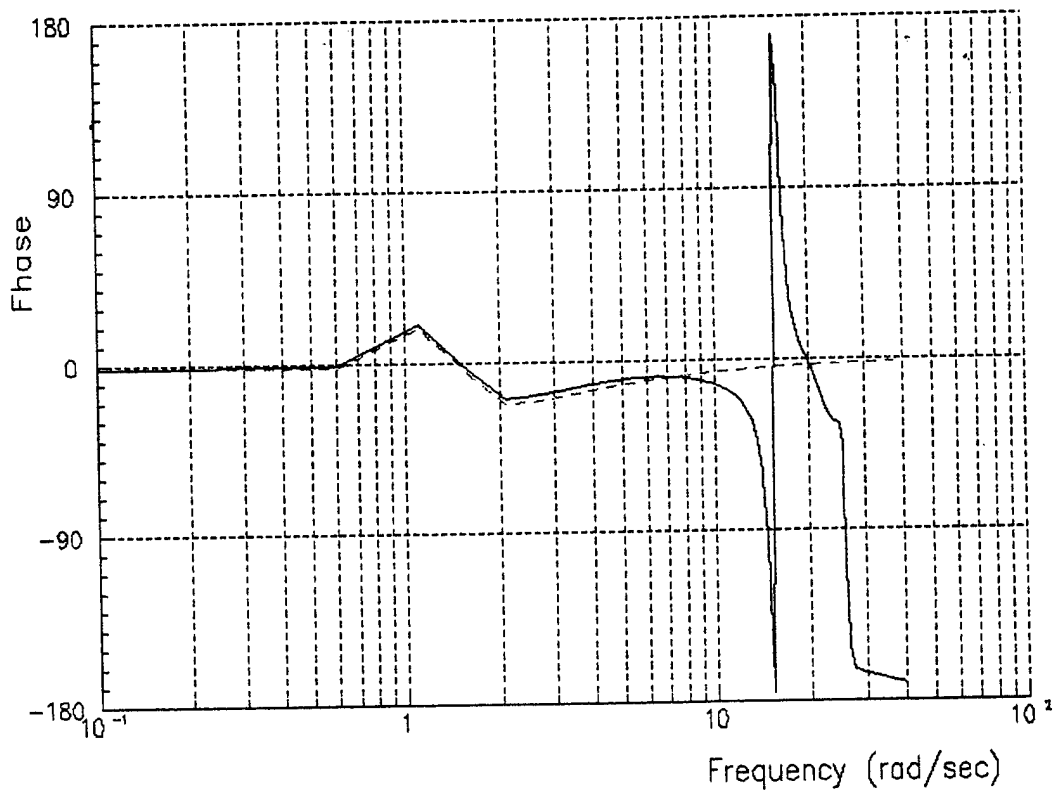
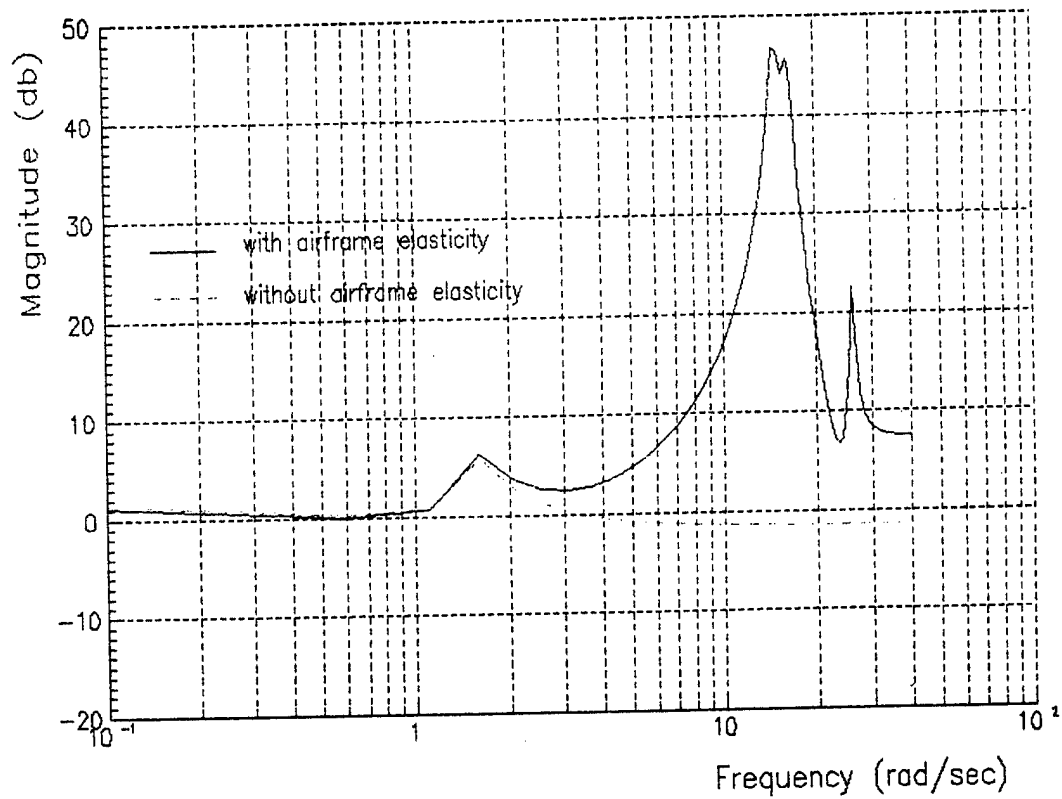


Fig. 3.2b Lateral-acceleration transfer function responses for the aircraft with and without airframe elasticity.

It should be mentioned that the phenomenon in question may present a problem for a maneuverable aircraft, since high frequency oscillations caused by structural elasticity appear on maneuverable aircraft as well. This type of oscillations appeared, for example, on a relatively light military aircraft (F-111 with external stores loading⁽³⁾).

This chapter of the report aims at theoretical and experimental validation of a possibility of roll high-frequency oscillations caused by a pilot for a certain combination of manipulator characteristics, structural elasticity and unmaneuverable aircraft dynamics.

3.2 UNMANEUVERABLE AIRCRAFT LATERAL MOTION MODEL COUPLED WITH ELASTIC MODES

Simplified linearized equations of aircraft lateral motion coupled with structural elastic modes can be written as follows:

$$\begin{cases} \dot{\beta} = Y_{\beta} \beta + \frac{g \cos \theta}{V} \phi + r \cos \alpha + p \sin \alpha + Y_{\delta_a} \delta_a + Y_{\delta_r} \delta_r + Y_{\beta} \frac{w}{V} \\ \dot{r} = N_{\beta} \beta + N_r r + N_p p + N_{\delta_a} \delta_a + N_{\delta_r} \delta_r + N_{\beta} \frac{w}{V} \\ \dot{p} = L_{\beta} \beta + L_r r + L_p p + L_{\delta_a} \delta_a + L_{\delta_r} \delta_r + L_{\beta} \frac{w}{V} \\ \phi = p - r \tan \theta \\ \ddot{\xi} + (D_K + D_A) \dot{\xi} + (G + B_A) \xi = R_a \delta_a + R_r \delta_r + R_w \delta_w \end{cases} \quad (3.1)$$

where $\xi = \xi(t)$ - is a vector of aircraft structural modes coordinates of dimension Nt , where Nt is a number of structural modes considered,
 w - is a side wind gust velocity.

The terms describing dynamic interaction of structural modes and rigid aircraft motion are excluded from the motion equations considered. The influence of static elastic deformation of an airframe is taken into account by means of special corrections of aerodynamic coefficients in motion equations (3.1) which describe an aircraft as a rigid body.

The matrix of aircraft structural stiffness G is diagonal, it consists of squares of structural mode natural frequencies in vacuum; the matrix of structural damping D_K is diagonal as well. Matrices G and D_K do not depend on flight conditions. Matrices of aerodynamic stiffness B_A , aerodynamic damping D_A and "control surfaces efficiency" R_a, R_r, R_w change due to flight conditions changing and depend on dynamic pressure and flight velocity V in a first approximation.

Roll rate \hat{p} , yaw rate \hat{r} and side acceleration \hat{n}_y , affecting a pilot or registered by control system sensors (located at a point with the coordinates x_s, z_s) are computed according to the following equations:

$$\hat{p}(t, x) = p(t) + \sum_{i=1}^{N_t} \varphi_i(x) \dot{\xi}_i(t)$$

$$\hat{r}(t, x) = r(t) + \sum_{i=1}^{N_t} \psi_i(x) \dot{\xi}_i(t)$$

$$\hat{n}_y(t, x, z) = \frac{V}{g} [\dot{\beta}(t) - r(t) \cos \alpha - p(t) \sin \alpha] - \phi(t) - \frac{x}{g} \dot{r}(t) + \frac{z}{g} \dot{p}(t) + \frac{1}{g} \sum_{i=1}^{N_t} [f_i(x) + z \varphi_i(x)] \dot{\xi}_i(t)$$

where

- $f_i(x), \varphi_i(x), \psi_i(x)$ - structural i-mode values :
- $f_i(x)$ - fuselage deformation along the y-axis, m;
- $\varphi_i(x)$ - fuselage torsion angle with respect to the x-axis, rad;
- $\psi_i(x)$ - fuselage bending angle with respect to the z-axis, rad;
- x_s, z_s - coordinates of the point considered, m.

A first approximation of elastic aircraft mathematical model takes into account 4 structural modes. Matrices $\hat{D}_A, \hat{B}_A, \hat{R}_a, \hat{R}_r, \hat{R}_w$ for cruise conditions ($H=11300\text{m}$, $M=0.825$, $q=1047\text{kg/m}^2$, $V=243\text{ m/sec}$) for aircraft weight 83000kg have the forms:

$$\hat{D}_A = \begin{bmatrix} 1.49 & 0.244 & -1.78 & 0.0 \\ 0.376 & 0.212 & 0.234 & 0.0 \\ 0.108 & 0.306 & 0.628 & 0.0 \\ 0.0 & 0.0 & 0.0 & 0.26 \end{bmatrix}, \hat{B}_A = \begin{bmatrix} 47.2 & 5.95 & -14.6 & 0.0 \\ 0.052 & 3.73 & 7.96 & 0.0 \\ 15.7 & 5.24 & 21.0 & 0.0 \\ 0.0 & 0.0 & 0.0 & 6.26 \end{bmatrix}$$

$$\hat{R}_a = \begin{bmatrix} 34.9 \\ 33.3 \\ 63.5 \\ 29.4 \end{bmatrix}, \hat{R}_r = \begin{bmatrix} 69.5 \\ 1.20 \\ -28.1 \\ 0.262 \end{bmatrix}, \hat{R}_w = \begin{bmatrix} 4555.7 \\ 27.0 \\ 51.0 \\ 37.0 \end{bmatrix}$$

Diagonal matrices G, D_K are the following:

$$G = \begin{bmatrix} 173.4 & 0.0 & 0.0 & 0.0 \\ 0.0 & 2219 & 0.0 & 0.0 \\ 0.0 & 0.0 & 244.3 & 0.0 \\ 0.0 & 0.0 & 0.0 & 683.2 \end{bmatrix}, D_K = \begin{bmatrix} 0.211 & 0.0 & 0.0 & 0.0 \\ 0.0 & 0.238 & 0.0 & 0.0 \\ 0.0 & 0.0 & 0.250 & 0.0 \\ 0.0 & 0.0 & 0.0 & 0.418 \end{bmatrix}.$$

As a result for cruise flight conditions structural modes equations can be written as follows:

$$\begin{bmatrix} \ddot{\xi}_1 \\ \ddot{\xi}_2 \\ \ddot{\xi}_3 \\ \ddot{\xi}_4 \end{bmatrix} + \begin{bmatrix} 1.703 & 0.244 & -0.178 & 0.0 \\ 0.376 & 0.450 & 0.234 & 0.0 \\ 0.108 & 0.306 & 0.878 & 0.0 \\ 0.0 & 0.0 & 0.0 & 0.678 \end{bmatrix} \times \begin{bmatrix} \dot{\xi}_1 \\ \dot{\xi}_2 \\ \dot{\xi}_3 \\ \dot{\xi}_4 \end{bmatrix} + \begin{bmatrix} 220.6 & 5.95 & -14.6 & 0.0 \\ 0.052 & 225.6 & 7.96 & 0.0 \\ -15.7 & 5.24 & 265.3 & 0.0 \\ 0.0 & 0.0 & 0.0 & 689.5 \end{bmatrix} \times \begin{bmatrix} \xi_1 \\ \xi_2 \\ \xi_3 \\ \xi_4 \end{bmatrix} = \\
= \begin{bmatrix} 34.9 \\ 33.3 \\ 63.5 \\ 29.4 \end{bmatrix} \delta_a + \begin{bmatrix} 69.5 \\ 1.20 \\ -28.1 \\ 0.262 \end{bmatrix} \delta_r + \begin{bmatrix} 45.7 \\ 27.0 \\ 51.0 \\ 37.0 \end{bmatrix} w$$

For cruise flight condition the values of aerodynamic derivatives of rigid aircraft equations considering static corrections for structural elasticity are given in the following table:

Derivative	Y	L	N
β	-0.1	-3.75	-2.2
p	0	-0.9	-0.076
r	0	-0.3	-0.33
δ_a	0	-0.8	0
δ_r	-0.02	-0.75	-1.05

Values of structural modes in different fuselage points are equal to

- in a cockpit
 $f = [-0.155 \ 0.219 \ -0.293 \ -0.971]$
 $\varphi = [0.0374 \ 0.0148 \ -0.021 \ 0.0027]$
 $\psi = [0.0093 \ -0.0092 \ 0.0276 \ 0.109]$
- in a control system sensors location
 $f = [-0.0323 \ 0.116 \ 0.035 \ 0.135]$
 $\varphi = [0.0326 \ 0.0107 \ -0.0185 \ 0.00455]$
 $\psi = [0.0048 \ -0.00015 \ 0.016 \ 0.017]$

$n_y / \delta_a, p / \delta_a$ - transfer functions models responses measured in a cockpit are presented in fig. 3.2.a,b.

Block-diagrams of lateral control system selected for simulation are given in fig.3.3.

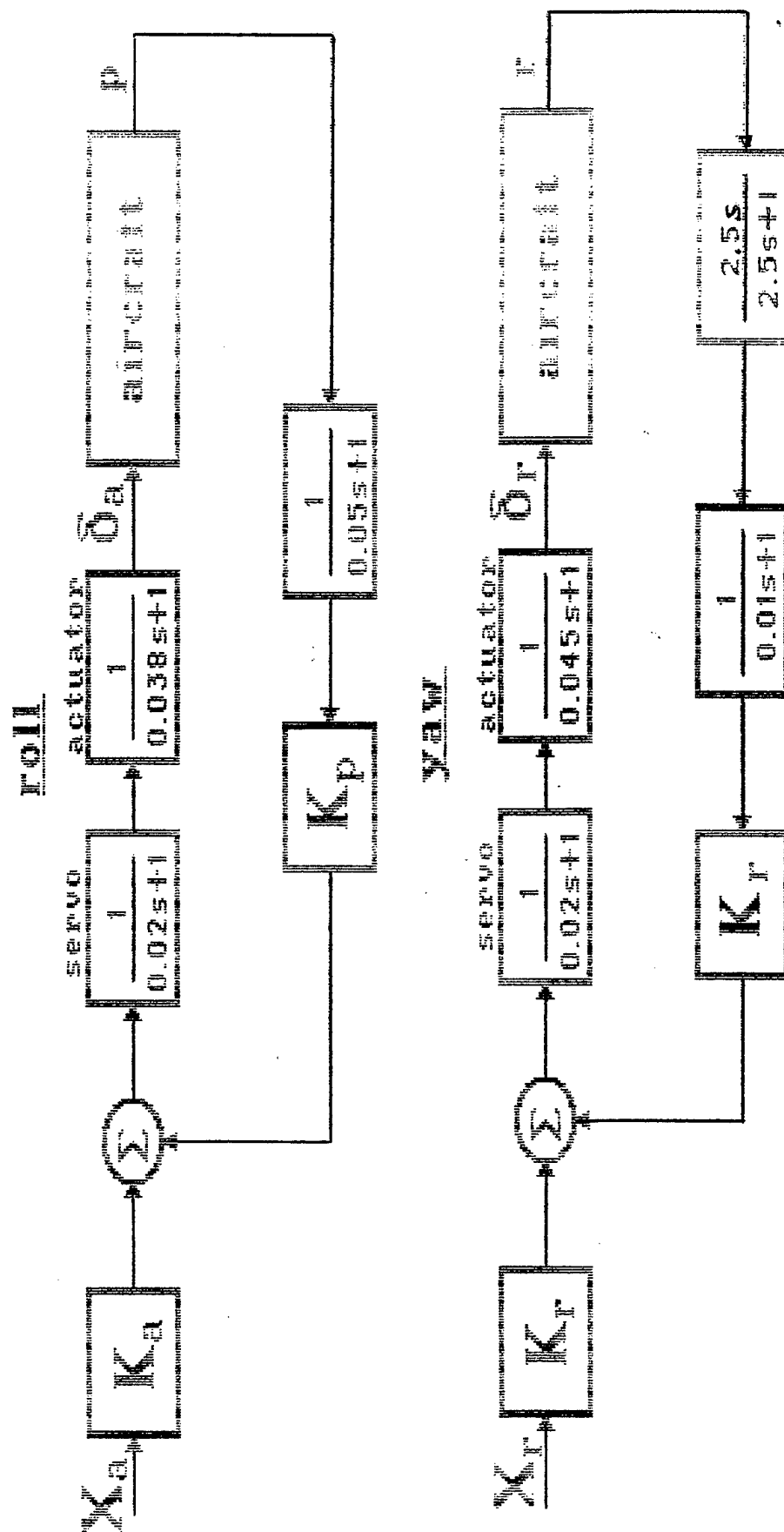


Fig.3.3. Block-diagrams of aircraft roll and yaw control system.

Feed-back and feed-forward gains of control system for cruise flight conditions are equal to the following:

$$K_q = 3.0 \text{ sec}; K_{n_z} = 0.087 \text{ rad/sec}; K_p = 0.6 \text{ sec}; K_r = 1.0 \text{ sec};$$

$$K_e = 0.0017 \text{ rad/mm}; K_a = 0.0052 \text{ rad/mm}; K_r = 0.003 \text{ rad/mm}$$

Coordinates of control system sensors are $x_s = 4.6 \text{ m}$, $z_s = 0$.

Longitudinal aircraft motion model for simulation is described with the following equations:

$$\begin{cases} \dot{\alpha} = -Z_{\alpha}\alpha + q - Z_{\delta_e}\delta_e \\ \dot{q} = M_{\alpha}\alpha + M_q q + M_{\dot{\alpha}}\dot{\alpha} + M_{\delta_e}\delta_e \end{cases}$$

$$n_z(t, x) = \frac{V}{g}[q(t) - \dot{\alpha}(t)] + \frac{x}{g}\dot{q}(t)$$

Aerodynamic coefficients accounting for static corrections for structural elasticity are given in the following table:

Derivative	Z	M
α	0.691	-2.034
p	-	-0.533
$\dot{\alpha}$	-	-0.221
δ_e	0.030	-2.38

Transfer functions models of side acceleration and roll rate referenced to an aileron deflection take the forms:

$$\frac{n_y}{\delta_e} = -0.187 \frac{(s+1.62)(s^2+0.88s+1.59)}{(s+0.83)(s^2+0.54s+2.2)} \frac{(s-7.2)(s+5.5)}{(s^2+1.6s+219)} \times$$

$$\times \frac{(s^2+0.71s+227)}{(s^2+0.41s+222)} \frac{(s^2-6.3s+555)}{(s^2+s+270)} \frac{(s^2+4.4s+631)}{(s^2+0.63s+678)}$$

$$\frac{p}{\delta_e} = \frac{2.44}{(s+0.83)} \frac{(s^2+0.44s+2.27)}{(s^2+0.54s+2.2)} \frac{(s^2+0.21s+221)}{(s^2+1.6s+219)} \frac{(s^2+1.19s+250)}{(s^2+0.41s+222)} \times$$

$$\times \frac{(s+9.3)(s-8.66)}{(s^2+s+270)} \frac{(s^2+0.678s+690)}{(s^2+0.63s+678)}$$

3.3 EXPERIMENTAL RESULTS

The results of high-frequency pilot assisted oscillations modeling are considered in this part of the work.

The experiments modeling aircraft dynamics on a flight simulator (see part 3.2) show the following:

1. Aircraft elastic modes influence high-frequency oscillations in a pilot-aircraft system to a considerable extent.

High-frequency oscillations were regularly observed in the course of experiments on the moving-base simulator for both step roll manipulator input and permanent manipulator deflections determined by a tracking task. This fact was mentioned by all the three pilots who took part in the experiments. In figs. 3.4, 3.5 the time histories for an elastic and rigid aircraft are given; the moving-base simulator was flown by one of the pilots. The comparison of the given time histories shows that high-frequency oscillations appeared on the elastic aircraft only.

The oscillations frequency remained about 2.5 Hz in all the cases regardless of a pilot and his piloting manner. This frequency coincides with that obtained during flight tests (fig. 3.1) and corresponds to the frequency of the first aircraft elastic mode (figs. 3.2a,b). The latter fact proves it was aircraft elasticity that caused oscillations in both ground-based and in-flight experiments.

2. The magnitude of such high-frequency oscillations depends on a resonant peak magnitude in elastic aircraft transfer function responses.

Figs. 3.5-3.8 show that as the first aircraft elastic mode peak becomes higher, the magnitudes of lateral and roll rate oscillations increase, the magnitudes being proportional to the elastic mode peak, see fig. 3.9.

As it is shown in fig. 3.10 the pilot ratings worsen as the peak magnitude increases. The threshold peak magnitude which corresponded to ratchet arising, was about 12.5% of the peak maximum value, according to the pilots. As the peak became higher, the pilots noticed the unfavorable effect of the accelerations. The attempts to counteract these disturbances failed. Smooth manipulator resetting to the neutral position or setting it free damped these oscillations.

3. Pilot-felt accelerations influence high-frequency oscillations considerably.

This follows from the comparison of the data obtained in the experiments while different degrees of freedom were engaged: roll and lateral displacement (fig. 3.5), roll only (fig. 3.11), no degrees of freedom switched on (fig. 3.12).

The data showed and the pilots noticed that aircraft oscillations arose on a moving simulator only. An aircraft oscillation tendency was observed even while only the roll degree was

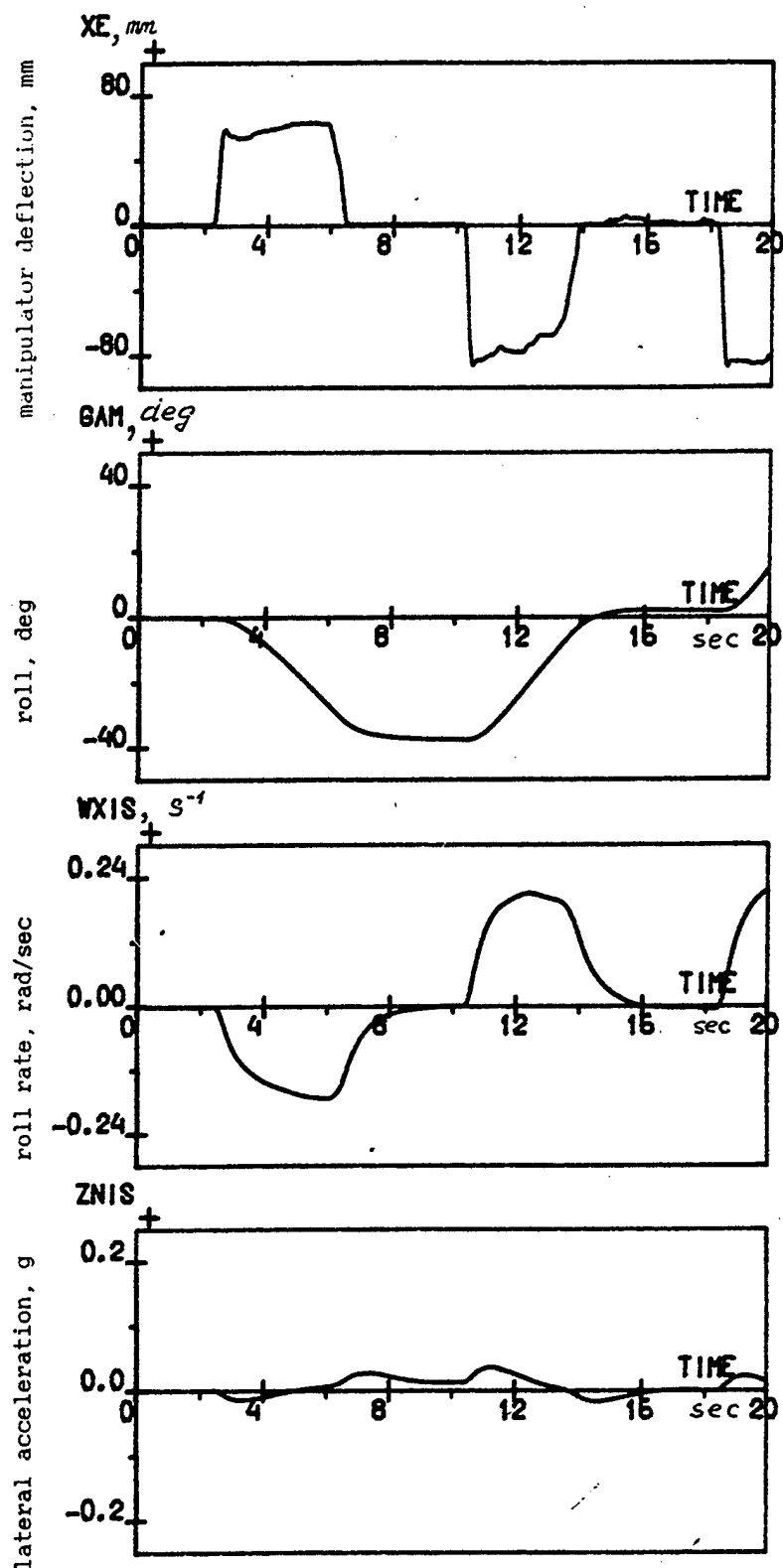


Fig.3.4. Time Histories of Aircraft as Rigid Body.

Elastic mode amplitude: $\bar{A} = 0$ Manipulator: central stick
 Motion simulated: roll, yaw, lat. displ. Aircraft gain: $K/K_n = 1$

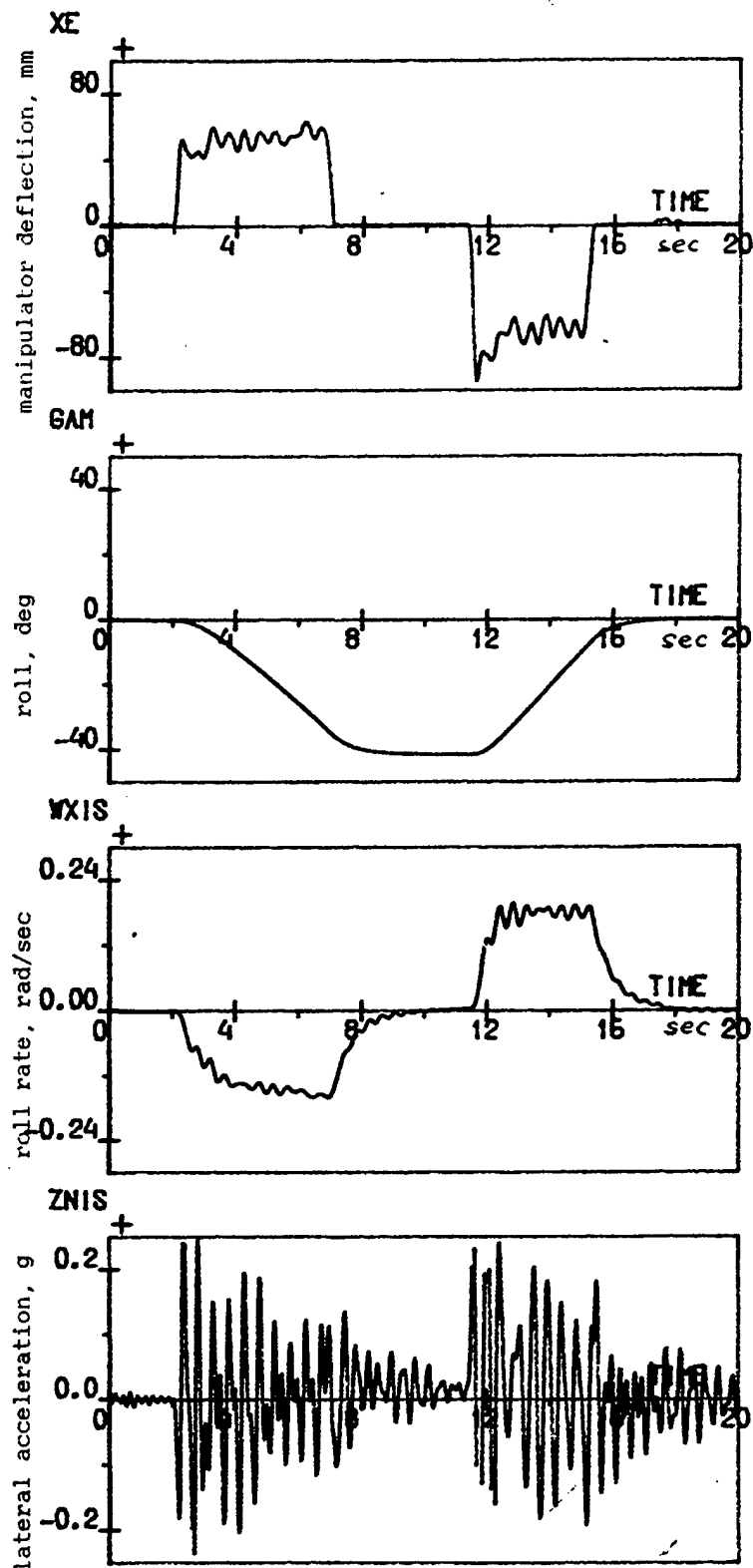


Fig.3.5. Time Histories of Elastic Aircraft

Elastic mode amplitude: $\bar{A} = 1$ Manipulator: central stick
 Motion simulated: roll, yaw, lat. displ. Aircraft gain: $K/K_n = 1$

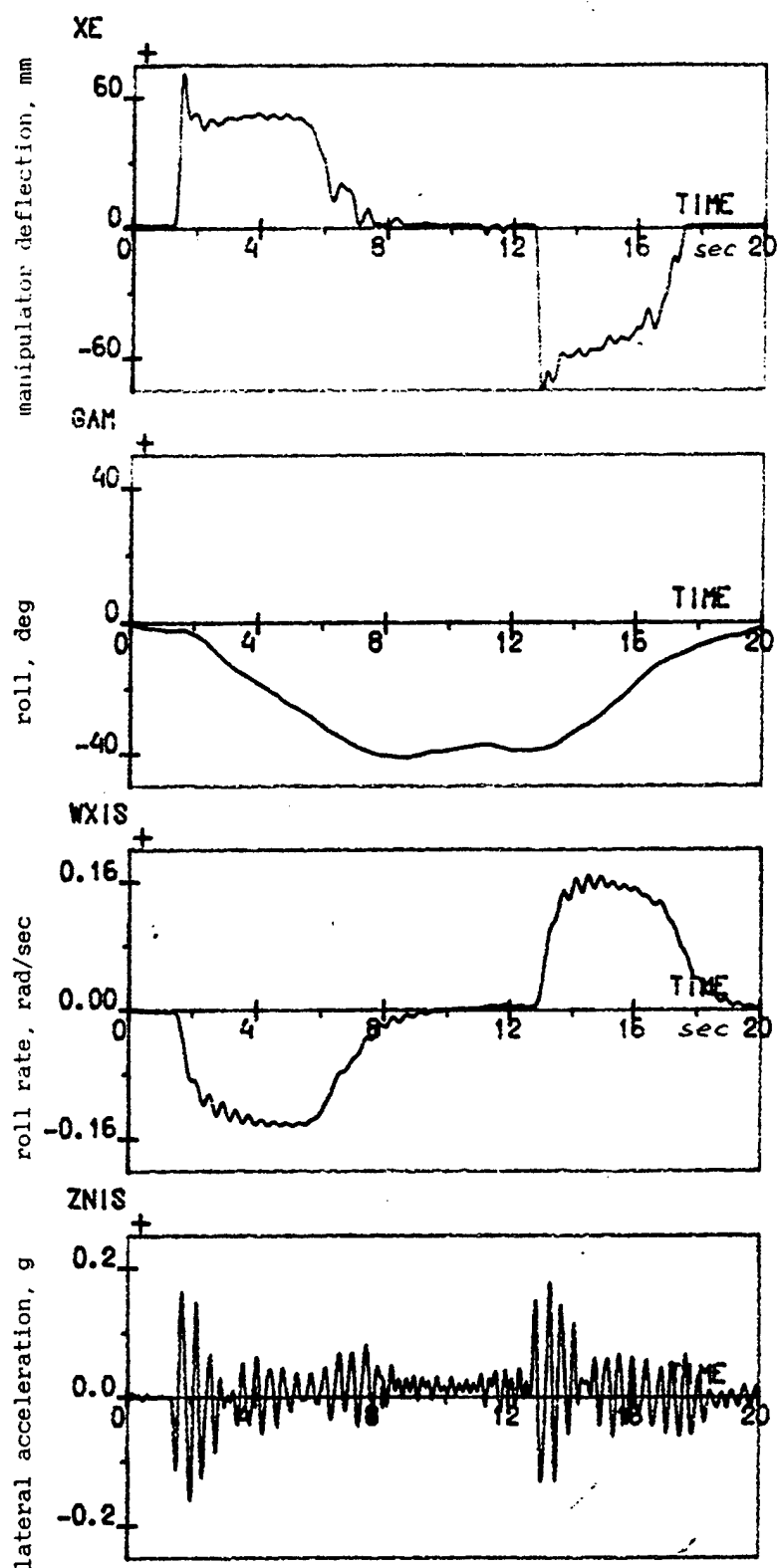


Fig.3.6. Time Histories of Elastic Aircraft

Elastic mode amplitude: $\bar{A} = 0.5$ Manipulator: central stick
 Motion simulated: roll, yaw, lat. displ. Aircraft gain: $K/K_n = 1$

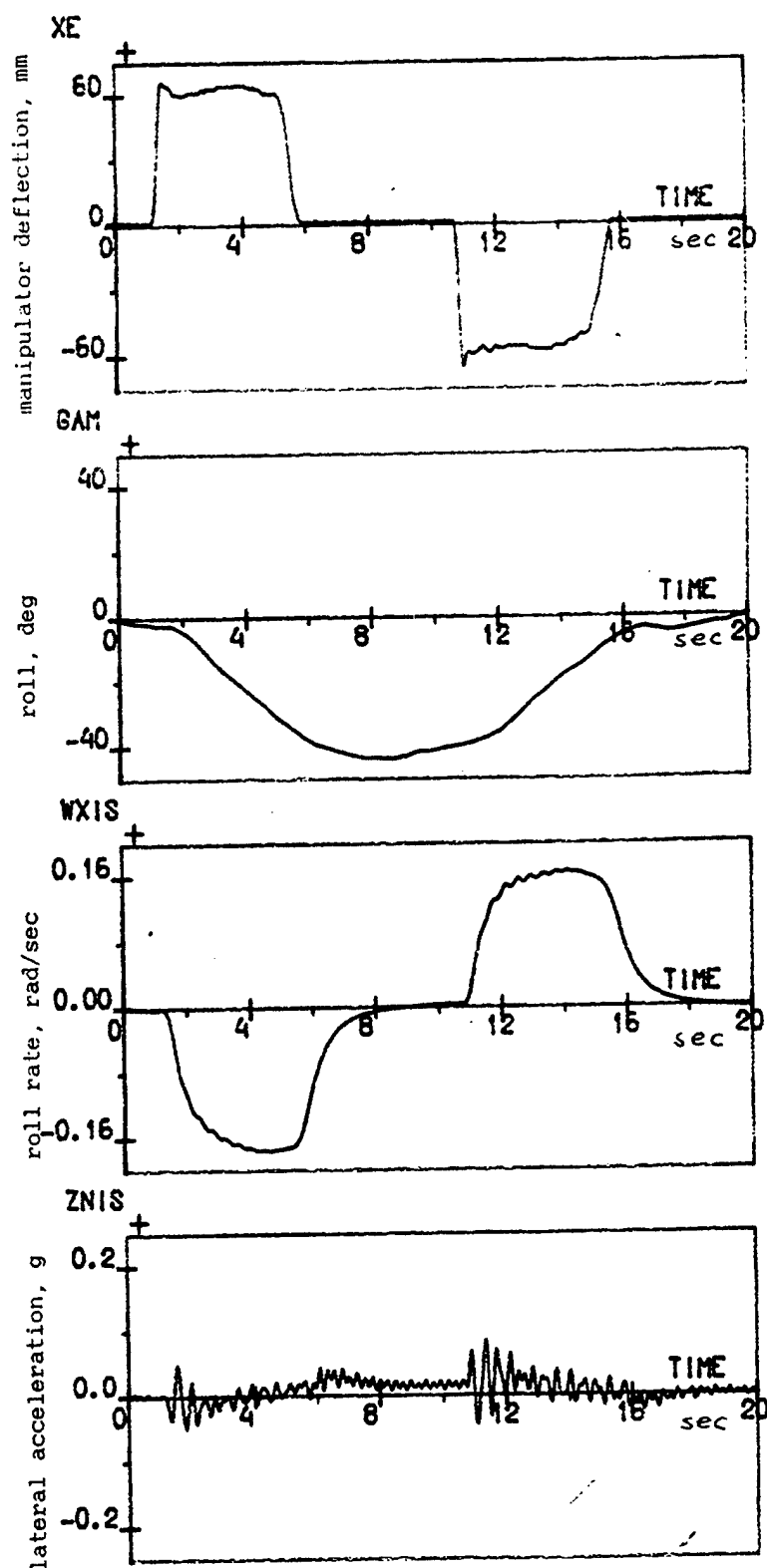


Fig.3.7. Time Histories of Elastic Aircraft

Elastic mode amplitude: $\bar{A} = 0.25$ Manipulator: central stick
 Motion simulated: roll, yaw, lat. displ. Aircraft gain: $K/K_n = 1$

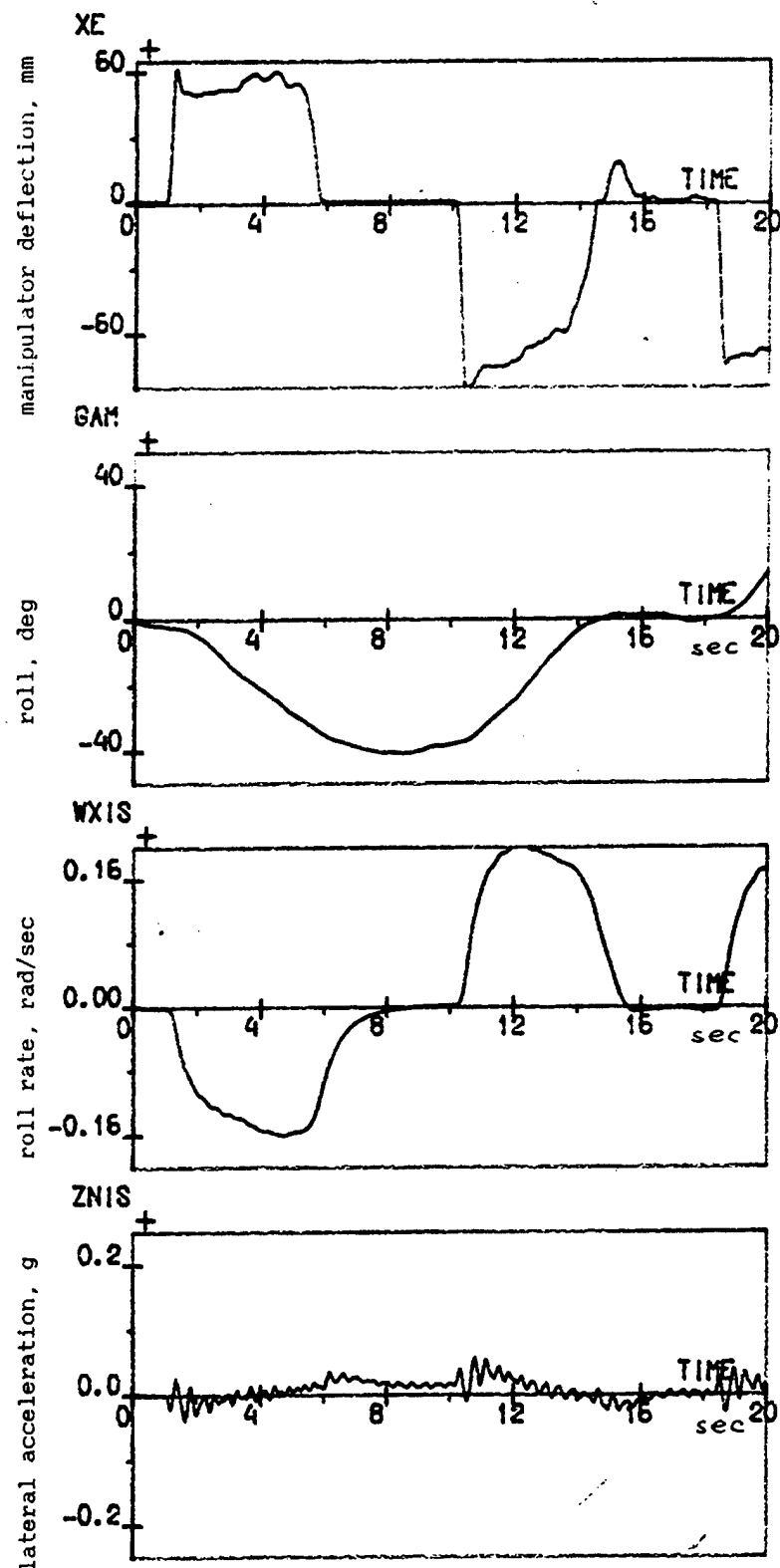


Fig.3.8. Time Histories of Elastic Aircraft

Elastic mode amplitude: $\bar{A} = 0.125$

Manipulator: central stick

Motion simulated: roll, yaw, lat. displ.

Aircraft gain: $K/K_n = 1$

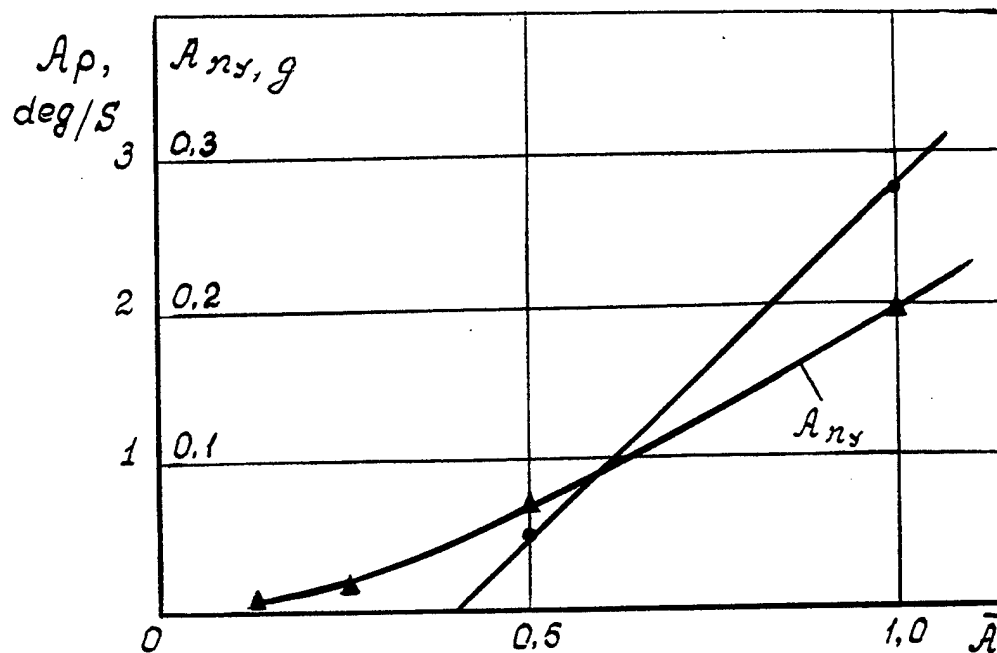


Fig.3.9. Elastic Mode Amplitude \bar{A} Influence on Roll Rate A_p and Lateral Acceleration A_{ny} Amplitudes.

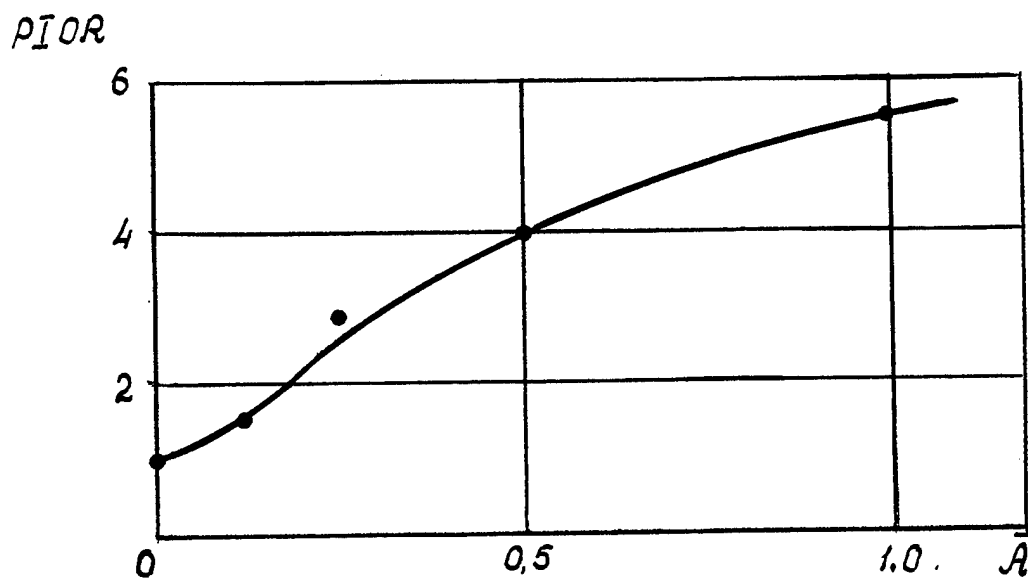


Fig.3.10. PIORs depending on Elastic Mode Amplitude \bar{A} .

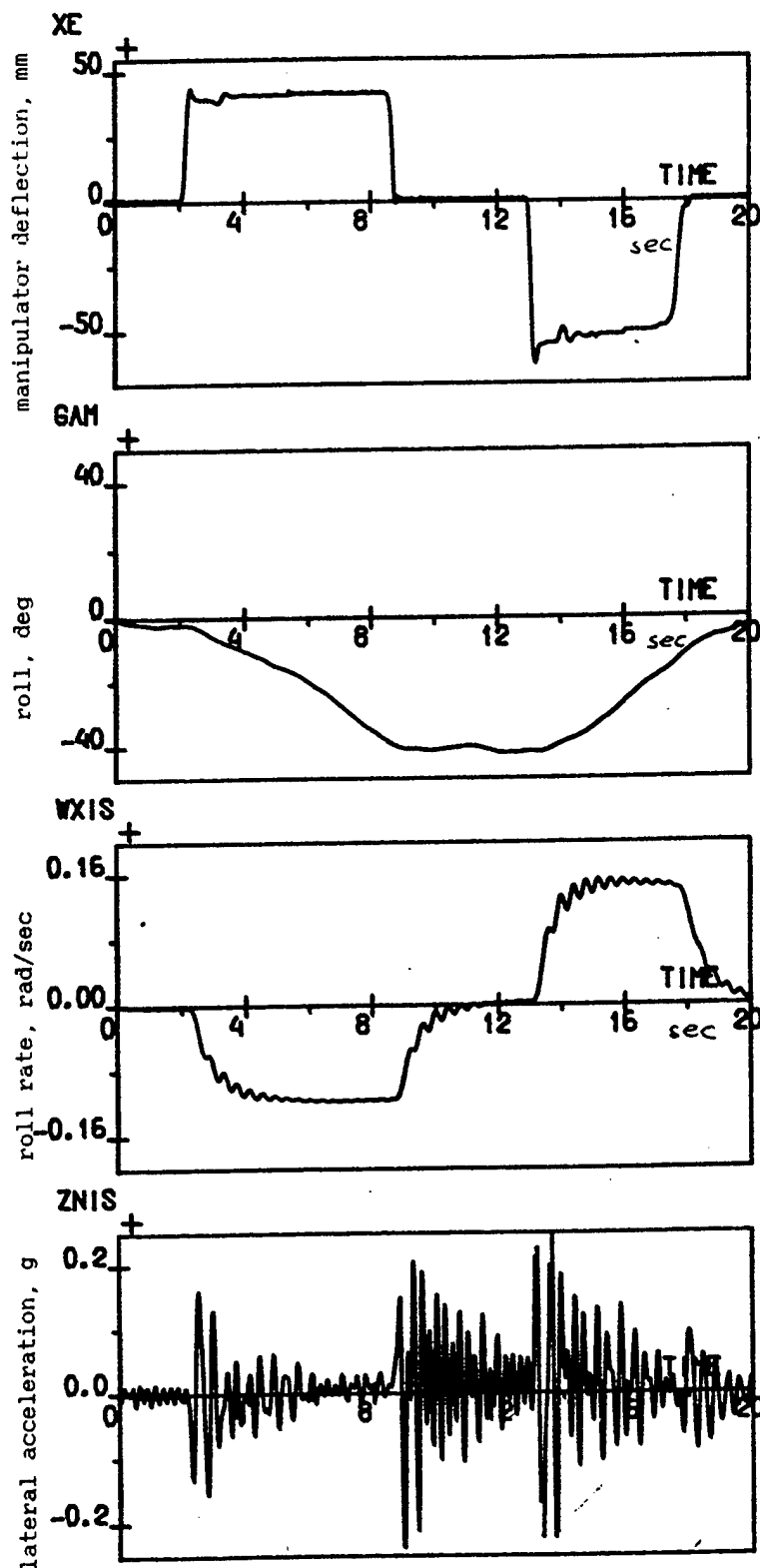


Fig.3.11. Time Histories of Elastic Aircraft

Elastic mode amplitude: $\bar{A} = 1$
 Motion simulated: roll

Manipulator: central stick
 Aircraft gain: $K/K_n = 1$

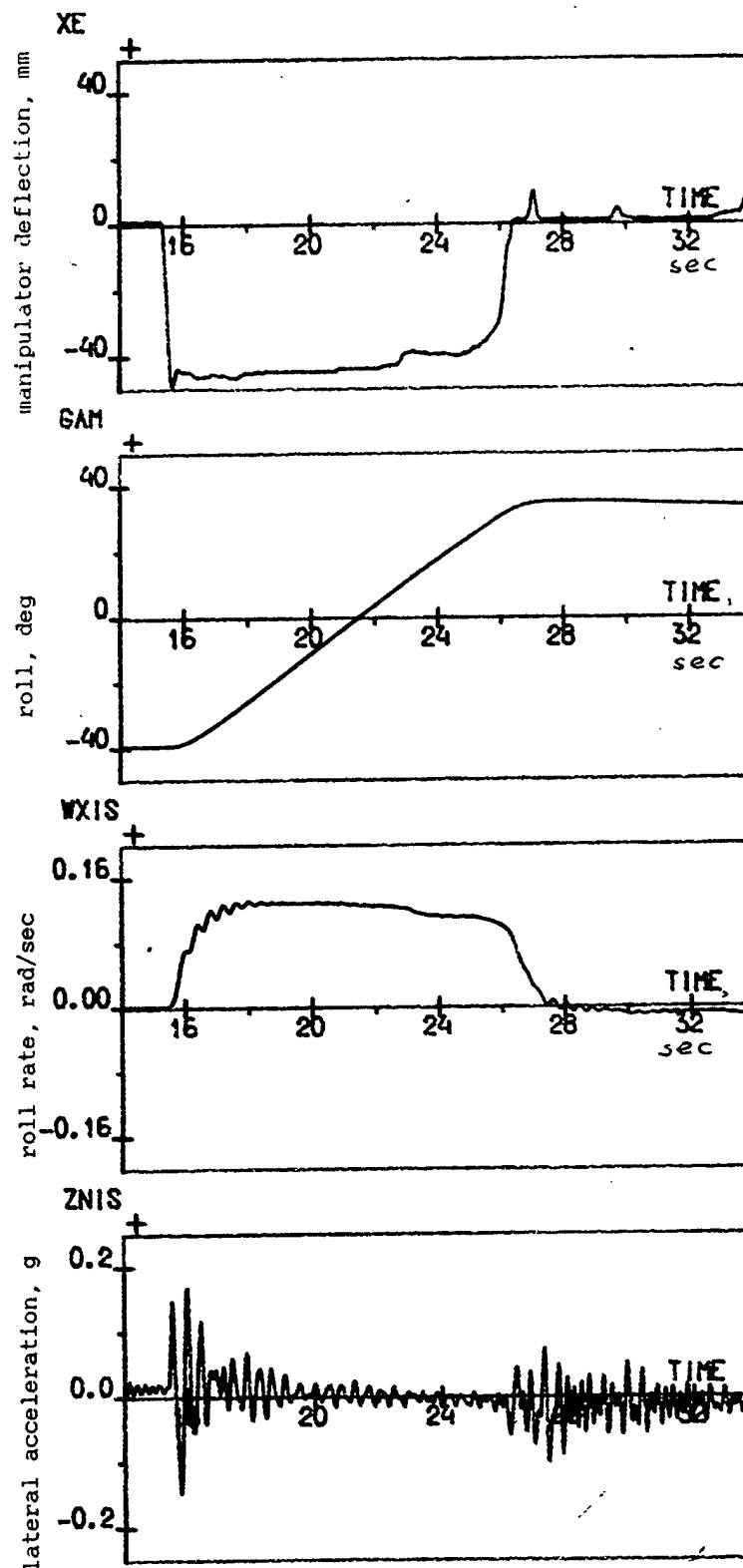


Fig.3.12. Time Histories of Elastic Aircraft

Elastic mode amplitude: $\bar{A} = 1$
 Motion simulated: absent

Manipulator: central stick
 Aircraft gain: $K/K_n = 1$

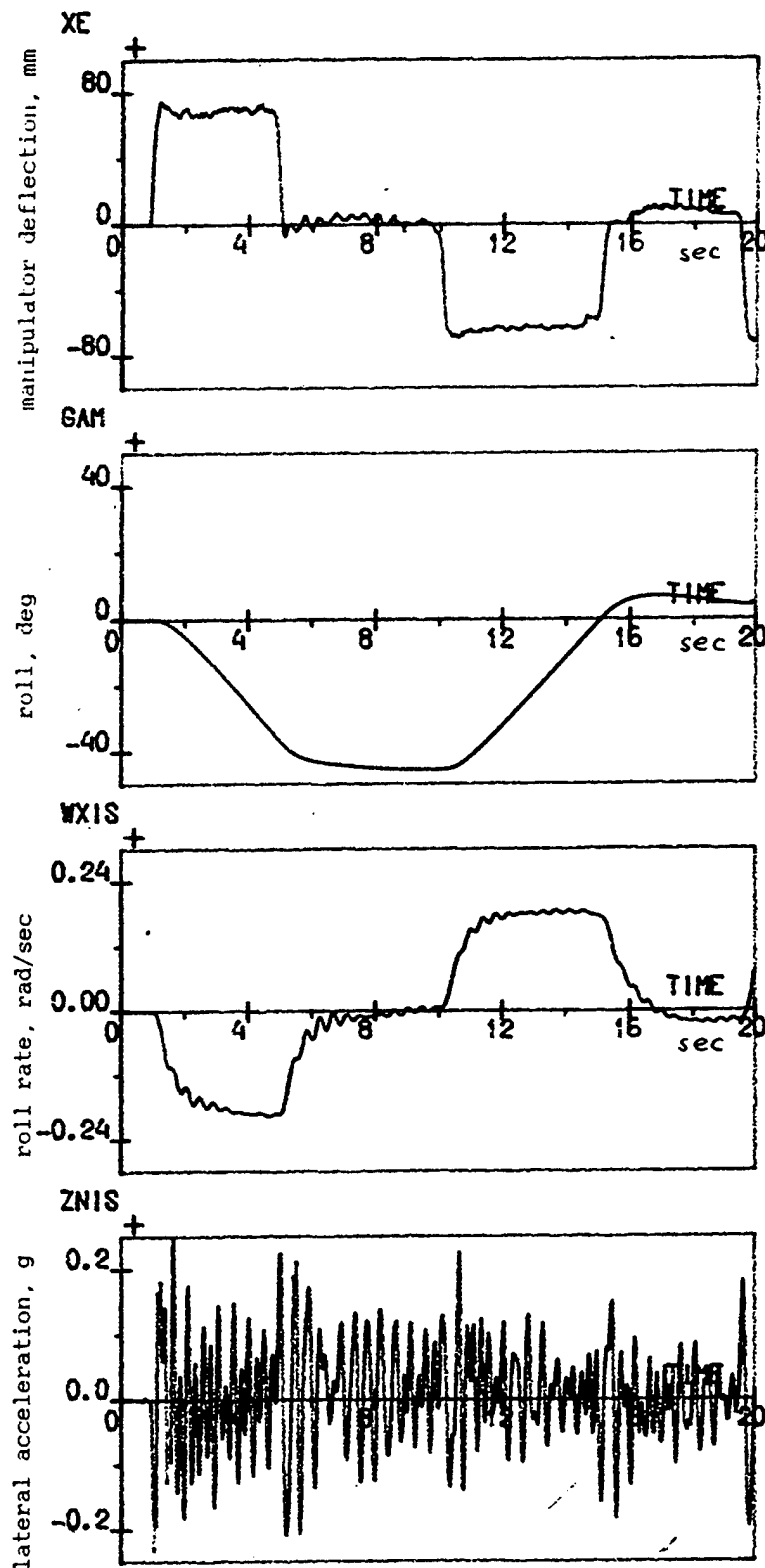


Fig.3.13. Time Histories of Elastic Aircraft

Elastic mode amplitude: $\bar{A} = 1$ Manipulator: side stick
 Motion simulated: roll, yaw, lat. displ. Aircraft gain: $K/K_n = 1$

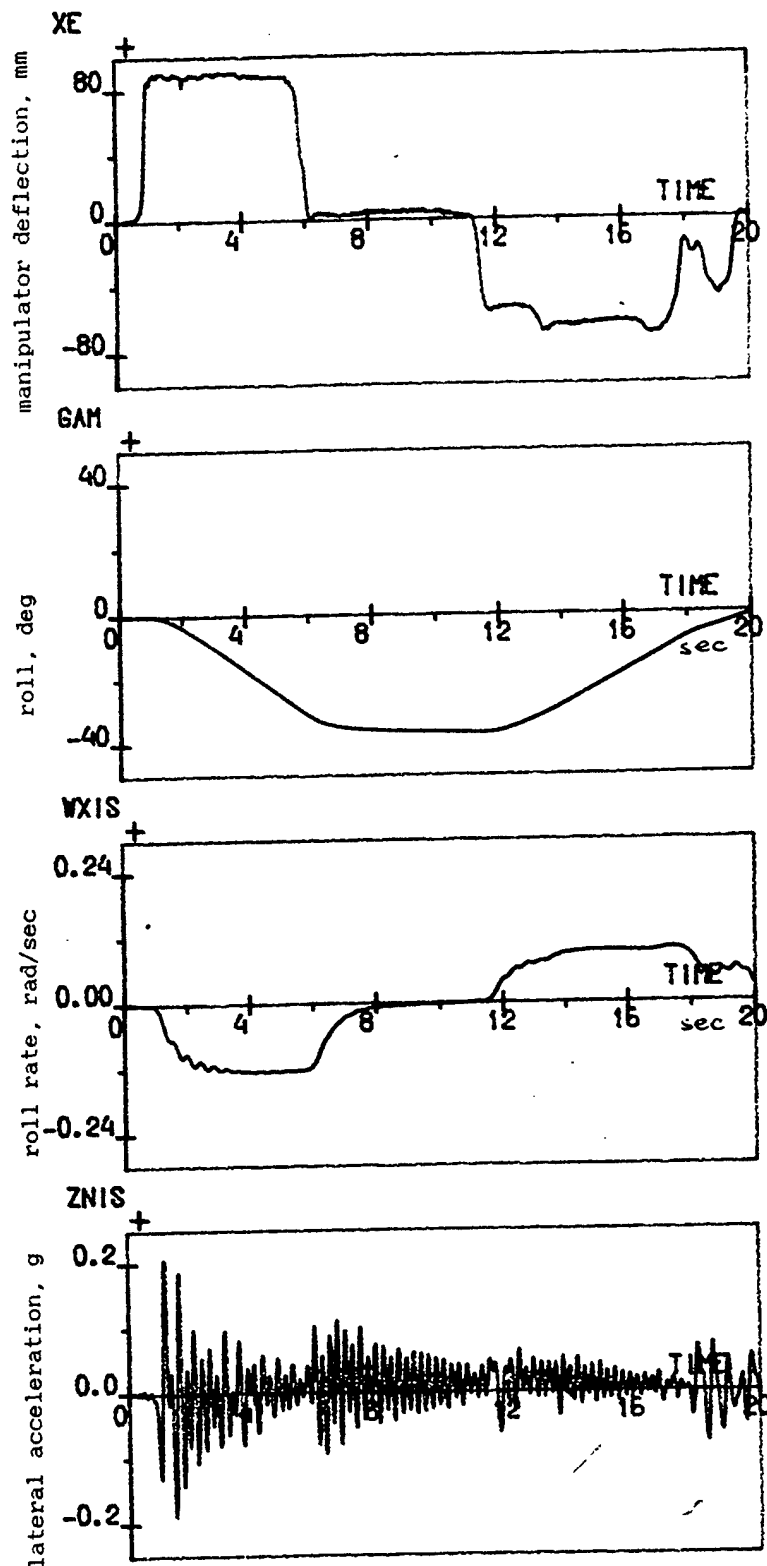


Fig.3.14a. Time Histories of Elastic Aircraft

Elastic mode amplitude: $\bar{A} = 1$ Manipulator: side stick
 Motion simulated: roll, yaw, lat. displ. Aircraft gain: $K/K_n = 0.5$

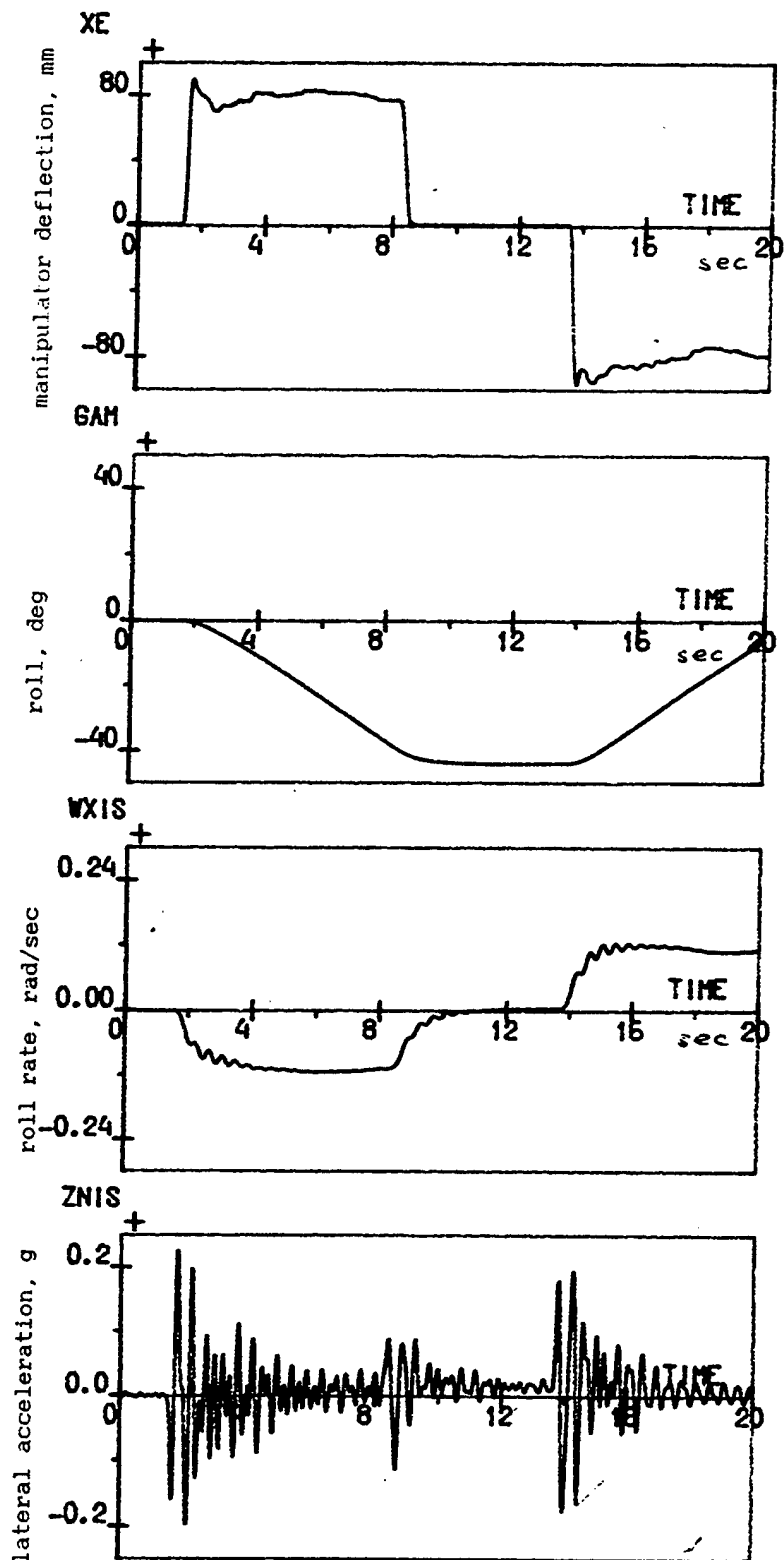


Fig.3.14b. Time Histories of Elastic Aircraft

Elastic mode amplitude: $\bar{A} = 1$ Manipulator: central stick
 Motion simulated: roll, yaw, lat. displ. Aircraft gain: $K/K_n = 0.5$

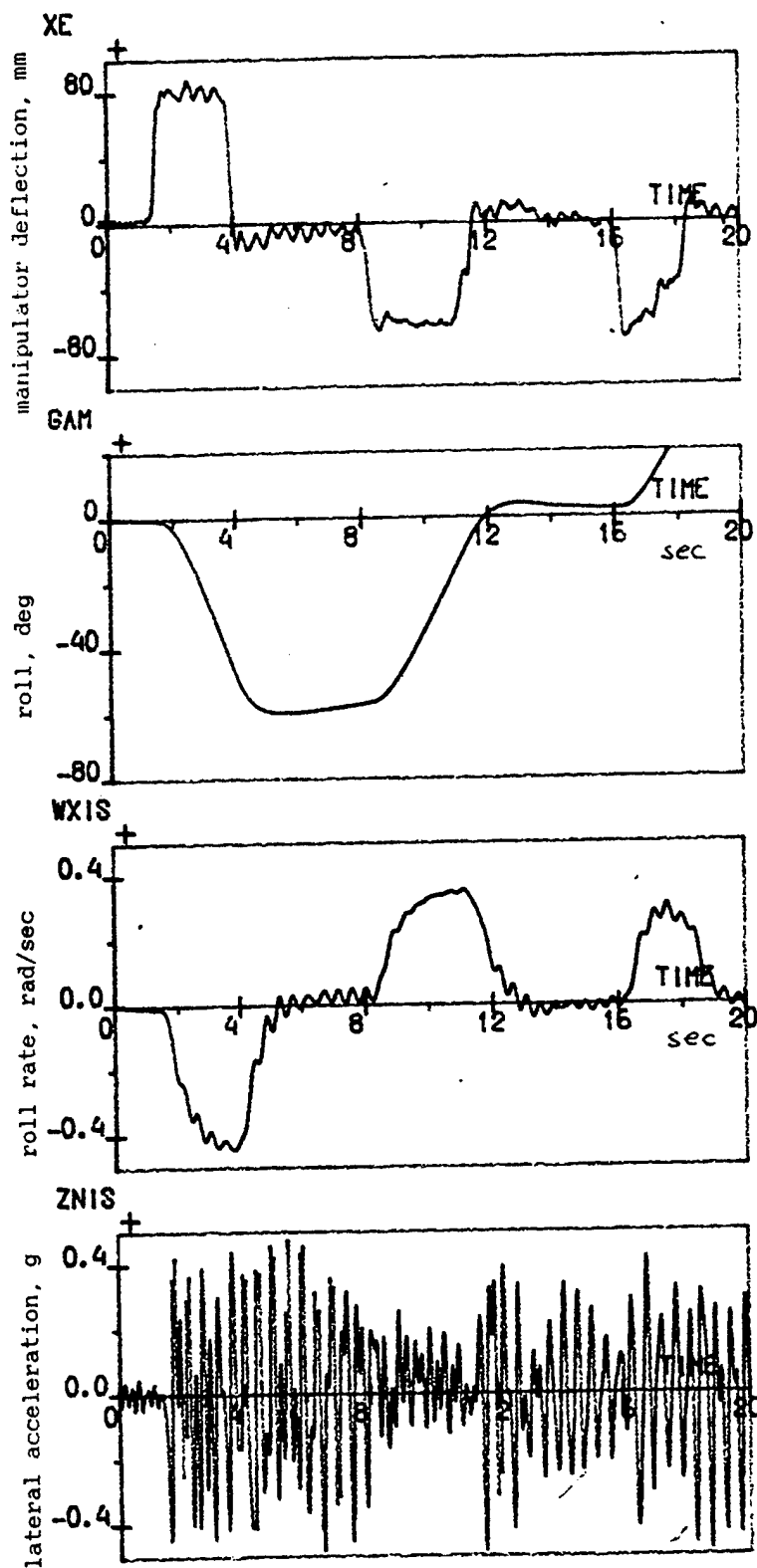


Fig.3.15. Time Histories of Elastic Aircraft

Elastic mode amplitude: $\bar{A} = 1$ Manipulator: side stick
 Motion simulated: roll, yaw, lat. displ. Aircraft gain: $K/K_n = 2$

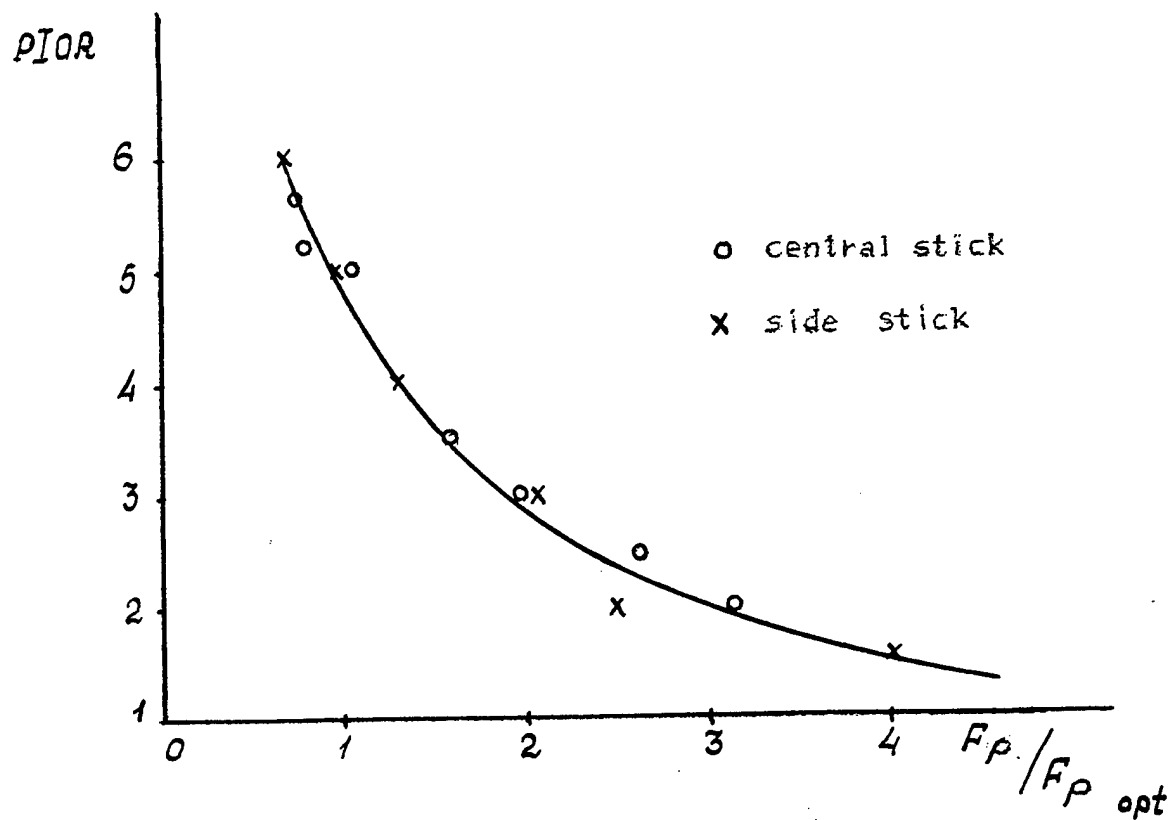


Fig.3.16. Lateral Control Sensitivity Influence on PIOR

switched on, but it was lateral accelerations that influenced this tendency greatly. An acceleration effect interfered with tracking task performance, thus, the piloting precision worsened.

4. The high-frequency oscillations are characteristic of both central and side sticks in spite of the latter having an armrest and a damping device, see time histories in figs. 3.5-3.7 for the central stick and figs. 3.13, 3.15 for the side stick.

A tendency to high-frequency oscillations depends on the direction of forces applied. This skewness depends on the manipulator type. In the case of a central stick the tendency is greater while the stick is deflected to the right, but for a side stick it is vice versa, see figs. 3.5 and 3.13. According to the pilots, difference in the type of skewness due to the type of a stick is accounted for by the fact that different muscle groups are engaged in controlling, these muscles having different dynamic and force characteristics. In the case of a central stick an arm and upper body are engaged, while in the case of a side stick with an arm on an armrest, only a forearm and a hand are used.

5. Aircraft command sensitivity affects high-frequency oscillations caused by structural elasticity to a considerable extent, which can be seen from the time histories (figs. 3.5, 3.14, 3.15) and from the relation of pilot rating to command sensitivity as well (fig. 3.16).

It should be mentioned that pilot ratings variation is accounted for by ratchet mainly, according to the pilots; if there is no ratchet observed aircraft gain variation does not influence pilot ratings. According to our data if aircraft gain is 2 times less in comparison with its optimum value, there are practically no high-frequency oscillations observed.

This peculiarity of command sensitivity effect on high-frequency oscillations caused by structural elasticity is in agreement with the data given in ⁽⁹⁾ concerning a command sensitivity effect on ratchet at low roll mode time constant values.

6. High-frequency oscillations are possible to simulate on a ground-based simulator with a motion system. It follows from all the data presented above.

According to the pilot who took part in the in-flight experiment (see time histories in fig. 3.1) and in the ground-based experiments (see time histories in fig. 3.17) high-frequency oscillations felt on the ground-based and in-flight simulators are basically the same. However, the oscillation tendency observed in flight experiments was less. It is accounted for by two facts: first, a miniwheel was used in flight while central and side sticks were used on a simulator; second, the command sensitivity characteristics differed.

It has been mentioned in some works (see, for example, ⁽⁹⁾) that ratchet caused by low roll mode time constant values is difficult to reproduce on a ground-based simulator. As to high-frequency oscillations caused by structural elasticity, our experience shows that this type of oscillations is easily reproduced and, thus, can be studied on a simulator.

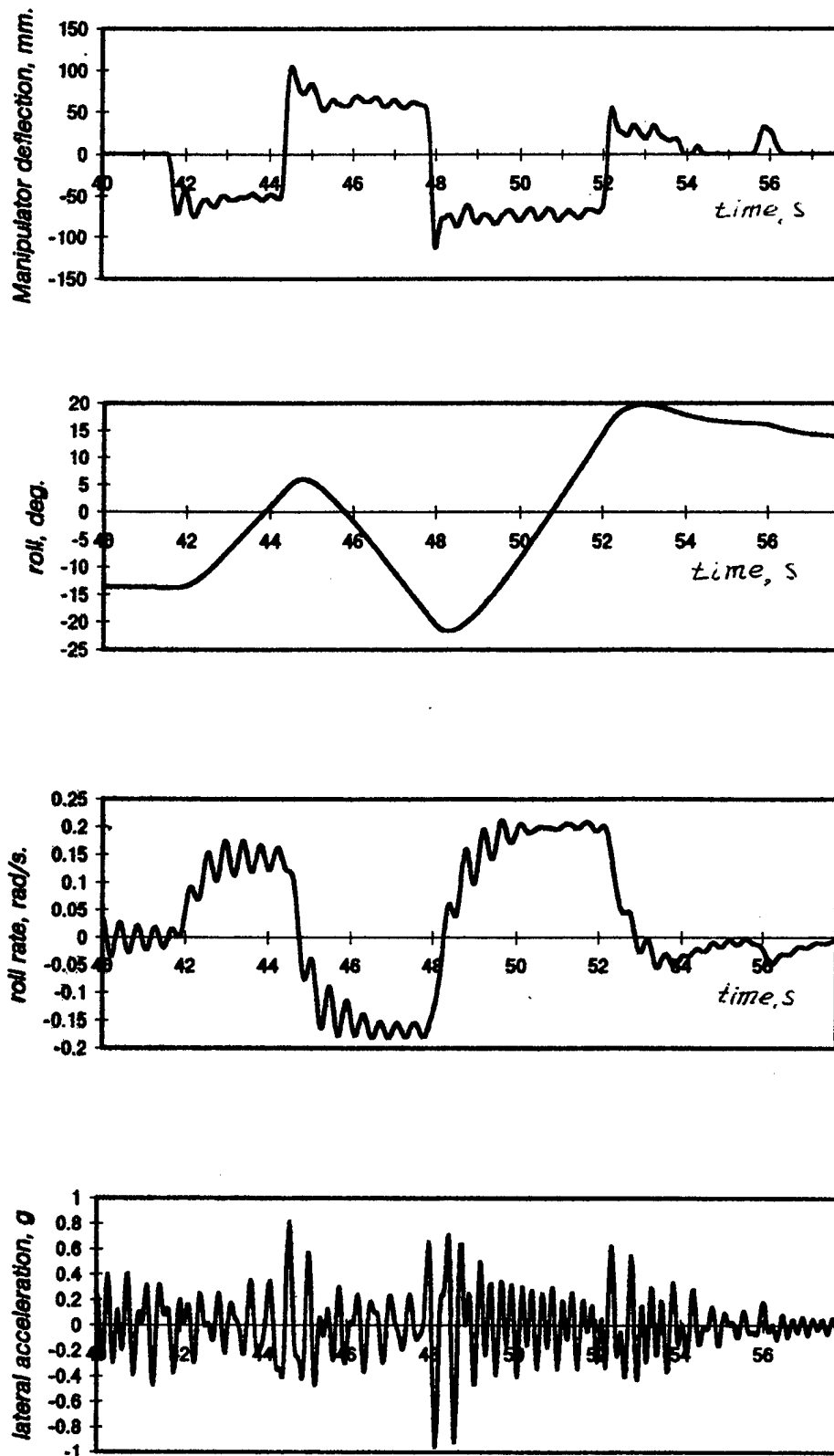


Fig.3.17. Time Histories of Elastic Aircraft

Elastic mode amplitude: $\bar{A} = 1$
 Motion simulated: roll

Manipulator: central stick
 Aircraft gain: $K/K_n = 1.5$

The experimental data concerning pilot describing functions will be considered in the next part.

3.4 ANALYSIS OF PILOT-AIRCRAFT SYSTEM CHARACTERISTICS

To reveal causes of high-frequency PIO and ways to preclude this phenomenon, let us consider the describing functions of a pilot and an open-loop pilot-aircraft system obtained in the course of the experiments, see figs. 3.18-3.21. In these figures the approximation of these describing functions in terms of a pilot transfer function model is shown as well. The pilot transfer function is as follows:

$$Y_p = K_p (T_i s + 1) e^{-s\tau} Y_{lm}, \quad (3.2)$$

where

K_p, T_i - pilot's gain and lead,

τ - pilot's equivalent time delay (as a combination of pilot's pure time delay and computer time delay).

In accordance with the diagram in fig. 1.14 Y_{lm} - transfer function model ($T_N = 0, P_{sp} = \infty$) can be presented as

$$Y_{lm} = \frac{1}{T_1^2 s^2 + 2\xi_1 T_1 s + 1} \frac{1}{T_2^2 s^2 + 2\xi_2 T_2 s + 1} \quad (3.3)$$

Let us consider the pilot/pilot-aircraft describing functions in figs. 3.18 and 3.19 for the case of roll motion described with

$$Y_c = \frac{K_c}{s} (T_R s + 1) \quad (3.4)$$

It can be seen that there is noticeable peaking in amplitude ratio at high frequencies (1-3 Hz) which is determined by limb-manipulator system dynamics. As a result a resonant peak in an open-loop pilot-aircraft system appears at these frequencies if values of roll mode time constant are low ($T_R = 0.1$ sec, fig. 3.18). The same type of peaking was observed by other investigators who analyzed ratcheting occurring on maneuverable aircraft in real flight. Some studies have shown (see ⁽⁹⁾, for example) that this peak magnitude is a measure of high-frequency PIO tendency caused by low roll mode time constant values. Roll high-frequency oscillations arise when a peak magnitude is about -6dB or more. Thus, the more the peak magnitude, the greater the PIO tendency.

If the roll mode time constant exceeds 0.5 sec which is typical of "rigid" unmaneuverable aircraft, resonant peaks are below -6dB. This can be seen from the describing functions presented in figs. 3.19 and 3.20: in the first case roll motion corresponded to eq.(3.4) where $T_R = 0.5$ sec; in

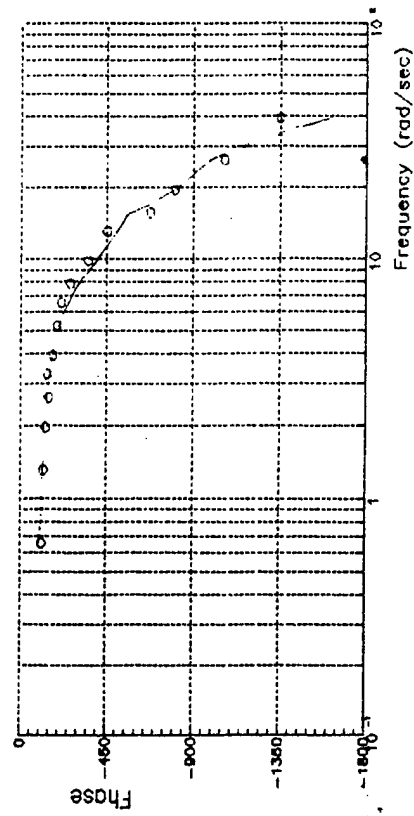
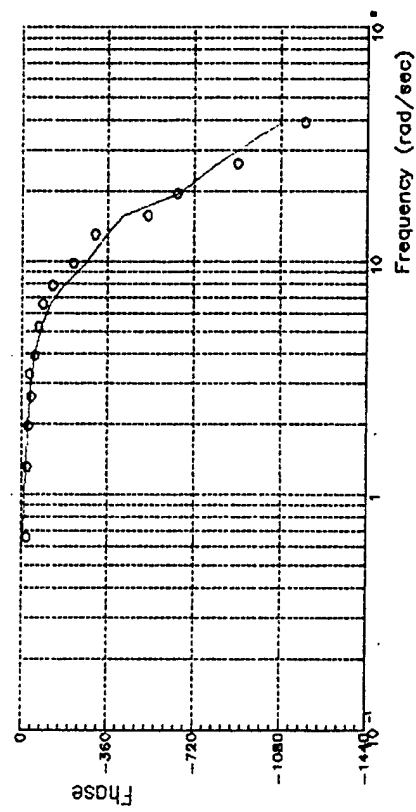
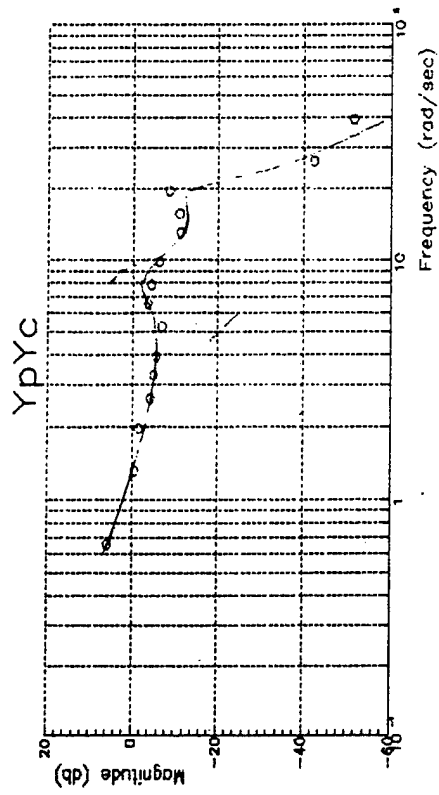
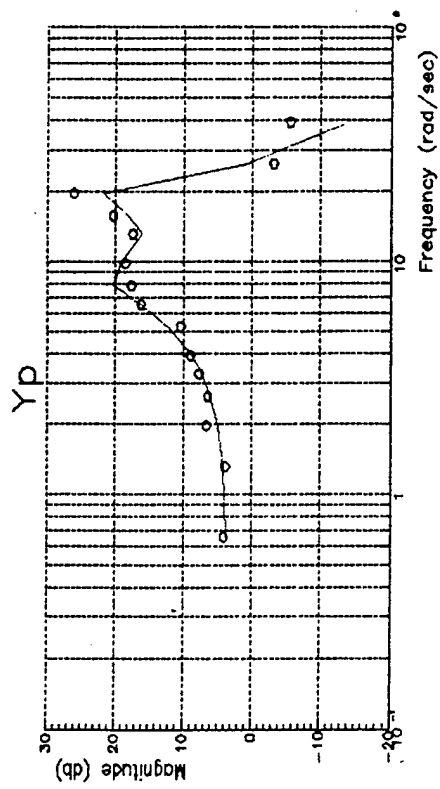


Fig.3.18.Pilot/Aircraft describing function
(isolated roll, $T_R = 0.1s$)

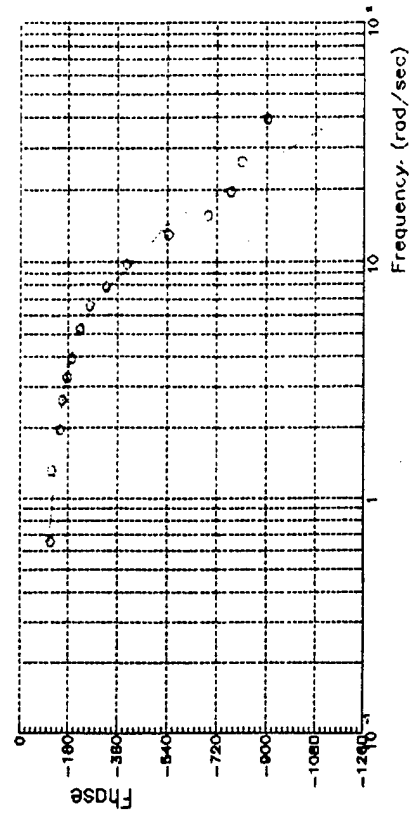
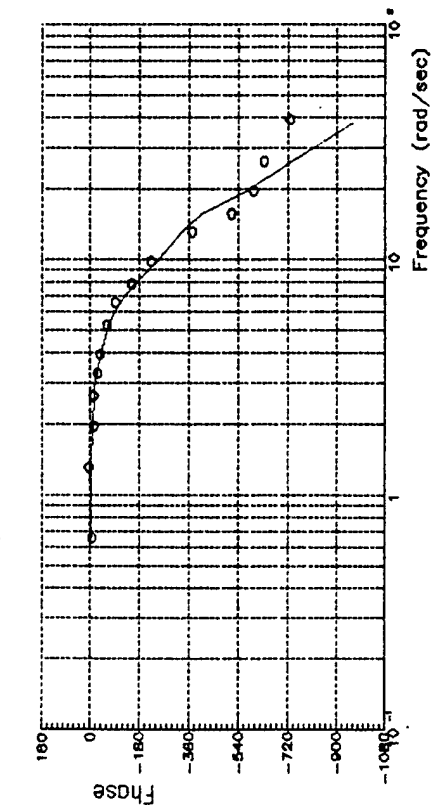
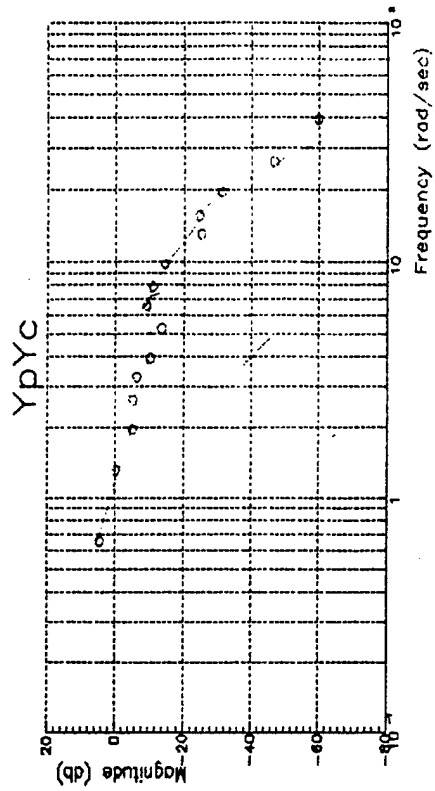
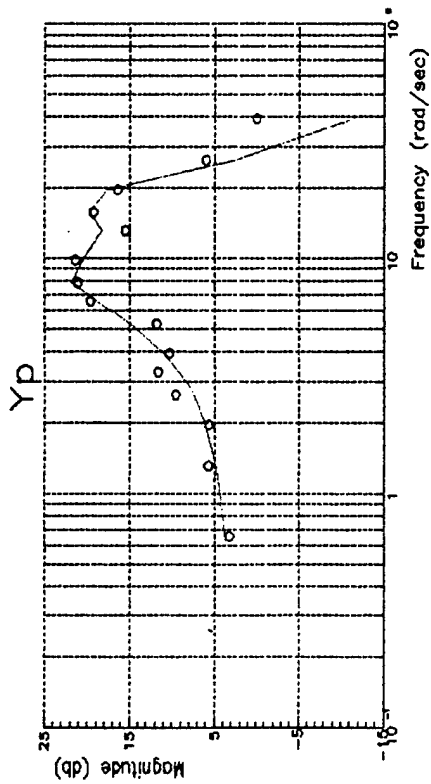


Fig.3.19.Pilot/Pilot-Aircraft describing function
(isolated roll, $T_r = 0.5s$)

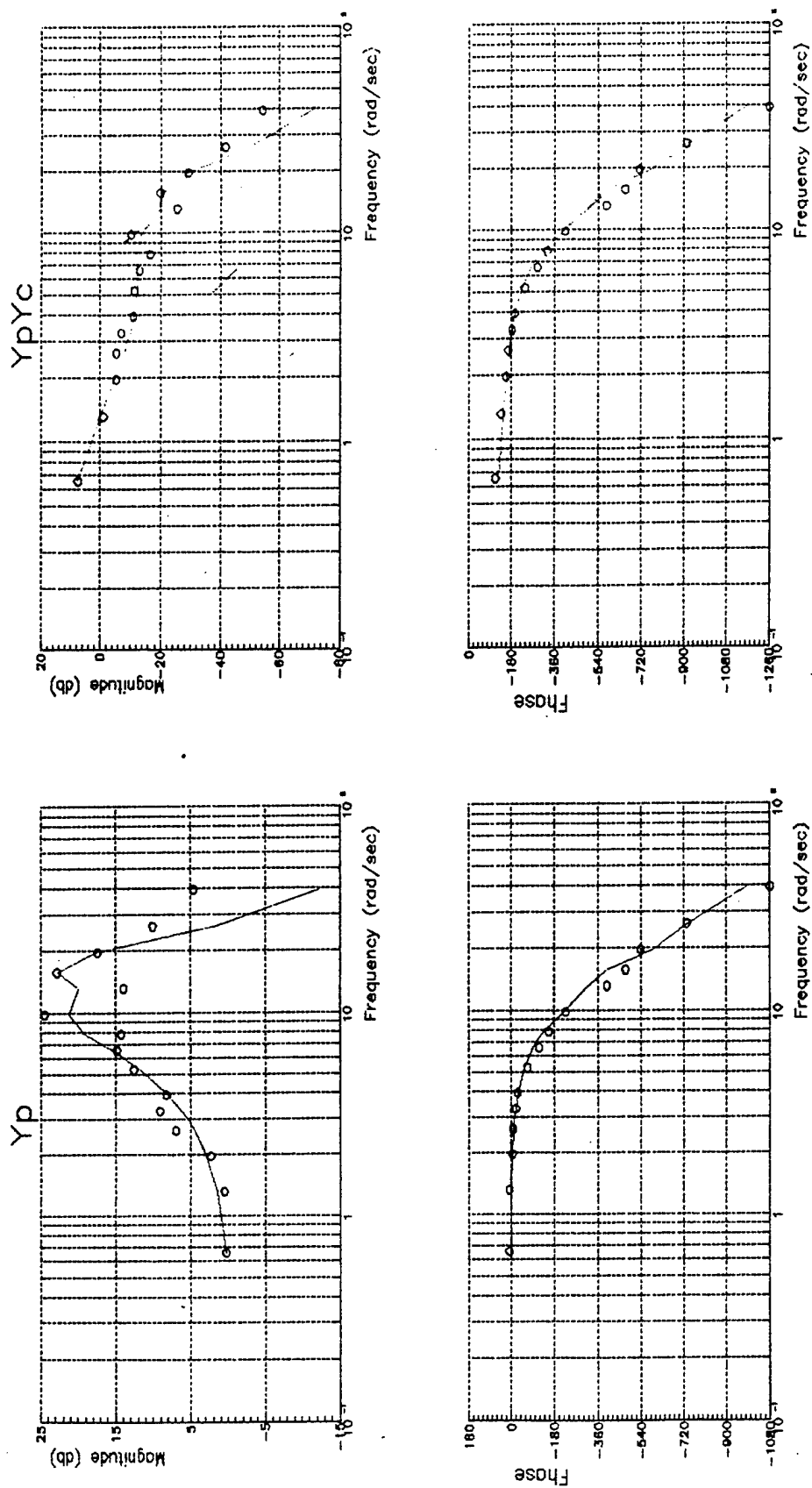


Fig.3.20 Pilot/Pilot-Aircraft describing function
(isolated roll, $T_r = 1.0s$)

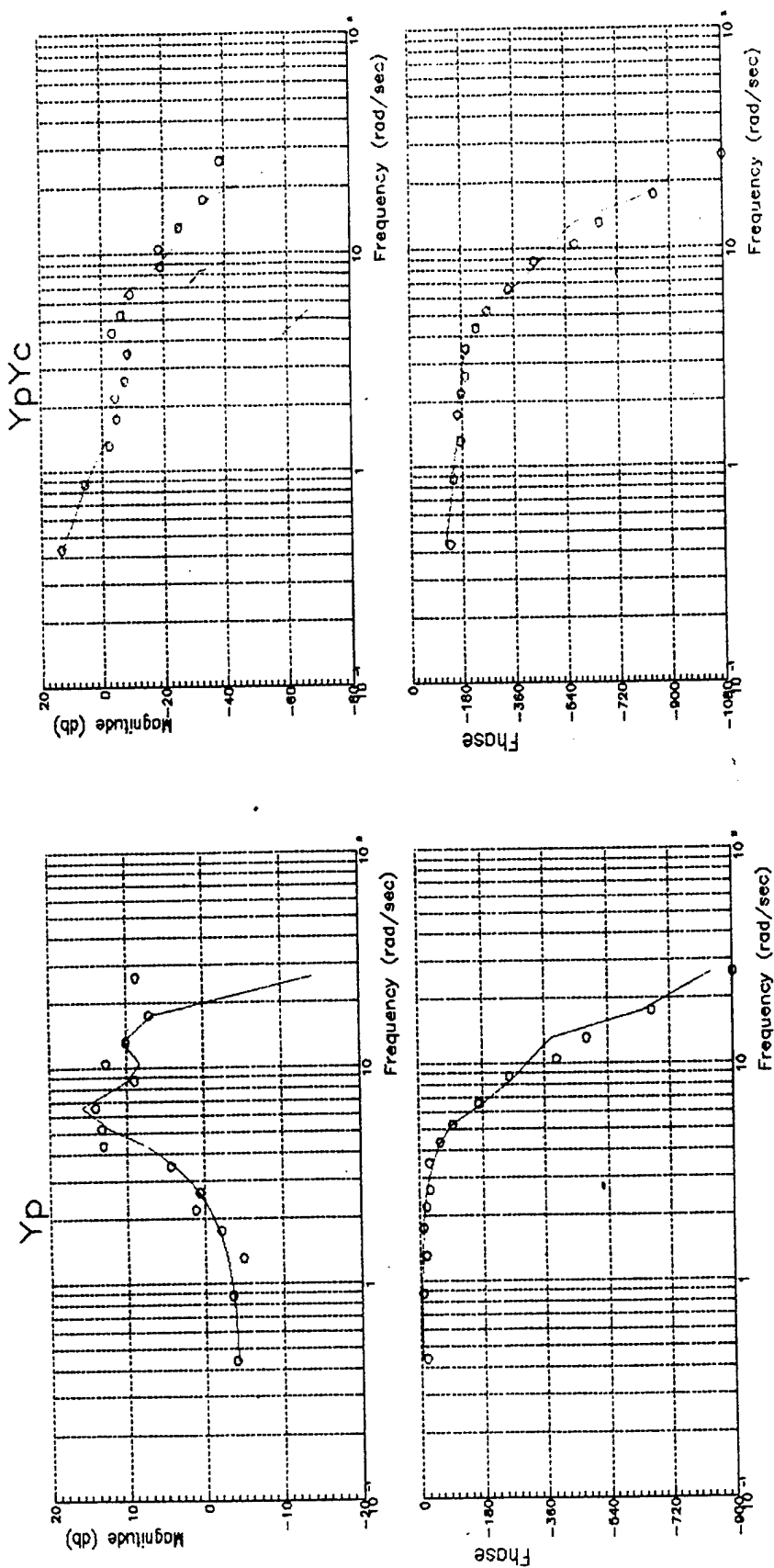


Fig. 3.21. Pilot/Pilot-Aircraft describing function

the second case roll motion corresponded to eq. (3.1) where $T_R = 1.2$ sec (structural elasticity was not taken into account). Thus, for a rigid unmaneuverable aircraft no ratcheting was observed neither in our experiments nor in other studies.

The experiments were conducted for an elastic unmaneuverable aircraft with various elastic mode amplitudes and control sensitivity characteristics. The experiments showed that if a resonant peak in $|Y_p Y_c|$ exceeded -6dB, high-frequency PIO arose. The pilot/pilot-aircraft describing functions are given in fig. 3.22 for the case when structural elastic modes (see eq.(3.1)) corresponded to real ones. (As mentioned above, in this case the PIO tendency was extreme.) For this case the resonant peak magnitude was up to +6dB.

These data have shown that the pilot and his neuromuscular system describing functions obtained in the experiments can be adequately approximated by transfer function models (3.2), (3.3).

The above mentioned facts allow us to conclude that both high-frequency oscillations on unmaneuverable aircraft due to their structural elasticity and ratchet phenomenon on maneuverable aircraft due to low values of roll mode time constant can be studied using pilot-aircraft model responses.

The pilot-aircraft model responses can be defined empirically or derived from pilot and limb-manipulator transfer functions models (3.2), (3.3). In the latter case a pilot's pure time delay can be assumed constant, for example, $\tau = 0.3$ sec; parameters K_p and T_l can be derived from "crossover model" as the data in figs. 3.18-3.21 prove:

$$Y_p(j\omega)Y_c(j\omega) = \frac{\omega_c}{j\omega} e^{-j\omega\tau},$$

where ω_c - pilot-aircraft crossover frequency ($|Y_p Y_c(j\omega_c)| = 1$) which does not depend on aircraft characteristics.

It should be mentioned that a limb-manipulator model has not been sufficiently developed yet. There is no clear idea of the order of a limb-manipulator model which would be adequate to analyze different cases of high-frequency PIO. It was concluded in ⁽⁹⁾ that a third-order transfer function model is enough to describe ratcheting caused by a low roll mode time constant. The pilot describing functions presented in figs. 3.18-3.21 show that there are two resonant peaks in pilot's amplitude ratio at the frequencies exceeding 1 Hz. These describing functions can be matched to a transfer function model of the fourth order. Comparing the experimental and calculated data showed that an adequate approximation of pilot-aircraft describing functions as well as the resonant peaks is achieved if transfer function model (3.3) is applied. We may conclude that while studying high-frequency PIO a limb-manipulator transfer function such as (3.3) can be with good reason applied.

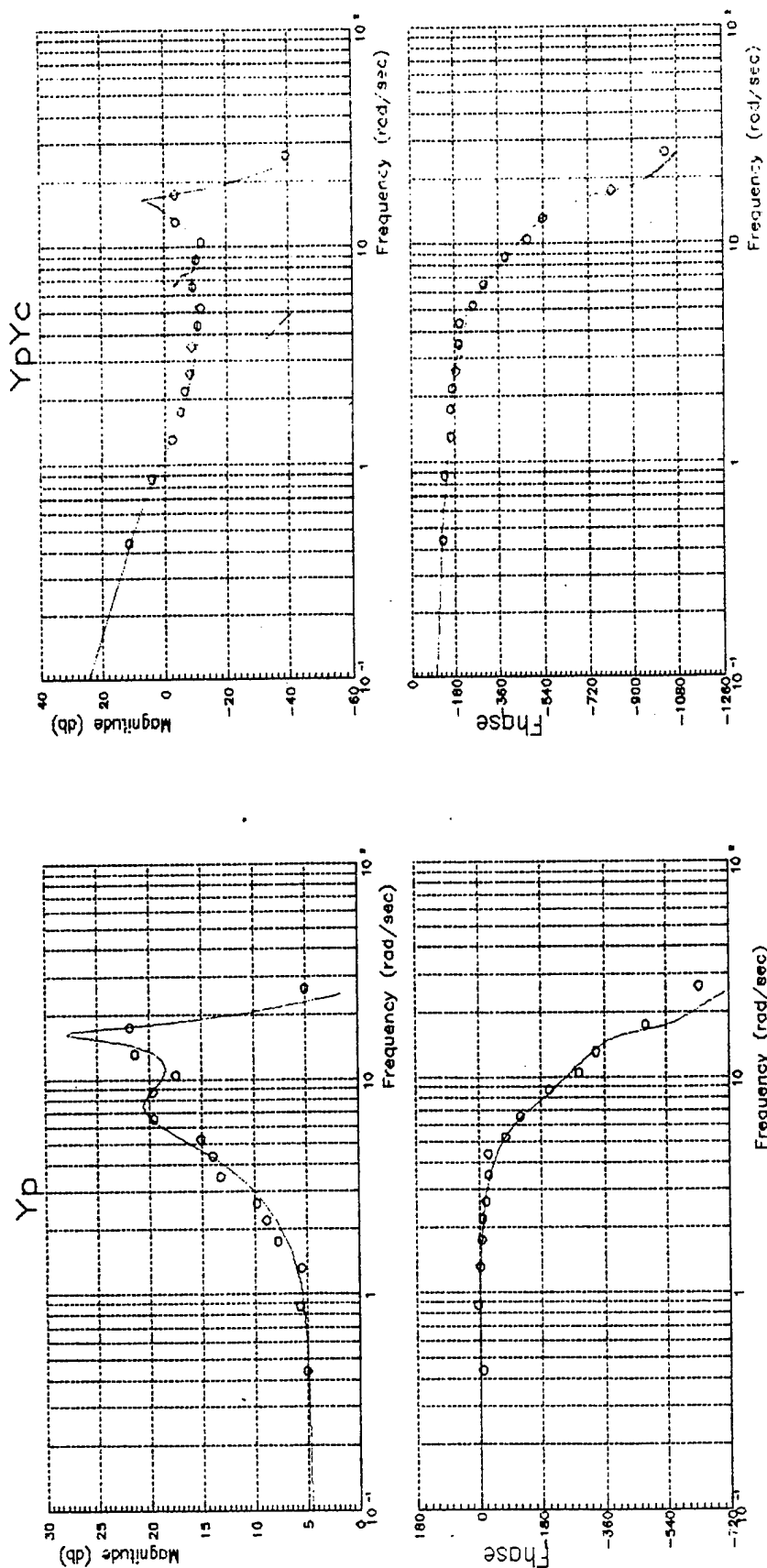


Fig.3.22. Pilot/Pilot-Aircraft describing function
(elastic aircraft, equations (3.1)).

It has been mentioned in the publications that parameters T_1, T_2, ξ_1, ξ_2 depend on a manipulator type and its feel system characteristics. They can be $T_{1,2} = 0.05 - 0.15 \text{ sec}$, $\xi_{1,2} = 0.05 - 1.0$.

In our experiments these parameter magnitudes were $T_1 = 0.12 \text{ sec}$, $\xi_1 = 0.2 \text{ sec}$, $T_2 = 0.055 \text{ sec}$, $\xi_2 = 0.1$. However, these parameters adjustment rules determined by a manipulator type and feel system characteristics have not been developed yet. This hampers an application of mathematical models of a pilot-aircraft system for high-frequency PIO analysis. These rules are also necessary for describing limb-manipulator system dynamics while developing controllability criteria and analyzing low-frequency PIO. Further studies to develop such adjustment rules should be carried out.

The pilot mathematical model considered here disregards pilot-felt lateral accelerations. Therefore, influence of these accelerations on low and high-frequency PIO should be studied in greater detail.

CONCLUSIONS

1. The technique of PIO experimental studies has been improved while modeling compensatory tracking task on a ground-based simulator.

It has been proved that ground-based PIO studies should be conducted on a moving-base simulator, since motion cues felt by a pilot can influence a PIO tendency greatly (in some cases the tendency is mitigated, in others it is intensified).

The technique has been improved to define, from experiments directly, a common pilot describing function and, at the same time, dynamic performance of closed loop limb-manipulator system. The technique suggests the use of two uncorrelated disturbance functions: one of them is the visual disturbance function, and the other is the manipulator force disturbance function generated in a feel system.

2. Main regularities of a feel system and control sensitivity characteristics effect on PIO have been revealed.

It has been shown that a decrease of command-response gradients and force gradient in comparison with their optimum values leads to PIO tendency intensification. Greater values of breakout forces at low values of force gradients mitigate PIO tendency.

As control sensitivity increases pilot gain adaptability to aircraft gain variation is upset. First, the pilot-aircraft model cut-off frequency becomes somewhat higher. Second, at the frequencies exceeding the cut-off value, pilot model amplitude ratio curves tend to converge. The amplitudes are practically the same when the frequency is about 0.7-1.0 Hz, in spite of the great difference in aircraft gains. The pilot phase remains about the same for all aircraft gains. This is accounted for by the fact that quite a number of muscle groups with various dynamic responses and displacement limits participate in deflecting a particular manipulator. This pilot peculiarity should be studied in greater detail, as it could form the basis for a mathematical method to evaluate the control sensitivity effect on PIO.

The criterion is proposed for an estimation of manipulator feel system and command sensitivity influence on PIO. The criterion allows a designer, first, to define optimum control sensitivity values for a tracking task for the given feel system characteristics, and, second, to estimate, in terms of PIO tendency, pilot ratings worsening in the case of characteristics deviation from their optimum values.

3. It has been shown that there is a tendency to high frequency oscillations on an unmaneuverable aircraft with certain characteristics of a manipulator, structural elasticity and aircraft dynamics.

High frequency PIO is possible to imitate on a moving-base simulator. According to the pilot the high frequency oscillations felt on ground-based and in-flight simulators are essentially the same.

Aircraft elastic modes affect considerably high frequency oscillations in a pilot-aircraft system. Their mere arising and their intensity depends on the magnitude of the first aircraft elastic mode. Their frequency corresponds to the frequency of the first elastic mode.

High frequency PIO intensity depends on limb-manipulator system characteristics as well; these characteristics are determined by the manipulator type and its feel system parameters. High frequency PIO appeared in the experiments with both central and side control sticks. High frequency PIO tendency depends on the direction of forces applied. This skewness, in its turn, depends on the manipulator type. In the case of a central stick the tendency is greater in the right direction, in the case of a side stick it is greater in the left direction.

Aircraft command-response gradients influence high frequency oscillations caused by structural elasticity to a considerable extent. As aircraft gain increases and pilot adaptability gets upset, a resonant peak in an open loop pilot-aircraft system is higher and, therefore, a PIO tendency is intensified.

Roll and lateral accelerations felt by a pilot play an important role in high frequency oscillations phenomenon. High frequency oscillations were observed only on the simulator with a moving base.

Causes of high frequency PIO and ways of its precluding can be adequately studied by means of analyzing pilot-aircraft model describing functions.

REFERENCES

1. Bjorkman, E. A., Silverthorn, J. T., Calico, R. A. Flight Test Evaluation of Techniques to Predict Longitudinal Pilot Induced Oscillations. - AIAA Guidance, Navigation and Control Conference, 1986. A Collection of Technical Papers, p.967-975.
2. Newell, F. D. and Wasserman, R. In-Flight Investigation of Pitch Acceleration and Normal Acceleration Bobweights. AFFDL-TR-69-3, April 1969.
3. McKay, K.. Summary of an AGARD Workshop on Pilot Induced Oscillation. AIAA - 1994.
4. Neal, T. R. and Smith, R. E. An In-Flight Investigation to Develop System Design Criteria for Fighter Airplanes. - AFFDL-TR-70-74, vol.1.
5. Smith, R. H. A Theory for Longitudinal Short Period Pilot Induced Oscillations. - AFFDL-TR-77-57.
6. Hodgkinson, J., Wood, J. R., Hoh, R. H. An Alternative Method of Specifying Bandwidth for Flying Qualities. - AIAA Paper No 82-1609.
7. Gibson, J. C. Piloted Handling Qualities Design Criteria For High Order Flight Control Systems. - AGARD-CP-333, 1982.
8. Johnston, D. E. and McRuer, D. T. Investigation of Interactions Between Limb-Manipulator Dynamics and Effective Vehicle Roll Control Characteristics in Roll Tracking. NASA CR-3983, 1986.
9. Johnston, D. E. and McRuer, D. T. Investigation of Limb-Sidestick Dynamic Interaction with Roll Control. - AIAA Paper No 85-1853.
10. Ónðíé÷éáíñòù, è óíðááēýáííñòù ñàííēáðíâ íà ðáæèlàð áçēáðà è ííñááēē. Éááēí Ì. À. Íáçíð íí làðáðēàēàì èííñòðáíííé íá÷àðē. ÍÍÒÈ ÒÁÆÈ, 1990ã.
11. Áþøááíñ, Á. Ñ., Ñòóáíáâ, Ð. Á. Àýðíāēíàìēēà ñàííēáðà. Àēíàìēēà íðíāíēüííāí è áíēíāíāí āāēæáíēý. Ì.: làøéííñòðíāíēà, 1979, 352 ñ.
12. Áóñüēíâ, Þ. Í., Çàāàéííâ, Á. È. Óíðááēáíēà ííēáðíí ñàííēáðíâ. Ì.: làøéííñòðíāíēà, 1980, 215 ñ.
13. Áððáííâ, À. Á., Íāēíáēēí, À. Á., Íðááðá÷áíñēēé À. Í., Ðíâ÷áíēí Á. Á. Éáð÷ēē, èàē æēíàìē÷āñēāý ñēñðàìà. Ì.: làøéííñòðíāíēà, 1992, 336 ñ.
14. Íāðááàðíâ, Á. Ñ. Íñíāáíííñòē óíðááēáíēý ñíāðáíáííùí íāíāíāððáííùí ñàííēáðíí íí èóðñó. ÅÈÈÈ 1DD0905, 1983.

15. Fedotov, I. I., Tarasov, A. .Z., Tatarnikov, K. A. Aircraft Handling Qualities Research and Criteria Development for Nonstationary/Nonlinear Situations. Final report on US Air Force sponsored research contract #SPC-94-4002.
16. Dubov, Yu. B., Zaichik, L. E., Yashin, Yu. P. The Investigation of Conditions Causing Pilot-Induced Oscillation in the Longitudinal Motion. Aircraft Flight Safety Conference, Zhukovsky, Russia, Aug. 31- Sept. 5, 1993.
17. Johnston, D. E. and Aponso, B. L.. Design Considerations of Manipulator and Feel Systems Characteristics on Roll Tracking. NASA CR-4111, 1988.
18. Watson, D. C. and Schroeder, J. A. Effects of Stick Dynamics on Helicopter Flying Qualities. AIAA-90-3477-CP, presented at the AIAA Guidance, Navigation and Control Conference, Portland, OR, Aug.1990.
19. Morgan, J. M. An Initial Study Into the Influence of Control Stick Characteristics on the Handling Qualities of a Fly-By-Wire Helicopter. AGARD Flight Mechanics Panel Symposium on Flying Qualities, Quebec City, Canada, Oct.1990.
20. Hess, R. A. Analyzing Manipulator and Feel-System Effects in Aircraft Flight Control. IEEE Transactions on Systems, Man, and Cybernetics. Vol.20, No.4, July/Aug.1990, pp.923-931.
21. Smith, Rodger R. Effects of FCS Dynamics on Fighter Approach and Landing Longitudinal Flying Qualities. AFFDL-TR-78-122, vol.1.
22. Rodchenko, V. V., Zaichik, L. E., Yashin, Yu. P., Perebatov, V. S., Lyasnikov, V. V. Investigation of Controllability Criteria of Unmaneuverable Aircraft Equipped with a Side Stick. Final report on US Air Force sponsored research contract #SPC-93-4046.

SECTION 3

IN-FLIGHT INVESTIGATION OF LARGE AIRCRAFT PILOT INDUCED OSCILLATION TENDENCY AND ITS CRITERIA DEVELOPMENT

**Sergey Boris, PhD
Maxim Grigoriev, PhD
V. Rogozin, PhD
V. Tchantchikov, PhD**

**GROMOV FLIGHT RESEARCH INSTITUTE
ZHUKOVSKY, RUSSIA**

CONTENTS

	Page
LIST OF FIGURES	223
ABBREVIATIONS	226
1.0 INTRODUCTION	227
1.1 BACKGROUND	227
1.2 PURPOSE	228
1.3 SEQUENCE OF ACTIONS	228
2.0 BRIEF REVIEW OF EXISTING PIO TENDENCY CRITERIA AND SELECTION OF A FEW ONES FOR FLIGHT RESEARCH	228
2.1 R. SMITH'S CRITERION	229
2.2 G. GIBSON'S CRITERION	229
2.3 BANDWIDTH CRITERION	232
2.4 "PILOT-IN-THE-LOOP" TECHNIQUE	234
3.0 SELECTION OF DYNAMIC CONFIGURATIONS PRONE TO PIO	240
3.1 SELECTION OF DYNAMIC CONFIGURATIONS	240
3.2 IMPLEMENTATION OF DYNAMIC CONFIGURATIONS IN THE MATH MODEL OF TU-154M IFS	243
4.0 DEVELOPMENT OF THE SOFTWARE FOR PIO GROUND-BASED AND IN-FLIGHT INVESTIGATION	245
4.1 SOFTWARE FOR MATH SIMULATION OF TU-154M IN-FLIGHT SIMULATOR	245
4.2 SOFTWARE FOR FREQUENCY RESPONSE ANALYSIS USING EXPERIMENTAL DATA	245
5.0 PRE-FLIGHT GROUND-BASED SIMULATION	246

5.1 SIMULATION IN MAI'S GROUND STATION	246
5.2 SIMULATION IN TSAGI'S FULL FLIGHT SIMULATOR	247
5.3 BASIC PRINCIPLES OF FLIGHT METHODS	247
5.3.1 PIO Provoking Technique	247
5.3.1.1 Display Format Symbology for Tracking Task	247
5.3.1.2 Command Signal Excitation Signal	250
5.3.2 Dynamic Configuration Characteristics	251
5.3.2.1 Longitudinal Short Term Dynamic Characteristics	251
5.3.2.2 Longitudinal Long Term Dynamic Characteristics	252
5.3.2.3 Lateral-Directional Dynamic Characteristics	257
5.3.2.4 Longitudinal and Lateral Dynamic Characteristics Coupling	257
5.3.2.5 Type of Hand Controller and Its Feel Characteristics	258
5.3.3 Power Actuator Dynamic Characteristics. The Saturation Influence on PIO Tendency	258
5.3.4 Influence of Pilot Station Location	260
6.0 FLIGHT INVESTIGATIONS IN THE TU-164M IN-FLIGHT SIMULATOR	260
6.1 DESCRIPTION OF TU-154M IN-FLIGHT SIMULATOR	260
6.2 FLIGHT METHODS. ENTIRE FLIGHT EVALUATION PROCEDURE	263
6.3 RESULTS OF FLIGHT INVESTIGATIONS	267
6.3.1 General Remarks and Pilot Assessment	267
6.3.2 R. Smith's Criterion	273
6.3.3 G. Gibson's Criterion	281

6.3.4	Bandwidth Criterion	284
6.3.5	"Pilot-In-The-Loop" Technique	286
CONCLUSIONS		292
REFERENCES		293

LIST OF FIGURES

	Page
Figure 2.1 ω_c Determination	230
Figure 2.2a,b Attitude Boundaries for Gibson's Criteria	231
Figure 2.2c,d Gibson's Parameters	233
Figure 2.3 Bandwidth Criteria	235
Figure 2.4 Pilot-in-the-Loop Technique	236
Figure 2.5 PIO Rating Scale 1	237
Figure 2.6 PIO Rating Scale 2	238
Figure 2.7 PIO Rating Scale 3	239
Figure 3.1 Short Period Parameters of Selected Configurations	241
Figure 3.2 Block Diagram of IFS Flight Control Law	244
Figure 5.1 HUD Format	249
Figure 5.2 Time History of Command Pitch Angle Signal	252
Figure 5.3a Comparison of Math Model and Full Flight Simulator Results Configuration I	253
Figure 5.3b Comparison of Math Model and Full Flight Simulator Results Configuration II	254
Figure 5.3c Comparison of Math Model and Full Flight Simulator Results Configuration III	255
Figure 5.3d Comparison of Math Model and Full Flight Simulator Results Configuration IV	256
Figure 5.4 Time History of $\dot{\delta}_e$ required During Target Tracking Task in FFS	259
Figure 6.1 General View of Tu-154M In-Flight Simulator	261

Figure 6.2 Tu-154M IFS Cockpit Layout	263
Figure 6.3 Evaluation Pilot Seat	264
Figure 6.4 Block Diagram of the Tupolev-154M IFS Experimental Flight Control System.....	265
Figure 6.5a Comparison of Full Flight Simulator Results and Tu-154M IFS Flight Configuration I	268
Figure 6.5b Comparison of Full Flight Simulator Results and Tu-154M IFS Flight Configuration II	269
Figure 6.5c Comparison of Full Flight Simulator Results and Tu-154M IFS Flight Configuration II	270
Figure 6.5d Comparison of Full Flight Simulator Results and Tu-154M IFS Flight Configuration IV	271
Figure 6.6 Time History of $\dot{\delta}_e$ Required During Target Tracking Task in Tu-154M IFS	272
Figure 6.7 Example of Sweep Execution	274
Figure 6.8 Example of Target Tracking Task	275
Figure 6.9a Example of Average Slope Determination (Configuration III) ...	277
Figure 6.9b Normalized Stick Force Spectrums	278
Figure 6.9c Normalized Stick Force Spectrums	279
Figure 6.9d Example of Parameter Determination (Configuration III)	280
Figure 6.10a,b Attitude Boundaries Results	282
Figure 6.10c,d Gibson's Criteria Results	283
Figure 6.11a Example of Bandwidth Criterion Parameters Determination (Configuration III)	285
Figure 6.11b Bandwidth Criteria Results	287
Figure 6.12a Comparison of Full Flight Simulator Results and Tu-154 IFS Flight Configuration I	288

Figure 6.12b	Comparison of Full Flight Simulator Results and Tu-154 IFS Flight Configuration II	289
Figure 6.12c	Comparison of Full Flight Simulator Results and Tu-154 IFS Flight Configuration III	290
Figure 6.12d	Comparison of Full Flight Simulator Results and Tu-154 IFS Flight Configuration IV	291

ABBREVIATIONS

DOF	- Degree of Freedom
FBW	- Fly-By-Wire
FCS	- Flight Control System
FRI	- (Gromov) Flight Research Institute
FFS	- Full Flight Simulator
FPV	- Flight-Path Vector
HDD	- Head-Down Display
HUD -	- Head-Up Display
IFS	- In-Flight Simulator
ILS	- Instrument Landing System
LAHOS	- Landing Approach of High Order System
MAI	- Moscow Aviation Institute
PFD	- Primary Flight Display
PIO	- Pilot Induced Oscillations
PR	- Pilot Rating
TsAGI	- Central Aero-Hydrodynamic Institute
VSS	- Variable Stability System

1. INTRODUCTION

1. 1 BACKGROUND

The Pilot Induced Oscillations (PIO) is an effect which has occurred in recent aviation practice rather often. It is a result of an unfavorable combination of airframe dynamics and flight control system (FCS) parameters emerged during high gain tracking flight task. PIO may be encountered both by fighters and transports especially by heavy transports with great mass and high inertia. For the latter type of aircraft countered on a great number of passengers, the PIO could become the problem of flight safety. That is why the present stage of PIO investigation will be the first one directed after all to the investigation of this effect for the large transports.

Modern aircraft encounters PIO in both longitudinal and lateral channels and may be coupled longitudinal-lateral PIO. As the first step of investigations longitudinal channel was chosen.

The latest versions of specifications contain various techniques for the PIO prediction but they provide no guidance in the area of precluding PIO tendency during flight control system (FCS) design stage. All techniques for PIO prediction have certain deficiencies; some of them are difficult in practical use, the other ones work well only for limited number of aircraft dynamic configurations. Almost all of them were developed for fighter type aircraft and all of them have no sufficient in-flight validation.

Meanwhile the PIO is known to be a phenomenon which is very difficult to truthfully reproduce in ground conditions. So any kind of PIO research should be checked and validated in actual flight conditions. For this purpose the In-Flight Simulator (IFS) with variable-in-flight dynamics and FCS parameters is a unique instrument. It allows us to combine all factors contributing to PIO as appropriate airframe nonlinear dynamics, FCS delays and peculiarities, pilot cues and anxiety etc.

This report proposes the initial experimental data on PIO obtained in Gromov Flight Research Institute using the Tu-154M IFS with variable-in-flight dynamic characteristics. The research program included the preflight investigation and preparation stage and the flight program. Because of the reasons beyond control only four flights were performed for the time being. Three test pilots of FRI participated in the program which comprised the flight evaluation of four dynamic configurations of transport aircraft against a few PIO criteria.

1. 2 PURPOSE

The IFS flight research, evaluation and validation of criteria predicting the PIO tendency and severity for transport aircraft.

1.3 SEQUENCE OF ACTIONS

In the frame of the preparation to experimental flights the sequence of the following actions was undertaken:

- review of existing PIO tendency criteria and selection of a few ones for further evaluation,
- selection of aircraft dynamic configurations prone to PIO,
- reproducing of dynamic configurations on the basis of math model of variable-in-flight dynamics IFS,
- assessment of the IFS dynamic configurations and method provoking PIO on the real time simulation station,
- development of the experimental flight method on PIO research I on the Full Flight Simulator (FFS) reproducing the IFS dynamic configurations.

The detailed description of both preflight research actions and experimental flight procedure and results is presented below.

2. BRIEF REVIEW OF EXISTING PIO TENDENCY CRITERIA AND SELECTION OF A FEW ONES FOR FLIGHT RESEARCH

In this work four PIO prediction techniques were selected for in-flight validation of their applicability for large aircraft. Three of them are simple in practical use and do not require pilot model identification from flight data. They are:

- a) Ralph Smith's longitudinal axis PIO prediction technique [1],
- b) J. C. Gibson's flying qualities prediction technique [2, 3],
- c) Hoh's bandwidth criterion [4],
- d) Also one "pilot-in-the-loop" technique developed by R. A. Hess and R. M. Kalteis [5] was chosen.

The explanation is that on one hand, the criteria selected showed the upward trend towards the experimental results and assumed the usage of parameters easily obtained from actual flight (may be except the last criterion which needs to obtain the "pilot-aircraft" frequency response from real experiment data). On the other hand, these criteria are all based on an entirely different premise from the physical point of view. Thus the further flight research is warranted to determine the real reasons of PIO.

2.1 R. SMITH'S CRITERION

Mr. Smith proposes a set of requirements for short-term longitudinal response (Fig. 2.1). His parameters include:

$$\Phi(i\omega_c) = -\frac{a_{z_p}}{F_s} (i\omega_c) - 14.3^* i\omega_c,$$

where: a_{z_p} - is normal acceleration at pilot station,

ω_c - criterion frequency, rad/s, approximately the crossover frequency of the pilot-aircraft system dynamics for pitch attitude tracking
- a function of aircraft dynamics and disturbance bandwidth:

$$\omega_c = 6.27 - 0.27 \frac{d|\theta / F_s(i\omega)|}{d\omega},$$

where: $\frac{d|\theta / F_s(i\omega)|}{d\omega}$ is determined by a first-order fit between 2.0 and 6.0 rad/s

Smith states that when controlling pitch attitude, if closed-loop damping is insufficient, a pilot may switch to normal-acceleration control. In that case phase margin of $n_z(i\omega)/F_s(i\omega)$, evaluated at the $\theta(i\omega)/F_s(i\omega)$ crossover frequency, is an indicator of pilot-induced oscillation tendency. His PIO criteria are:

$$\Phi(i\omega_c) \geq -160^\circ \text{ when } -122^\circ \geq \frac{\theta}{F_s}(i\omega_c) \geq -130^\circ, \text{ for level 1;}$$

$$\Phi(i\omega_c) \geq -220^\circ \text{ when } -148^\circ \geq \frac{\theta}{F_s}(i\omega_c) \geq -165^\circ, \text{ for level 2.}$$

Level 3 floors exist, but data to establish them are lacking.

Note: presented boundaries were established for fighter aircraft, so for large aircraft they may differ.

2.2 G. GIBSON'S CRITERIA

Fig. 2.2a shows optimum aircraft pitch attitude response boundaries for precision control tasks, in which the crossover frequency of 0.3 Hz is inherently assumed. To apply this criterion, the aircraft attitude response to the stick input is plotted so that its open-loop amplitude at 0.3 Hz is 0 dB. The phase difference between this and the 0 dB closed-loop line (upper boundary) represents the allowable pilot phase lag for optimum tracking. If this criterion

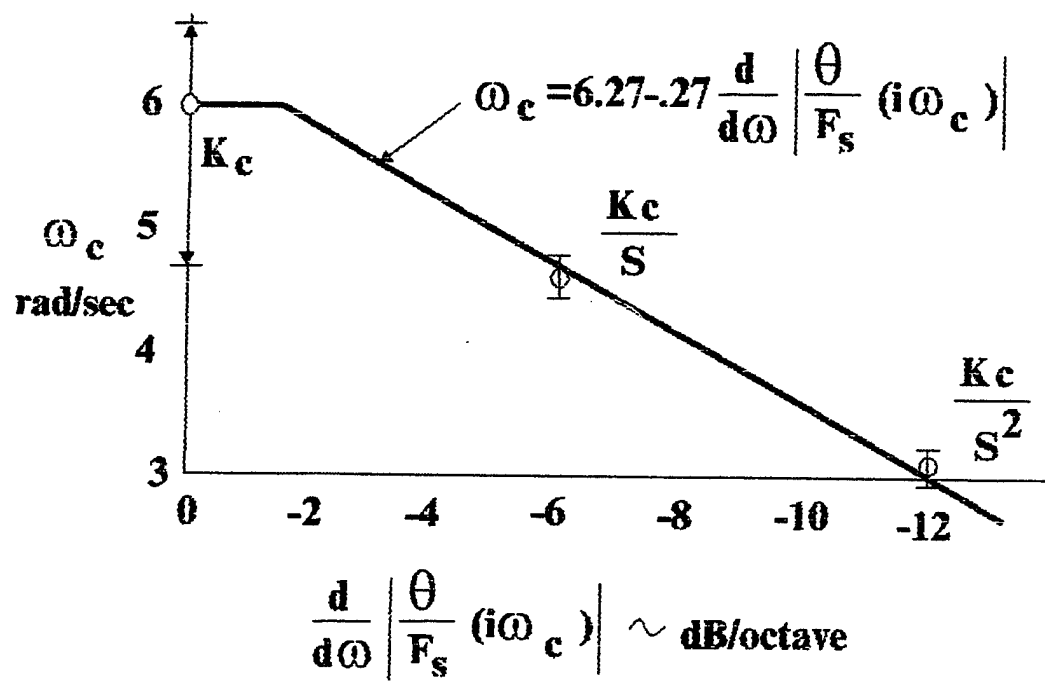
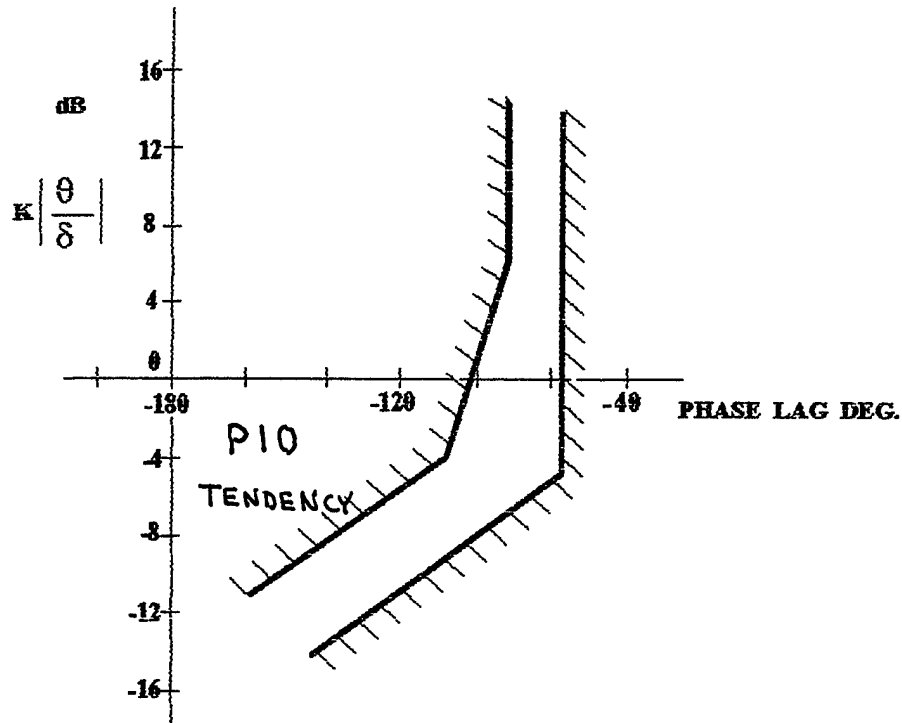


Figure 2.1 ω_c Determination

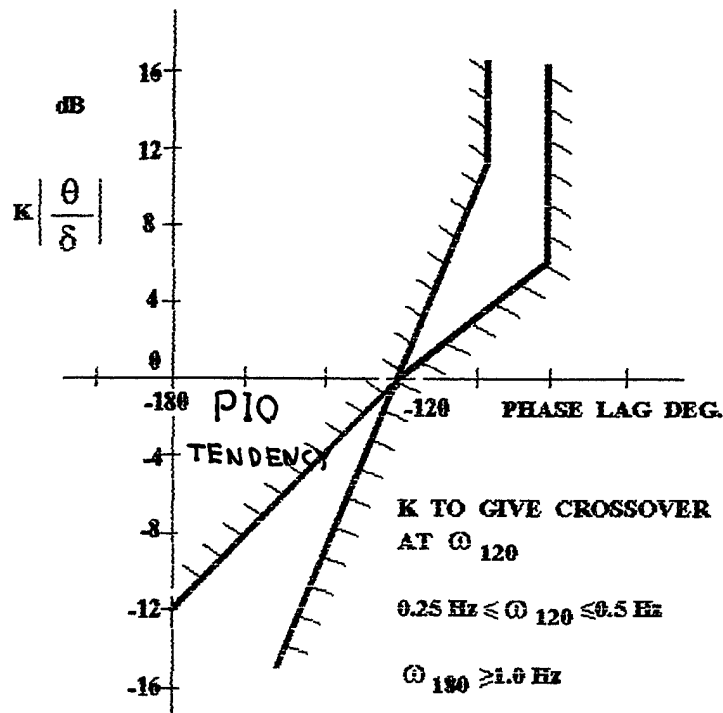
Gibson's Criteria.

UP-AND-AWAY FLIGHT



a) ATTITUDE BOUNDARIES FOR 0.3 Hz CROSSOVER FREQUENCY

LANDING



b) ATTITUDE BOUNDARIES FOR LANDING

Figure 2.2a,b Attitude Boundaries for Gibson's Criteria

is satisfied, all the pilot phase lag can be attributed to his time delay and no further equalization is required from him.

Mr. Gibson also proposed a mechanism for the initiation of landing PIO. The PIO starts when the pilot begins to perceive the attitude oscillation in the stick pumping activity in the flare maneuver. The latter seems to be a subconscious testing of the pitch control by pumping at a frequency where pitch acceleration is nearly in phase with the stick, and at an amplitude of about 6 deg/s^2 . In consequence the attitude oscillation is 180 degrees out of phase with the stick, so that the pilot is already "set up" for a PIO if he consciously detects it. Fig. 2.2c shows an open-loop criterion. However, a further factor is that no PIO can occur if the response amplitude at 180 degrees phase lag is so low that even stop-to-stop stick inputs generate only a small oscillation e.g. 2 or 3 degrees attitude.

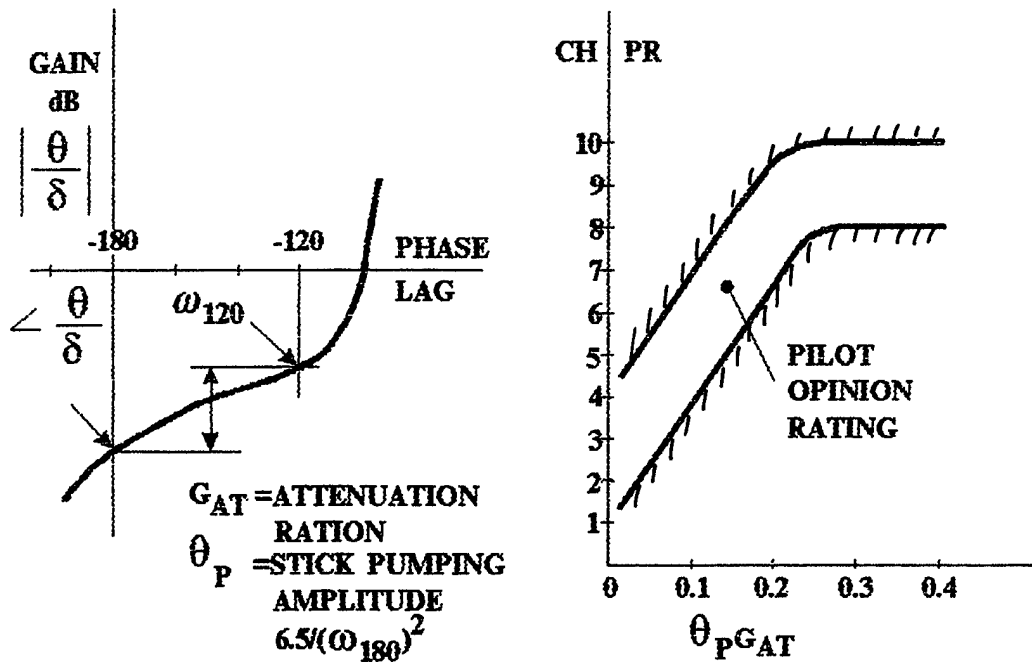
The boundaries shown in Fig 2.2b divide the response regions into two at a bandwidth limit set by the frequency at which phase lag is 120 degrees. Above this frequency, the PIO tendency at touchdown is determined as in Fig. 2.2c, and responses satisfying the boundaries automatically achieve low PIO criterion values. Below the bandwidth frequency the responses useful for flight path control are defined. The satisfactory range of bandwidth limit frequencies lies between 0.25 and 0.5 Hz.

The other parameter characterizing the PIO has proved to be the phase rate at which the pitch attitude phase lag increases with frequency in the PIO lag crossover region, equally applicable to the landing or to target tracking task. By the nature of the attitude frequency response, if the frequency is low and the attitude attenuates only slowly towards the cross over region of the phase rate is large. If the phase frequency is high and there is substantial attenuation, the phase rate is low. The gain margin is increased, the stick pumping amplitude is reduced and the tendency to PIO is decreased automatically by designing a low phase rate into the control laws. This simple attitude parameter alone is almost sufficient to quantify the tendency to high order PIO, Fig 2.2d.

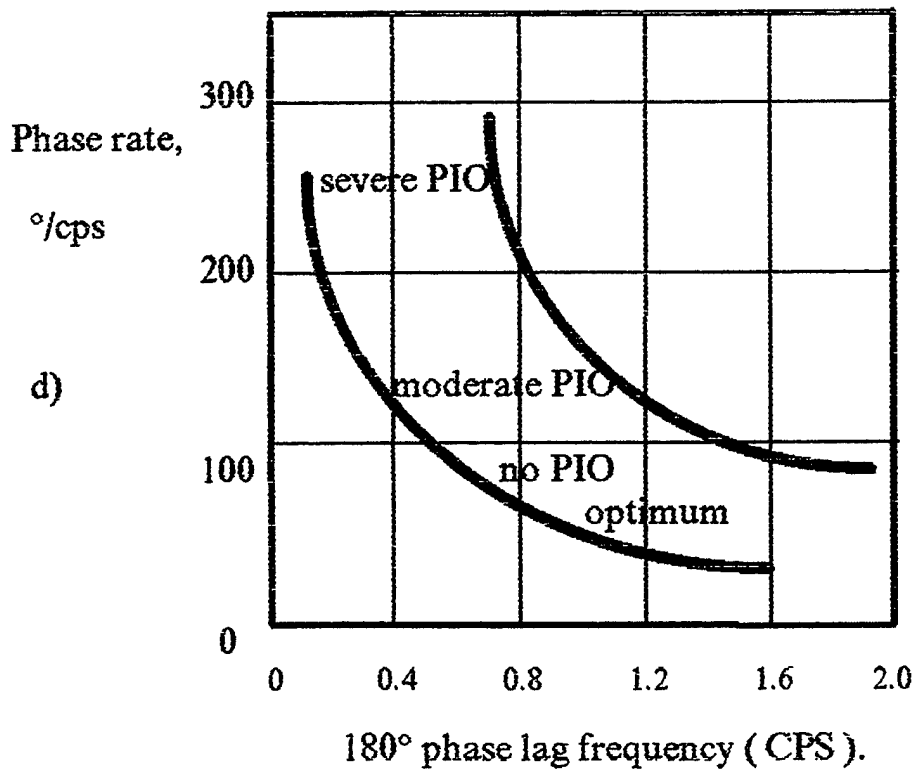
2.3 BANDWIDTH CRITERION

The criterion is based on an idea that bandwidth ω_{Bw} is a key measure of the quality of an airplane's handling characteristics in a tight tracking situation. The bandwidth is the frequency at which the phase margin is 45 degrees (ω_ϕ) or the gain margin is 6 dB (ω_G), whichever frequency is lower. Handling qualities depend not only on the value of bandwidth ω_{Bw} but also on the shape of the phase curve at frequencies above ω_{Bw} . Rolloffs in phase are well represented by the following parameter [6]:

Gibson's Criteria.



C) LANDING PIO CRITERION.



d) Trends of phase rate of "FCS-aircraft" system.

Figure 2.2c,d Gibson's Parameters

$$\tau_P \geq - \frac{\Phi_2 \omega_{180} + 180^\circ}{57.3 \cdot 2 \omega_{180}}$$

These two factors (ω_{BW} and τ_P), define handling qualities, see Fig. 2.3.

2.4 "PILOT-IN-THE LOOP" TECHNIQUE

The "Pilot-in-the-loop" technique proposed by R. A. Hess and R. M. Kalteis states:

- 1) crossover frequency of "pilot-aircraft" open-loop $|Y_p Y_c(i\omega)|$ must be more than 1.5 - 2 rad/s;
- 2) slope of $|Y_p Y_c(i\omega)|$ must be no less than - 20 dB/decade for at least one half decade below the minimum crossover frequency. Below this frequency, flat amplitude characteristics would be acceptable. Fig. 2.4 shows the resulting frequency domain boundary.

During this work three PIO rating scales (Fig. 2.5, 2.6, 2.7) were evaluated [7, 8, 9]. These scales will be mentioned as Scale 1, 2, and 3 correspondingly.

This review exposed the problem concerning the PIO research and explains the forthcoming weight placed on these problems, so we can conclude the following:

- a) The amount of real flight data is insufficient to validate of existing and for developing of a new criteria;
- b) Most of the criteria concerns only highly maneuverable aircraft and don't cover the requirements for transport aircraft;
- c) Criteria are based mostly on the representative parameters of the amplitude and phase frequency responses of "FCS-aircraft" and "pilot-FCS-aircraft" systems,
- d) Most of the criteria indicates only probability of PIO occurrence but don't predict severity of PIO to be encountered.

Analysis performed made it possible to draw the following conclusions forming the basis of PIO research suggested:

Item a) confirms the importance of special in-flight investigations on PIO problem in spite of the previous investigations.

According to item b) it is necessary to check in flight applicability of PIO criteria to large transport aircraft.

According to item c) special flight test regimes, which permit "pilot-FCS-aircraft" frequency response determination were proposed for ground based and in-flight investigations.

As for item d) our opinion is that PIO criteria should predict pilot ratings of aircraft PIO tendencies according to some PIO - rating scale. So it is necessary to validate the existent PIO rating scales or (in case of unsatisfactory results) develop a new one based on the extensive statistical flight data.

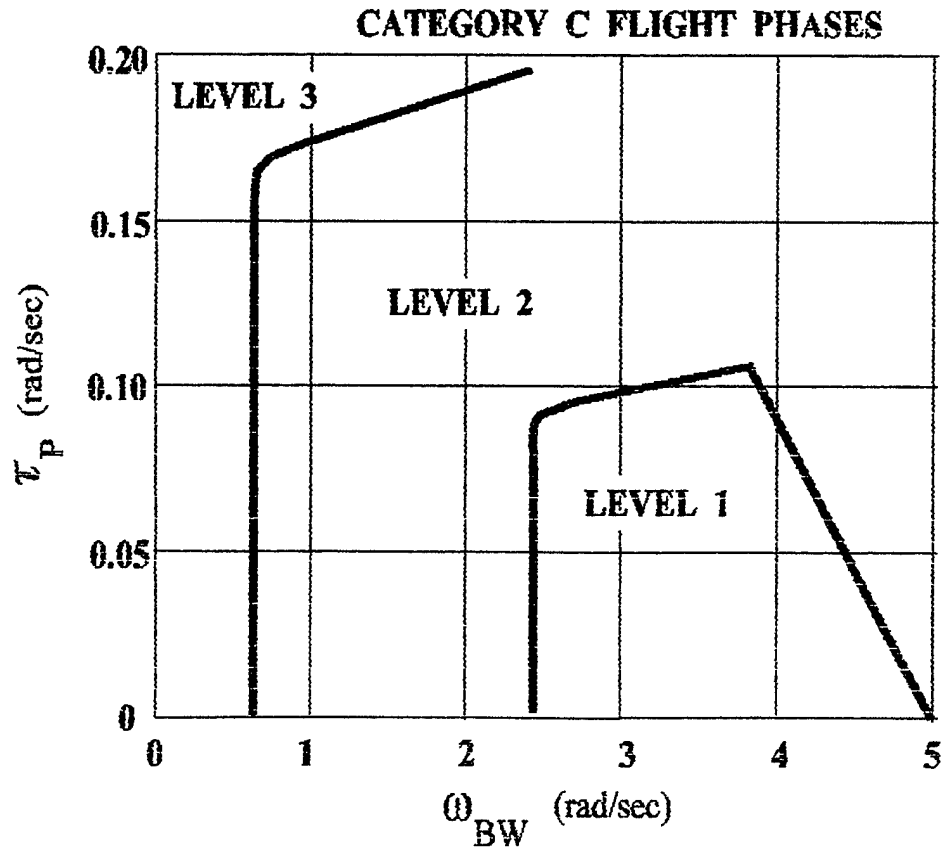
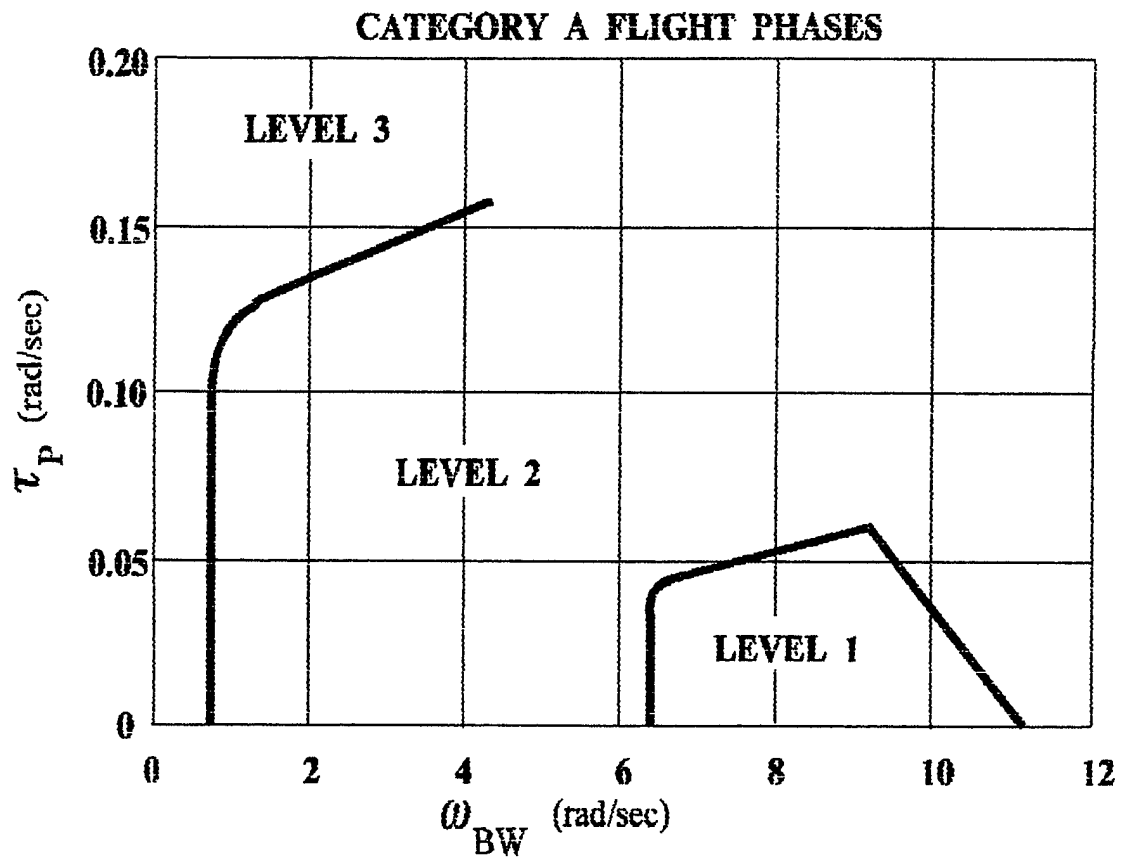


Figure 2.3 Bandwidth Criteria

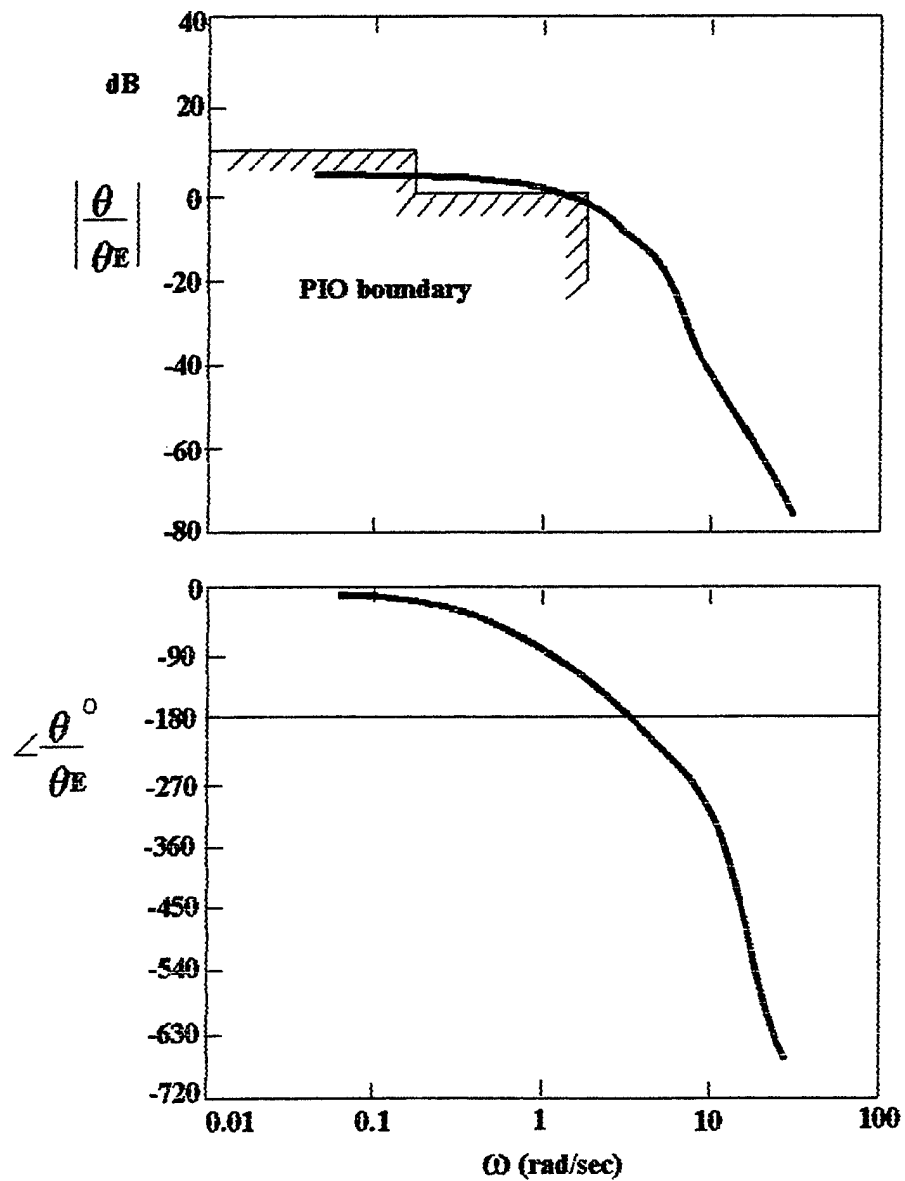


Figure 2.4 Pilot-in-the-Loop Technique

DESCRIPTION	Numerical rating
No tendency for pilot to induce undesirable motions	1
Undesirable motions tend to occur when pilot initiates abrupt maneuvers or attempts tight control. These motions can be prevented or eliminated by pilot technique.	2
Undesirable motions easily induced when pilot initiates abrupt maneuvers or attempts tight control. These motions can be prevented or eliminated but only at sacrifice to task performance or through considerable pilot attention and effort.	3
Oscillations tend to develop when pilot initiates abrupt maneuvers or attempts tight control. Pilot must reduce gain or abandon task to recover.	4
Divergent oscillations tend to develop when pilot initiates abrupt maneuvers or attempts tight control. Pilot must open loop by releasing or freezing the stick.	5
Disturbance or normal pilot control may cause divergent oscillation. Pilot must open control loop by releasing or freezing the stick.	6

Figure 2.5 PIO Rating Scale 1

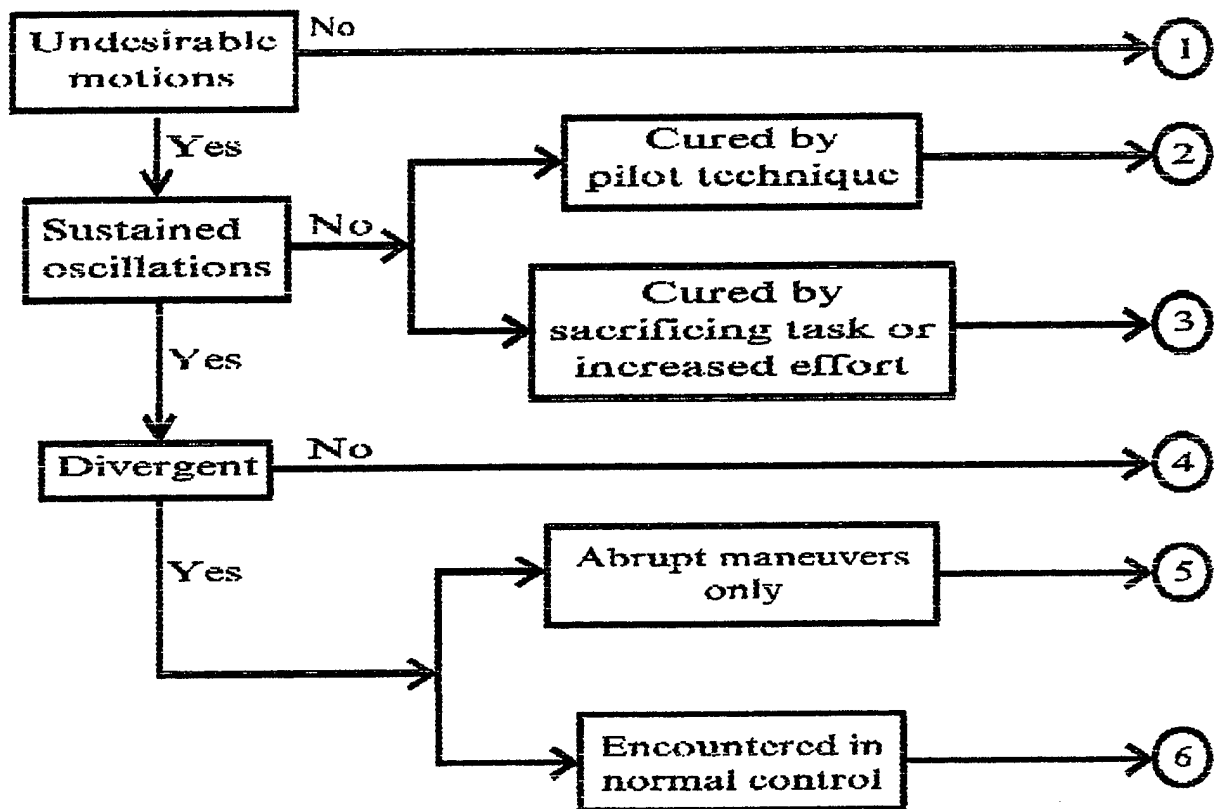


Figure 2.6 PIO Rating Scale 2

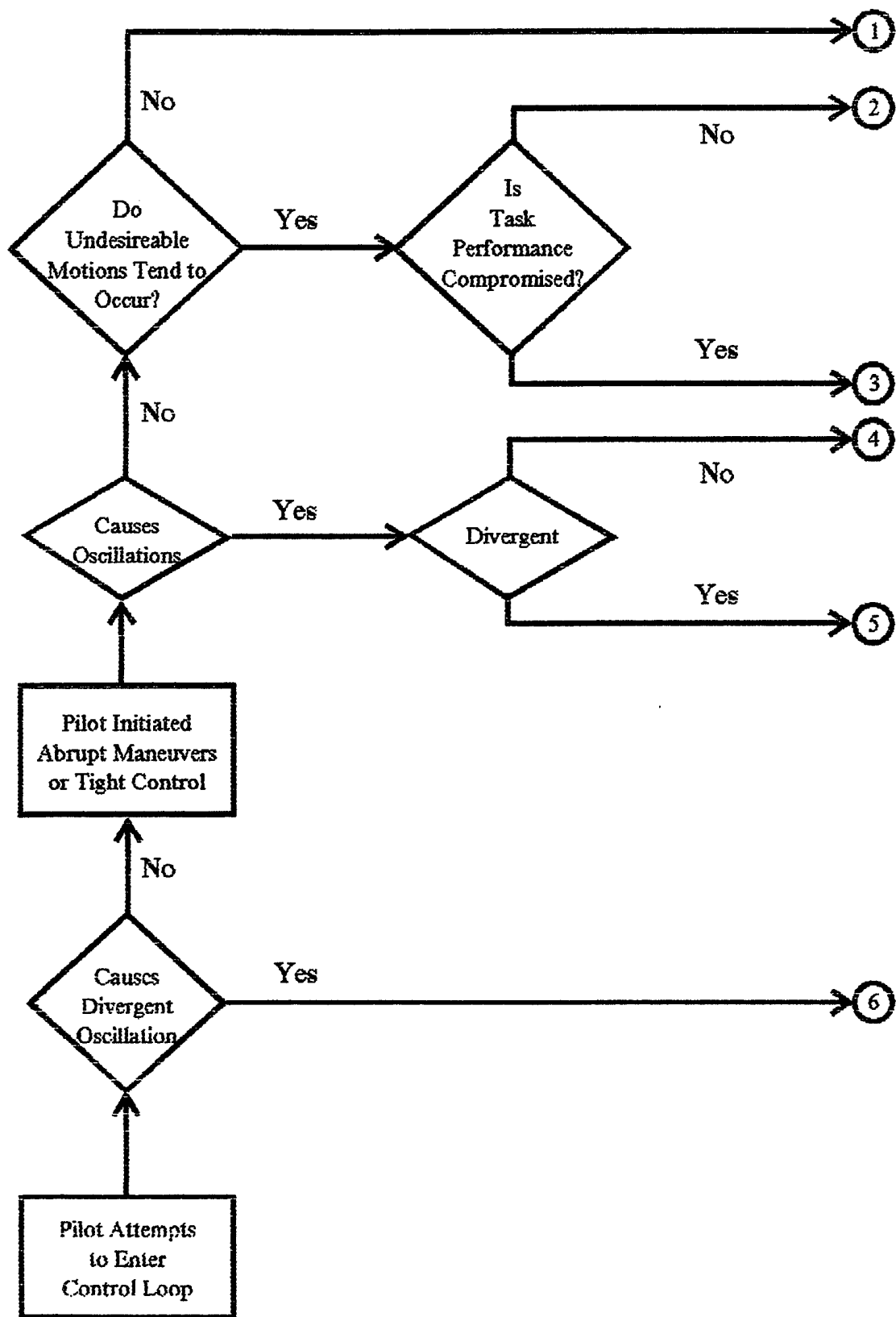


Figure 2.7 PIO Rating Scale 3

3. SELECTION OF DYNAMIC CONFIGURATIONS PRONE TO PIO

3.1 SELECTION OF DYNAMIC CONFIGURATIONS

As for selection of dynamic configurations prone to PIO, it is important to note some practical moments. From the very beginning it was assumed that the main restriction imposed on the project may be the number of experimental flights. Under these conditions it was necessary to limit the number of dynamic configurations being selected for the flight assessment. But to guarantee the reliability of future flight results these configurations selected had to satisfy the following requirements:

- they had to be the most prone to PIO (compared to other possible configurations),
- their proness had to be already checked and validated in actual flight,
- these limited number of configurations had to cover the possible wide spectrum of different types of frequency characteristics of various dynamic configurations prone to PIO.

As a starting point, the LAHOS [7] data base was used as the only one that was recently proposed with the most comprehensive results (although for the approach and landing regimes only). Three of the total 49 LAHOS'es configurations were selected as those covering the different aircraft dynamics (Fig. 3.1). Using the LAHOS'es numbering they are configurations 1-4, 2-10 and 4-10, which pitch rate to pilot control input transfer functions could be described in the form

$$\frac{\theta}{\delta_{ES}} = K_{\theta} \frac{(\tau_{\theta_2} S + 1)}{S \left(\frac{S^2}{\omega_{SP}^2} + \frac{2\zeta_{SP}}{\omega_{SP}} S + 1 \right)}$$

where the short term characteristics which were originally taken from the approach regime are presented in the table.

Category C		$n_z/\alpha = 4.5 \text{ g/rad}$		$\tau_{\theta_2} = 14\text{sec}$	
Parameters	Configurations	1-4	2-10	4-10	
	ζ_{SP}	0.74	0.57	1.06	
	ω_{SP}	1.0	2.3	2.0	

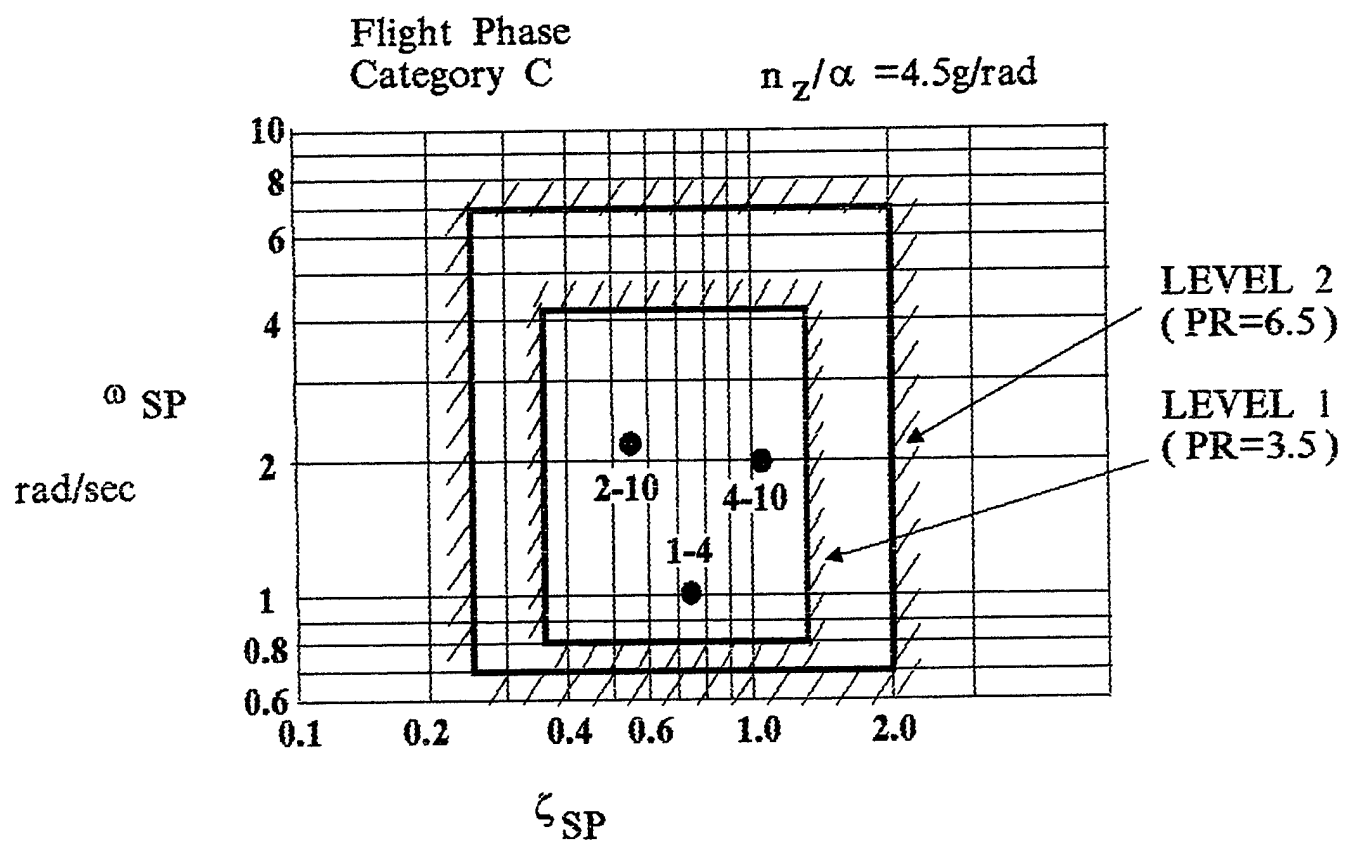


Figure 3.1 Short Period Parameters of Selected Configurations

As in the LAHOS program these configurations were evaluated in combination with the additional control system dynamics described as the appropriate filters:

$$\frac{1}{0.5 \cdot S + 1} \quad - \text{ for configuration 1-4,}$$

$$\frac{16}{S^2 + 2 \cdot 0.7 \cdot 4 \cdot S + 16} \quad - \text{ for configurations 2-10, 4-10.}$$

Note that all of configurations selected were evaluated by the pilots as those being very prone to PIO.

To make these configurations closer to the characteristics of large transport with highly augmented digital FCS additionally the rather large time delay of $\tau_d = 0.25$ sec was implemented in the loop. These time delays occur in the closed control loop due to digital control law implementation, the existence of phase lags associated with high-order control system dynamics and digital PFD symbology generation dynamics. The range of time delays encompasses values encountered in operational aircraft and were considered reasonable in recent experimental research [10]. Besides the IFS Tu-154M inherent dynamics was considered as the base one for all kinds of comparative evaluations during the ground and flight simulation.

Summarizing the following dynamic configurations with the identification names written below were

Configuration	Identification
modified 1-4	I
modified 2-10	II
modified 4-10	III
base Tu-154M	IV

All these configurations were evaluated in combination with the sidestick to make the possible PIO more strongly marked in the presence of light-force and small-displacement hand controller. The evaluation was also done to research the PIO against this background (unfortunately later during the Full Flight Simulator stage because of the sidestick malfunctions, some configurations were partly evaluated with central stick).

As the initial step, it was planned to research the PIO criteria against the dynamic characteristics of above mentioned configurations.

Note: At the same time the math model of hypothetical Very Large Transport Aircraft of landing weight about 500 t was developed. In general, the dynamics of such type aircraft with highly augmented FCS could be

characterized by high inertia, large equivalent time delay, rather slow response. So as the second step we planned to evaluate a set of PIO criteria against this dynamic configuration. But in the end, it was not unfortunately done because of the flight number restriction.

3.2 IMPLEMENTATION OF DYNAMIC CONFIGURATIONS IN THE MATH MODEL OF Tu-154 IFS

Practical realization of PIO prone configurations for their further implementation onboard the Tu-154M IFS via experimental digital Variable Stability System (VSS) was performed by the following procedure.

To realize the dynamic configurations based on the LAHOS'es ones it was decided to use the most simple feedback response method. The IFS is not currently equipped with any direct lift control device. So the matching of the numerator time constant τ_{θ_2} of the pitch rate to pilot input transfer function θ/Fs was done on the following conditions:

- the average operational flight weight 70 t and center of gravity position 32% MAC were taken for the IFS,
- the indicator airspeed about $V_{IAS} = 450$ km/hour (260.-270 kt) was assigned to provide the safe margin of angle of attack to stall during the IFS maneuvering,
- the height of 4,200 m (14,000 ft) was assigned to finally match the value of τ_{θ_2}

Note: under these flight conditions the Tu-154M aircraft base dynamic short term characteristics are as follows:

$$\zeta_{sp} = 0.64 \quad \omega_{sp} = 1.62 \text{ rad/sec} \quad n_z/\alpha = 13.5 \text{ rad/sec}$$

Then short period frequency ζ_{sp} and damping ω_{sp} of θ/Fs transfer functions were adjusted by means of pitch rate and normal acceleration feedback gains. Concrete values of these feedback gains were calculated initially for pure IFS aerodynamics (without actuator dynamics) for chosen flight conditions. After that the necessary LAHOS'es prefilters were added in the VSS forward path to form in the IFS the configuration prone to PIO.

To take into account the dynamic characteristics of IFS's servo and power actuators, the matching of IFS full math model frequency response to those for LAHOS'es θ/FS transfer functions was finally performed and appropriate compensation lead filter was inserted additionally in the VSS forward path. Thus the VSS control law has the final form shown in Fig. 3.2.

As the actuator rate limit is of particular importance in PIO research and is known to greatly influence the PIO tendency, the preliminary assessment of maximum elevator deflection rate which could be reached in forthcoming

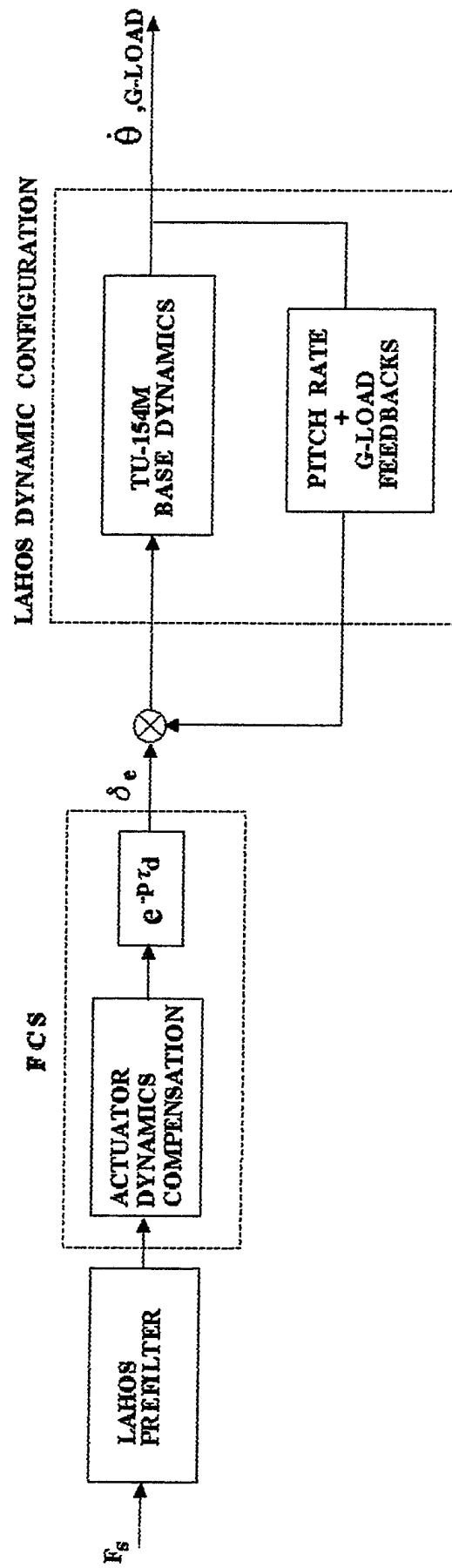


Figure 3.2 Block Diagram of IFS Flight Control Law

flights was done. Therefore, for all cases of dynamic configurations, the IFS expected dynamics was simulated. The sweep excitation pilot control inputs of worthwhile amplitude and frequency were taken from actual flight and injected in the input. The results showed that actuators saturation and control surfaces deflection limits were not encountered.

4. DEVELOPMENT OF THE SOFTWARE FOR GROUND-BASED AND IN-FLIGHT PIO INVESTIGATION

4.1 SOFTWARE FOR MATH SIMULATION OF Tu-154M IN-FLIGHT SIMULATOR

The math model of Tu-154M In-Flight Simulator (IFS) is a full 6 DOF model. Equations for aerodynamic moments and forces, Euler angles and cinematic equations which relate body and earth axis systems are in continuous form and are integrated by 4-th order Runge-Kutt's method. Digital FCS filters and actuators models are realized in difference equation form and integrated by Tustin algorithm. The derivatives of non-dimensional coefficients for aerodynamic forces and moments are second order functions of Mach number, flap deflection and angle of attack. These functions were identified during special identification flight test program. The actuator models include deadzones and control surfaces speed and deflection limitations, also determined from special ground and flight tests.

4.2 SOFTWARE FOR FREQUENCY RESPONSE ANALYSIS USING EXPERIMENTAL DATA

During these ground-based and in-flight investigations, two methods for experimental frequency response determination were used.

The first is based on the classical methods of spectral analysis and the second one is the modified Fourie coefficients method, developed by MAI. The first method presupposes the pilot natural control inputs for "pilot-aircraft" control loop excitation and does not require any special command signal. The only restriction imposed is that the level of excitation shall be of amplitude worthwhile for further quantitative processing and analysis.

The second method requires a special generator for "pilot-aircraft" loop excitation. This generator must provide input signal, which consists of the sum of sinusoids of certain amplitudes and frequencies. Therefore, this pseudorandom input signal has discrete spectrum. MFC method calculates frequency response only for frequencies of these generated sinusoids and can't calculate a frequency response for other frequencies so you can't calculate the frequency response for continuos spectrum of input signal by this method.

This is a drawback, but because of the small number of input sinusoids the modified Fourier coefficients method works faster than the spectral analysis.

5. PRE-FLIGHT GROUND-BASED SIMULATION

Ground-based simulation was considered as a preflight stage dedicated to the development of experimental flight methods which provide both pilot experiment familiarization and training, flight safety and high quality flight data collection. This stage was organized in two steps.

The first step was the real-time simulation in the MAI ground station where the FRI developed software for IFS dynamics real-time simulation was implemented. The was the preliminary pilot's assessment of IFS dynamics, the dynamic configurations prone to PIO justification and the principles of PIO provoking validation.

Then the positive results had to be transferred to TsAGI's 6 DOF Full Flight Simulator for detailed research and development of forthcoming PIO flight research methods as a second step of ground simulation.

5.1 SIMULATION IN MAI's GROUND STATION

MAI's ground station is organized on the basis of commercial PC-computer connected with a right-hand sidestick mounted on the operator's seat. The computer comprises the software for real-time simulation of IFS motion reproducing the PIO prone dynamic configurations. The monitor screen of standard size realizes the simplified format of head-up display symbology. The particular feature of the format is the moveable mark of tracking angle error in the longitudinal channel presented in natural pilot view scale. The pseudorandom signal excited the mark at given flight conditions of level flight. The task of FRI's pilot participating in the simulation was to null out the error centering the mark and trying not to exceed the "permissible" error value (the detailed description of simulation procedure is presented below). During the tracking the pilot inadvertently excited the "pilot-aircraft" closed-loop and entered the PIO.

Preliminary FRI test pilot's comments validated implemented IFS dynamics, general points of experimental procedure, PIO provoking technique and PIO proness of chosen configurations.

5.2 SIMULATION IN TsAGI's FULL FLIGHT SIMULATOR

The main volume of preflight research dedicated to experimental flight technique development was carried out in the TsAGI's Full Flight Simulator (FFS) with participation of FRI engineering staff and test pilots.

The FFS is a 6 DOF moving base simulator with large amplitude (of $\pm 1.2...1.5$ m linear and $\pm 30^\circ...60^\circ$ angular displacement) and high response motion characteristics. The left-hand pilot seat of the two crew member cockpit is equipped with central stick, right-hand sidestick and two PFD's. The implemented software represented the FRI Tu-154M IFS base dynamics and the dynamic configurations selected for in-flight research. Since the FFS was not equipped with a HUD like the Tu-154M IFS, it was decided to use the head-down monitor of one of the PFD's during the experiments.

Three FRI test pilots took part in the simulations. The general organization and all particular moments comprising the flight methods and technique of forthcoming flights were evaluated during the simulations in environmental conditions close to actual flight.

The main results formed the experimental flight methods which are presented in the next subsection.

5.3 BASIC PRINCIPLES OF FLIGHT METHODS

5.3.1 PIO Provoking Technique

The special PIO provoking technique was developed and used both in ground and flight simulation. Application of this technique would help the pilot to subjectively evaluate PIO proneness of particular configuration, would provide experimental data to use some objective methods for PIO tendencies evaluation and would provide the necessary safety level. This technique is similar to the so-called target tracking procedure. The pilot task was to trim the aircraft in level flight and perform tracking in the longitudinal channel as defined by the pitch command bar on the PFD. During a certain time period, the pilot had to attempt, first, to keep the command bar centered and, second, try not to exceed the maximum "permissible" tracking error level which was indicated by two fixed horizontal bars. The detailed description of this technique's components is presented in the next subsections.

5.3.1.1 Display Format Symbology for Tracking Task

In the beginning it was necessary to use both the HDD and HUD of IFS to provoke the PIO in the experimental flights. Since the limitation of the number flights became evident, it was decided to use only one of the displays. So the

dilemma of what of kind of IFS displays should be preferably used in the coming flight program was encountered. The answer was found in the FFS stage.

Initially the HDD in the FFS was used to simulate the HDD format of IFS. The appropriate format (most applicable for IFS experimental flights) was implemented in the display of the ground simulator. The ILS mark of this format was used as the command pitch attitude symbol against the pitch indicator scale typical of transport aircraft. The result was that for all PIO prone dynamic configurations tested no provoking excitation of command bar caused the PIO in "pilot-aircraft" closed control because of the small pitch indication scale. So the pilot didn't clearly feel PIO tendencies.

After some attempts, the acceptable pitch angle scale was found which caused the pilot to enter PIO (at least in ground simulation) and was of practical interest so long as the scale defined was close to one typical of the HUD. The concrete value of the pitch angle scale finally accepted was 1.5 pitch angle deg/cm (0.63 pitch angle deg/inch) which approximately corresponds to the scale of IFS's HUD which conformed to the outside view.

Thus, it was decided to use the HUD during the IFS experimental flights, but preflight ground simulation tests were conducted with the HDD for which the format and pitch angle scale were modified to make them close to IFS HUD.

The sketch of the HUD format utilized in the IFS is shown in Fig. 5.1. It is rather standard so only the central part symbols directly associated with PIO excitation are worthy of some explanation.

The center of the circular body with a cranked wing is a flight-path vector symbol (FPV). The task was mechanized by displaying the error between the actual pitch attitude and a programmed pitch attitude command signal. To make the task a compensatory tracking one (since the modern criteria are based primarily on the single-axis compensatory tracking principle), this error is presented by the position of a small circle (command symbol) relative to the FPV symbol which is practically only slightly movable during the PIO excitation maneuvering in level flight. The error is zero when the pilot managed to match the FPV and pitch attitude error symbols.

It was very important to bring the task closer to more realistic conditions of pilot tight control operation in "pilot-aircraft" closed loop, i.e. to make the tracking task more stringent for the pilot. For this purpose the maximum "permissible" error zone was established in the HUD format which is depicted in the figure as two bars on both sides of the FPV symbol. These bars are fixed relative to the FPV mark and move across the screen as a single piece. The width of the mentioned zone changed from one evaluation run to another. The

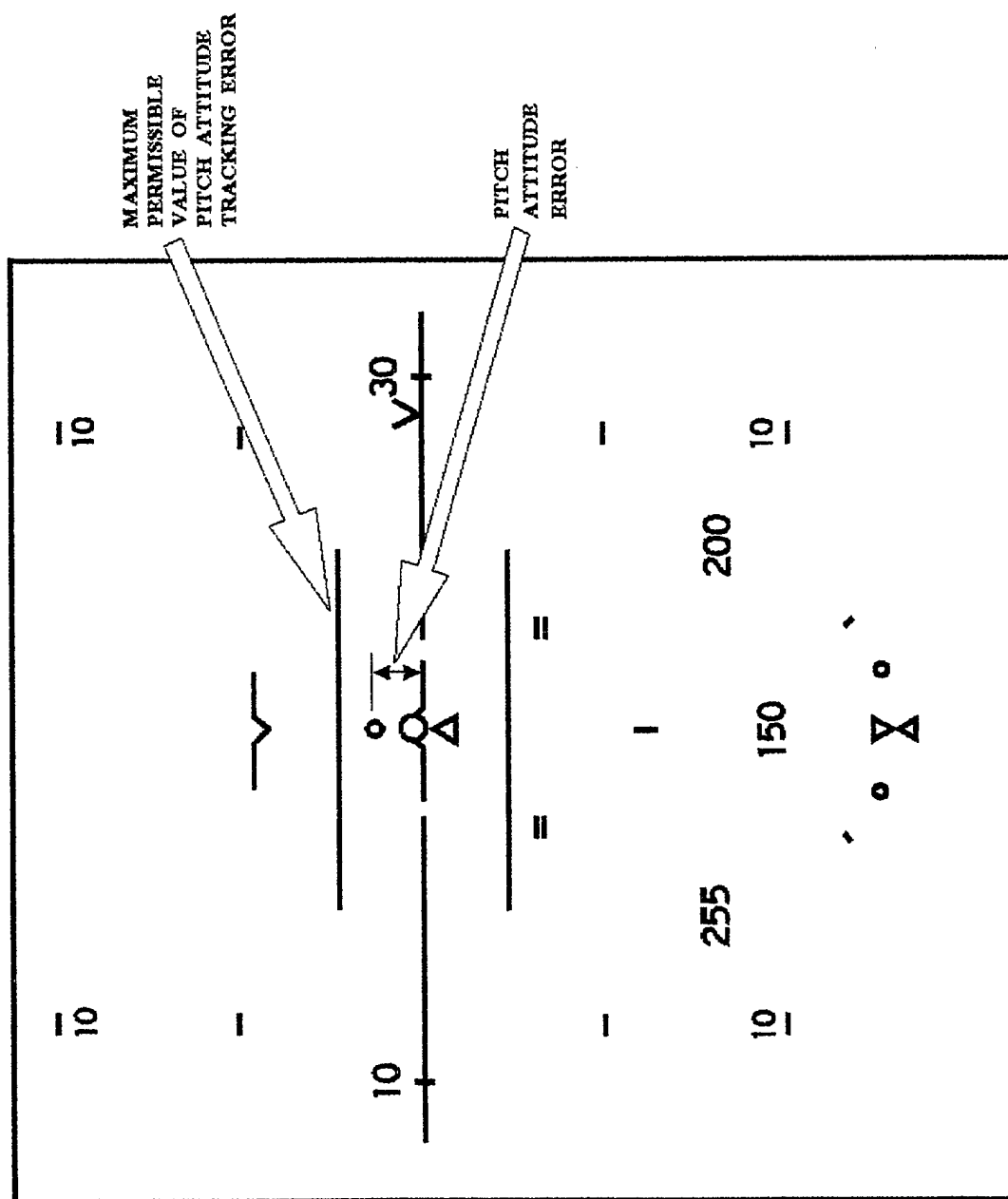


Figure 5.1 HUD Format

more narrow zone would make the pilot work harder, therefore, initiating the more intensive and aggressive manner of pilot controlling and provoking the PIO. During the ground simulation "trial and error" procedure, it was found that the pitch attitude error "permissible" range of $\pm 1^\circ \dots 2^\circ$ is correct and could provoke the PIO tendency. On one hand, it reasonably aggravates the tracking task and makes it closer to the natural piloting task. On the other hand, the value of $\pm 1^\circ \dots 2^\circ$ is one that is still within the average pilot's ability to perform the tracking by not exceeding this boundary.

5.3.1.2 Command Symbol Excitation Signal

The input command signal (its form was suggested by MAI) excited the pitch attitude error symbol (small circle) which was a pseudorandom signal made up of a sum of 15 sinusoids approximating the rectangular spectrum:

$$i(t) = \sum_{i=1}^{15} A \sin(\omega_i t)$$

where parameters of this formula are presented in the table below.

i	1	2	3	4	5	6	7	8
ω_i , rad/s	0.26	0.52	0.785	1.05	1.31	1.57	2.09	2.62

i	9	10	11	12	13	14	15
ω_i , rad/s	3.14	3.93	4.36	6.28	7.85	10.5	15.7

Before injecting into the display format, the resulting signal was filtered. The form of this filter was as:

$$S(\omega) = \frac{1}{(\omega^2 + \omega_i^2)^2},$$

where $\omega_i = 0.5$ rad/sec.

While choosing both frequency and amplitude spectrums of the summed signals, the pilot assessment and engineering analysis of the resulting effect were also considered. These spectrums were corrected based on the approach as follows:

- to make them much closer to the ones in tight tracking tasks (like formation flight, pitch attitude stabilization while flying under disturbance conditions etc.),
- to have a relatively high level of excited closed control loop parameters providing the acceptable accuracy of flight data processing,
- on the whole, the integral displacement of command symbol over an experimental run should not cause the significant change of aircraft

trajectory as a result of pilot tracking efforts; only slight thrust lever inputs were needed to correct the aircraft trajectory (the thrust control manual mode was used),

- to avoid as far as possible achieving of actuator saturation,
- to avoid exceeding the maximum angle of attack and g-load during the command signal tracking.

Two other factors that impacted the total duration of each evaluation run. On one hand, the method of flight data analysis presupposes that the process is the time stationary one, thus each evaluation run should be rather long and the pilot control manner should not significantly change during this time frame. On the other hand, the run should not be very long thus avoiding pilot tiredness and change in the manner of piloting.

Each experimental run total duration finally chosen was $T \approx 120$ sec. The time history of the command signal excited by the pitch attitude error symbol is shown in Fig. 5.2.

FRI test pilots evaluated the spectrum of the command signal as reasonable after a small training target tracking task was performed with a good quality without achieving actuators saturation. It was confirmed that the amplitude of command signal is sufficient, and that during tracking, there are no dangerous normal accelerations or high angle of attack encountered.

5.3.2 Dynamic Configuration Characteristics

5.3.2.1 Longitudinal Short Term Dynamic Characteristics

The short period dynamic configuration characteristics selected were initially realized inside the Tu-154M IFS math model by means of a response feedback method using the g-load and pitch attitude signals and appropriate filters provided for certain dynamic configurations. As is apparent from the frequency response characteristics in Fig. 5.3, the VSS ensured close similarity of the IFS real-time math model to the given dynamic configurations. The real-time simulation in the FFS proved the prones of dynamic configurations to PIO and justified the flight regime chosen ($V_{IAS} \approx 450$ km/hour, $H \approx 4.2$ km).

5.3.2.2 Longitudinal Long Term Dynamic Characteristics

For all dynamic configurations selected, the long term (phugoid) response characteristics were those of the Tu-154M base aircraft, only slightly modified by the longitudinal feedback gains used to achieve the desirable short period dynamics. The long term characteristics didn't change during the experiments; since some weight change didn't impact the long term characteristics significantly and the airspeed was held constant. The latter was due to a slight influence of long term characteristics on the aircraft airspeed and to necessary

15

$$i(t) = \sum_{i=1}^15 A \sin(\omega_i t)$$

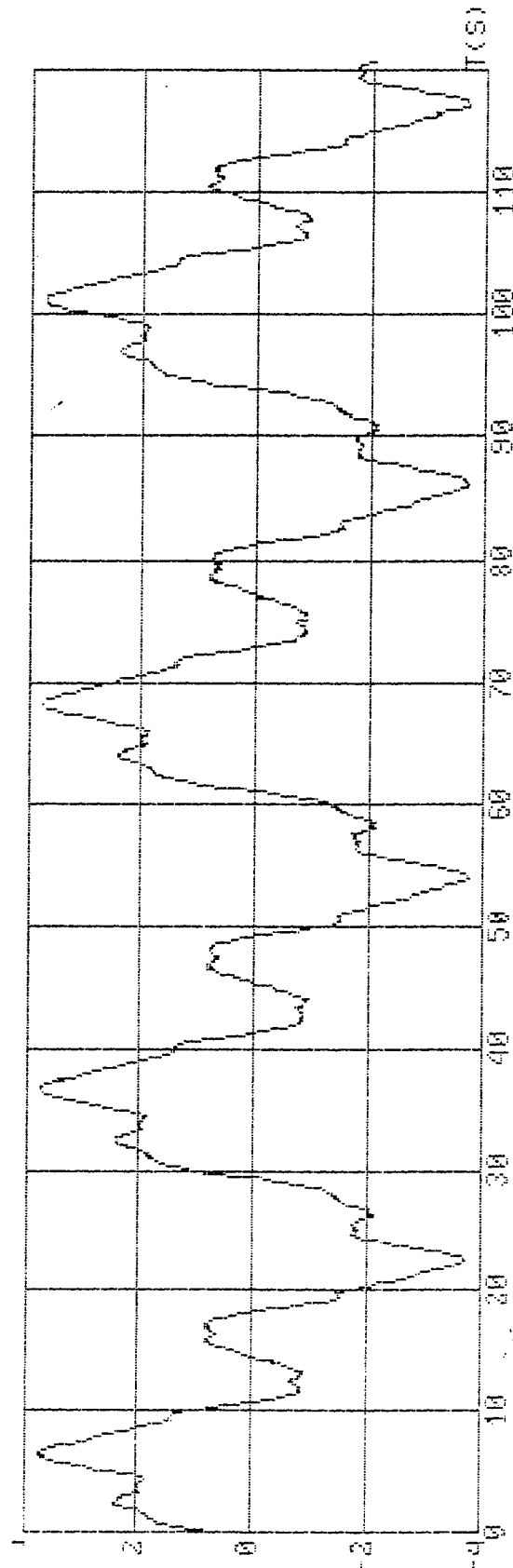


Figure 5.2 Time History of Command Pitch Angle Signal

Configuration I

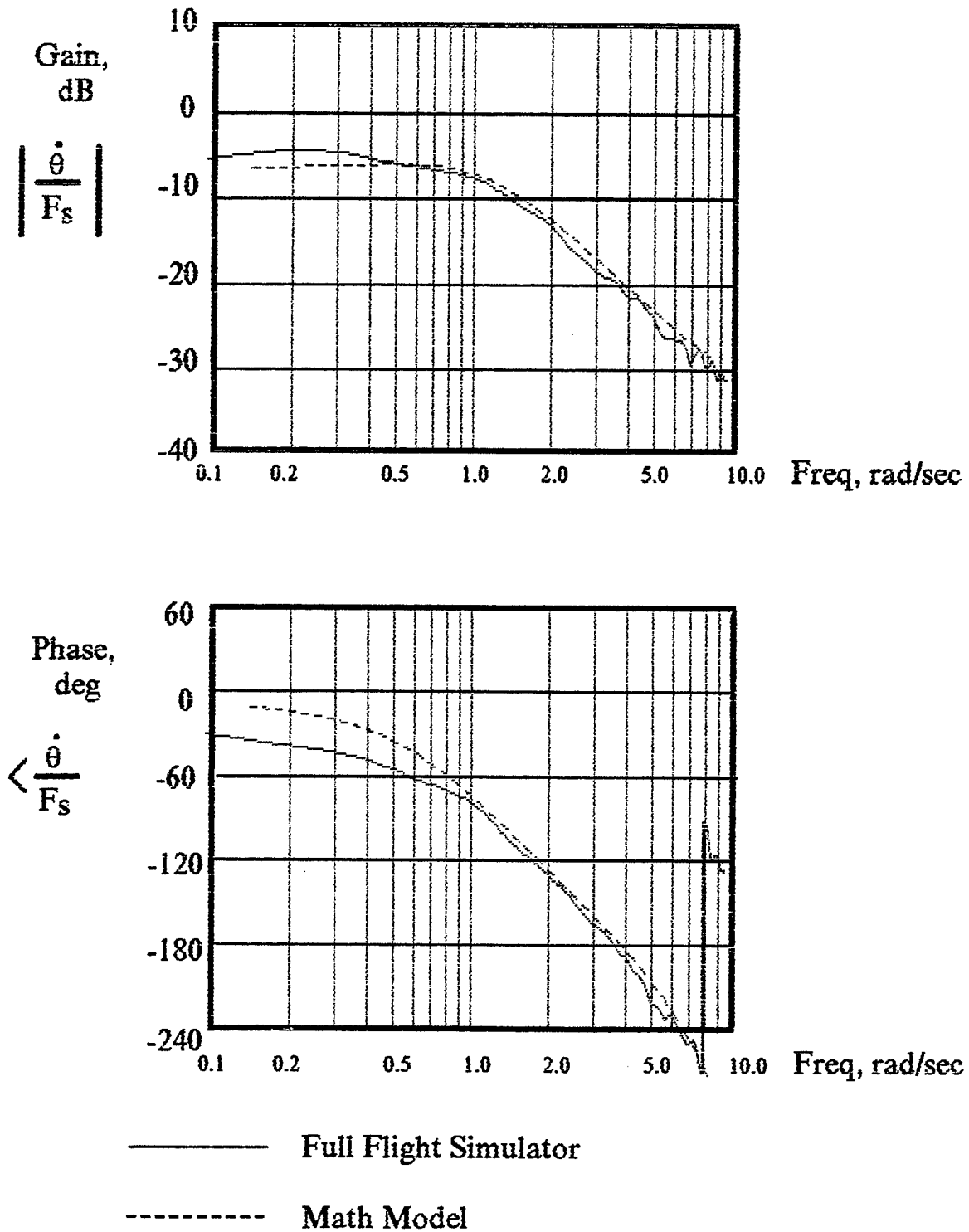


Figure 5.3a Comparison of Math Model and Full Flight Simulator Results

Configuration II

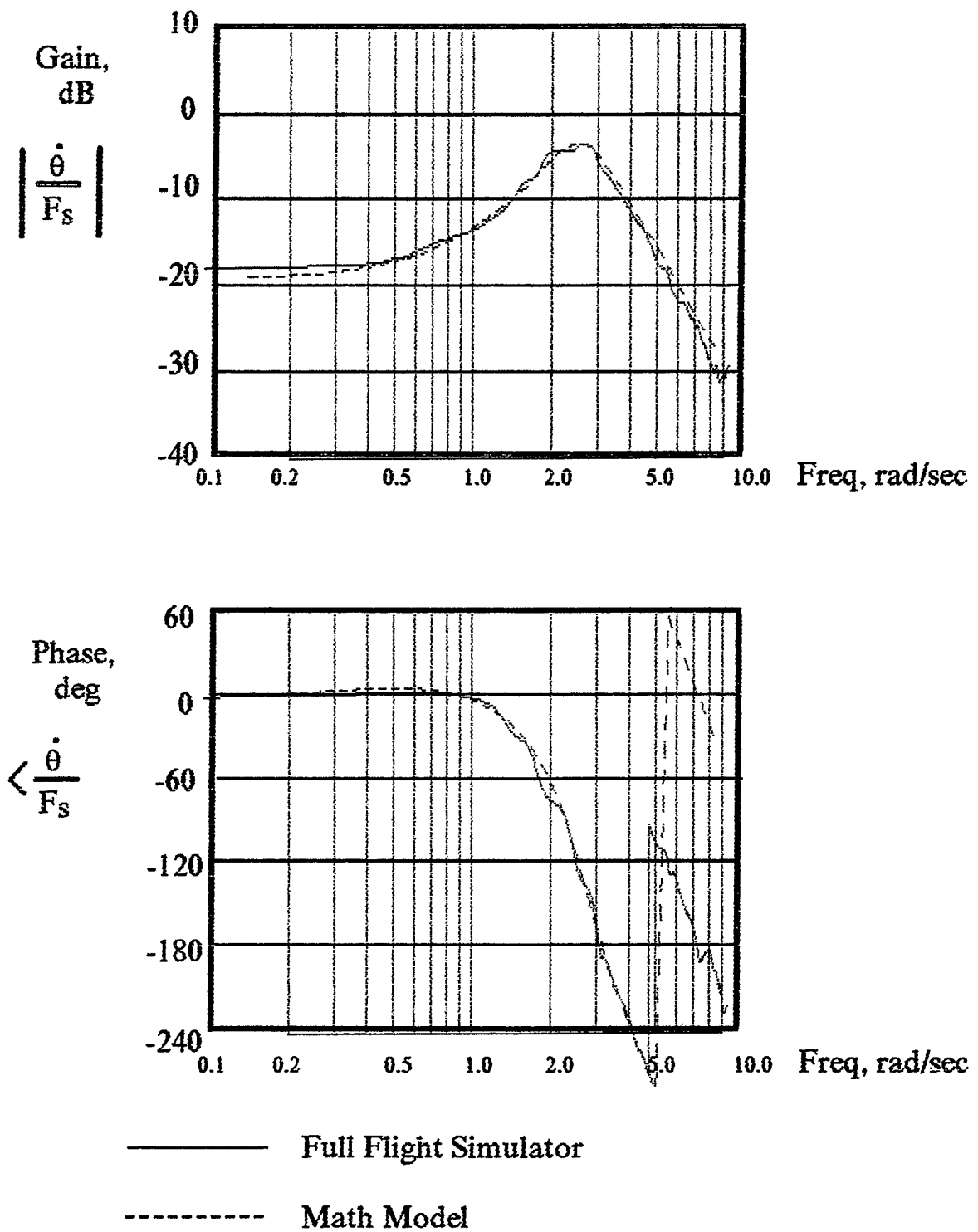


Figure 5.3b Comparison of Math Model and Full Flight Simulator Results

Configuration III

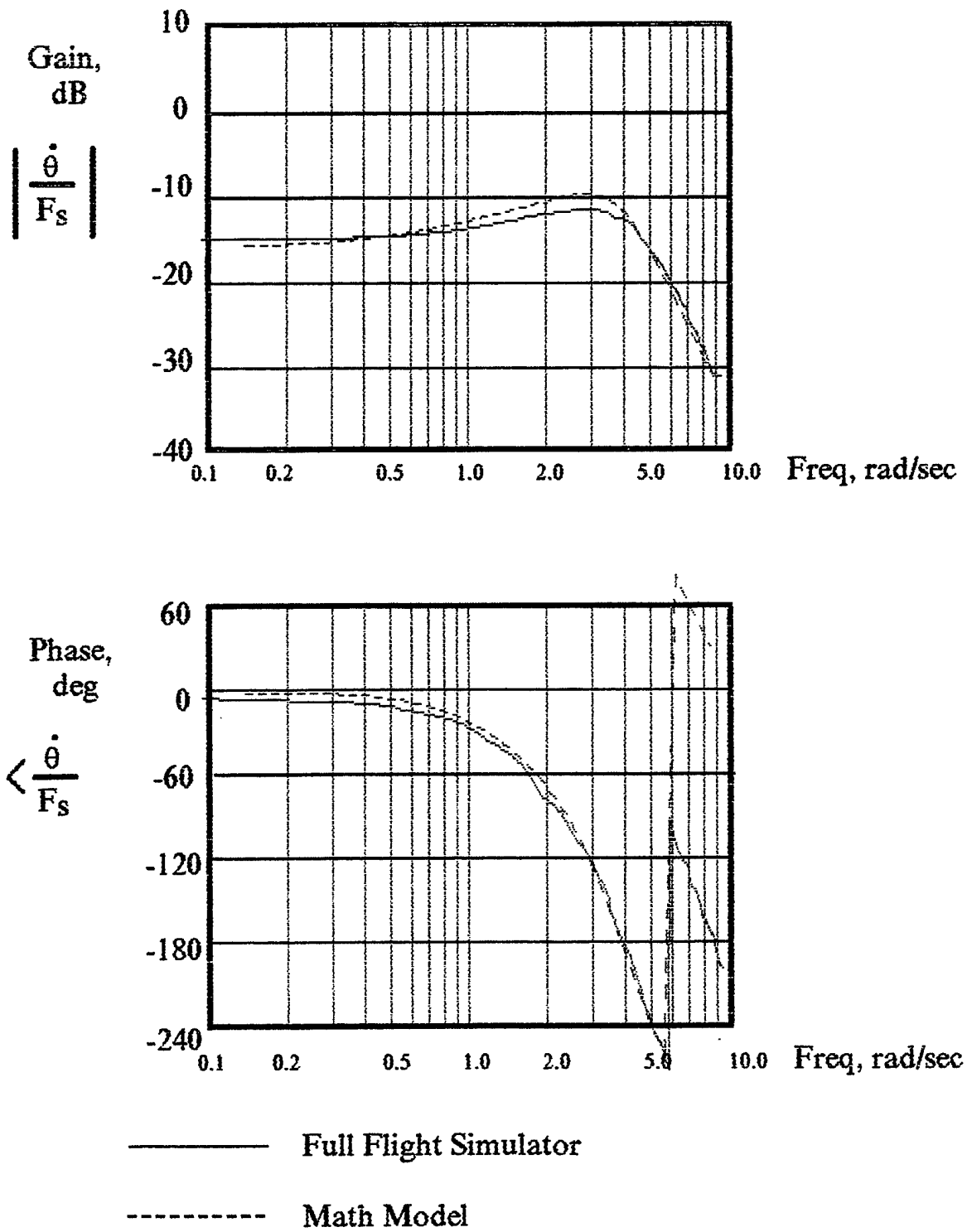


Figure 5.3c Comparison of Math Model and Full Flight Simulator Results

Configuration IV

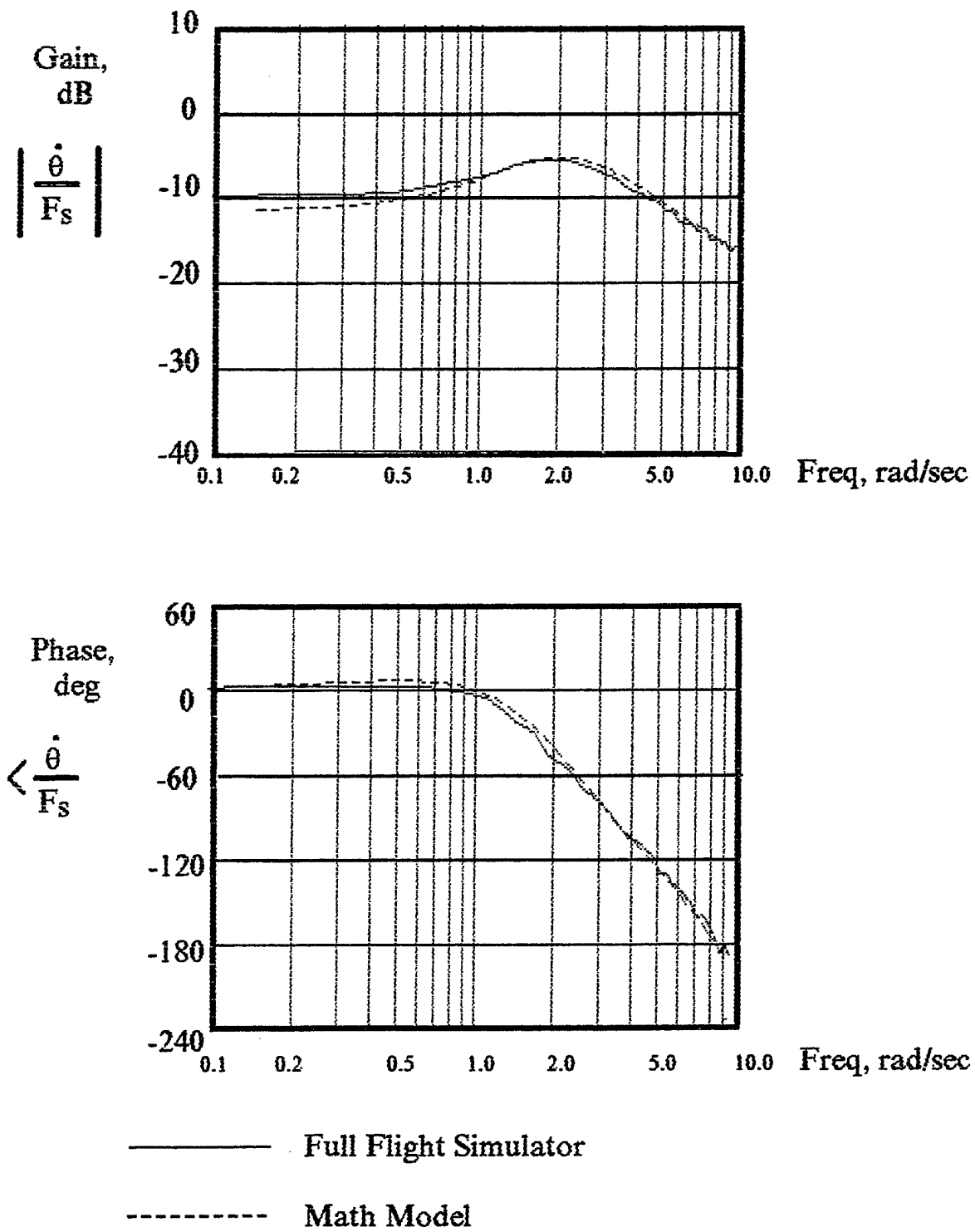


Figure 5.3d Comparison of Math Model and Full Flight Simulator Results

pilot efforts to maintain the airspeed constant in the manual mode (the attempt to utilize the autothrust mode gave negative results because of engine response delay which was assessed by the research pilots as unacceptable in such a task). The change in altitude during the experiment runs was also rather small.

For assigned airspeed $V_{IAS} \approx 450$ km/hour (~ 240 kt) and aircraft average operational weight $G \approx 70t$, the long term pitch characteristics were as follows:

$$\omega_{PH} = 0.092 \text{ rad/sec,}$$

$$\xi_{PH} = 0.02,$$

$$T_{PH} = 68 \text{ sec.}$$

Under the given flight conditions the IFS is on the positive slope branch of the power required versus airspeed curve.

5.3.2.3 Lateral - Directional Dynamic Characteristics

For all dynamic configurations selected and the flight regime assigned, the lateral-directional characteristics were those of the Tu-154M base aircraft, namely:

$$\omega_d \approx 0.95 \text{ rad/sec,}$$

$$\xi_d \approx 0.6,$$

$$|\phi/\beta|_d \approx 0.9,$$

$$\tau_r \approx 0.4 \text{ sec,}$$

$$\tau_s \approx 70. \text{ sec}$$

5.3.2.4 Longitudinal and Lateral Dynamic Characteristics Coupling

During the FFS sessions the acceptability of gain ratio between the control surfaces and stick positions (control sensitivity) were evaluated. The same was done with longitudinal/lateral dynamic characteristics coupling for configurations selected.

Based on the pilot comments as a result of pilot free maneuvering evaluations, the gain ratio for each dynamic configurations was adjusted in the pitch channel. The optimal gain ratio selected was then fixed for subsequent PIO tendency evaluation runs while testing this concrete configuration.

The dynamic characteristics of the lateral-directional channels were assessed by the pilots as acceptable in spite of some disharmony of poor longitudinal and "good" lateral dynamics. Thus, there were no reasons to change anything in this respect during the flights.

5.3.2.5 Type of Hand Controller and Its Feel Characteristics

The right-hand sidestick was chosen for the experimental flights as a rather evident result of both the central and sidestick preliminary evaluations in the FFS. The sidestick revealed a greater tendency of "pilot-aircraft" closed control loop to PIO.

The feel system characteristics were chosen based on the previous extensive experience of sidestick research in the Tu-15M IFS and were fixed for all the configurations evaluated in the flight program:

	pitch	roll
spring gradient (kg/cm)	1.3	0.9
breakout force (kg)	± 0.5	± 0.35

The forces are measured at the grip middle point located at the distance of ~12 cm from the pivot point.

The sidestick utilizes the force sensors to measure the pilot command inputs. Thus, the feel system dynamic characteristics were included in the FCS while determining the frequency response characteristics of the control loop.

5.3.3 Power Actuator Dynamic Characteristics. The Saturation Influence on PIO Tendency

There was a priori recognition of the pitch channel actuator rate limitation impact on PIO tendency while flying the IFS. During the ground simulation sessions, the appropriate evaluation of actuator saturation was made; and if it were reached in experimental flight, how it would influence the PIO tendency.

The pitch channel actuator rate limit is $\dot{\delta}_e=24$ deg/sec. While simulating in the FFS, the pitch actuator rate was varied from 15 deg/sec through infinity. Naturally the influence of low rate actuator on PIO phenomenon was confirmed. It manifested itself somewhere about $\dot{\delta}_e < 20$ deg/sec depending on the dynamic configuration characteristics, piloting manner, etc. At $\dot{\delta}_e=24$ deg/sec (inherent in IFS) the impact of actuator rate limit was insignificant. This fact was substantiated both by pilot ratings and simulation data analysis. The latter showed that in case of $\dot{\delta}_e=24$ deg/sec the "pilot-aircraft" closed loop system frequency response characteristics had still been close to those with unlimited pitch actuator rate (Fig. 5.4).

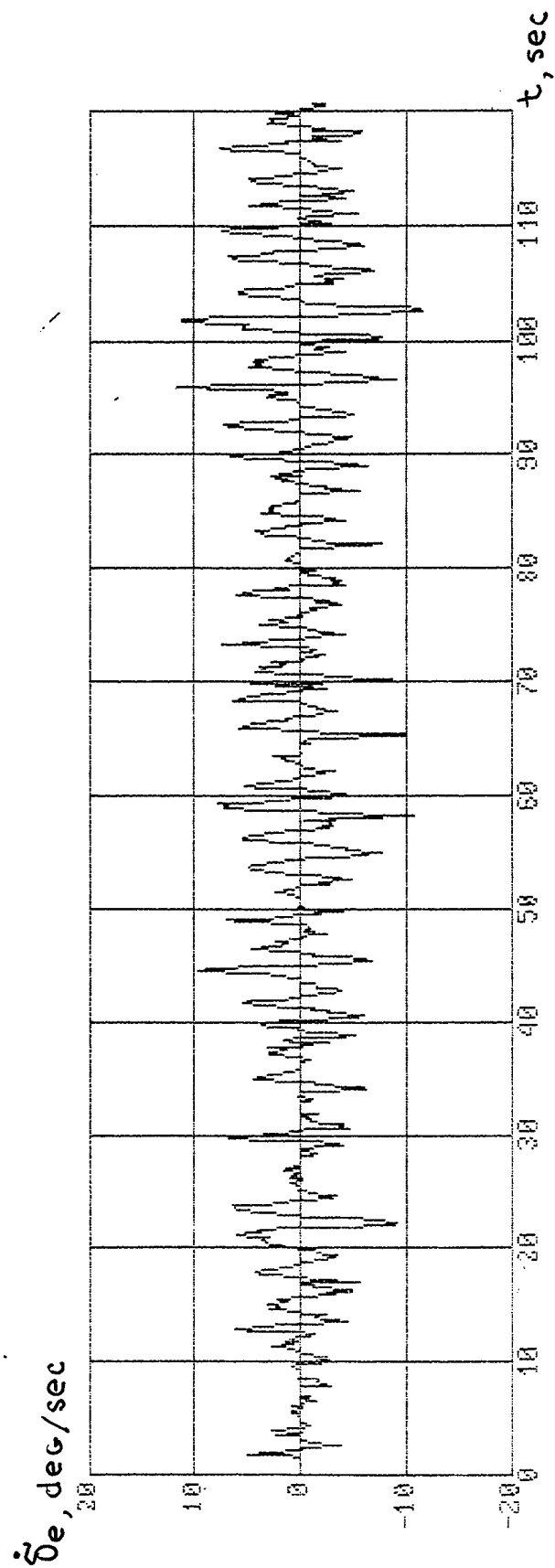


Figure 5.4 Time history of $\dot{\delta}_e$ required during target tracking task in FFS.

Nevertheless, the attempt was made to display the symbols on the PFD indicating the maximum limited and actual actuator rates during the experiment along with the above mentioned symbols. The simulation results revealed that such information really reduces the necessary actuator rates since it changes the pilot's manner of performing the tracking. It was finally considered unnatural for the pilot and was rejected.

To assure good results the test pilot was asked to "simulate" the "average" pilot without an extremely aggressive manner of aircraft piloting.

5.3.4 Influence of Pilot Station Location

The pilot station location relative to the center of gravity position $L \approx 26$ m was taken into account while simulating the IFS dynamic response in the FFS. However, no regular preflight investigations were conducted in the FFS as the Tu-154M IFS has currently no means to simulate the pilot station at different locations relative to the center of gravity.

The above stated basic principles of flight methods were involved in the flight evaluation procedure which is presented in section 6.2

6.0 FLIGHT INVESTIGATIONS IN Tu-154M IN-FLIGHT SIMULATOR

6.1 DESCRIPTION OF Tu-154M IFS

The experimental flights were carried out in the IFS developed by FRI based on the Tupolev-154M 3-engine jet transport aircraft (Fig. 6.1). The IFS is intended for the flight research such as:

- developing digital and analog flight and engine control systems,
- evaluating new pilot controllers, including sidesticks, control wheels, trust levers etc.,
- particular dynamic phenomena investigations and advanced handling qualities criteria development,
- development of advanced HDD/HUD formats,
- human factors research.

The IFS utilizes the normal cockpit, with the evaluation pilot sitting in the left seat and the safety pilot in the right (Fig. 6.2). The safety pilot has the conventional mechanical controls and instruments. He is warned of any imminent failures or system limits. The safety pilot can manually take control of the aircraft by pressing any of several buttons located on his controls or by

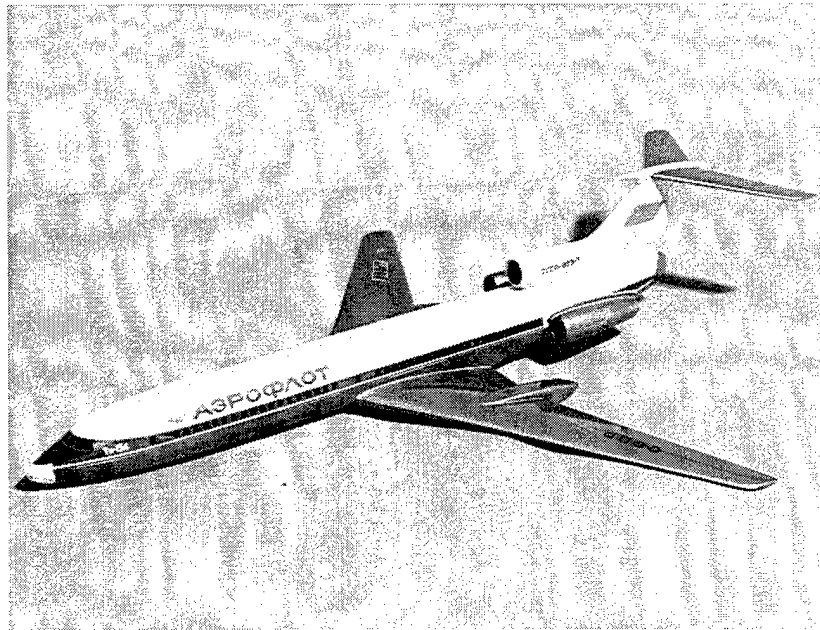


Figure 6.1 General View of Tu-154M In-Flight Simulator

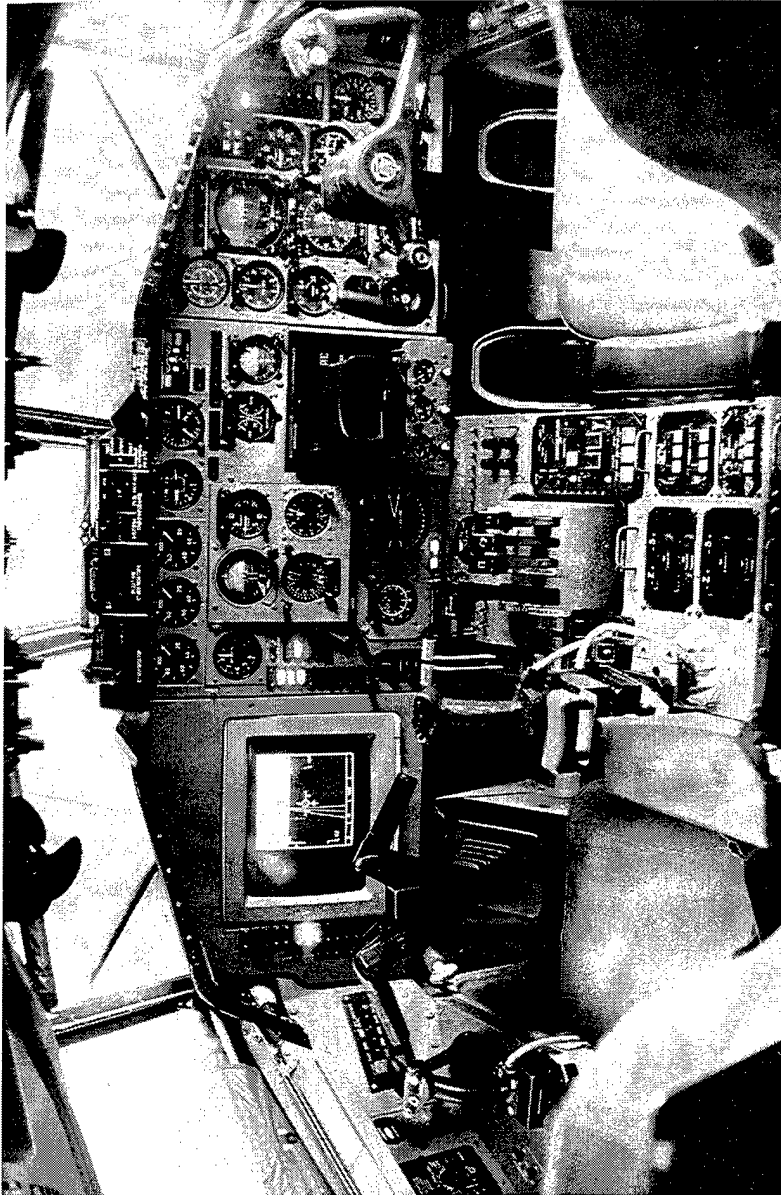


Figure 6.2 Tu-154M IFS Cockpit Layout

moving his control wheel past certain thresholds. Automatic system disengagement only occurs if the angle of attack or g-load approach limits or the second failure of the experimental FCS or the associated electronic components occurs.

The evaluation pilot is in the left seat (Fig. 6.3) and controls the IFS through completely separate fly-by-wire (FBW) controls (currently an experimental central stick and a right-hand sidestick are installed). A wide variety of hand control parameters can be changed in advance or during the flight as needed.

The left seat displays consist of head-down and head-up displays. The HDD is a modified commercial color computer monitor. The HUD was adapted from a fighter aircraft unit, and mounted inverted from the ceiling. The displays for both units are generated using a modified commercial minicomputer. Different preprogrammed displays can even be modified in flight as needed.

The experimental fly-by wire system comprises the triplex analog and nonredundent digital FCSs. The block-diagram of the experimental FCS and its attachment to the mechanical system is shown in Fig. 6.4. The analog FBW is intended for simulation of simple control laws. The digital FBW is utilized for control laws of any complexity and airframe dynamics simulation. The digital system is based on a modified microVAX-2 digital computer. This includes all components for the aerodynamics, flight control laws, engine response, and control feel characteristics.

From a functional point of view (as in present experimental flights) the digital FCS may be presented as two parts:

- the variable-in-flight dynamics or Variable Stability System (VSS) responsible for airframe dynamics simulation,
- the other part is intended for experimental flight control and engine control laws simulation.

The IFS is equipped with flight data acquisition system which uses a tape recorder. Also, the telemetry station may be used for ground flight data acquisition, processing and monitoring.

Normal crew of the IFS consists of two pilots, a navigator, a project engineer, a simulation system engineer and an acquisition system engineer.

6.2 ENTIRE FLIGHT EVALUATION PROCEDURE

Each flight took approximately 1.5 hours. Totally two or three dynamic configurations selected along with the Tu-154M IFS base configuration were

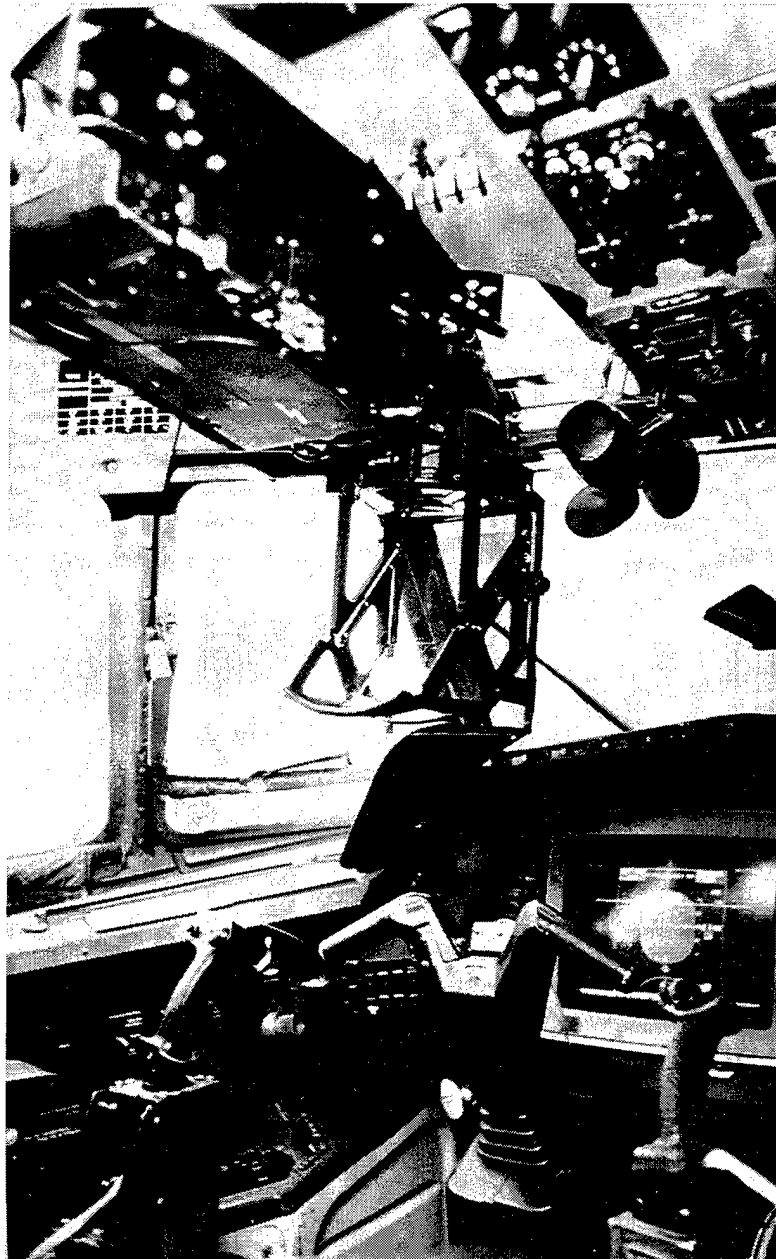


Figure 6.3 Evaluation Pilot Seat

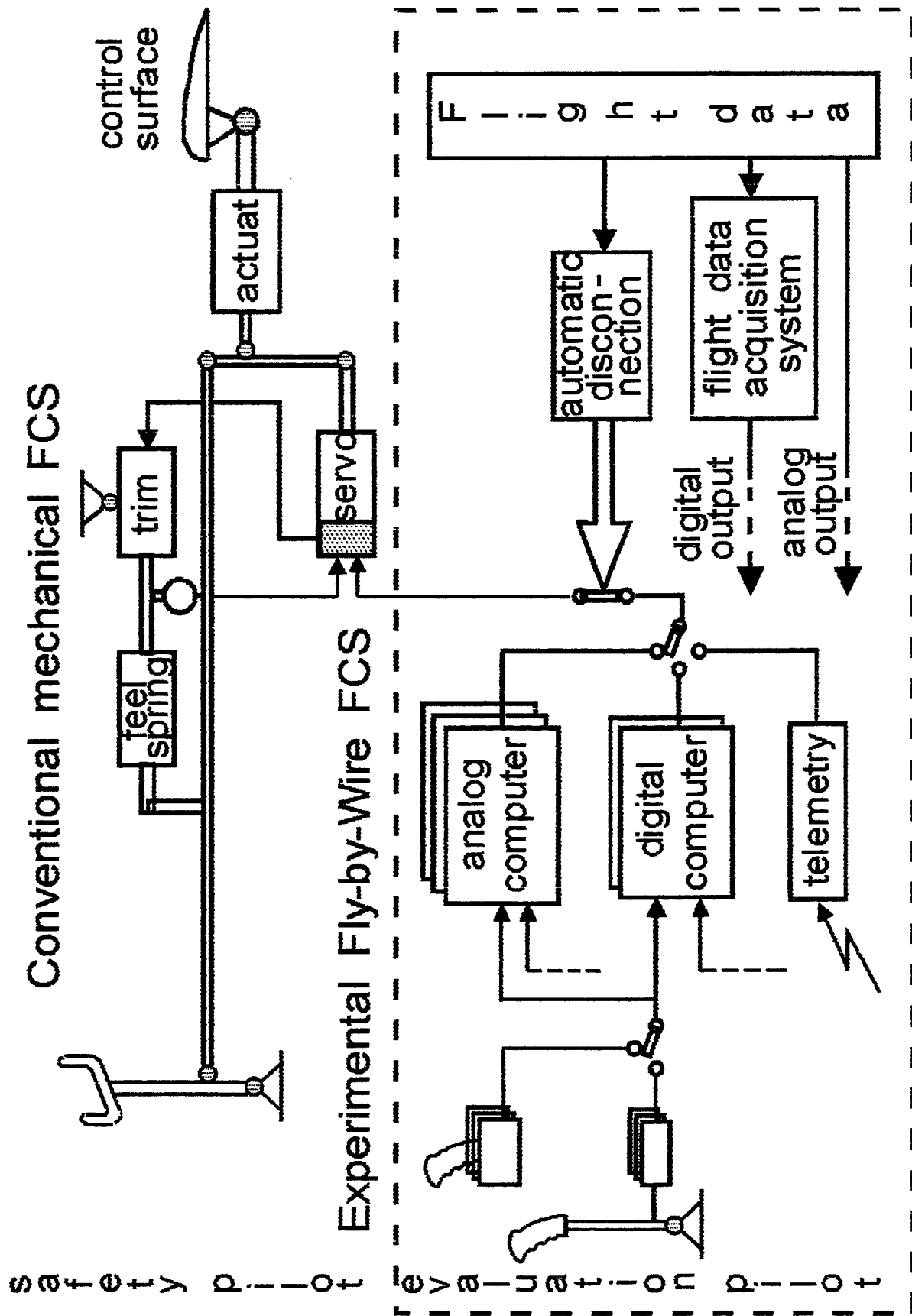


Figure 6.4 Block diagram of the Tupolev-154M IFS experimental Flight Control System.

evaluated in a generally random order. One or two extra evaluations may be performed in case of some failure in previous attempts.

During the flight each dynamic configuration (except the base one) was evaluated four times: at first twice with pitch attitude error "permissible" range of $\pm 2^\circ$, then twice again with the smaller range of $\pm 1^\circ$.

The general order of experimental flight was as follows:

1. The evaluation pilot was given control of IFS at an altitude of $H \approx 4.2$ km and airspeed of $VIAS \approx 450$ km/hour, with aircraft in flight configuration (flaps/slats retracted, gear up), initial flight weight $G \approx 73...75$ tons, with right-hand sidestick and experimental digital FCS engaged by the onboard research engineer while the VSS was realizing a certain dynamic configuration.

2. The evaluation pilot (having no prior knowledge of the configuration characteristics) was to take control and perform any flight maneuvers he likes to select, optimal from his viewpoint in pitch gearing ratio and familiarize himself with the given configuration for 2...4 minutes.

3. Then the evaluation pilot performed in level flight, so-called frequency sweeps in the longitudinal channel for more reliable "FCS-aircraft" loop frequency response characteristics identification in the given flight conditions.

4. The evaluation pilot trimmed the aircraft in level flight with thrust control engaged in manual mode. Then the research engineer set the $\pm 2^\circ$ pitch attitude "permissible" range. Shortly after the HUD command signal was activated, the evaluation pilot performed the tracking as defined by the pitch attitude error command signal during approximately 120 sec. Level flight was to be maintained (not exceeding bank angle of 3 degrees). The small thrust lever position correction could be made by the safety pilot if necessary. The pilot was keep imperatively to two partly conflicting conditions:

- try to center the command signal symbol with stringent demand not exceed the boundary of "permissible" range even if he really failed to do it well,
- try to "play a role" of "averaged pilot" with "average" degree of aggressiveness while striving for tight tracking.

5. After the command symbol stopped the evaluation pilot trimmed the initial level flight position and repeated the evaluation run once more.

6. The pitch attitude error boundary of $\pm 1^\circ$ was set by the research engineer. The evaluation pilot performed the tracking task twice under conditions of above stated item 5.

7. The next configuration was engaged by the research engineer while the evaluation pilot was asked to assign both the overall rating using the Cooper-Harper rating scale and PIO ratings by means of three special PIO scales (Figs. 2.5, 2.6, 2.7).

8. The next dynamic configuration (in order unknown for the evaluation pilot) was evaluated in accordance with contents of items 2 through 7.

During the evaluation runs the task performance was recorded on tape for post flight processing and analysis.

6.3 RESULTS OF FLIGHT INVESTIGATIONS

6.3.1 General Remarks and Pilot Assessment

Four experimental flights were performed. During this work four configurations (basic and three PIO prone ones) were evaluated by three test pilots in accordance with the above presented methods. In general, the pilot managed to sustain the evaluation procedure. They have noted that in the case of actual flight tracking tasks, the pilot's perception differed to a certain degree from the ground simulator because of real flight anxiety and environment. Also, they remarked that there was a markedly unnatural difference between poor longitudinal handling qualities and good lateral ones that could be rarely encountered in real practice. The flights confirmed that it is very important to motivate the pilot in such a way that he would be trying to be within the "permissible" range of pitch attitude error at any price while tracking. Only in this case would he entered a PIO and not back out of the loop settling for a lower level of performance.

The results obtained from both the sweep excitation maneuvers and tracking task showed that the IFS reproduced rather well the dynamics of configurations selected and previously evaluated in ground simulation (Figs. 6.5a...6.5d).

As to the problem of actuator rate saturation in the pitch channel, the analysis indicated that in most cases the pilots managed to be within actuator rate limits (Fig. 6.6). This fact validated "automatically" since in the case of actuator rate limit achievement the "FCS-aircraft" control loop became significantly nonlinear and yielded too much (and therefore clearly noticeable) scatter in frequency response characteristics.

In the pilot assessment of dynamic configurations, configuration I was evaluated as having very slow response with large time delay. Because of this, during selection of optimal pitch gearing ratio, pilots chose the twice lower value compared to the basic configuration which then affected the results of tracking task.

Configuration II was evaluated as having very a oscillatory response with large time delay. Pilots chose pitch gearing ratios 15% lower than for basic configuration. This configuration received the poorest pilot ratings.

Configuration III was evaluated as somewhat sluggish. Pilots chose the same pitch gearing ratio as for the basic configuration.

Configuration I

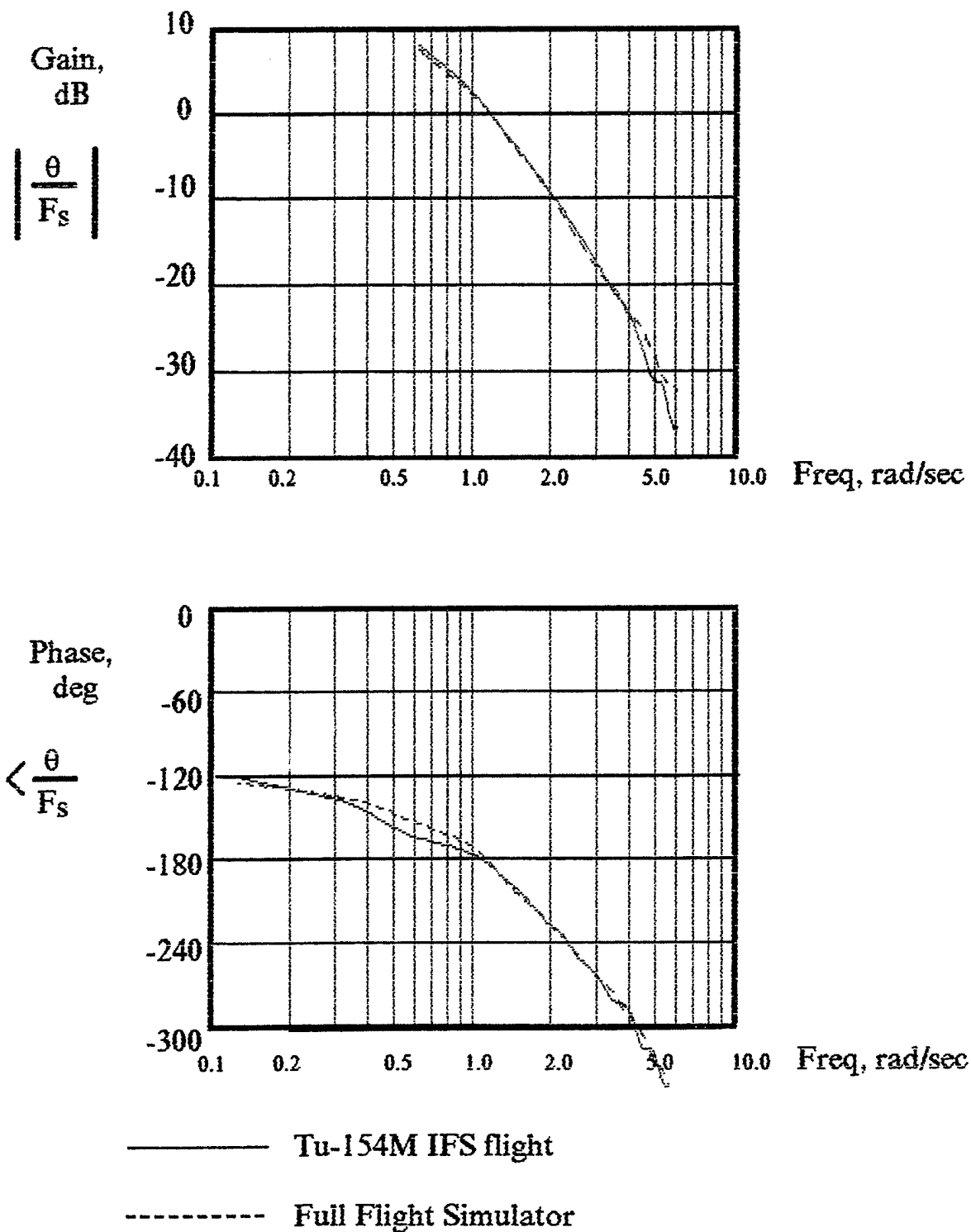


Figure 6.5a Comparison of Full Flight Simulator Results and Tu-154M IFS Flight

Configuration II

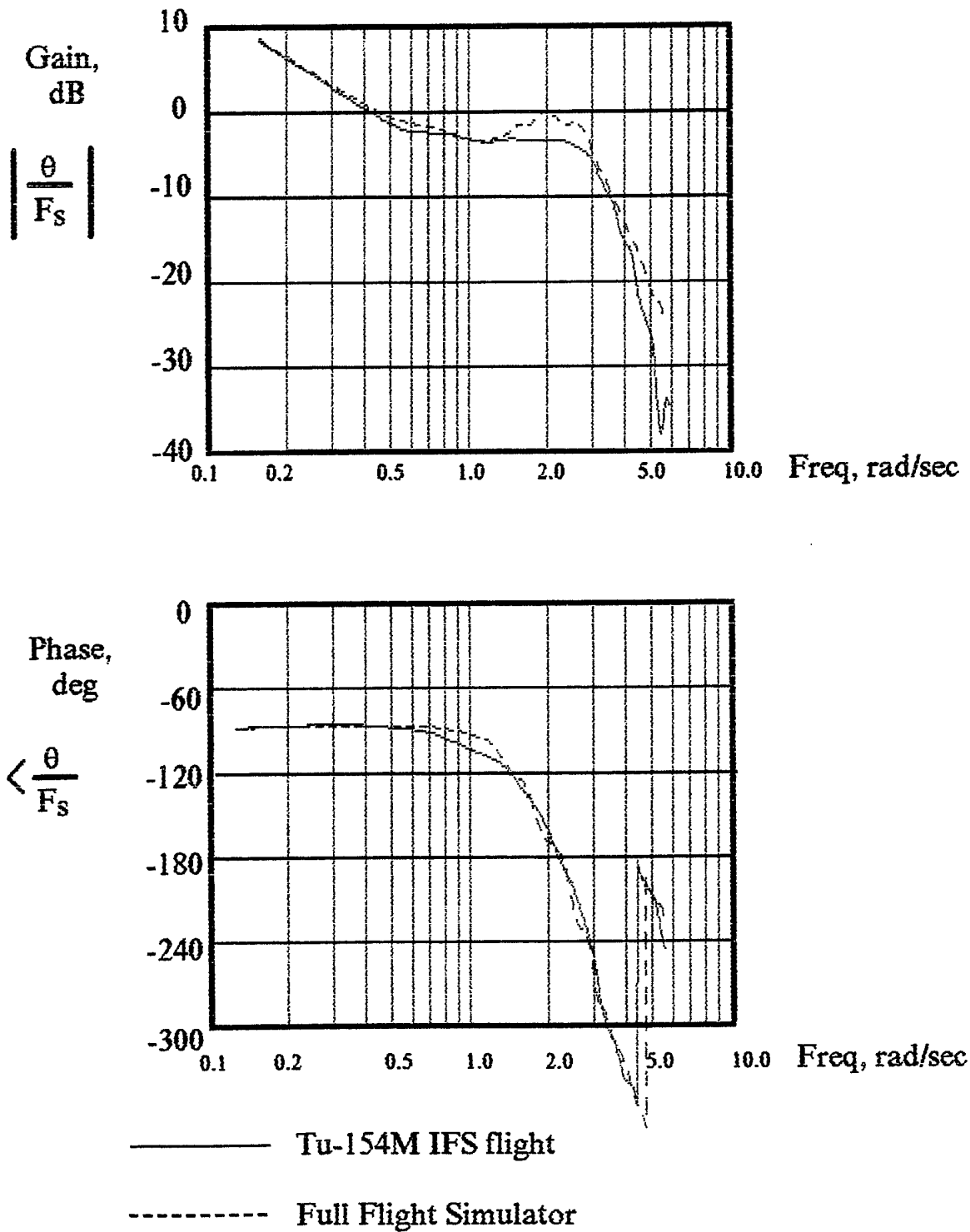


Figure 6.5b Comparison of Full Flight Simulator Results and Tu-154M IFS Flight

Configuration III

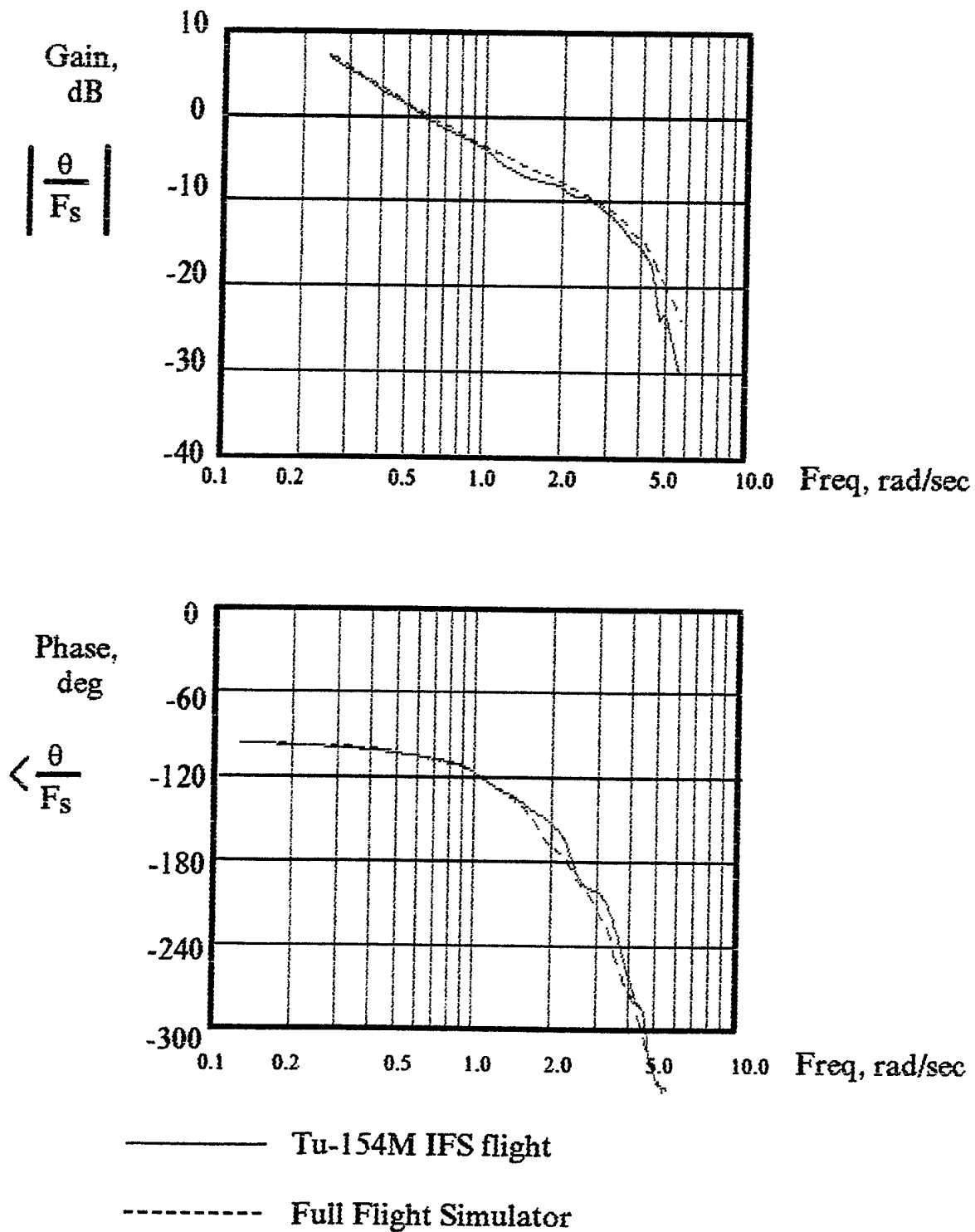


Figure 6.5c Comparison of Full Flight Simulator Results and Tu-154M IFS Flight

Configuration IV

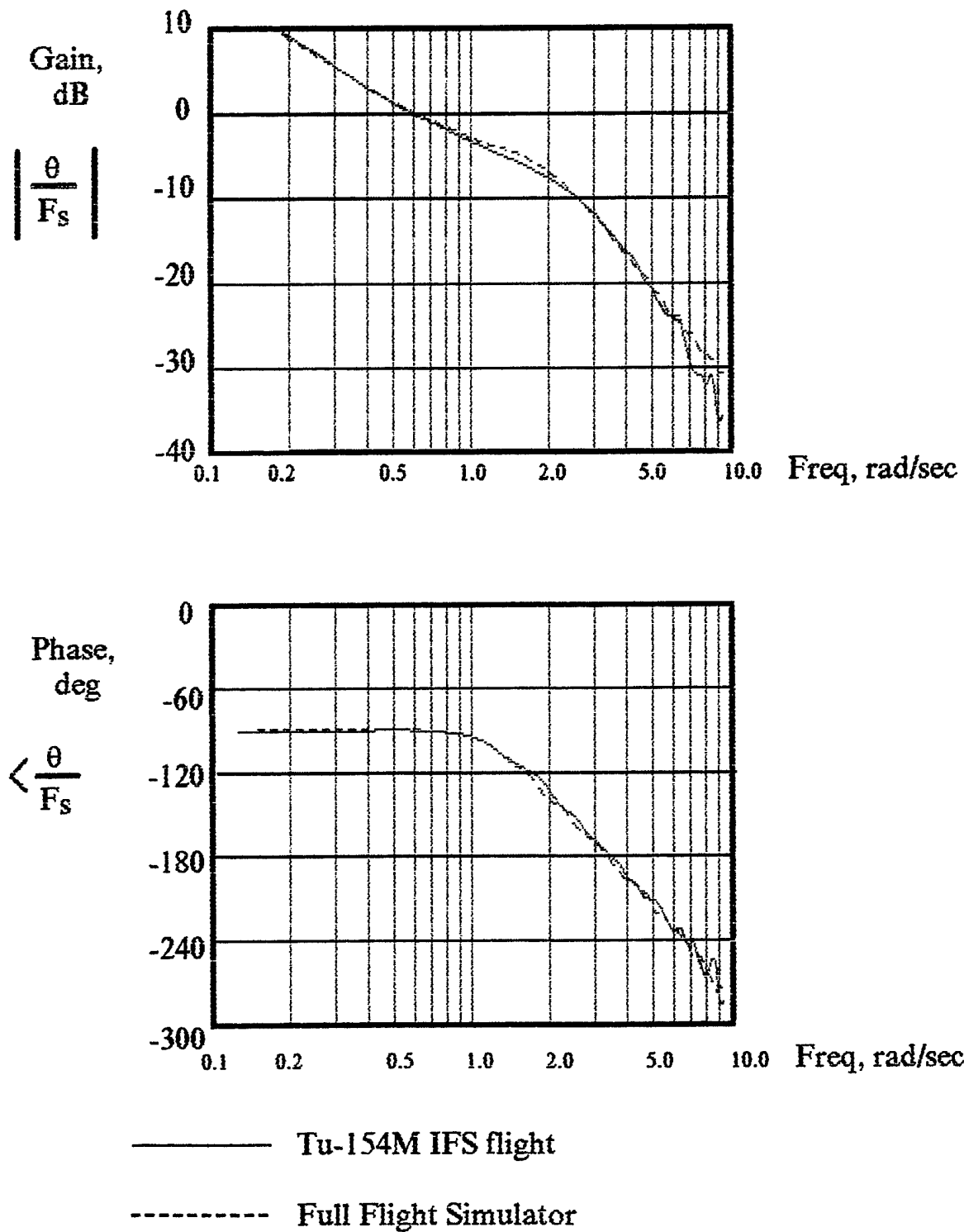


Figure 6.5d Comparison of Full Flight Simulator Results and Tu-154M IFS Flight

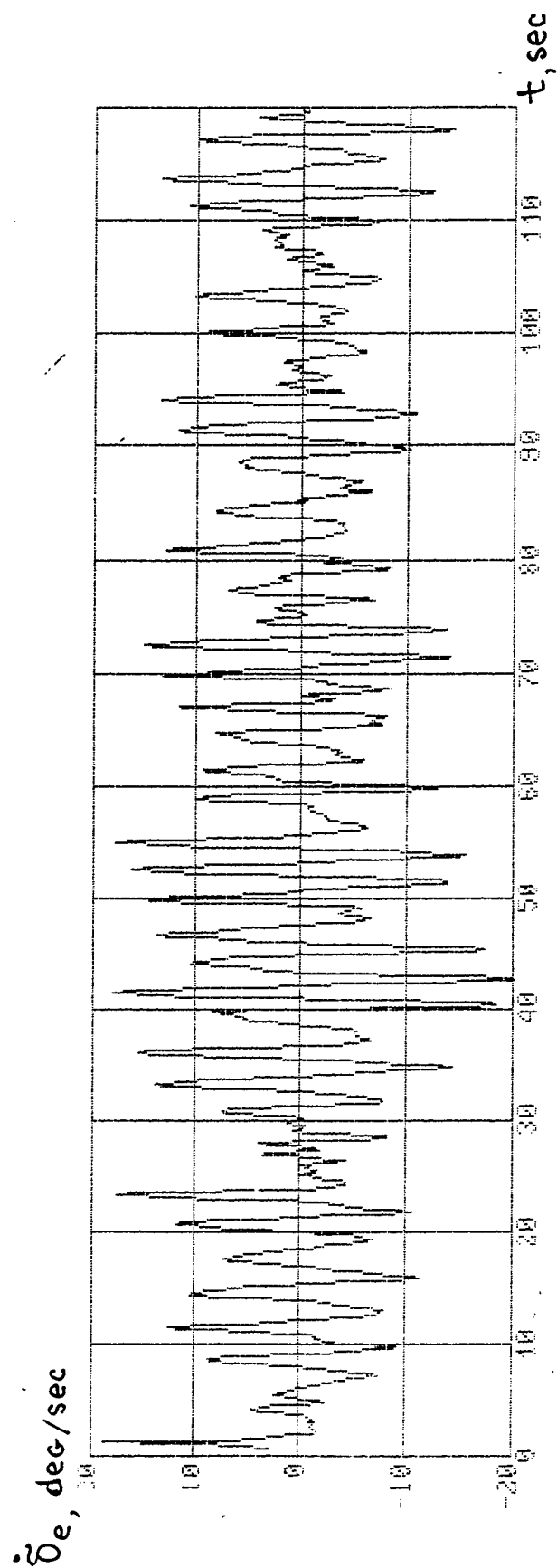


Figure 6.6 Time history of $\dot{\delta}_e$ required during target tracking task in Tu-154M IFS.

Handling qualities pilots ratings according to the Cooper-Harper scale along with PIO pilot ratings according to special PIOR scales are presented in the following table.

Configuration	CHPR		PIOR					
			Scale 1		Scale 2		Scale 3	
	FFS	Flight	FFS	Flight	FFS	Flight	FFS	Flight
I	3.8	4.0-5.5	3.4	3.8-4.0	3.0	3.0-3.2	3.0	3.0
II	4.0-4.2	6.5-8.0	3.2-3.8	4.0-4.2	3.3	3.5-3.8	3.5	3.5-3.0
III	2.2	2.0-3.5	1.7-1.8	2.6-2.8	2.0	2.0	1.8	2.2-2.3
Basic	3.2	2.5	2.2-2.7	1.8-2.2	2.2	1.6-1.8	2.2	1.8-2.0

Some scatter in pilot ratings is clearly explained by too limited flight time.

It is apparent from this table that PIO prone configurations received worse ratings in flight than during ground-based simulation. According to pilot comments, this is because during flight, pilots feel some additional aircraft motion (even if it is comparable with the moving base FFS accounting distance between center of gravity position and pilot seat) and can more clearly identify possible deficiencies of aircraft dynamics and its influence on task performance and flight safety. It is interesting to note that configurations with low PIO tendency received better ratings during ground-based simulation than the basic configuration.

During ground-based and in-flight evaluations, pilots also were asked to make a comparative assessment of PIOR scales. The most suitable scale for ground-based and in-flight evaluation was shown to be Scale 1, mainly because it contains a rather detailed description and explanation for each PIO rating. But the table form is less convenient in practical use in comparison with the more visually perceptible "tree-like" scale. Scale 2 (Scale 3 as well) has a very good "tree-like" form, but it is desirable to have more explanations for each PIO rating. As the pilots were often prone to use values between integer ratings, in the future it may be worth combining Scales 1 and 2 in order to have every choice of PIO rating according to a "tree-like" form with complete comments (as in Scale 1) describing aircraft behavior and the pilot compensation required.

6.3.2 R. Smith's Criterion

The R. Smith's Criterion assumes that there can be a frequency at which the power spectral density of the pilot's normal acceleration due to pitch attitude tracking is "sufficiently" narrowband. If such a frequency exists, there is a high probability during a high gain tracking task the pilot will switch from tracking pitch to tracking the normal acceleration he feels at that frequency; i.e., the frequency is said to be "subjectively predictable." A suggested

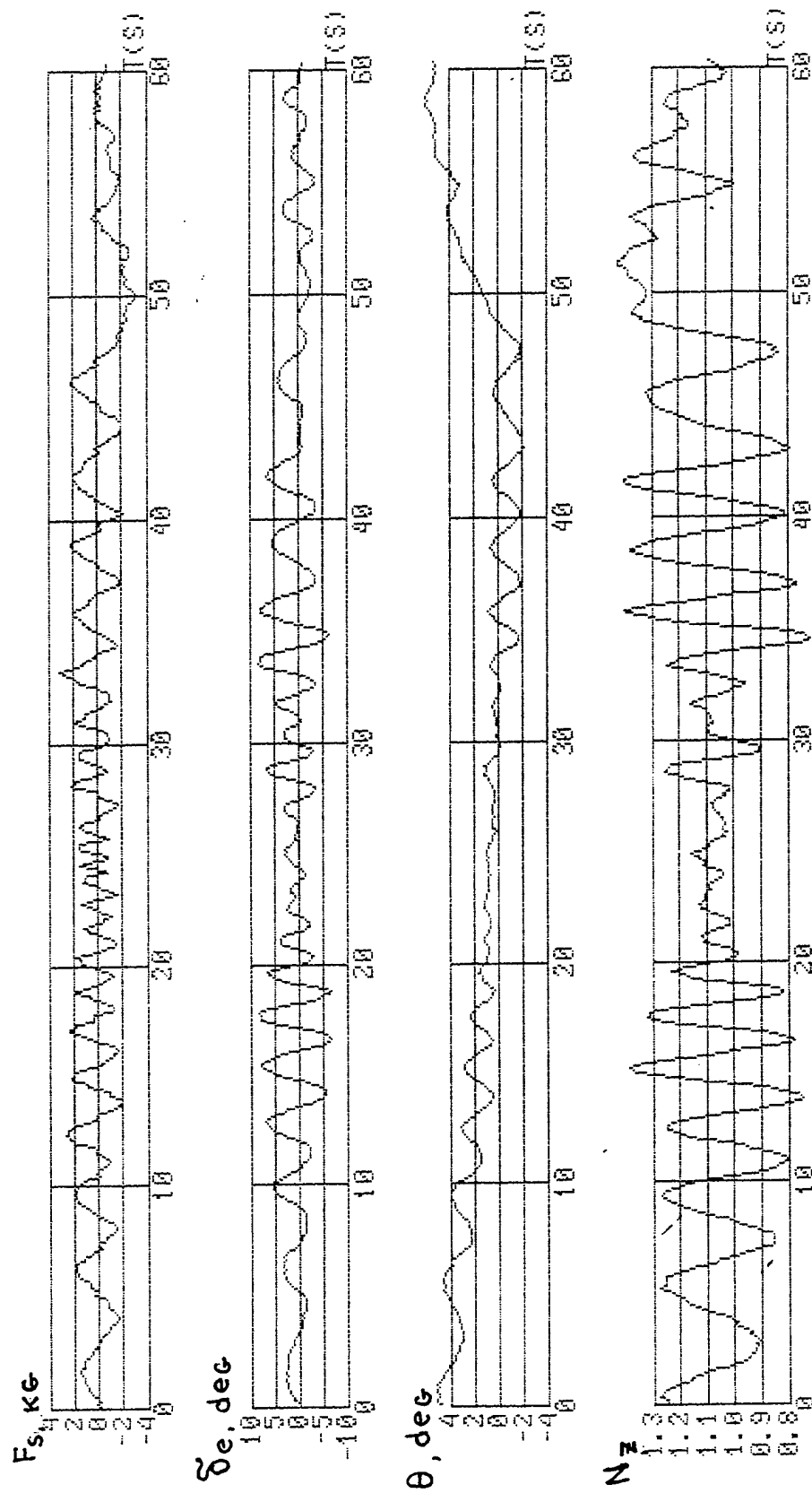


Figure 6.7 Example of sweep excitation.

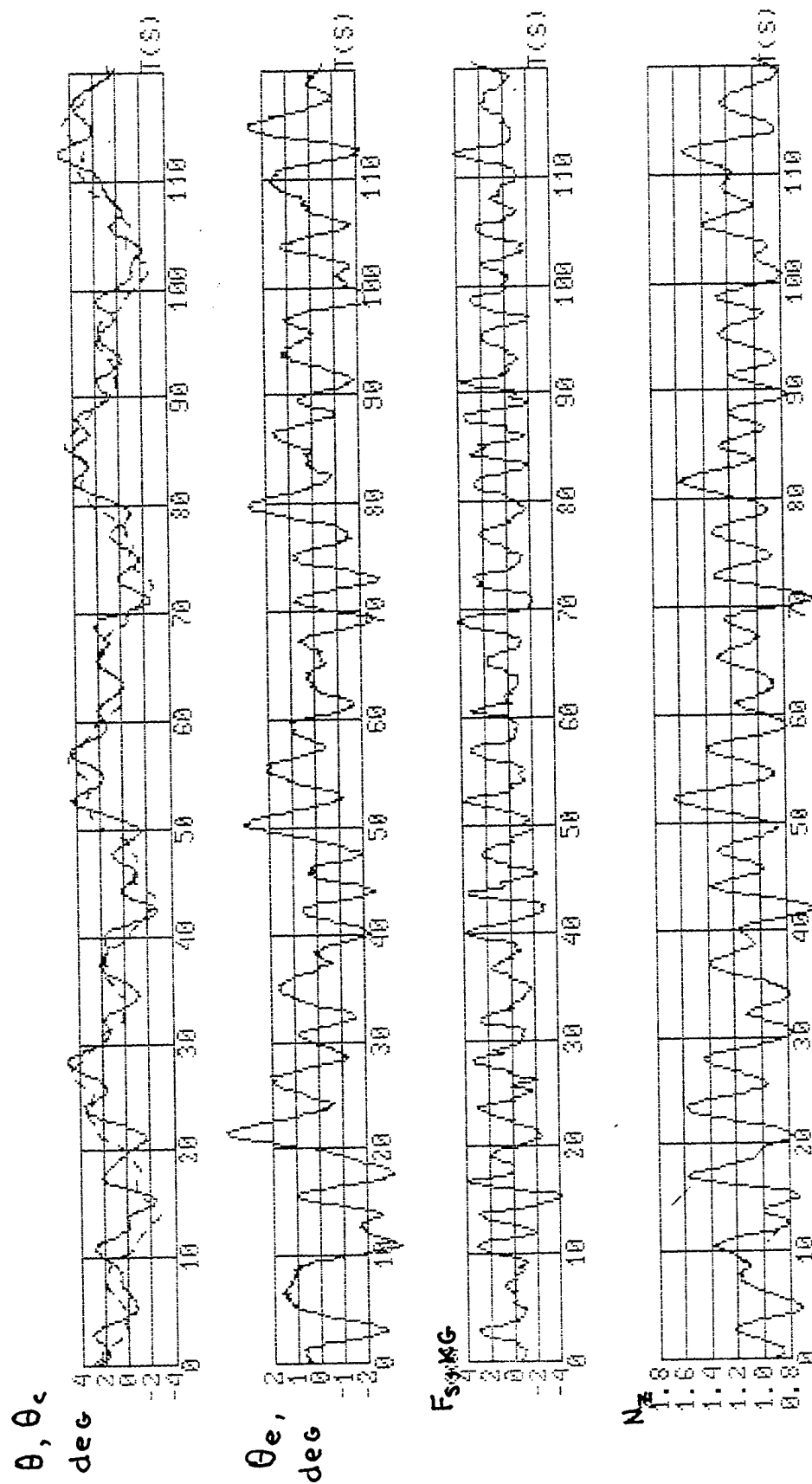


Figure 6.8 Example of target tracking task.

threshold for the magnitude of normal acceleration the pilot must sense to attempt acceleration tracking is $|a_{zp}/q(\omega_c)| > 0.012 \text{ g/deg/sec}$. This parameter is known as Smith's magnitude criterion. If the phase margin of the pilot-felt normal acceleration to stick force dynamics is less than zero (sometimes the slightly positive value of 10...15 degrees is taken) at the subjectively predictable frequency, then the aircraft will have the tendency to PIO at that frequency.

The parameters of tracking task determined according to R. Smith's procedure yielded the following results.

The value m of the average slope of the magnitude of the experimental θ/F_s transfer function was defined as it is shown in Fig. 6.9a for all dynamic configurations. These values of m provided for the appropriate calculated meanings of crossover frequencies ω_c for all configurations.

From the other side the same parameters ω_c have been determined from ground simulation and flight experiment based on the normalized power spectral density obtained for stick force activity (Figs. 6.9b, 6.9c). The comparison of calculated and actual flight frequency meanings indicated along the frequency axis shows that ω_c predicted for the PIO prone configurations are very close to actual peaks in pilot's control inputs power spectral density obtained during tracking in actual flight.

Fig. 6.9d demonstrates the example of determination of parameters which are necessary components of Smith's Criterion

$$\Phi(i\omega_c) = p \frac{a_{zp}}{F_s} (i\omega_c) - 14.3 * i\omega_c,$$

namely:

magnitude and phase for n_{zp}/q ,

calculated function $\Phi(i\omega_c)$.

Simultaneously the n_z/F_s magnitude along with the q/F_s (Fig. 6.9d) are used to check the Smith's magnitude criterion $|a_{zp}/q(\omega_c)| > 0.012 \text{ g/deg/sec}$.

To check the conditions

$$\Phi(i\omega_c) \geq -160^\circ \text{ when } -122^\circ \geq \frac{\theta}{F_s}(i\omega_c) \geq -130^\circ. \text{ for level 1;}$$

$$\Phi(i\omega_c) \geq -220^\circ \text{ when } -148^\circ \geq \frac{\theta}{F_s}(i\omega_c) \geq -165^\circ. \text{ for level 2}$$

of R. Smith's criterion the phase of θ/F_s for ω_c frequencies were determined.

R. Smith's Criterion

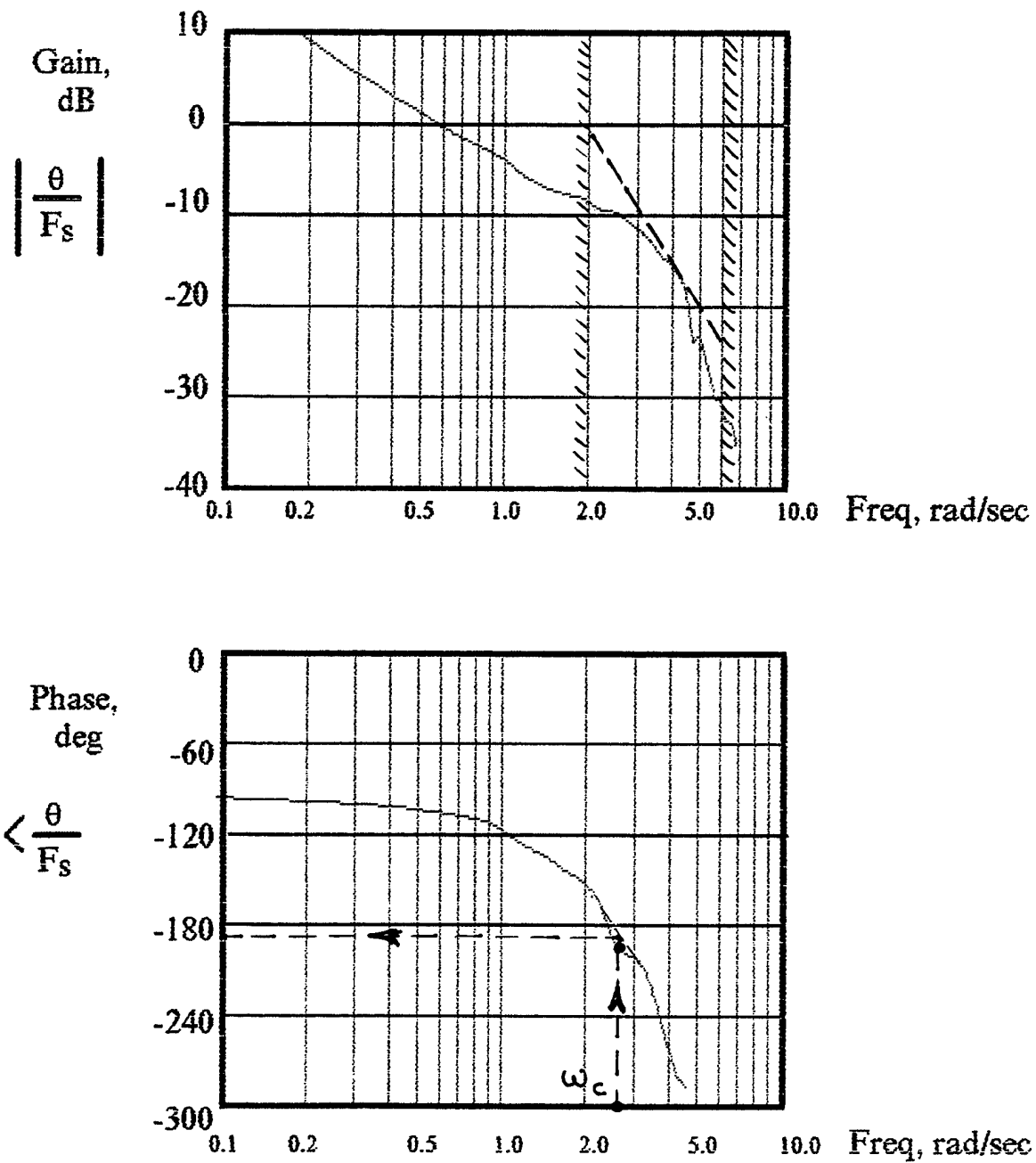
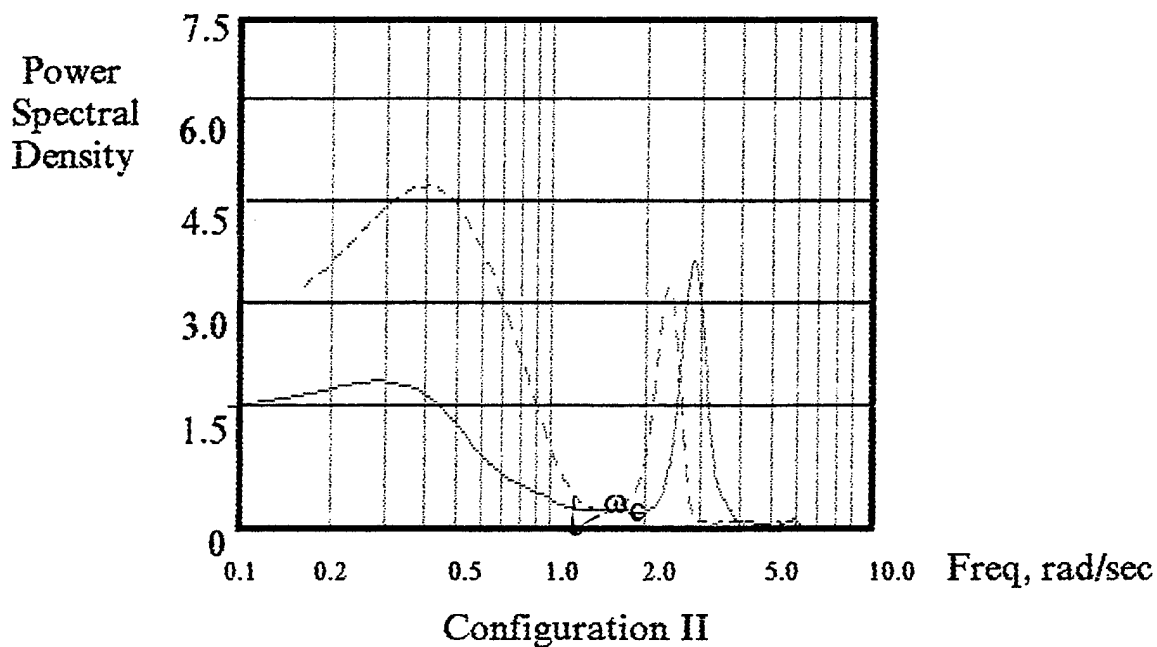
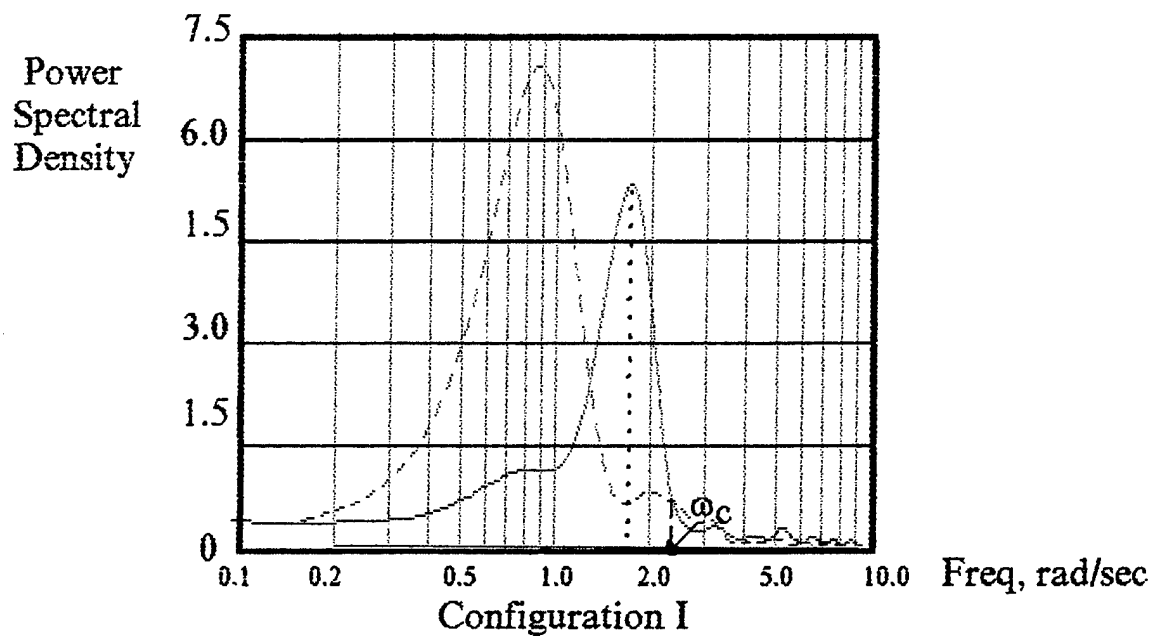
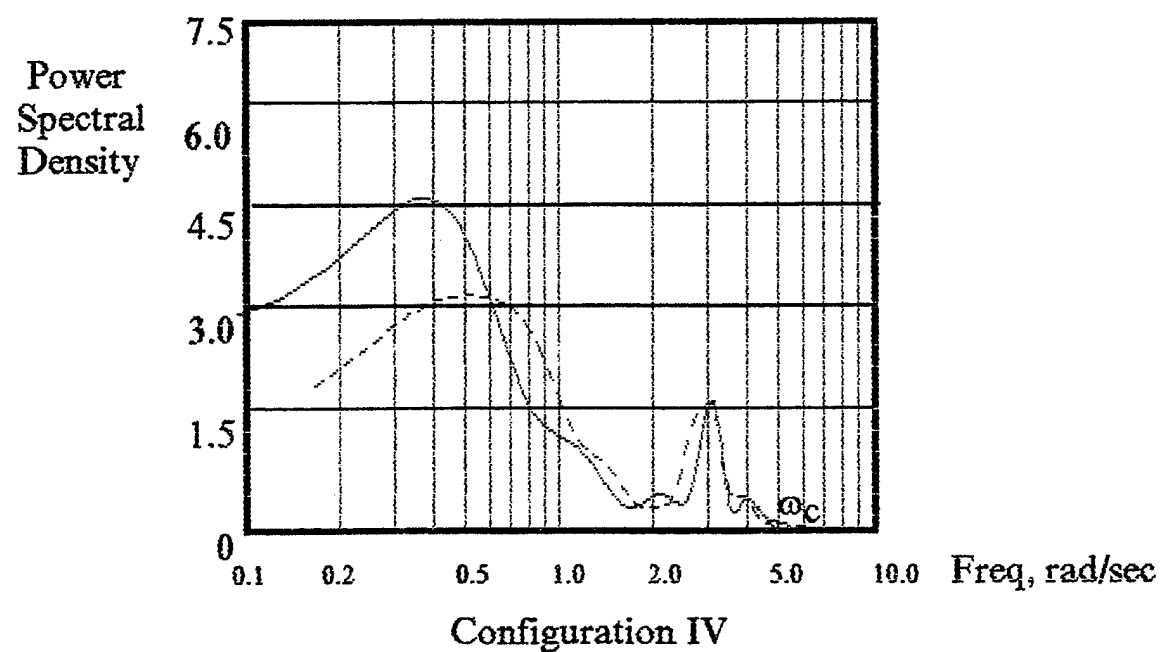
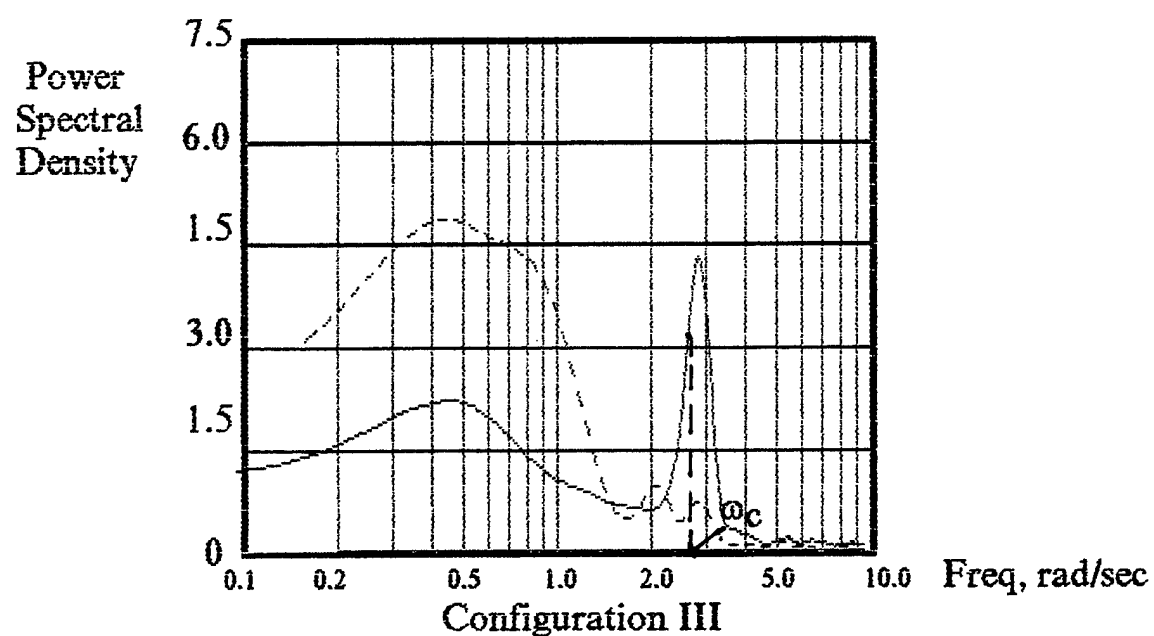


Figure 6.9a Example of Average Slope Determination (Configuration III)



— Tu-154M IFS flight
 - - - Full Flight Simulator

Figure 6.9b Normalized Stick Force Spectrums



— Tu-154M IFS flight
 - - - Full Flight Simulator

Figure 6.9c Normalized Stick Force Spectrums

R. Smith's Criterion

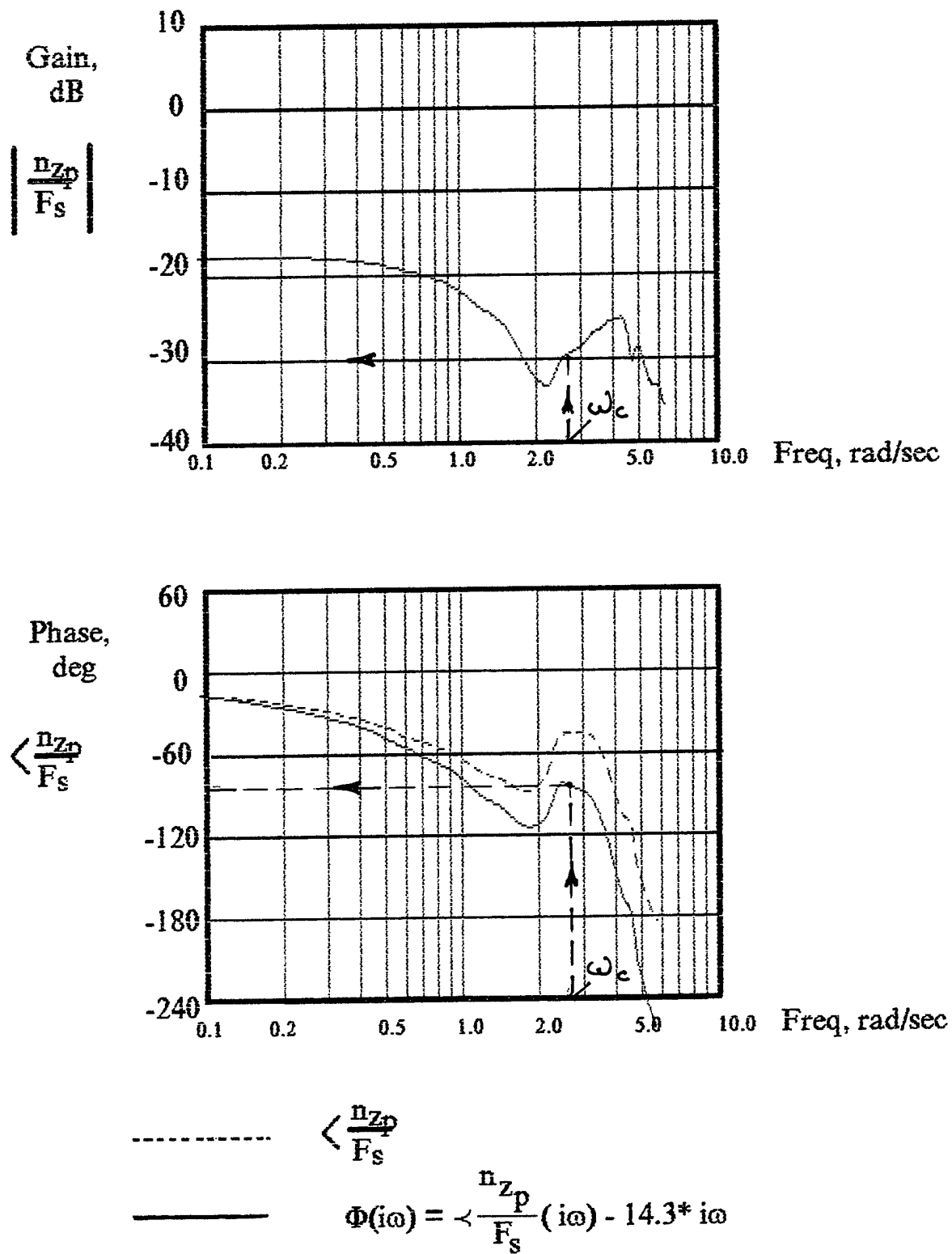


Figure 6.9d Example of Parameter Determination (Configuration III)

The results of calculation are summarized in the following table.

Configuration.	q rad/sec	$p \frac{\theta}{F_S}(i\omega_c)$	$\Phi(i\omega_c)^\circ$	$ n_{zp}/q(i\omega_c) $ g/sec/sec
I	2.22	-240	-180	0.04
II	1.14	-110	-80	0.10
III	2.49	-186	-80	0.042
Basic	3.5	-180	-70	0.056

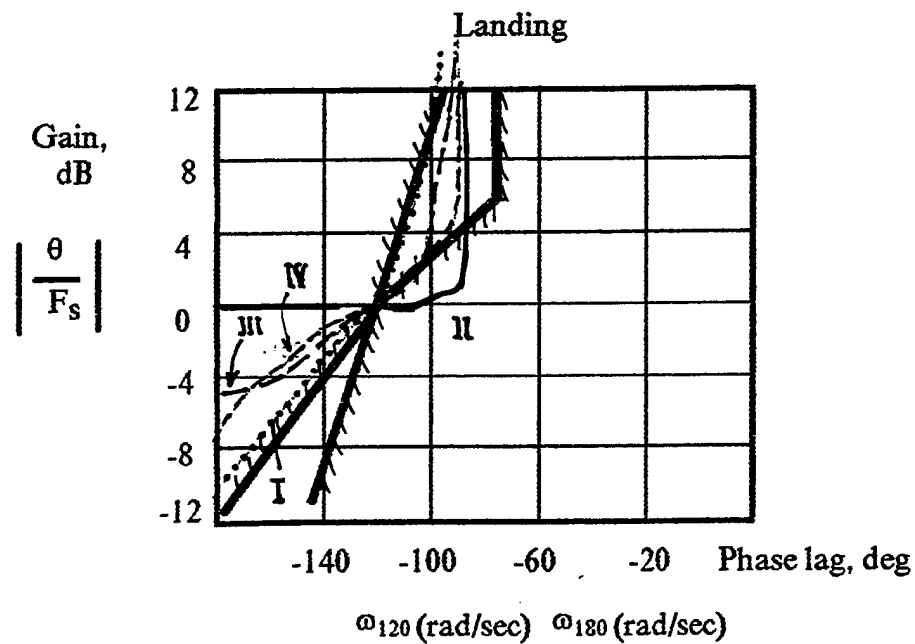
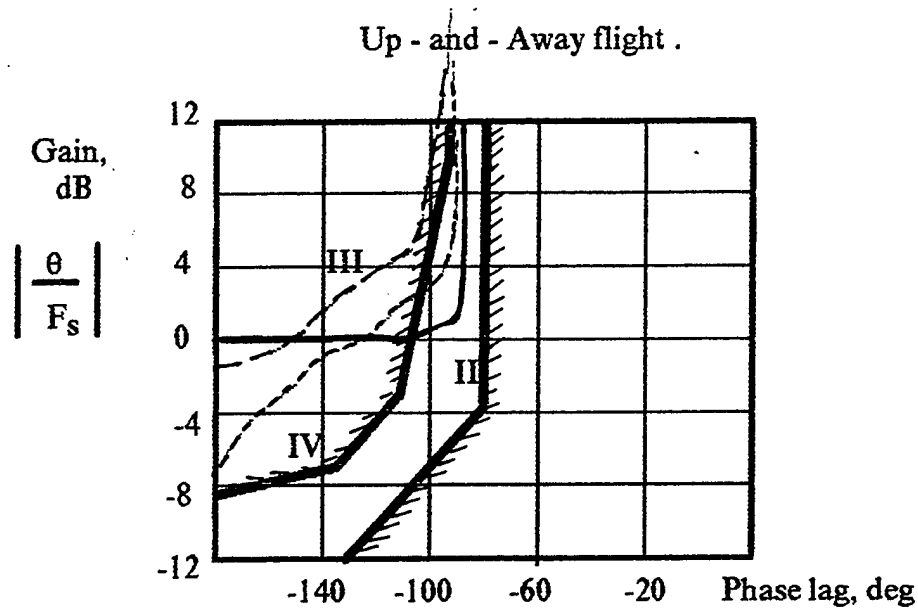
Thus we can see that even for "good" base configuration this criterion does not work properly in our case ($\frac{\theta}{F_S}(i\omega_c)$ is much lower than the lowest boundary). Besides, values of $\Phi(i\omega_c)$ are much higher than the recommended ones because for large aircraft, the distance between the center of gravity position and pilot seat is much longer than for fighter aircraft. Nevertheless, values of ω_c predicted for PIO prone configurations are very close to actual peaks in the pilots control inputs power spectral densities, obtained during target tracking regimes, see Figs. 6.9b, c.

6.3.3 G. Gibson's Criterion

The results of experimental flights applied to Gibson's criterion are presented in the Fig. 6.10 both for up-and-away flight and landing. It can be seen that for up-and-away flight (Fig. 6.10a), the correlation between these results and pilot PIO ratings is rather poor. So the Configuration I was rated by the pilots as not the most prone to PIO, but in the phase region of -180 degrees the appropriate curve lies far above the others, though for the curves corresponding to other configurations the present order is correct.

Attitude boundaries for landing yield correct PIO tendency prediction for configurations II, III and IV. The PIO region is near -180° phase lag and in this region configuration II lies higher than configuration III, which, in its turn lies higher than configuration IV. Besides, configuration IV has the maximum values of ω_{120} and ω_{180} , which nevertheless are lower than criterion requirements. For configuration I, the situation is not so obvious. Its frequency response is the nearest one to the boundaries proposed, so it seems this configuration should have the least PIO tendency. But according to pilot comments, it is not true and an explanation may be that this configuration has very low values of ω_{120} and ω_{180} . Thus for this criterion, attitude boundaries and those for ω_{120} and ω_{180} should be modified.

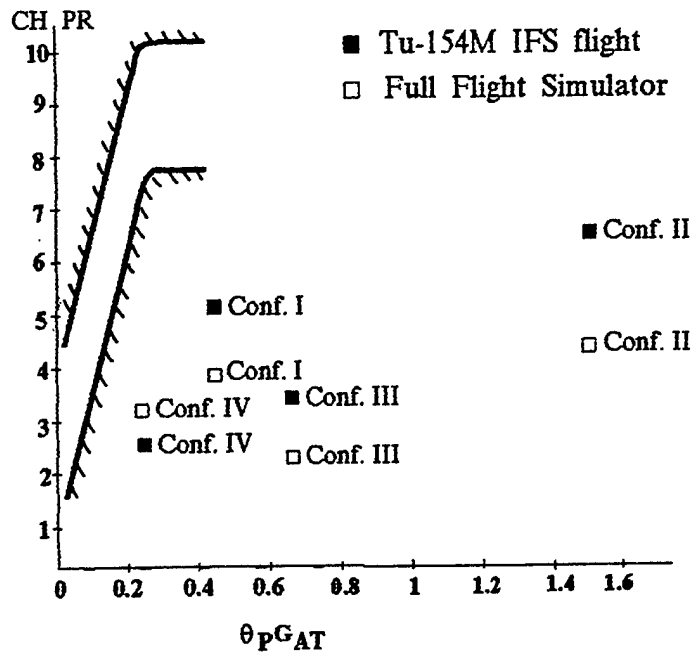
Gibson's Criteria



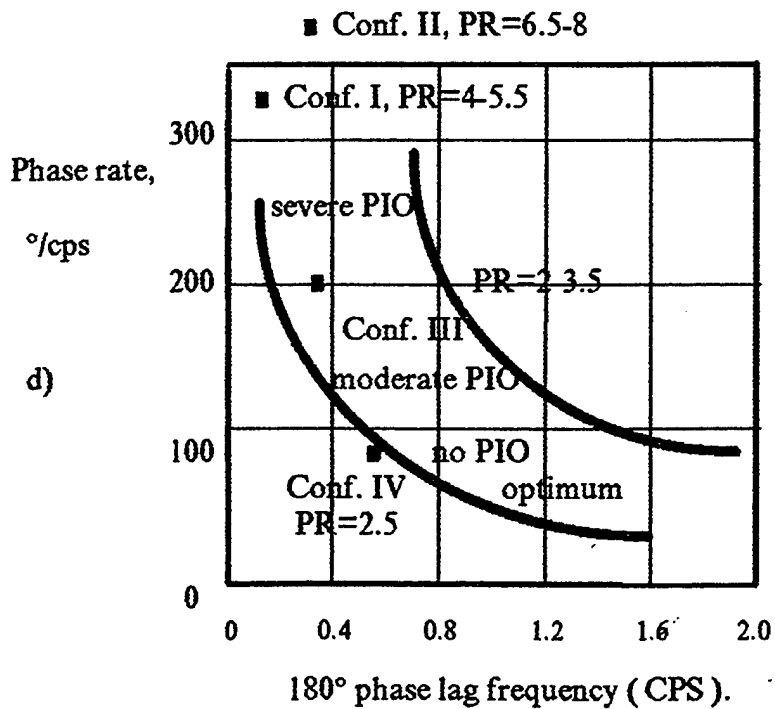
conf. I	0.12	1.05
conf. II	1.44	2.08
conf. III	1.0	2.35
conf. IV	1.76	3.5

Figure 6.10a,b Attitude Boundaries Results

Gibson's Criteria.



c) LANDING PIO CRITERION RESULTS.



d) Trends of phase rate of "FCS-aircraft" system.

Figure 6.10c,d Gibson's Criteria Results

Summarizing the results presented in Fig. 6.10c and in the table below it can be stated that this criterion, in general, properly reflects the interdependence of dynamic configurations in accordance with subjective pilot ratings while applying all types of pilot's rating scales. Nevertheless, the correlation between PR and parameter $\theta_p G_{AT}$ suggested as PIO criterion is rather poor, and in all cases, the PIO region boundaries should be shifted in the right-down direction for transport aircraft.

Configuration	G_{AT}	θ_p	$G_{AT}\theta_p$
I	21.7 dB	6	0.48
II	0 dB	1.5	1.5
III	5.0 dB	1.18	0.66
Basic	7.4 dB	0.54	0.23

The most hopeful results are yielded while applying the other Gibson's Criteria based on utilizing trends of phase rate of "FCS-aircraft" system, see Fig. 6.10d (the author stated that this criterion replaced the previous one). One can see that all configurations are located strictly in the order corresponding to average pilot's PIO ratings and the correlation is reasonable. The criterion boundary even seems to be applicable for transport aircraft.

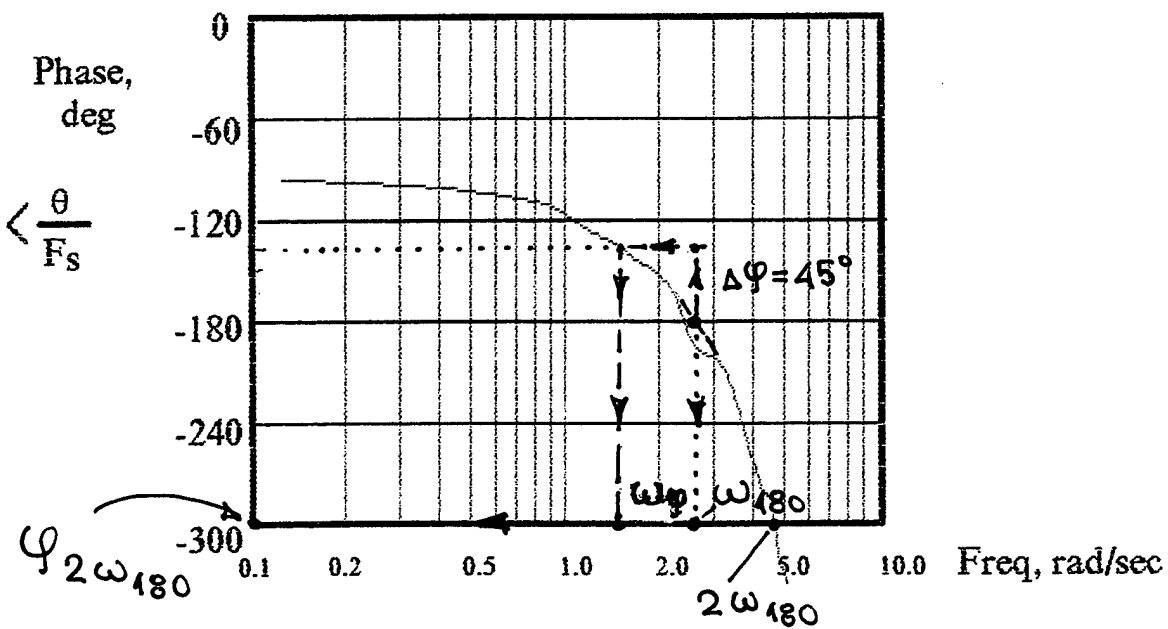
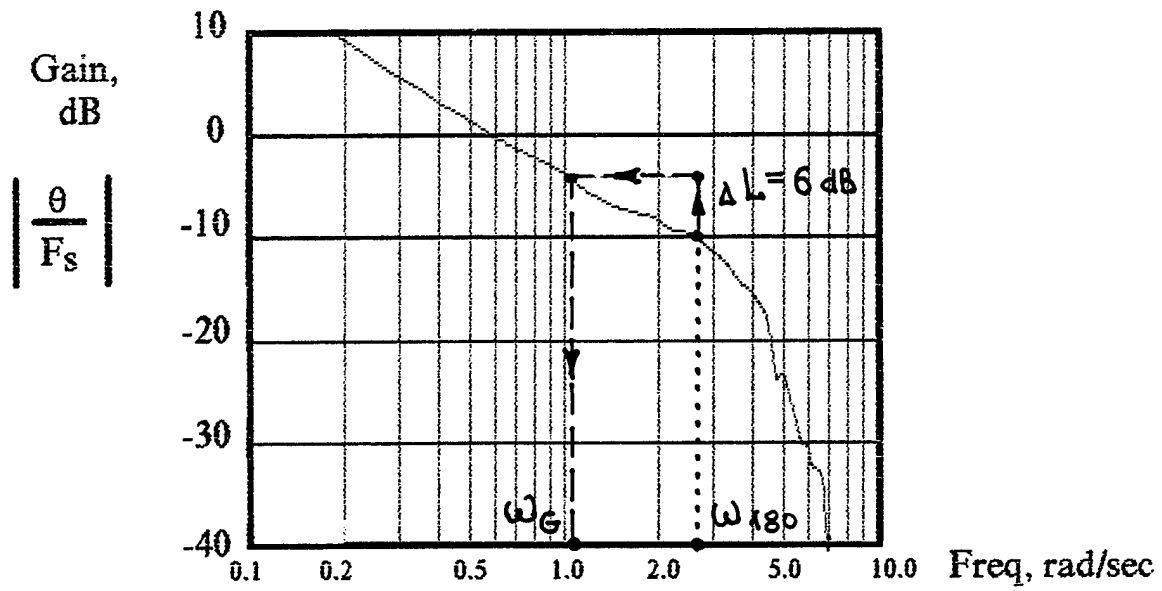
6.3.4 Bandwidth Criterion

Bandwidth criterion does not directly predict PIO tendency or rating, but predicts levels of handling qualities based on phase delay τ_p and system bandwidth ω_{BW} of open-loop pitch to stick force dynamics. Phase delay can be thought of as a measure of the slope of the phase curve of this loop dynamics. A rapid phase rolloff (steep slope) at frequencies within the pilot's bandwidth of control indicates the presence of higher order lag dynamics which contribute to equivalent system time delay. Phase delay is usually numerically similar to equivalent system time delay, and is much easier to calculate.

The results of parameters ω_{BW} and τ_p definition due to expression

$$\tau_p \geq - \frac{\varphi_2 \omega_{180} + 180^\circ}{57.3 \cdot 2 \omega_{180}},$$

are summarized in the following table. The example of determination of the components of the above mentioned formula is presented in Fig. 6.11a.



$$\omega_{BW} = \min(\omega_G, \omega_\phi)$$

Figure 6.11a Example of Bandwidth Criterion Parameters Determination (Configuration III)

Configuration	ω_ϕ rad/sec	ω_G rad/sec	ω_{BW} rad/sec	$2\omega_{180}$ rad/sec	$\phi_{2\omega_{180}}$ degrees	τ_P sec
I	0.3	0.7	0.3	2.1	-235	-0.46
II	1.6	0.31	0.31	4.16	-350	-0.71
III	1.38	1	1	4.7	-300	-0.44
Basic	2	2.05	2.	7	-240	-0.15

These results are plotted in Fig. 6.11b. It is rather obvious that the general tendency of pilot ratings is predictable, but for large aircraft much lower values of ω_{BW} and much higher values of τ_P are acceptable, comparatively with fighter aircraft.

6.3.5 "Pilot-In-The-Loop" Technique

The technique for predicting an aircraft susceptibility to longitudinal PIO is based entirely on the characteristics of the "pilot-aircraft" open-loop transfer function $|Y_P Y_C(i\omega)|$. Namely,

- if the open-loop crossover frequency ω_c of $Y_P Y_C$ does not exceed 2.0 rad/sec, and
- if the amplitude of $Y_P Y_C$ is less than 10 dB at a frequency one decade below the 2.0 rad/sec crossover frequency, then the aircraft should be considered to be susceptible to longitudinal PIO.

Both elements of this criterion relate indirectly to the closed-loop transfer function θ/θ_c .

The author mentioned in his papers that the PIOs are most probable at frequency ω_{180} while the amplitude characteristic θ/θ_e is within the "PIO region" area.

Results of this technique, presented in Figs. 6.12a, b, c, d revealed the following tendency. The more prone the configuration is to PIO, the lower the crossover frequencies of "pilot-aircraft" frequency response and the less the gain margins. From an accurate comparative consideration of θ/θ_e frequency characteristics for all dynamic configurations, it becomes noticeable that some correlation exists between configuration PIO proneness due to amplitude criterion requirements satisfaction. To validate this correlation and boundaries location, more statistical flight results should be obtained.

Bandwidth Criterion

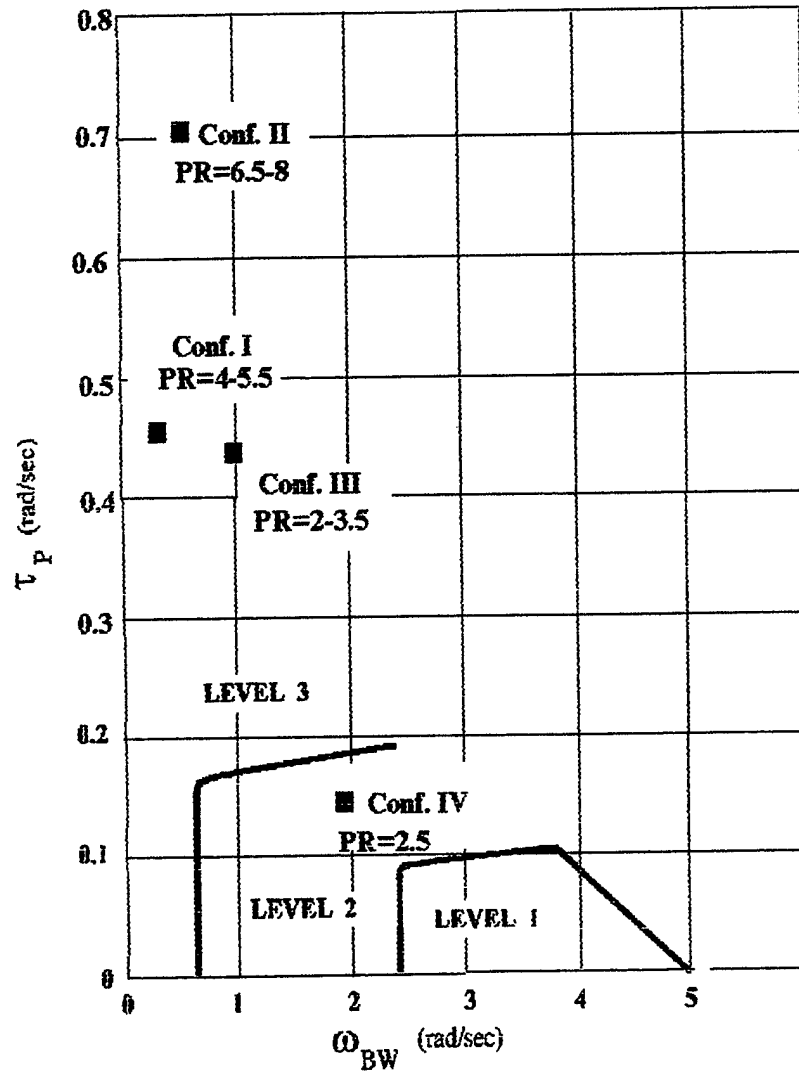


Figure 6.11b Bandwidth Criteria Results

"Pilot-in-the-loop Technique"

Configuration I

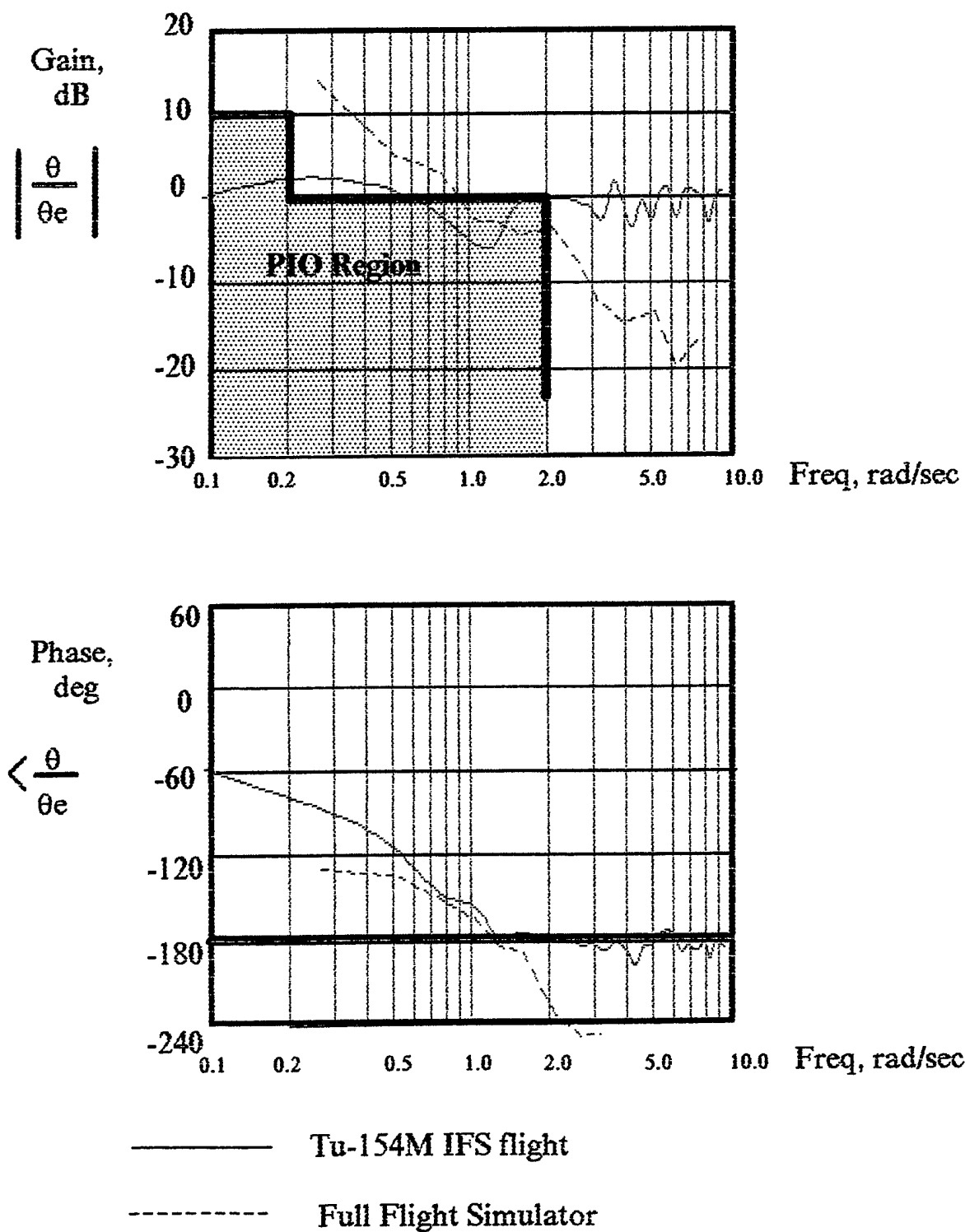


Figure 6.12a Comparison of Full Flight Simulator Results and Tu-154 IFS Flight Configuration I

"Pilot-in-the-loop Technique"

Configuration II

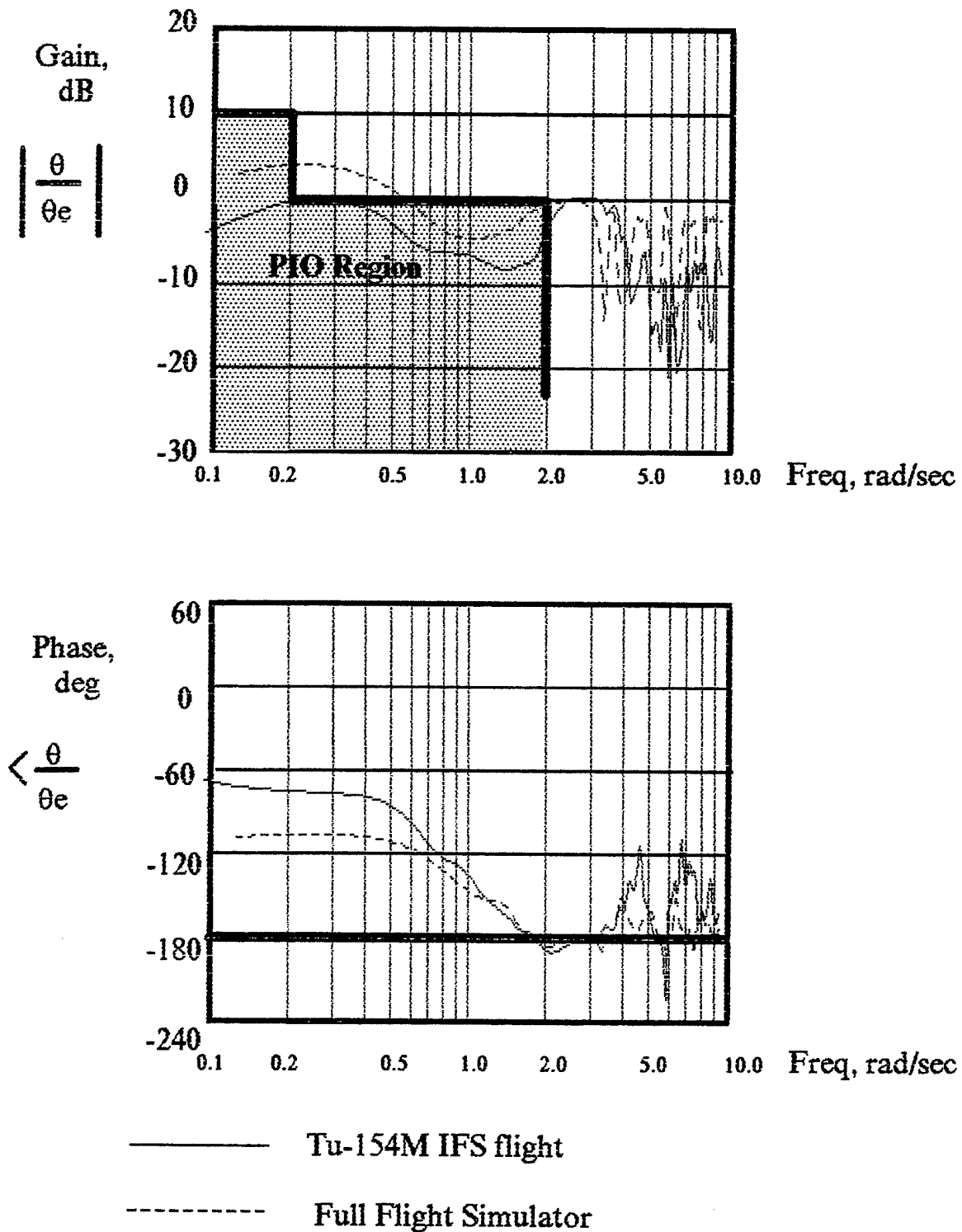


Figure 6.12b Comparison of Full Flight Simulator Results and Tu-154 IFS Flight Configuration II

"Pilot-in-the-loop Technique"

Configuration III

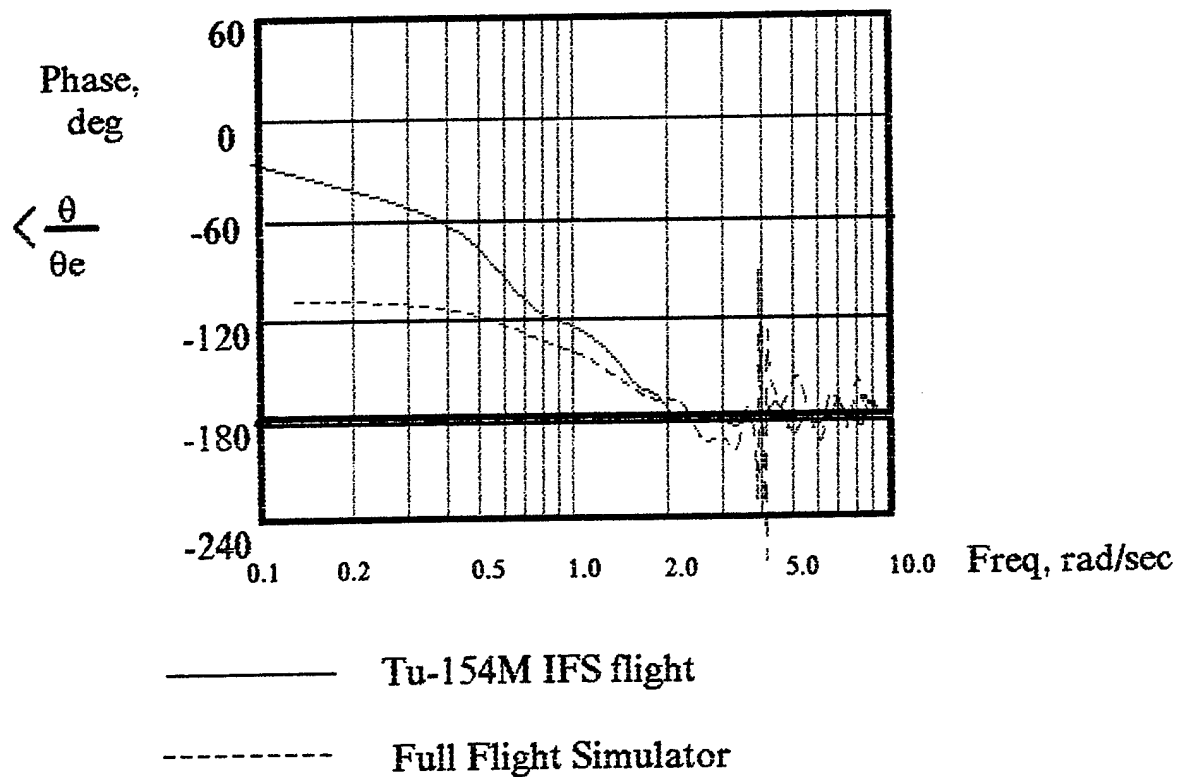
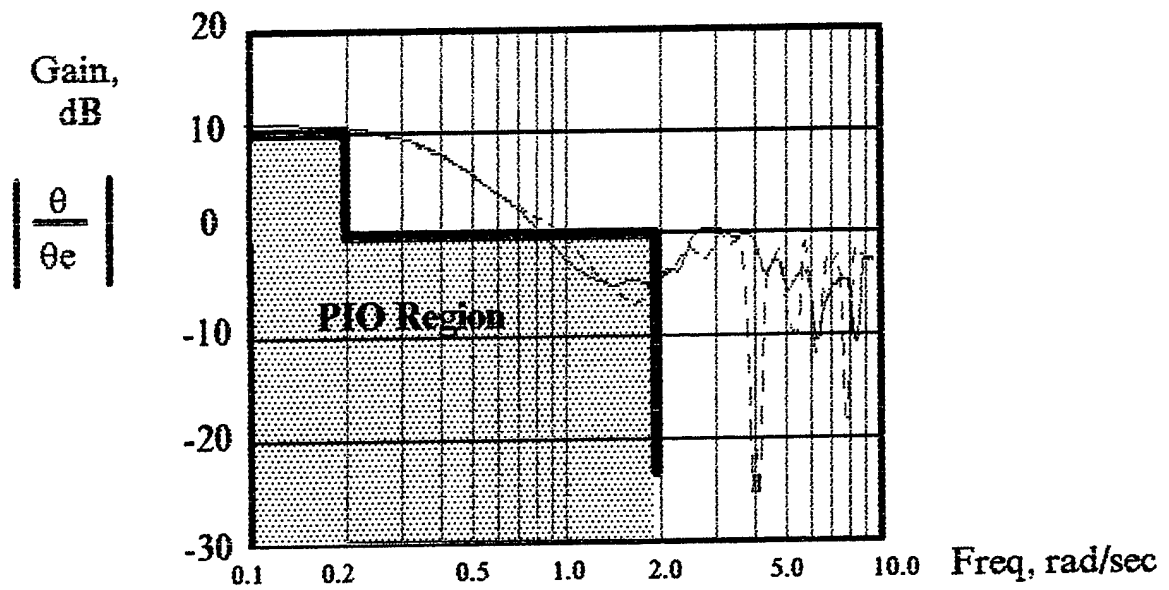


Figure 6.12c Comparison of Full Flight Simulator Results and Tu-154 IFS Flight Configuration III

"Pilot-in-the-loop Technique"

Configuration IV

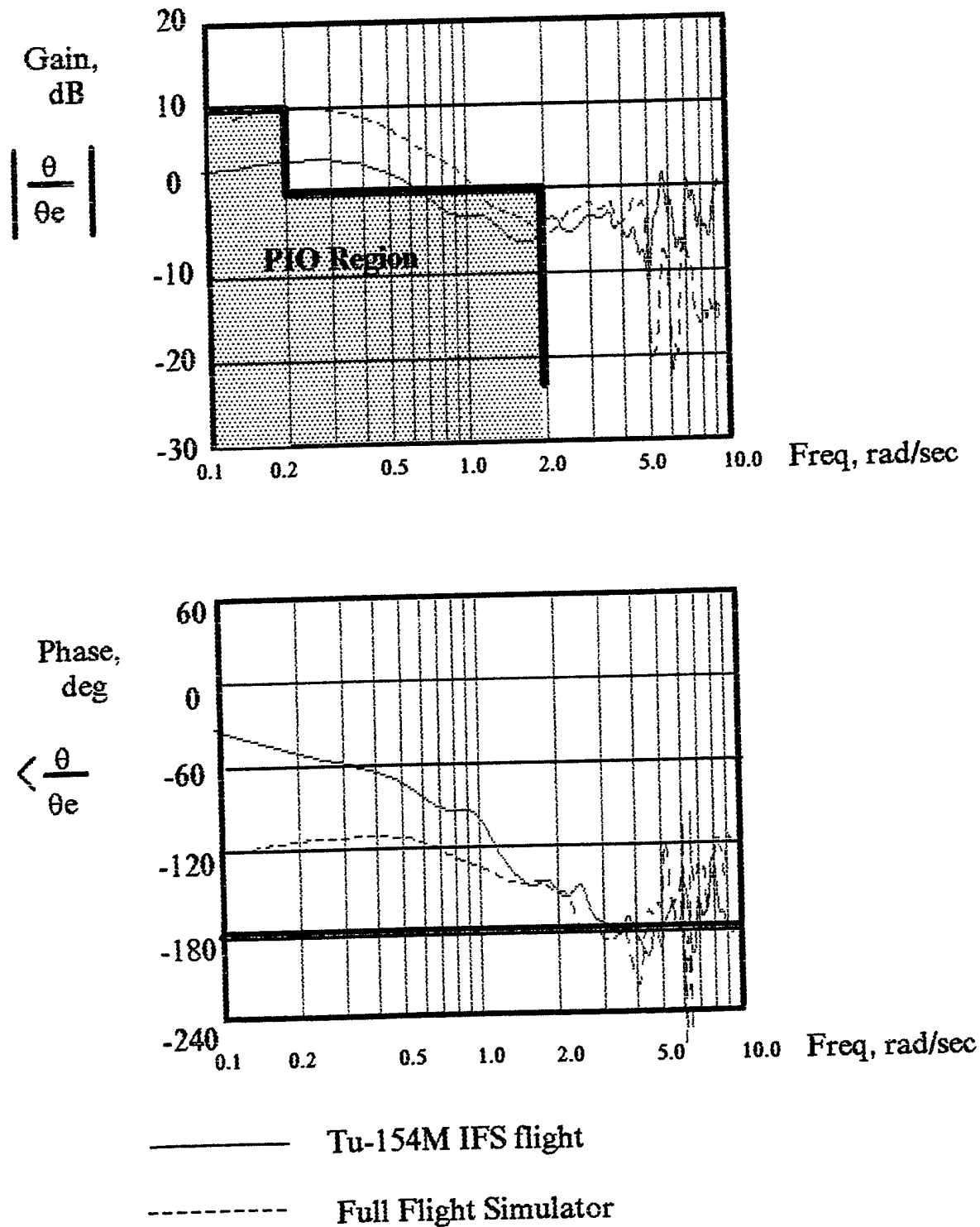


Figure 6.12d Comparison of Full Flight Simulator Results and Tu-154 IFS Flight Configuration IV

CONCLUSIONS

1. A few PIO criteria (namely, R. Smith's criterion, G. Gibson's criterion, bandwidth criterion and "pilot-in-the-loop" technique) were selected and investigated in the Tu-154M variable-in-flight dynamics In-Flight Simulator reproducing rather wide range of transport aircraft and control system characteristics. The flight results indicated that practically all criteria (may be Smith's in less degree) are capable of revealing the tendency of transport aircraft to PIO in appropriate cases. These results correlate unequivocally with pilot ratings and are, in general, in conformity with results obtained in previous experiments by other investigators.

2. For the transport aircraft, the values of parameters characterizing one or another PIO criterion and indicating the PIO tendency or onset are to be significantly corrected in comparison with parameters obtained previously for maneuverable aircraft. The boundaries indicating the domains of the appropriate PIO tendency criteria on the planes of PIO characteristic parameters are to be essentially shifted.

3. Based on limited pilot experience, the most preferable variant of PIO Pilot Rating Scale seems to be the combination of Scale 1 and Scale 2 which comprises the convenient "tree-like" form (Scale 2) and a rather detailed description of aircraft behavior occurred (Scale 1). As the pilots were often prone to use the values between integer ratings, perhaps some intermediate decimal values and appropriate word descriptions should be added.

4. The flight method utilized in the experimental flights reproduced the tight tracking task aggravated by an additional stringent requirement for the pilot to be within the limits of pitch attitude error while tracking. This method proved to be one which provoked the PIO tendency and provided for flight data acquiring for further reasonable frequency characteristics determination, including those for closed control loop "pilot-aircraft."

5. To define exactly the PIO criteria parameters and outline the corrected PIO onset boundaries, further in-flight research experiments should be undertaken (embracing more dynamic configurations, different pilots with diverse piloting manners, different hand controllers and feel characteristics, lateral dynamic characteristics influence etc.) directed at collecting the comprehensive statistical flight data.

6. As the PIO phenomenon criteria development are to be based on the comprehensive flight data of different dynamic and flight control system parameters and the frequency response characteristics of the control loop are primarily required, the variable-in-flight dynamic In-Flight Simulator is the most suitable instrument for such investigations.

REFERENCES

1. Moorhouse, D. J. And Woodcock, R. J. "Present Status of Flying Qualities Criteria for Conventional Aircraft." AGARD Conference Proceedings ¹ 333, Criteria for Handling Qualities of Military Aircraft, April 1982.
2. Gibson, J. C. "Piloted Handling Qualities Design Criteria for High Order Flight Control Systems." AGARD Conference Proceedings ¹ 333, Criteria for Handling Qualities of Military Aircraft, April 1982.
3. Gibson, J. C. "Handling Qualities for Unstable Combat Aircraft." ICAS Proceedings, 1986
4. Hoh, R. H., et al. "Bandwidth - A Criterion for Highly Augmented Airplanes." AGARD Conference Proceedings ¹ 333, Criteria for Handling Qualities of Military Aircraft, April 1982.
5. Hess, R. A. and Kalteis, R. M. "Technique for Predicting Longitudinal Pilot-Induced Oscillations." Journal of Guidance, Control, and Dynamics, vol. 14, number 1, 1991, p.p. 198-204.
6. Green, F. B., Hoffman, S. K. "Design and Development of a Three-Axis Augmentation System for a Class III STOL Assault Transport." AIAA paper 86 - 2709.
7. Smith, R. E. "Effects of Control System Dynamics on Fighter Approach and Landing Longitudinal Flying Qualities." AFFDL-TR-78-122, vol. 1 March 1978.
8. Powers, B. G. "Space Shuttle Pilot-Induced Oscillations Research Testing." AGARD-AG-262, 1984.
9. Bjorkman, E. A. et al. "Flight Test Evaluation of Techniques to Predict Longitudinal Pilot Induced Oscillations." AIAA paper 86-2253.
10. Hess, R. A. "Effects of Time Delays on Systems Subject to Manual Control." J. Guidance, July-August, 1984.